



Design, synthesis and study of the biological and biophysical activity of antimicrobial peptides

Ariadna Grau Campistany



Aquesta tesi doctoral està subjecta a la llicència **Reconeixement- Compartitqual 3.0. Espanya de Creative Commons.**

Esta tesis doctoral está sujeta a la licencia **Reconocimiento - Compartitqual 3.0. España de Creative Commons.**

This doctoral thesis is licensed under the **Creative Commons Attribution-ShareAlike 3.0. Spain License.**

DISSERTATION

**Design, synthesis and study of the biological and
biophysical activity of antimicrobial peptides**

Ariadna Grau Campistany

Program of doctorate in Organic Chemistry
Department of Organic Chemistry
Faculty of Chemistry
University of Barcelona

Francesc Rabanal Anglada
Department of Organic Chemistry
Faculty of Chemistry
University of Barcelona

Yolanda Cajal Visa
Department Physical Chemistry
Faculty of Pharmacy
University of Barcelona

*‘...forget conventionalisms;
forget what the world thinks of you stepping out of your place;
think your best thoughts,
speak your best words,
work your best works,
looking to your own conscience for approval.’*

Susan B. Anthony

Suposo que com tot en aquest món, la forma més fàcil d'escriure uns agraïments és començant per l'inici, per com va començar tot. Per tant, hauria de començar donant-vos les gràcies a vosaltres Francesc i Yolanda, perquè vosaltres va ser els que va confiar en les meves possibilitats, independentment del que un paper o un número pogués dir, va ser capaçs de veure més enllà i donar-me la oportunitat de fer aquest viatge conjuntament. Amb vosaltres no només he pogut aprendre i créixer com a científic sinó que he rigut i he plorat creixent també així com a persona. Heu sigut únics i mai oblidaré els meus jefes de doctorat, acabi on acabi!!!

A tota la gent que vaig trobar al entrar en el grup, Montse, Roser, Núria i Silvia, em va obrir les portes del lab i del món de les polimixines, tot i estar juntes poc temps va ser prou per veure que sou genials!!

A les meves noies, Natàlia, Helena i Clàudia, ha sigut un autèntic plaer ensenyar-vos i compartir allò que sé (poc, però bé!). He gaudit moltíssim treballant amb vosaltres i heu fet possible que el nostre en ocasions solitari laboratori tornés a ser una petita família.

Moltíssimes gràcies a tota la gent del departament de fisicoquímica, perquè tot i no ser una farmacèutica, va ser capaçs de confiar en els meus coneixements. Gràcies també per tots els riures, les mini-explosions, i bogeries vàries, conseqüència de tantes hores dins un laboratori. Un gràcies molt especial a la M^a Asunció per ser una alumna molt avantatjada jiji!! A la Tere per ser sempre tant amable amb mi. Evidentment, no m'oblido de la M^a Antònia, ha sigut genial (adjectiu que estic usant per descriure que ha sigut millor que bé o molt bé o molt i molt bé) compartir aquesta etapa amb tu, has sigut com una segona mami (la primens és la Yolanda jiji)!

Especial gràcies a la Dra. M^a Àngels Manresa, per ser capaç de fer de mi, la petita química, una petita microbiòloga, encenent dins meu el gusanillo del interessant món de la microbiologia. Gràcies també a la gent de micro, en especial a en Nacho, Andreu i Jho, tot i no ser-hi sempre allà amb vosaltres, i no ser del lab 100%, em va fer sentir part del vostre grup, i us estaré sempre agraïda. No em puc oblidar de la Carme i la M^o Jesús, per ajudar-me tantíssim, fer-me riure sempre que havia de preparar material i compartir confidències entre autoclau i autoclau!

Now, I move to a different country, and consequently I have to change language. I would have never imagined that the experience of moving abroad, to a completely different country, working in a different lab, would turn out to be what it was. I always say that it was the best and worst experience of my life. I became a much better scientist and a much more mature person (never forgetting the tiny dragon inside me!).

Firstly, I want to thank Anne Ulrich for giving me the great opportunity of working in your laboratory, especially without knowing me personally, in a way you blindly trusted that I was a good worker, and I hope I lived up to your expectations. Especial thanks to Erik, with whom I shared lots of hours, especially lots of NMR and with whom I learned a lot. Thank you to all the people in the Institute, and especially thanks to the people in the lab. Papia and Jonathan, thanks for making me feel comfy and part of the group, even if I was the crazy loud Spanish girl, and thank you Sabine, Tamta and Christina, because even if we didn't actually work together you were great colleagues with whom I shared lots of laughter. My most especial thanks to Sarah, you were my first friend and most special friend, you are an awesome scientist and a best person, never forget it!!!

Thank you to all the people I met in Karlsruhe for making me feel like in home!!! Thank you Coral and Clàudia for being my tiny safe Catalunya while living in Germany!! And of course also thank you to the funding agencies, DAAD and EMBO.

Per acabar suposo que només em queda agrair a la meva família.

Gràcies Mare i Mame per donar-me una gran educació i ser el meu pilar de suport, sense vosaltres no seria on sóc ara. Sé que no ha sigut fàcil, i heu hagut de treballar molt, però espero que veurem convertida en doctora us faci orgullosos de la vostra filla. Gràcies per fer l'esforç de venir a Alemanya a veurem, estant allà em vaig adonar de com és d'important la família (tot i que al cap de dos dies ja estava cansada de vosaltres jiji). Gràcies Mireia per estar allà, quan he estat malament i quan he estat bé, fent les nostres xerradetes, i no oblidem per polemitzar sempre que fos necessari i gràcies al Ale per preguntar sempre com anava la tesi! Finalment, gràcies Avi, per inculcar l'interès per inventar en mi, tot i no estar amb nosaltres espero que estiguis orgullós de la teva néta!

I never imagined that life could change so drastically; from one day to another someone comes to your life and turns you around. That's why my last thanks is to you, Marco, for being here, coping with me complaining about the thesis, about working for so many hours (even taking me to work on holidays!!) and about life in general. You have been my second and strongest pillar. Thank you also for so many beautiful moments and so much more we have left to come. Thank you also to your family, for making me feel part of it, even if sometimes communication is not easy, and for being so supportive!!!!

Per acabar, només dir que si em deixo alguna persona, moltes gràcies per tot!!! To finish, just say that if I forgot someone, thank you so much for everything!!!

És una tonteria de quan ets petit, però sempre he cregut que estava destinada a fer coses grans. Crec doncs que 3 anys d'esforços, escriure una tesi doctoral i convertir-me en la Dra. Grau-Campistany és potser l'inici de tot això. Un camí llarg i farragós però que tinc moltes ganes de recórrer!!!

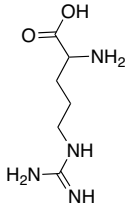
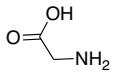
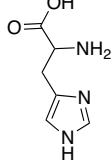
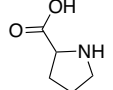
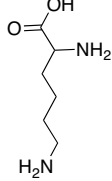
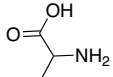
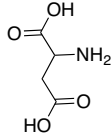
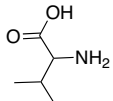
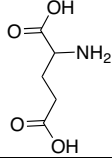
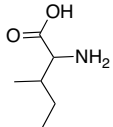
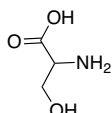
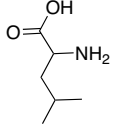
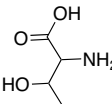
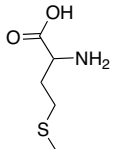
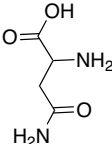
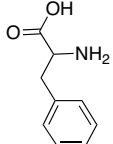
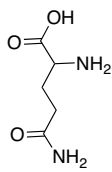
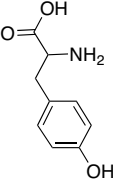
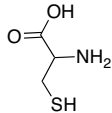
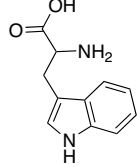
ABBREVIATIONS AND APPENDICES

List of abbreviations

AA	Amino acid
AC	Active centres
ACN	Acetonitrile
AMP	Antimicrobial peptide
ANTS	1-aminonaphthalene-3,6,8-trisulfonic acid
aq	Aqueous
ATCC	American Type Culture Collection
B₀	Magnetic field
Boc	<i>tert</i> -Butoxycarbonyl
BOX	bis-(1,3-dibutylbarbituric acid)-trimethine oxonol
tBu	<i>tert</i> -Butyl
CD	Circular dichroism
CFU	Colony-forming unit
CHCA	Cyano-4-hydroxycinnamic acid
CP	Cross-polarization
CSA	Chemical shift anisotropy
dansyl	Dimethylaminonaphthalene-5-sulfonyl
DCM	Dichloromethane
DEPC	1,2-dierucoyl- <i>sn</i> -glycero-3-phosphocholine
DEPG	1,2-dierucoyl- <i>sn</i> -glycero-3-phospho-(1'- <i>rac</i> -glycerol)
DIC	Diisoproylcarbodiimide
DIEA	Diisopropylethylamine
DLPC	1,2-dilauroyl- <i>sn</i> -glycero-3-phosphocholine
DLPG	1,2-dilauroyl- <i>sn</i> -glycero-3-phospho-(1'- <i>rac</i> -glycerol)
DMF	Dimethyl formamide
DMoPC	1,2-dimyristoleoyl- <i>sn</i> -glycero-3-phosphocholine
DMPC	1,2-dimyristoyl- <i>sn</i> -glycero-3-phosphocholine
DMPG	1,2-dimyristoyl- <i>sn</i> -glycero-3-phospho-(1'- <i>rac</i> -glycerol)
DMSO	Dimethyl sulfoxide
DOPC	1,2-dioleoyl- <i>sn</i> -glycero-3-phosphocholine
DOPG	1,2-dioleoyl- <i>sn</i> -glycero-3-phospho-(1'- <i>rac</i> -glycerol)
DPH	1,6-diphenyl-1,3,5-hexatriene
DPX	<i>N,N'</i> - <i>p</i> -xylenebis(pyridinium bromide)
DSM / DSMZ	Deutsche Sammlung von Mikroorganismen und Zellkulturen
Et	Ethyl
eq	Equivalent
f	Functionalization
F	Fluorescence
FA	Fatty acid
FC	Flow cytometry
FID	Free induction decay
Fmoc	9-fluorenylmethoxycarbonyl
FRET	Fluorescence resonance energy transfer
h	Hours
HBTU	<i>O</i> -(Benzotriazol-1-yl)- <i>N,N,N',N'</i> -tetramethyluronium hexafluorophosphate

HCl	Hydrochloric acid
HEPES	4-(2-Hydroxyethyl)piperazine-1-ethanesulfonic acid
HOBt	Hydroxybenzotriazole
HPLC	High pressure liquid chromatography
RP-HPLC	Reverse phase high pressure liquid chromatography
LB	Luria broth
LC	Liquid chromatography
LPS	Lipopolysaccharide
Lyso-MPC	1-myristoyl-2-hydroxy- <i>sn</i> -glycero-3-phosphocholine
MBHA	4-methylbenzhydramine
MDR	Multidrug-resistant
Me	Methyl
MHB	Mueller-Hinton broth
MIC	Minimum inhibitory concentration
min	Minutes
MRSA	Methicillin-resistant <i>Staphylococcus aureus</i>
NBD	7-nitrobenzofurazan
NBD-PE	1,2-dimyristoyl- <i>sn</i> -glycero-3-phosphoethanolamine- <i>N</i> -(7-nitro-2-1,3-benzoxadiazol-4-yl)
NMR	Nuclear magnetic resonance
ssNMR	Solid-state nuclear magnetic resonance
SPPS	Solid phase peptide synthesis
OD	Optical density
OM	Outer membrane
PAS	Principal axes system
PI	Propidium iodide
POPC	1-palmitoyl-2-oleoyl- <i>sn</i> -glycero-3-phosphocholine
POPE	1-palmitoyl-2-oleoyl- <i>sn</i> -glycero-3-phosphoethanolamine
POPG	1-palmitoyl-2-oleoyl- <i>sn</i> -glycero-3-phospho-(1'- <i>rac</i> -glycerol)
ppm	Part per million
PxB	Polymyxin B
PxBN	Polymyxin B nonapeptide
py	Pyrene
s	Seconds
TES	Triethylsilane
TEM	Transmission electron microscopy
TFA	Trifluoroacetic acid
TIS	Triisopropylsilane
TMA-DPH	<i>N,N,N</i> -trimethyl-4-(6-phenyl-1,3,5-hexatrien-1-yl)phenylammonium <i>p</i> -toluenesulfonate
TSA	Tryptone soya agar
TSB	Tryptone soya broth
UV	Ultraviolet
wt	Wild type

Appendix 1: Structure and 3- and 1- letter codes of the common amino acid residues.

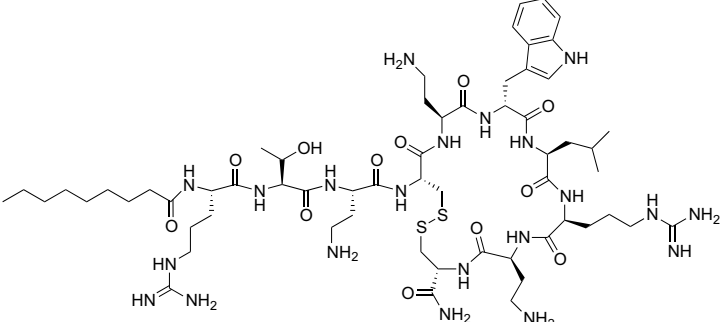
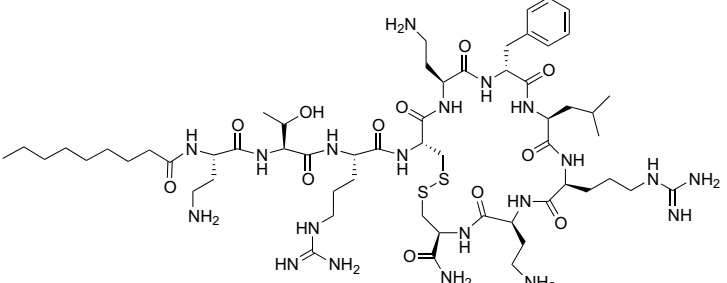
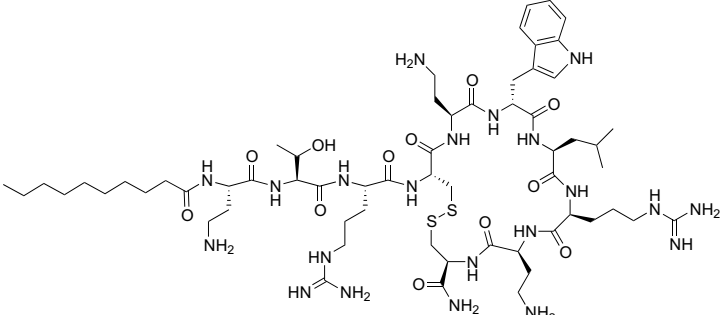
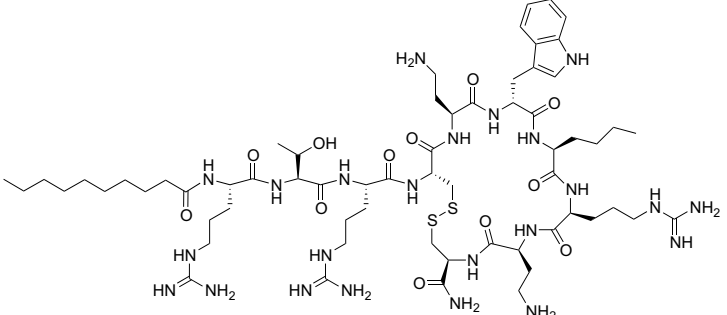
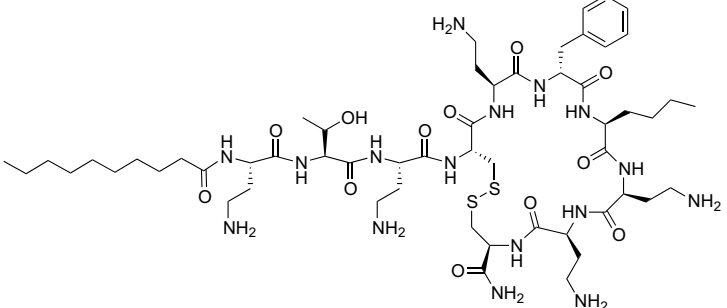
AMINO ACID	STRUCTURE	AMINO ACID	STRUCTURE
Arginine Arg R		Glycine Gly G	
Histidine His H		Proline Pro P	
Lysine Lys K		Alanine Ala A	
Aspartic Acid Asp D		Valine Val V	
Glutamic Acid Glu E		Isoleucine Ile I	
Serine Ser S		Leucine Leu L	
Threonine Thr T		Methionine Met M	
Asparagine Asn N		Phenylalanine Phe F	
Glutamine Gln Q		Tyrosine Tyr Y	
Cysteine Cys C		Tryptophan Trp W	

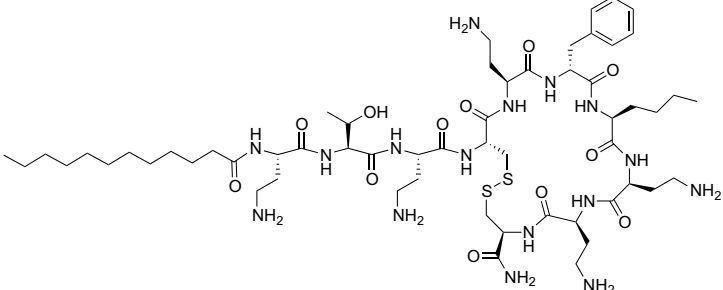
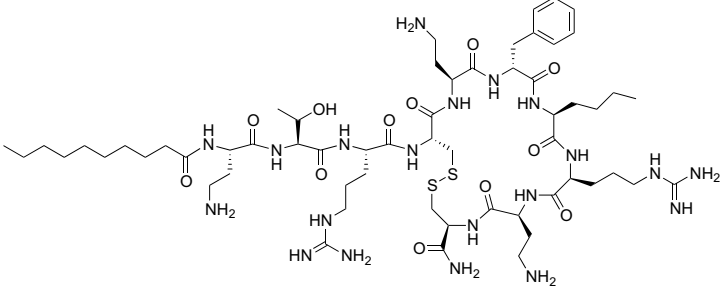
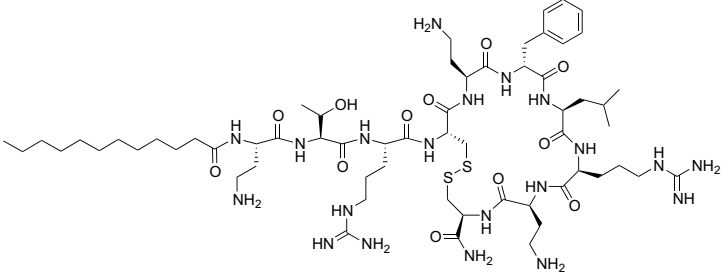
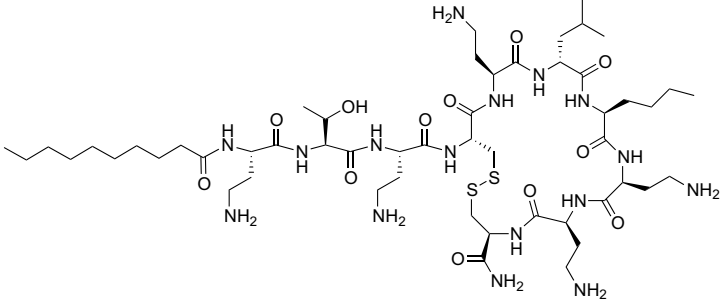
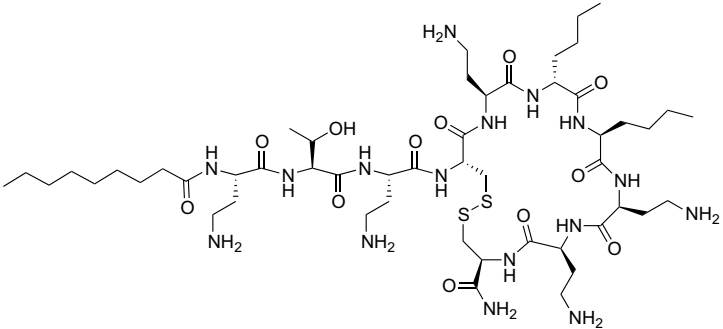
Appendix 2: Structure and three-letter code of the special amino acid residues used in this thesis.

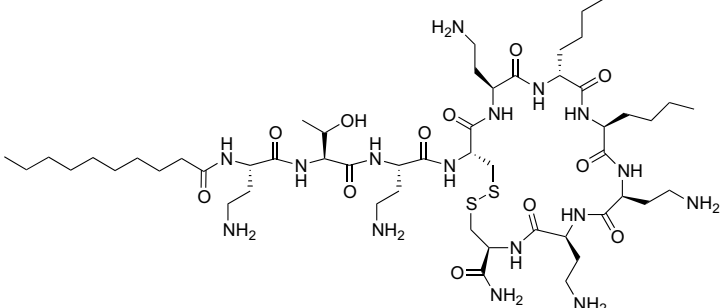
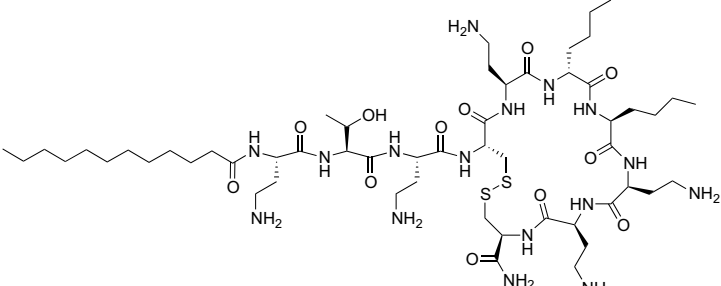
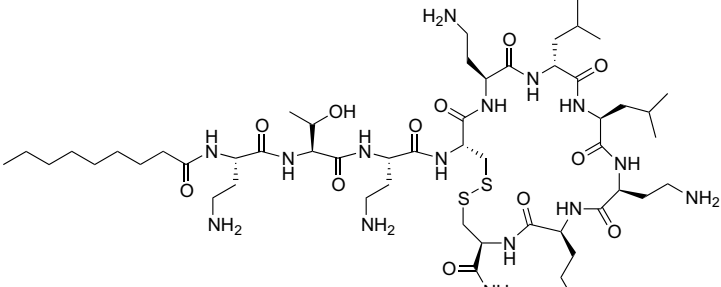
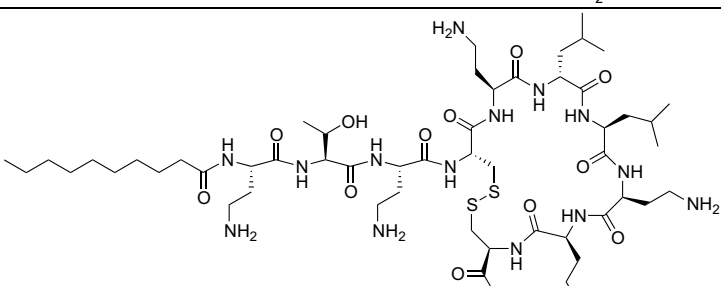
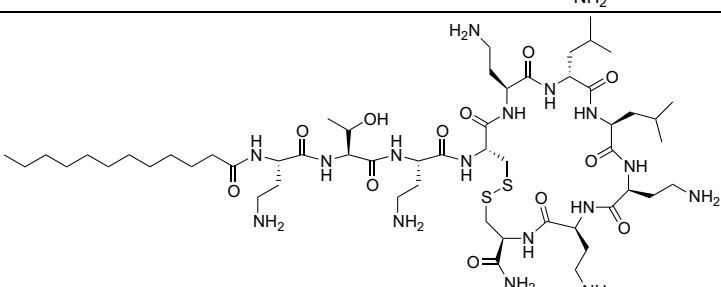
AMINO ACID	STRUCTURE
Diaminobutyric acid Dab	
Ornithine Orn	
Norleucine Nle	

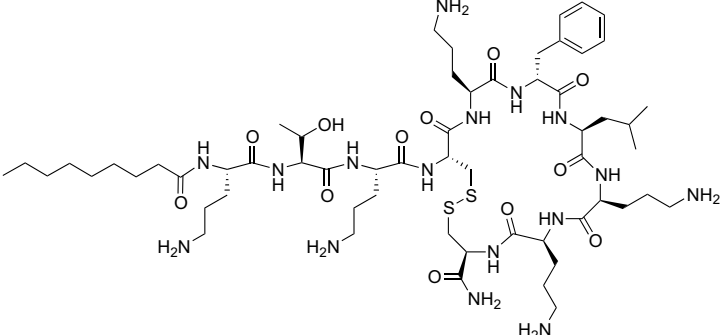
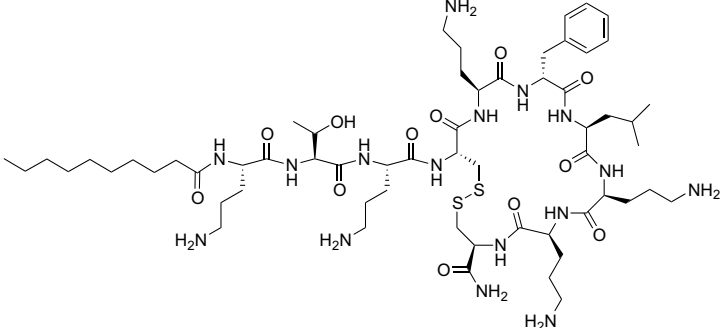
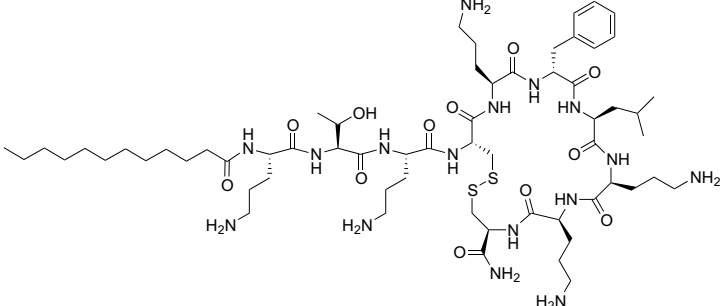
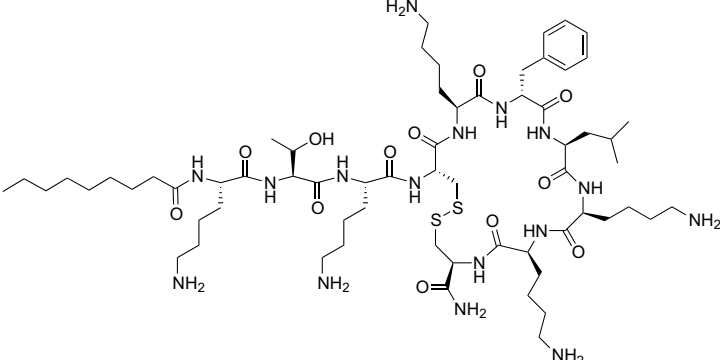
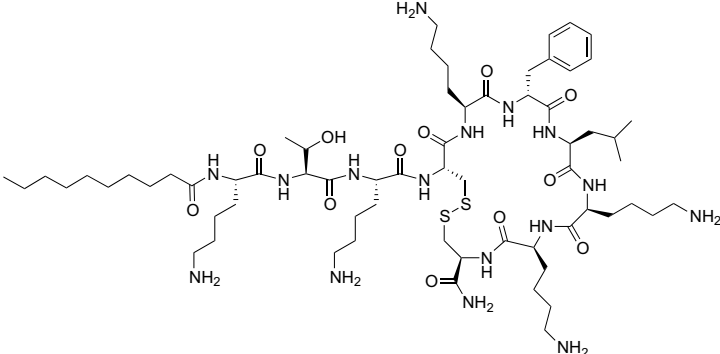
Appendix 3: Sequence and structure of the synthetic polymyxin analogues used in this thesis. The amino acid residues are in three-letter code, D-amino acids are denoted in *italics* and underlined residues denote bond formation.

Peptide	Sequence	Structure
1	nonanoyl-Arg-Thr-Dab- <u>Cys</u> -Dab- <i>Phe</i> -Leu-Arg-Dab- <u>Cys</u>	
2	decanoyl-Arg-Thr-Dab- <u>Cys</u> -Dab- <i>Phe</i> -Leu-Arg-Dab- <u>Cys</u>	
3	dodecanoyl-Arg-Thr-Dab- <u>Cys</u> -Dab- <i>Phe</i> -Leu-Arg-Dab- <u>Cys</u>	

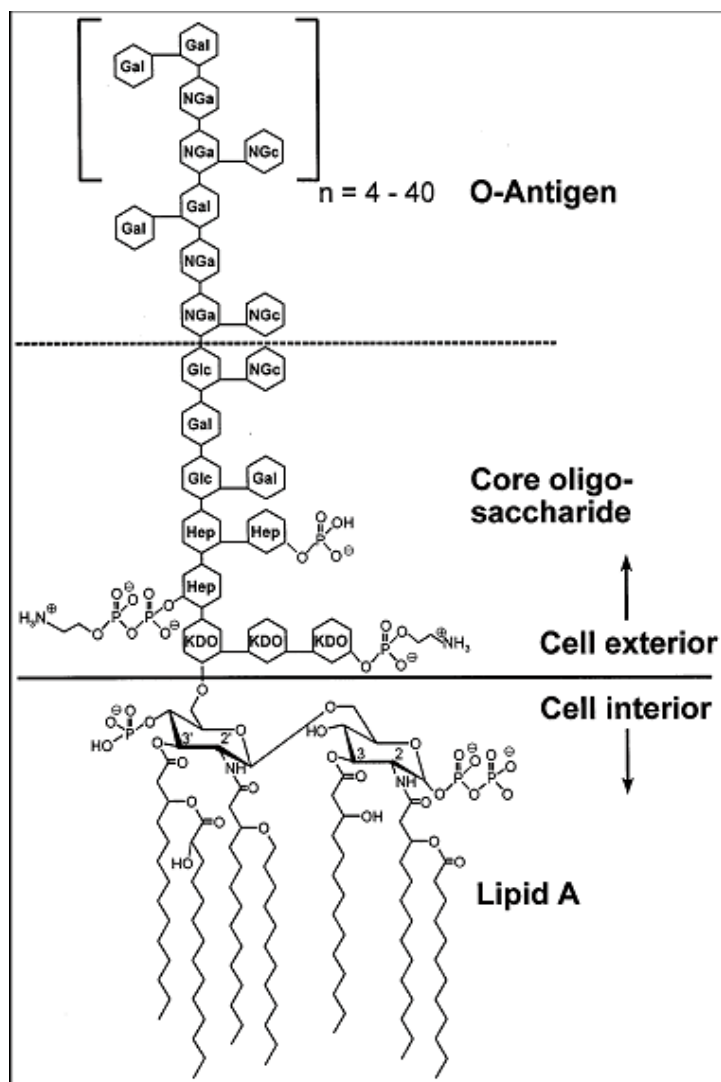
4	<p>nonanoyl-Arg-Thr-Dab- <u>Cys</u>-Dab-Trp-Leu-Arg- Dab-<u>Cys</u></p>	 <p>The structure shows a nonanoyl chain (9 carbons) attached to an Arginine residue. The peptide backbone continues with Threonine, Dab, Cysteine (forming a disulfide bridge with another Cysteine), Dab, Tryptophan, Leucine, Arginine, Dab, and another Cysteine. Various side chains are shown, including guanidino groups, hydroxyl groups, and an indole ring.</p>
5	<p>nonanoyl-Dab-Thr-Arg- <u>Cys</u>-Dab-Phe-Leu-Arg- Dab-<u>Cys</u></p>	 <p>The structure shows a nonanoyl chain (9 carbons) attached to a Dab residue. The peptide backbone continues with Threonine, Arginine, Cysteine (forming a disulfide bridge with another Cysteine), Dab, Phenylalanine, Leucine, Arginine, Dab, and another Cysteine. Side chains include guanidino groups, hydroxyl groups, and a phenyl ring.</p>
6	<p>decanoyl-Dab-Thr-Arg- <u>Cys</u>-Dab-Trp-Leu-Arg- Dab-<u>Cys</u></p>	 <p>The structure shows a decanoyl chain (10 carbons) attached to a Dab residue. The peptide backbone continues with Threonine, Arginine, Cysteine (forming a disulfide bridge with another Cysteine), Dab, Tryptophan, Leucine, Arginine, Dab, and another Cysteine. Side chains include guanidino groups, hydroxyl groups, and an indole ring.</p>
7	<p>decanoyl-Arg-Thr-Arg- <u>Cys</u>-Dab-Trp-Nle-Arg- Dab-<u>Cys</u></p>	 <p>The structure shows a decanoyl chain (10 carbons) attached to an Arginine residue. The peptide backbone continues with Threonine, Arginine, Cysteine (forming a disulfide bridge with another Cysteine), Dab, Tryptophan, Nle, Arginine, Dab, and another Cysteine. Side chains include guanidino groups, hydroxyl groups, and an indole ring.</p>
8	<p>decanoyl-Dab-Thr-Dab- <u>Cys</u>-Dab-Phe-Nle-Dab- Dab-<u>Cys</u></p>	 <p>The structure shows a decanoyl chain (10 carbons) attached to a Dab residue. The peptide backbone continues with Threonine, Dab, Cysteine (forming a disulfide bridge with another Cysteine), Dab, Phenylalanine, Nle, Dab, Dab, and another Cysteine. Side chains include guanidino groups, hydroxyl groups, and a phenyl ring.</p>

<p>9</p>	<p>dodecanoyl-Dab-Thr-Dab- <u>Cys</u>-Dab-Phe-Nle-Dab- Dab-<u>Cys</u></p>	 <p>The structure shows a dodecanoyl chain (12 carbons) attached to a Dab residue. This is followed by a Thr residue, another Dab residue, a Cys residue, a Dab residue, a Phe residue, an Nle residue, another Dab residue, and a final Cys residue. The Cys residues are linked by a disulfide bridge (S-S).</p>
<p>10</p>	<p>decanoyl-Dab-Thr-Arg- <u>Cys</u>-Dab-Phe-Nle-Arg- Dab-<u>Cys</u></p>	 <p>The structure shows a decanoyl chain (10 carbons) attached to a Dab residue. This is followed by a Thr residue, an Arg residue, a Cys residue, a Dab residue, a Phe residue, an Nle residue, an Arg residue, and a final Cys residue. The Cys residues are linked by a disulfide bridge (S-S).</p>
<p>11</p>	<p>dodecanoyl-Dab-Thr-Arg- <u>Cys</u>-Dab-Phe-Leu-Arg- Dab-<u>Cys</u></p>	 <p>The structure shows a dodecanoyl chain (12 carbons) attached to a Dab residue. This is followed by a Thr residue, an Arg residue, a Cys residue, a Dab residue, a Phe residue, a Leu residue, an Arg residue, and a final Cys residue. The Cys residues are linked by a disulfide bridge (S-S).</p>
<p>12</p>	<p>decanoyl-Dab-Thr-Dab- <u>Cys</u>-Dab-Leu-Nle-Dab- Dab-<u>Cys</u></p>	 <p>The structure shows a decanoyl chain (10 carbons) attached to a Dab residue. This is followed by a Thr residue, another Dab residue, a Cys residue, a Dab residue, a Leu residue, an Nle residue, another Dab residue, and a final Cys residue. The Cys residues are linked by a disulfide bridge (S-S).</p>
<p>13</p>	<p>nonanoyl-Dab-Thr-Dab- <u>Cys</u>-Dab-Nle-Nle-Dab- Dab-<u>Cys</u></p>	 <p>The structure shows a nonanoyl chain (9 carbons) attached to a Dab residue. This is followed by a Thr residue, another Dab residue, a Cys residue, a Dab residue, two Nle residues, another Dab residue, and a final Cys residue. The Cys residues are linked by a disulfide bridge (S-S).</p>

<p>14</p>	<p>decanoyl-Dab-Thr-Dab- <u>Cys</u>-Dab-Nle-Nle-Dab- Dab-<u>Cys</u></p>	 <p>The structure shows a decanoyl chain (10 carbons) attached to a Dab residue. This is followed by a Thr residue, a Dab residue, a Cys residue, another Dab residue, two Nle residues, another Dab residue, a second Dab residue, and finally a Cys residue. The Cys residues are linked by a disulfide bridge (S-S).</p>
<p>15</p>	<p>dodecanoyl-Dab-Thr-Dab- <u>Cys</u>-Dab-Nle-Nle-Dab- Dab-<u>Cys</u></p>	 <p>The structure is identical to entry 14, but the decanoyl chain is replaced by a dodecanoyl chain (12 carbons).</p>
<p>16</p>	<p>nonanoyl-Dab-Thr-Dab- <u>Cys</u>-Dab-Leu-Leu-Dab- Dab-<u>Cys</u></p>	 <p>The structure shows a nonanoyl chain (9 carbons) attached to a Dab residue. This is followed by a Thr residue, a Dab residue, a Cys residue, another Dab residue, two Leu residues, another Dab residue, a second Dab residue, and finally a Cys residue. The Cys residues are linked by a disulfide bridge (S-S).</p>
<p>17</p>	<p>decanoyl-Dab-Thr-Dab- <u>Cys</u>-Dab-Leu-Leu-Dab- Dab-<u>Cys</u></p>	 <p>The structure shows a decanoyl chain (10 carbons) attached to a Dab residue. This is followed by a Thr residue, a Dab residue, a Cys residue, another Dab residue, two Leu residues, another Dab residue, a second Dab residue, and finally a Cys residue. The Cys residues are linked by a disulfide bridge (S-S).</p>
<p>18</p>	<p>dodecanoyl-Dab-Thr-Dab- <u>Cys</u>-Dab-Leu-Leu-Dab- Dab-<u>Cys</u></p>	 <p>The structure is identical to entry 17, but the decanoyl chain is replaced by a dodecanoyl chain (12 carbons).</p>

<p>19</p>	<p>nonanoyl-Orn-Thr-Orn- <u>Cys</u>-Orn-<u>Phe</u>-Nle-Orn- Orn-<u>Cys</u></p>	
<p>20</p>	<p>decanoyl-Orn-Thr-Orn- <u>Cys</u>-Orn-<u>Phe</u>-Nle-Orn- Orn-<u>Cys</u></p>	
<p>21</p>	<p>dodecanoyl-Orn-Thr-Orn- <u>Cys</u>-Orn-<u>Phe</u>-Nle-Orn- Orn-<u>Cys</u></p>	
<p>22</p>	<p>nonanoyl-Lys-Thr-Lys- <u>Cys</u>-Lys-<u>Phe</u>-Nle-Lys- Lys-<u>Cys</u></p>	
<p>23</p>	<p>decanoyl-Lys-Thr-Lys- <u>Cys</u>-Lys-<u>Phe</u>-Nle-Lys- Lys-<u>Cys</u></p>	

<p>24</p>	<p>dodecanoyl-Lys-Thr-Lys- <u>Cys-Lys-Phe-Nle-Lys-</u> <u>Lys-Cys</u></p>	
<p>N</p>	<p>nonanoyl-Arg-Thr-Dab- <u>Cys-Dab-Gly-Gly-Arg-</u> <u>Dab-Cys</u></p>	
<p>NN</p>	<p>nonanoyl-Arg-Thr-Dab- Ser-Dab-Phe-Leu-Arg- Dab-Ser</p>	
<p>8N</p>	<p>Thr-Dab-Cys-Dab-Phe- Nle-Dab-Dab-Cys</p>	



Appendix 4: Chemical structure of LPS from *E. coli*. It is situated in the external monolayer of the OM and is formed by three covalently joined parts: (i) the proximal region which is strongly anchored in the membrane, is the hydrophobic region constituted by a polar lipid of unusual structure, the lipid A, also known as endotoxin, which can trigger fever, diarrhea, erythrocyte lysis and potentially lethal anaphylactic shock; (ii) the distal region, also known as hydrophilic region or antigen-O, formed by different polysaccharides that unfold as filaments from the surface of the membrane, (iii) the oligosaccharide core, it is localized in the surface of the membrane connecting the two other regions and is the responsible of the majority of the serological properties of LPS. (Hep) L-glycerol-D-manno-heptose; (Gal) galactose; (Glc) glucose; (KDO) 2-keto-3-deoxyoctonic acid; (NGa) N-acetyl-galactosamine; (NGc) N-acetyl-glucosamine. From: (Magalhães et al., 2007).

Appendix 5: Structure of the headgroups of the lipids used in this thesis (R = acyl chain).

LIPID HEADGROUPS	STRUCTURE
Phosphatidylcholine PC	
Phosphatidylethanolamine PE	
Phosphatidylglycerol PG	

Appendix 6: Structure of the lipids used in this thesis (the X depends on the headgroup used, shown in the previous table).

LIPIDS	STRUCTURE
DEPx Px(22:1(13Z)/22:1(13Z))	
DOPx Px(18:1(9Z)/18:1(9Z))	
POPx Px(16:0/18:1(9Z))	
DMPx Px(14:0/14:0)	
DMoPx Px(14:1(9Z)/14:1(9Z))	
Lyso-MPx Px(14:0/0:0)	
DLPx Px(12:0/12:0)	

INDEX

1. INTRODUCTION	1
1.1. Bacterial resistance and the antibiotic crisis	3
1.2. Antimicrobial peptides	4
1.2.1. Mechanism of action of AMPs	4
1.2.2. Antimicrobial peptides used in this thesis	8
1.2.2.1. Polymyxins	8
1.2.2.2. Peptidyl-glycine-leucine-carboxamide (PGLa) and its derivative MSI-103	9
2. OBJECTIVES	11
3. SECTION A – POLYMYXIN ANALOGUES	15
A.1. ANALOGUE DESIGN AND SYNTHESIS	17
A.1.1. Overview of polymyxin synthetic analogues.....	17
A.1.2. Design of novel polymyxin synthetic analogues	22
A.1.3. Chemical synthesis of the polymyxin analogues.....	25
A.2. <i>IN-VITRO</i> ANTIBACTERIAL ACTIVITY DETERMINATION	28
A.2.1. Bacterial ATCC strains	28
A.2.2. Resistant and multidrug-resistant strains	37
A.3. STUDY OF THE MECHANISM OF ACTION	41
A.3.1. Biological membranes	41
A.3.2. Biophysical study.....	43
A.3.2.1. Monolayers as model membranes, a tool to study peptide-lipid interactions	43
A.3.2.2. Liposomes as model membranes, a tool to study peptide-lipid interactions	45
A.3.2.3. Biophysical study of the polymyxin analogues.....	50
A.3.2.3.1. Determination of peptide binding to LPS	51
A.3.2.3.2. Aggregation of vesicles induced by peptide interaction	54
A.3.2.3.3. Lipid mixing between vesicles due to peptide interaction	55
A.3.2.3.4. Permeabilization of the lipid membrane induced by peptide interaction.....	58
A.3.2.3.5. Determination of the fluidity of the membrane by fluorescence polarization	59
A.3.2.3.6. Tryptophan fluorescence measurements:.....	64
A.3.2.3.6.1. Modification of the emission spectra of tryptophan due to peptide binding	65
A.3.2.3.6.2. Tryptophan fluorescence anisotropy to determine peptide binding.....	67
A.3.2.3.6.3. Quenching of tryptophan fluorescence by acrylamide to determine peptide insertion	69
A.3.2.3.6.4. Fluorescence resonance energy transfer to determine peptide binding	71
A.3.3. Flow cytometry as a tool to determine the effect of the novel polymyxin analogues on bacteria	74

A.3.3.1. Fundamentals of flow cytometry.....	74
A.3.3.2. Results from FC experiments for the novel polymyxin analogues.....	76
A.3.4. Transmission electron microscopy as a tool to determine the effect of the novel polymyxin analogues on bacteria.....	81
A.4. DISCUSSION SECTION A – New broad-spectrum, cyclic antibacterial lipopeptides with high activity	85
4. SECTION B – MSI-103 ANALOGUES.....	89
B.1. DESIGN AND SYNTHESIS OF MSI-103 ANALOGUES TO STUDY THE EFFECT OF LENGTH ON ACTIVITY	91
B.1.1. Design of MSI-103 analogues.....	91
B.1.2. Chemical synthesis of MSI-103 analogues.....	93
B.2. <i>IN-VITRO</i> ANTIBACTERIAL AND HAEMOLYTIC ACTIVITY DETERMINATION.....	94
B.2.1. Antibacterial activity.....	94
B.2.2. Haemolytic activity	95
B.3. STUDY OF THE MECHANISM OF ACTION – Investigation of the pore formation hypothesis.....	97
B.3.1. Circular dichroism spectroscopy.....	97
B.3.1.1. Fundamentals of circular dichroism spectroscopy	97
B.3.1.2. Results from CD experiments for KIA peptides	98
B.3.2. Biophysics experiments – Vesicle leakage	100
B.3.3. Solid-state nuclear magnetic resonance spectroscopy	103
B.3.3.1. Fundamentals of NMR spectroscopy	103
B.3.3.2. Single-pulse experiment	105
B.3.3.3. Spin interactions	105
B.3.3.3.1. Chemical shielding.....	106
B.3.3.4. ³¹ P-ssNMR as a tool to study phospholipids	108
B.3.3.5. ¹⁵ N-ssNMR as a tool to study peptide orientation in lipid membranes	109
B.3.3.6. ³¹ P- and ¹⁵ N-ssNMR to study the orientation of the KIA peptides in lipid membranes.....	110
B.4. DISCUSSION SECTION B – Length dependent activity of α-helical amphipathic membrane bound peptides.....	118
5. CONCLUSIONS	121
6. EXPERIMENTAL PART.....	125
6.1. MATERIALS AND METHODS.....	127
6.1.1. SECTION A.....	127
6.1.1.1. Chemical synthesis of the polymyxin analogues	127
6.1.1.1.1. Solvents.....	127
6.1.1.1.2. Reagents.....	127
6.1.1.1.3. Instruments.....	128
6.1.1.1.4. Methods	128
6.1.1.1.4.1. Qualitative ninhydrin assay.....	128

6.1.1.1.4.2. Hydrolysis and amino acid analysis..	129
6.1.1.1.4.3. SPPS.....	129
6.1.1.1.4.4. Cleavage, deprotection and cyclization of the lipopeptides.....	130
6.1.1.1.4.5. RP-HPLC	131
6.1.1.1.4.6. Mass spectrometry MALDI-TOF	131
6.1.1.2. Evaluation of the biological activity, minimum inhibitory concentration determination.....	131
6.1.1.2.1. Material used.....	131
6.1.1.2.2. Methods	132
6.1.1.3. Study of the mechanism of action	133
6.1.1.3.1. Solvents.....	133
6.1.1.3.2. Reagents.....	133
6.1.1.3.3. Instruments.....	134
6.1.1.3.4. Methods	135
6.1.1.3.4.1. Preparation of liposomes.....	135
6.1.1.3.4.2. Kinetics of insertion into monolayers of LPS.....	135
6.1.1.3.4.3. Dansyl-PxB binding and displacement assay	135
6.1.1.3.4.4. Aggregation of liposomes measured as light scattering at 90°.....	136
6.1.1.3.4.5. Fluorescence assay for lipid mixing .	136
6.1.1.3.4.6. ANTS/DPX fusion assay for leakage or mixing of aqueous compartments	136
6.1.1.3.4.7. Polarization	136
6.1.1.3.4.8. Modification of the emission spectra of tryptophan	137
6.1.1.3.4.9. Tryptophan fluorescence anisotropy.	137
6.1.1.3.4.10. Quenching of tryptophan fluorescence by acrylamide.....	137
6.1.1.3.4.11. Fluorescence resonance energy transfer	137
6.1.1.3.4.12. Flow cytometry	138
6.1.1.3.4.13. Transmission electron microscopy .	138
6.1.2. SECTION B.....	139
6.1.2.1. Chemical synthesis of the MSI-103 analogues	139
6.1.2.1.1. Solvents.....	139
6.1.2.1.2. Reagents.....	139
6.1.2.1.3. Instrument	139
6.1.2.1.4. Methods	140
6.1.2.1.4.1. SPPS.....	140
6.1.2.1.4.2. Cleavage and deprotection of the peptides	140

6.1.2.1.4.2. RP-HPLC	140
6.1.2.2. Evaluation of the biological activity, antibacterial and haemolytic activity determination	141
6.1.2.2.1. Material used.....	141
6.1.2.2.2. Methods	141
6.1.2.2.2.1. MIC assay	141
6.1.2.2.2.2. Haemolysis assay	141
6.1.2.3. Study of the mechanism of action	142
6.1.2.3.1. Solvents.....	142
6.1.2.3.2. Reagents.....	142
6.1.2.3.3. Instruments.....	142
6.1.2.3.4. Methods	143
6.1.2.3.4.1. Circular dichroism spectroscopy.....	143
6.1.2.3.4.2. Vesicle leakage assay.....	143
6.1.2.3.4.3. Solid-state NMR	144
6.2. EXPERIMENTAL <u>SECTION A</u>	145
6.3. EXPERIMENTAL <u>SECTION B</u>	149
7. SUMMARY OF THE THESIS IN CATALAN	151
8. REFERENCES	181

1. INTRODUCTION

1.1. Bacterial resistance and the antibiotic crisis

The global emergence and spread of multidrug-resistant bacteria (defined as resistant to three or more antibacterial drug classes) is an important clinical problem. Some factors that have contributed to the development of bacterial resistance include inappropriate use of antibiotics, such as the overuse of powerful, broad-spectrum antibiotics, the presence of antibiotics in the food/livestock industry and the inclusion of antimicrobials in household products (Aiello & Larson, 2003; Arnold, 2007). The World Health Organization recognizes antimicrobial resistance as one of the three greatest threats to human health (Fauci, 2001). However, the antimicrobial pipeline remains unacceptably lean, in fact, the ESKAPE pathogens (*Enterococcus faecium*, *Staphylococcus aureus*, *Klebsiella pneumoniae*, *Acinetobacter baumannii*, *Pseudomonas aeruginosa* and *Enterobacter* species) have outpaced the drug discovery process (Boucher et al., 2009; Rice, 2008). The number of antimicrobial agents approved by the United States Food and Drug Administration (FDA) and the European Medicines Agency (EMA) has sharply decreased over the last 25 years (Figure 1). This has left few treatment options for the most stubborn forms of methicillin-resistant *Staphylococcus aureus*. The picture is even bleaker for infections caused by Gram-negative bacteria, which are occasionally resistant to all the antibiotics now in the market. All these facts have made it necessary to launch different initiatives and efforts towards discovering new, safe and effective antimicrobials in the next decade (Theuretzbacher, 2012). All this work is beginning to crystallize: 22 new antibiotics have been launched since 2000 and approximately 60 compounds are currently in active clinical development (Butler, et al., 2013).

In this context, there is now renewed interest in the search for drugs that have more than one target on the bacterial cell, rather than a specific chiral receptor or enzyme, with a focus on modes of therapy with mechanisms less likely to promote resistance. Antimicrobial peptides are a class of antibiotics that have attracted great interest in the last few years because they rarely spur the development of resistant organisms. They are a diverse group of molecules that share a few common features, the most important is that their main target is the lipid bilayer itself, and in consequence to develop genetic resistance is very costly for bacteria.

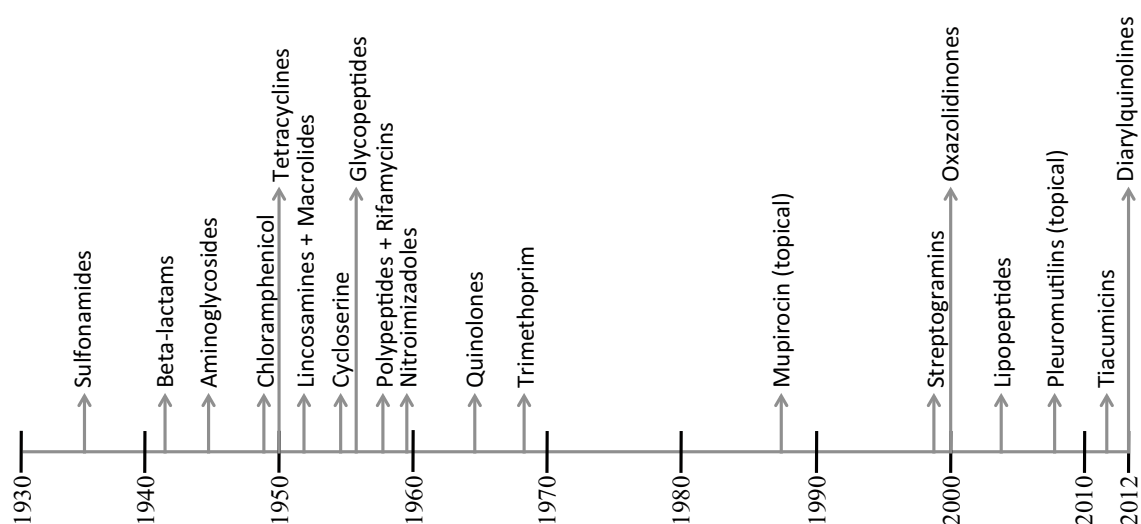


Figure 1: Between 1935 and 1968, 14 classes of antibiotics (with novel mechanisms of action) were introduced for human use; since then only 7 new classes have been described, including Tiacumicins in 2011 (approved antibiotic Fidaxomicin) and Diarylquinolones in 2012 (approved antibiotic Bedaquiline).

1.2. Antimicrobial peptides

Antimicrobial peptides are natural weapons produced by a variety of organisms, from single-celled microbes to vertebrates (Zasloff, 2002). To date more than 2000 have been identified in nature and they are listed in the Antimicrobial Peptide Database (<http://aps.unmc.edu/AP/main.php>). They are very diverse in their sequences, length (generally short) and structures (some of them are linear while others are cyclic sometimes due to disulphide bridges, with a variety of secondary structures) but they all seem to adopt an amphipathic conformation with opposing hydrophobic and polar charged faces that allows them to interact and disrupt selectively negatively charged microbial membranes. They can be classified as follows (Brogden, 2005):

- **Anionic peptides**, such as daptomycin and the amphibian peptide Maximin-H5.
- **Linear cationic α -helical peptides**, as for example magainin 2 and cecropins.
- **Anionic and cationic peptides enriched for specific amino acids**, like tryptophan-rich indolicin from cattle and Dab-rich polymyxins.
- **Peptides that contain cysteine and form disulphide bonds**, such as defensins and protegrins.
- **Peptide fragments of larger proteins**, as for example lactoferricin from lactoferrin.

Multiple studies have shown that AMPs have very good activities (in the micromolar range), and broad spectrum of activity against a range of bacteria, fungi, enveloped viruses and parasites (Brown & Hancock, 2006) and represent a promising novel class of antibiotics. Traditionally, the search for novel AMPs involved the identification of active peptides from natural sources followed by the design of synthetic peptide analogues, but nowadays design is accompanied by structure-function studies, or *de novo* design that includes high-throughput combinatorial library screening, structure-based modelling, predictive algorithms and the introduction of non-coded modifications to conventional peptide chemistry (Fjell, et al., 2012). Some AMPs have even been discovered through sequence searches within large proteins (such as lactoferricin or haemoglobin). Some examples of AMPs introduced in the market or in advanced stages of development can be found in Table 1 (Butler et al., 2013; Fjell et al., 2012; Hancock & Sahl, 2006).

1.2.1. Mechanism of action of AMPs

Although the mode of action of antimicrobial peptides involves disrupting the integrity of the bacterial membrane in different ways, new evidence points to intracellular targets, including DNA and protein synthesis, protein folding, enzymatic activity and cell wall synthesis. In any case, membrane interactions are important even for intracellular-targeting peptides, because they must translocate through the lipid membrane. Diverse studies have indicated that the interaction of AMPs with the bacterial membranes is specifically based on their structural properties. It is thus their sequence, size, cationic nature, hydrophobicity and amphipathicity that govern their interaction with target cells (Nguyen, et al., 2011; Yeaman, 2003).

According to the Shai-Matsuzaki-Huang model (Huang, 2000; Matsuzaki, 1999; Shai, 1999), unstructured peptides in solution adopt a three-dimensional structure when interacting with the bacterial membrane and fold into amphiphilic molecules, with

Table 1: Representative antimicrobial peptides in different stages of the drug-discovery process (M = Market).

Name	Description	Activity	Phase	Mode of action
Polymyxin B	10-amino acid lipopeptide	Antibacterial Gram-	M	Membrane
Colistin (Polymyxin E)	10-amino acid lipopeptide	Antibacterial Gram-	M	Membrane
Nisin	34-amino acid polycyclic peptide	Antibacterial Gram+	M	Membrane
Daptomycin	13-amino acid lipopeptide	Antibacterial Gram+	M	Membrane
Telavancin	Lipoglycopeptide	Antibacterial Gram+	M	Cell wall inhibition
PGLa	21-amino acid peptide	Broad-spectrum antibacterial	M	Membrane
Dalbavancin	Lipoglycopeptide	Antibacterial Gram+	III	Cell wall inhibition
Surotomycin	11-amino acid lipopeptide	Antibacterial Gram+	III	Membrane
Oritavancin	Lipoglycopeptide	Antibacterial Gram+	III	Cell wall inhibition
LL-37	37-amino acid peptide (human cathelicidin)	Broad-spectrum antibacterial	II	Membrane
LTX-109	3-amino acid peptide, synthetic antimicrobial peptidomimetic (SAMP)	Broad-spectrum antibacterial	II	Membrane
IMX942	13-amino acid peptide	Broad-spectrum	I	Immunomodulation
POL7080	14-amino acid peptide, synthetic antimicrobial peptidomimetic (SAMP)	Antibacterial Gram- (especially <i>P.aeruginosa</i>)	I	Target the β -barrel protein LptD, involved in outer-membrane biogenesis of LPS
HB1345	6-amino acid lipopeptide	Broad-spectrum antibacterial	Pre-clinical	Immunomodulation
NAB739	9-amino acid PxB analogue	Antibacterial Gram-	Early pre-clinical	Membrane

positively charged side chains directly interacting with the anionic lipid headgroups of the bacterial membrane. The lipids are then displaced by the peptides, causing a thinning of the outer leaflet of the bacterial membrane. Right after this, the peptides aggregate and form a channel that allows for peptide translocation into the interior of the target cell (Figure 2). At this point, there are three different models that have been proposed to explain the method of pore formation: the carpet model, the barrel-stave model and the toroidal pore (wormhole) model (Brogden, 2005; Hancock, et al., 2006; Zasloff, 2002):

- **The carpet model** describes the disruption of the membrane at high local peptide concentrations (Shai, 1999). The presence of negatively charged lipids is important for a peptide carpet to form, as they help to reduce the repulsive electrostatic forces between positively charged peptides. High local peptide concentrations can be achieved, when cationic peptides phase-separate into domains rich in acidic phospholipids (Bechinger, 1999). This mechanism is used to describe the mode of action of dermaseptins.
- **The barrel-stave** or transmembrane helical bundle is the classical picture to explain the formation of pores. Above a threshold concentration peptides aggregate and align to an inserted state (Matsuzaki, 1999; Shai, 1999). Discrete openings are proposed to form, with the hydrophobic face of the peptide interacting with the non-polar lipid acyl chains and the hydrophilic face of the peptide forming the interior of the pore (Toke, 2005). This mechanism is observed predominantly for peptides where not too many cationic residues will accumulate in the highly restricted volume of the pore interior (Bechinger, 1999; Bechinger & Lohner, 2006). Alamethicin is assumed to form this type of pore (Yang, et al., 2001).
- **The wormhole** or **toroidal pore model** is an extension of the transmembrane helical bundle. To relieve the bilayer from unfavourable stress induced by the accumulation of peptide molecules in the outer leaflet, the layers bend continuously from one membrane leaflet to the other like the inside of a doughnut (Toke, 2005). Peptides translocate stochastically to the inner leaflet (Matsuzaki, 1999; Matsuzaki, et al., 1995b). Negatively charged phospholipid head groups together with positively charged peptides line the wall of the pore to reduce repulsive interactions due to the high positive charge density of the peptides (Bechinger & Lohner, 2006; Matsuzaki, et al., 1996). Such a pore structure was first proposed for melittin and magainin (Yang et al., 2001) upon the observation that magainin induces rapid lipid flip-flop coupled with pore formation (Matsuzaki et al., 1996).

There does not appear to be one model that fits all peptides, with various factors contributing to the process of pore formation. The actual antimicrobial activity in order to kill bacteria resides in part in the disruption of the bacterial cell membrane, which can occur in a number of ways. These include membrane depolarization, permeabilization or creation of pores which could cause cellular contents to leak out, degradation of cell walls, and alteration of the lipid composition in the membrane bilayer which could lead to the disturbance of membrane functions (Straus & Hancock, 2006; Zasloff, 2002).

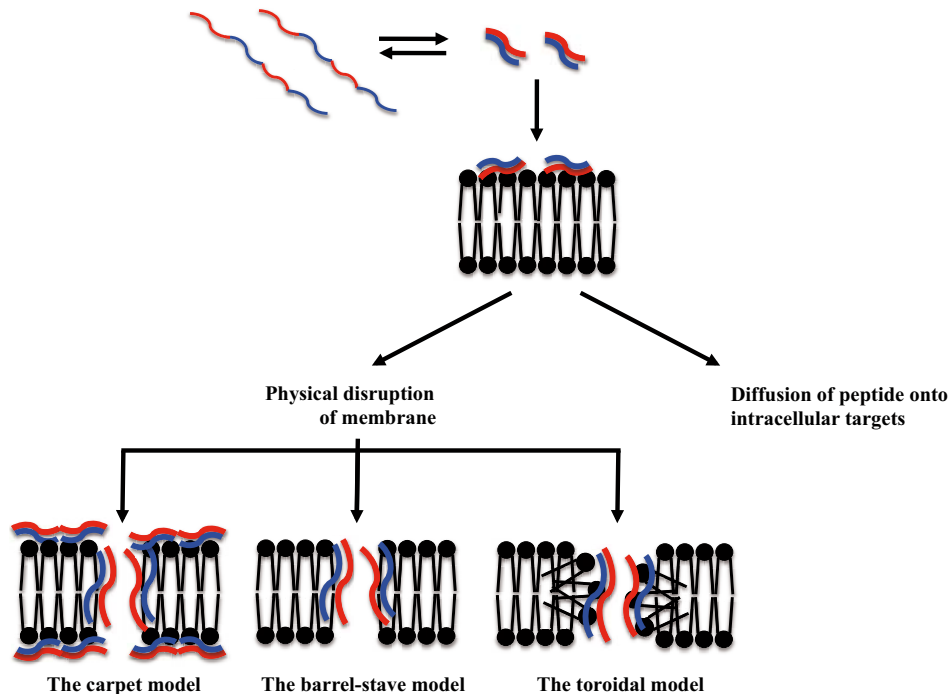


Figure 2: The Shai-Matsuzaki-Huang model describes the activity of AMPs as a stepwise event. First, the AMP binds to the membrane surface. When a threshold concentration is reached, membrane perturbation occurs. Three cooperative permeabilization mechanisms are illustrated. The hydrophilic and hydrophobic regions of the peptide are shown in red and blue respectively.

A variety of techniques have been used to assess the mechanisms of antimicrobial peptide activity. Each method provides a slightly different view of peptide activity and no single technique is capable of adequately determining the mechanism of action of AMPs. Such techniques include:

- Biophysical studies with model membranes: To provide insights into mechanisms of activity and therefore determine the type of damage induced by the peptides, we can study the interaction of AMPs with phospholipids in model membranes (liposomes or monolayers), of single or mixed lipids in order to mimic the different composition of bacterial membranes. The use of fluorescent dyes can also be useful, such as encapsulated dyes to detect the formation of pores or labelled lipids to determine the effect on the bilayer (Nguyen et al., 2011).
- Microscopy: The use of microscopy techniques to visualize the morphological effects of AMPs on microbial cells has helped identify general target sites. Scanning and transmission electron microscopy have been used to demonstrate the ultrastructural damaging effects of antimicrobial peptides (Hartmann et al., 2010). This analysis has shown that different peptides have different effects on microbial cells, indicating that they might have different target sites or mechanisms of activity.
- Circular dichroism or oriented circular dichroism: The orientation and secondary structure of an AMP bound to a lipid bilayer can be measured fast and easily by circular dichroism (Bürck et al., 2008; Greenfield, 2007).
- Flow cytometry: Flow cytometry in conjunction with different dyes can be used to determine the effects of the peptides on bacteria, such as propidium iodide to detect membrane permeability or bis-(1,3-dibutylbarbituric acid) trimethine oxonol [DiBAC₄(3)] to detect depolarization of the membrane (Alvarez-Barrientos, et al., 2000).

- Solid-state NMR spectroscopy: Solid-state NMR measures the secondary structure, orientation and penetration of AMPs into lipid bilayers in the biologically relevant liquid-crystalline state (Bechinger, 1999; Strandberg & Ulrich, 2004). These data help define the interactions of AMPs with bacterial membranes and the effects of peptide and membrane composition on activity (Strandberg et al., 2008; Strandberg, et al., 2012b; Strandberg, et al., 2006).

1.2.2. Antimicrobial peptides used in this thesis

1.2.2.1. Polymyxins

As previously introduced, emergence of bacterial pathogens with acquired resistance to almost all available antibiotics, namely “superbugs”, is a growing medical concern in hospital and healthcare settings. The major challenge is regarding the treatment of multidrug-resistant Gram-negative bacteria, such as *P. aeruginosa* or *A. baumannii*, since very few new antibiotics in the drug development pipeline are active against these strains. Consequently, there has been a resurgence of old antibiotics, such as polymyxins discovered in the 1940s (Ainsworth, et al., 1947), as drugs of last resort for the treatment of infections caused by MDR Gram-negative pathogens, despite their toxicity (nephro- and neurotoxicity) and the lack of clinical efficacy data (Landman, et al., 2008; Pogue, et al., 2011)

Polymyxin B and colistin are two secondary metabolite nonribosomal cyclic lipopeptides produced by the soil bacterium *Bacillus polymyxa*, and are the two polymyxins used clinically. Both are specific and highly potent against Gram-negative bacteria. They share a common primary sequence, with five positive charges due to L- α,γ -diaminobutyric acid (Dab), the only difference being at position 6, which is occupied by D-Phe in PxB and D-Leu in colistin (Figure 3).

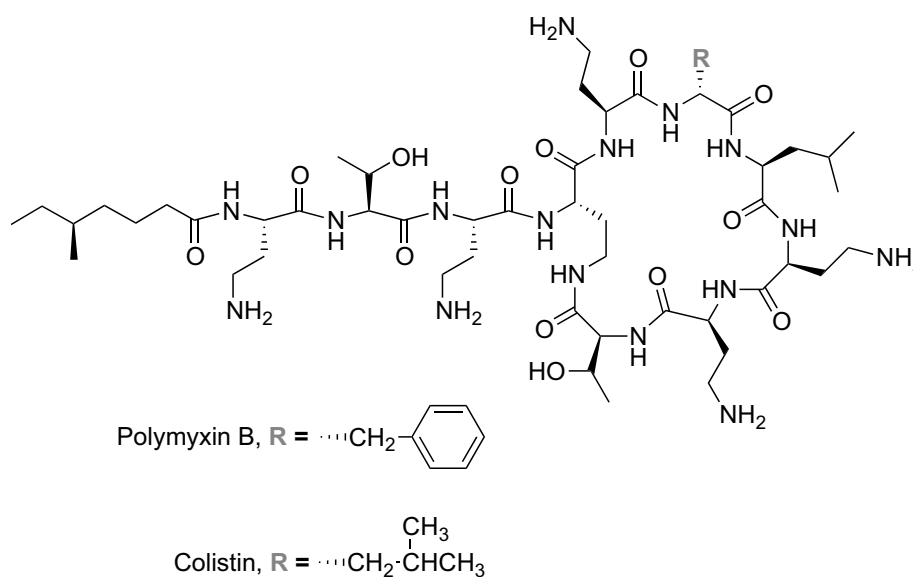


Figure 3: Structure of polymyxin B and colistin, both lipopeptides used in this thesis.

The mechanism of action of polymyxins, and in particular of PxB, has been studied in detail (Velkov, et al., 2010). The initial target is the anionic lipopolysaccharide in the outer membrane of Gram-negative bacteria, resulting in OM permeabilizing action. The

high affinity for LPS binding can be attributed to the polycationic character of PxB together with its amphipathicity, and the polar and hydrophobic domains folding in two distinct faces when binding to the bacterial membrane. LPS binding results in divalent cation displacement, and leads to PxB self-promoted uptake into the periplasmic space (Hancock & Chapple, 1999). This process is necessary but not sufficient for bacterial killing, and subsequent interaction with the cytoplasmic membrane is necessary for antibiotic activity (Hancock & Chapple, 1999; Zhang, et al., 2000). The next step remains unclear at the molecular level, but biophysical studies with model membranes have given insight into the mechanism of bacterial killing by PxB. One possibility involves the insertion of PxB into the cytoplasmic membrane and the disruption of its integrity via membrane thinning or pore formation. However, several reports clearly show that permeabilization or depolarization of the membrane take place only at concentrations of polymyxin well above the minimal inhibitory concentration, and thus other mechanisms of bactericidal action should be considered (Yeaman, 2003).

A more consistent mechanism of action is based on the formation of periplasmic membrane contacts between outer and inner membranes. According to this model, once in the periplasmic space, PxB forms contacts between the two enclosed phospholipid interfaces and promotes a fast exchange of certain phospholipids. The resulting changes in the membrane lipid composition trigger an osmotic imbalance that leads to bacterial stasis and cell death. This phenomena has been proposed as the mechanism of antibacterial action of PxB and several other antibiotic peptides, including cecropins (Oh, et al., 1998a; Oh et al., 2000; 1998b), and has major implications in bacterial resistance, since it would not be susceptible to generate stable genetic resistance. In fact, acquisition of resistance by a sensitive microbial strain against antimicrobial peptides is surprisingly improbable (Zasloff, 2002).

1.2.2.2. Peptidyl-glycine-leucine-carboxamide (PGLa) and its derivative MSI-103

Peptidyl-glycine-leucine-carboxamide (PGLa) is a linear peptide of 21 amino acid residues (GMASKAGAIAGKIAKVALKAL-NH₂) belonging to the magainin family of antimicrobial peptides. It is a highly charged and hydrophobic peptide that in aqueous solution has no well-defined secondary structure, but adopts an amphipathic α -helical structure, upon binding to lipid bilayers (Bechinger 1998; Wieprecht 2000). PGLa was originally found in the skin secretion of the South African clawed frog *Xenopus laevis* (Hoffmann, et al., 1983; Richter, et al., 1985) and it exhibits significant broad-spectrum antibacterial activity while possessing negligible haemolytic activity (Soravia, et al., 1988).

MSI-103, with sequence (KIAGKIA)₃-NH₂, was designed starting from the sequence of PGLa but it was optimized and simplified by using only four different amino acids in a repeated heptamer and increasing the positive charge while keeping the overall amphipathic character of the peptide (Blazyk, 2001; Maloy & Kari, 1995). This designed peptide was found to adopt an α -helical structure in a lipid environment and demonstrated higher antimicrobial activity than PGLa with low haemolytic side effects (Blazyk, 2001; Strandberg et al., 2007) and a higher rate of fusion (Wadhvani, et al., 2012), probably due to the higher positive charge and a stronger propensity of MSI-103 to dimerize and form higher-order oligomers (Figure 4).

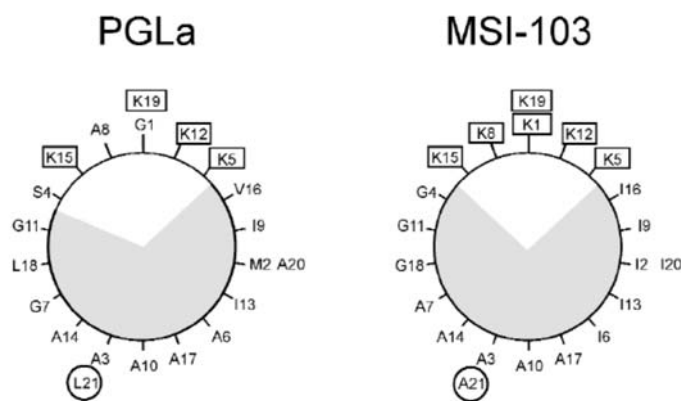


Figure 4: Helical wheel projections of the amphiphilic α -helical peptides PGLa and MSI-103. Charged residues are marked by rectangles, and the C-terminal amino acid by a circle. The hydrophobic sector is shaded.

PGLa was proposed to kill bacteria through formation of transmembrane channels (Soravia et al., 1988). Using ^2H - and ^{19}F - solid-state NMR, the helical PGLa was found to undergo a concentration-dependent realignment at ambient temperature in fluid phase synthetic lipid bilayers consisting of dimyristoylphosphatidylcholine and dimyristoylphosphatidylglycerol at the lipid molar ratio of 3 to 1 (Glaser, et al., 2004; Glaser et al., 2005; Strandberg et al., 2006). Through these experiments, PGLa was shown to reside in a surface alignment (S-state) at low peptide-to-lipid ratios (P/L) of 1/200 or lower and to adopt a tilted alignment (T-state) at high P/L ratios of 1/50 or higher.

In the case of MSI-103, it was also studied using ^2H - and ^{19}F - solid-state NMR in different lipid membranes where, like PGLa, this helical peptide demonstrated a concentration-dependent realignment, adopting an S-state at low concentrations and a T-state at high concentrations (Strandberg et al., 2008). However, this orientation was found to be highly affected by the lipid composition (Strandberg, et al., 2012b). When unsaturated lipids were used, or more generally in bilayers with a negative spontaneous curvature, only the S-state was found, even at high peptide concentration. On the other hand, in saturated lipids, and in the presence of lyso-lipids or more generally in bilayers with a positive spontaneous curvature, the T-state was found at higher peptide concentrations. However, the detailed mechanism of action of MSI-103 has not yet been established, but the helical peptide is proposed to permeabilize bacteria by formation of pores like its parent peptide.

2. OBJECTIVES

The main objectives of this thesis were the following:

- Design and synthesize new lipopeptides based on the structure of polymyxins in order to obtain novel antimicrobial compounds with a broad spectrum of activity, and in particular activity against resistant and multidrug-resistant bacteria. In addition, the design should facilitate the chemical synthesis and future scale-up of production of the analogues.
- Investigate the mechanism of action of the peptides using different techniques, such as biophysical techniques based on fluorescence using liposomes and monolayers as model membranes, and flow cytometry and transmission electron microscopy using bacteria.
- Study the effect of length in the activity (antibacterial and haemolytic) by synthesizing a series of peptides with different length (from 14 to 28 amino acid residues) based on the same repeating units as MSI-103.
- Study the ability of MSI-103 peptides to form pores in a transmembrane orientation like its parent peptide PGLa, by using biophysical techniques such as solid-state NMR, and determine the minimum length needed for the peptides to span the membrane.

3. SECTION A – POLYMYXIN ANALOGUES

A.1. ANALOGUE DESIGN AND SYNTHESIS

A.1.1. Overview of polymyxin synthetic analogues

In view of the excellent antimicrobial activity of natural polymyxins and the relatively low prevalence of resistance, it is understandable the substantial effort made into discovery of polymyxin analogues with improved microbiological, pharmacological, and toxicological profiles (Velkov et al., 2010). An overview of the main modifications and their results is made in the following lines:

1) Modifications on the N-terminal side acyl tripeptide.

The molecular model of the PxB-LPS complex allowed the characterization of the conformation of PxB when bound to the LPS and thus the different interactions of the components of the molecule (Figure 5) (Pristovsek & Kidric, 1999; 2004).

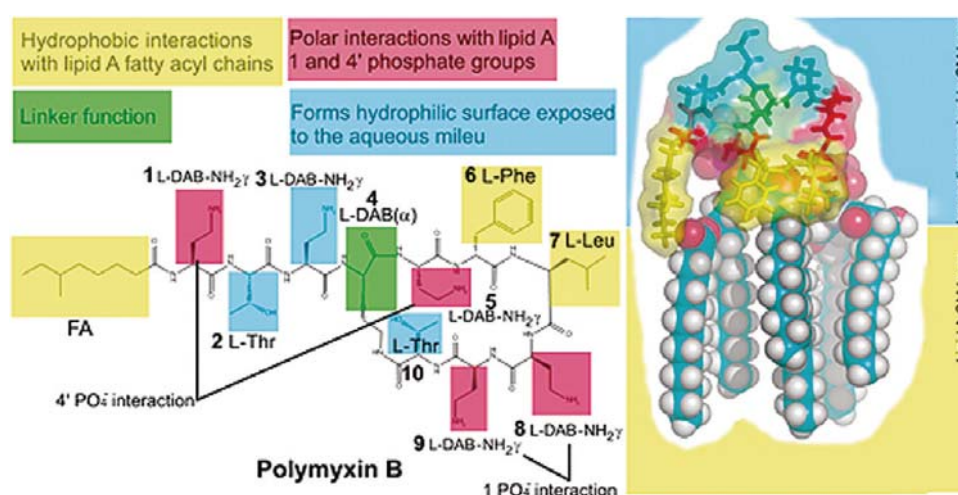


Figure 5: Schematic diagram of the molecular model of the complex PxB-LPS, the key contacts between PxB and the lipid A component of LPS are summarized (FA = fatty acid). From: (Velkov et al., 2010).

It is known that the function of the fatty acid is to penetrate the OM and disrupt the packing of the lipid A fatty acyl chains. In fact, the fatty acid is crucial for the activity of polymyxins as it is the driving force for the complexation with the LPS (Howe et al., 2007; Srimal, et al., 1996).

The importance of the fatty acid was demonstrated with the characterization of polymyxin nonapeptides, polymyxins that lack the N-terminal fatty acyl-Dab¹ segment, retain the capacity to bind to LPS but are devoid of antimicrobial activity (Vaara & Vaara, 1983b). It must be noted that nonapeptides have lower toxicity profiles than the original compounds (Tsubery et al., 2005) and consequently the toxicity of polymyxins can be partially attributed to the N-terminal fatty acid (Vaara et al., 2008). It becomes then evident the number of research groups focused on generating N α -analogues with lower toxicity but good antimicrobial profile.

Analogues with various fatty acids with aliphatic or hydrophobic ring structures have been described, such as ciclohexylbutanoyl or 4-biphenylacetyl, these had a comparable antimicrobial activity to that of PxB but displayed a higher affinity to LPS (Okimura, et al., 2007). Contrarily, a pyrene-substituted analogue synthesized in our group (Clausell, et al., 2006), afterwards tested by the Sakura group, and

Fmoc-N-terminal analogues (Tsubery, et al., 2001) showed no improvement in activity compared to that of PxB. The latest reported analogue of this type, CB-182,804, from Cubist Pharmaceuticals, containing a (2-chlorophenyl)-carbamic acid replacing the fatty acid, demonstrated very high activity against multi-drug resistant Gram-negative pathogens but its development was discontinued after Phase I in 2010 (Quale et al., 2012; Sader, et al., 2010).

The effect of the fatty acyl chain length on antimicrobial activity has been extensively studied (Ohki, et al., 2007; O'Dowd et al., 2007; Visser et al., 2003), but in all cases it was found out that chains of intermediate length are optimal (C7-C9), whereas longer (C14) and smaller (< C7) chained analogues display poor antimicrobial activity.

In conclusion, as seen in the data described in the literature, the antimicrobial activity of polymyxins seems to correlate with the bulkiness and length of the N α -substituents. If we take a look again at the molecular model of the LPS-PxB complex, we can clearly see that very long, bulky or hydrophilic N α substituents sterically hinder the OM insertion.

2) Modifications on the charged residues.

It has always been clear that the positive charges present in the molecule are crucial for its antimicrobial activity, in fact, if we block all the free amino groups we obtain a completely inactive compound (Barnett, et al., 1964). Many reports can be found in the literature of analogues with chemical modifications in the Dab residues (Figure 6), such as acetylation, deamination or reaction with dimethylaminonaphthalene-5-sulfonyl to name a few (Schindler & Teuber, 1975; Srinivasa & Ramachandran, 1978; Teuber, 1974). The majority of the analogues obtained were devoid of antimicrobial activity, however, some examples can be found where modifications in the Dab residues gave place to active molecules (Weinstein, et al, 1998; Witzke & Heding, 1976). In general, those derivatives that contain positively charged or polar substituents display better activity than PxB but in contrast, those analogues with Dab side chains substituted by lipophilic groups, so with reduced cationic character, appear to have an increased activity against Gram-positive bacteria.

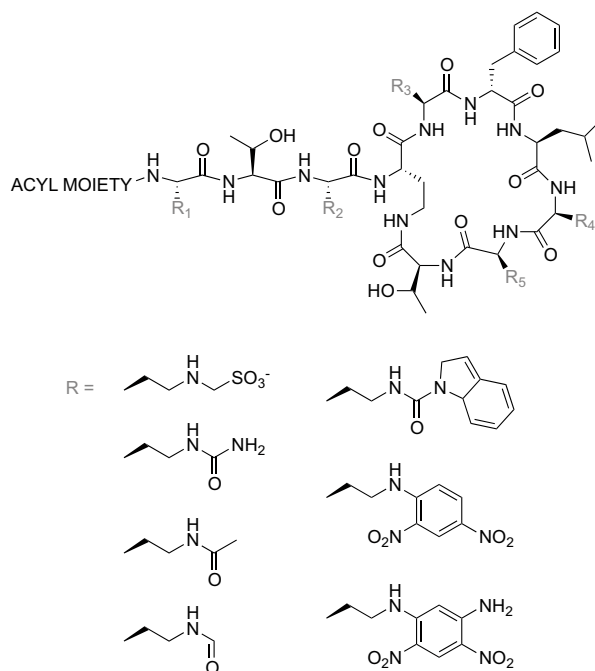


Figure 6: Example of polymyxin analogues with chemical modifications in the Dab residues.

Another approach is the substitution of the Dab residues with neutral or basic amino acids. For example, the substitution of Dab residues for Arg or His residues does not affect the ability to bind to LPS (Porro, 1993; 1995; Porro & Vaara, 1996).

An important conclusion extracted from the studies of the *Sakura group* was that the Dab residues within the heptapeptide cycle (Dab^{5,8,9}) are more important for the antimicrobial activity than those in the N-terminal segment, as observed when substituting the Dab residues for Ala (Kanazawa et al., 2009) or neutral 2-aminobutyric acid (Vaara et al., 2008), in the case of substitution of positions 5, 8 or 9 the activity drops significantly but not for positions 1 or 3.

In addition to cationic character, length of the amino acid side chain is crucial for activity. Analogues with 2 methylene groups (Dab) have higher activity than those with four (Lys), three (Orn) or one (2-amino-4-guanidinobutyric acid) methylene groups (Tsubery, et al., 2000b; 2002). This can be explained using the model of the PxB-LPS complex where optimal distance between the amino acid side chains and the lipid A phosphates is needed.

As summary, the key features of the Dab residues are the cationic character, the two-methylene length of the side chain and the spatial distribution of the charges, which makes the Dab residues, specially those within the cycle, indispensable for activity.

3) Modifications on the hydrophobic region D-Phe⁶/D-Leu⁶-Leu⁷.

The function of the hydrophobic dipeptide segment contained in the heptapeptide ring is to insert into the bacterial OM and stabilize LPS complexation via hydrophobic interactions between the amino acid side chains and the fatty acyl chains of lipid A. As said before, PxB and colistin have the same primary sequence but differ in position 6, occupied by a D-Phe in the case of PxB and a D-Leu in colistin.

Several attempts have been made to modify the hydrophobic segment in order to obtain better antimicrobials, for example substitution of D-Phe⁶ for D-Trp, D-Ala and L-Phe, or the substitution of Leu⁷ for Trp, such analogues maintain the antimicrobial activity and the LPS binding ability (Kanazawa et al., 2009). These results seem to suggest that a loss on hydrophobicity or lack of a D-configuration in the hydrophobic cycle are not crucial for activity, however it can be explained by a decrease in hydrophobicity in positions 6 and 7 being compensated by the hydrophobicity of the N-terminal fatty acid. In contrast, if both residues are substituted by Gly, we obtain an inactive analogue due to the complete loss of hydrophobicity (Kanazawa et al., 2009).

In our group, a disulphide cycle analogue containing a Dab in position 7, giving place to a permutation in the hydrophobic segment (D-Phe⁶-Dab⁷-Leu⁸) was synthesized. This lipopeptide showed a loss in selectivity for lipids that exchange through vesicle-to-vesicle contacts and a lower permeabilizing activity towards artificial vesicle membranes. While an analogue with D-Trp in substitution of D-Phe did show binding to vesicles and formation of vesicle-to-vesicle contacts (Clausell, et al., 2005).

Finally, a series of analogues containing dipeptide mimics of the D-Phe⁶-Leu⁷ segments such as, δ -aminovaleric acid, 4-phenyl-4-carboxymethylpiperidine or m-aminomethylbenzoic acid, just to mention some, were reported, but none of these analogues were active (Visser et al., 2003).

We can conclude that the D-Phe⁶/D-Leu⁶-Leu⁷ segment forms a needed hydrophobic domain, but it is not a highly specific domain, as the only needed characteristic is hydrophobicity.

4) Modifications of the size of the cyclic peptide ring.

The molecular model of the PxB-LPS complex reveals that the precise 23-atom size of the heptapeptide ring is indispensable for the electrostatic and hydrophobic contact points with LPS, that is why not many attempts have been made to modify the structure. The first reported analogues with an additional Dab residue, and consequently a bigger ring, resulted in much less active peptides (Vogler & Studer, 1966; Vogler, et al., 1961). Other analogues with a 20 to 26-membered ring have been tested, all of which presented a reduced OM permeabilizing activity (Tsubery, et al., 2000a; 2000b).

Clearly, the 23-atom ring seems essential for efficient binding to LPS and subsequent OM permeabilizing activity.

5) Modifications on the linear tripeptide.

By means of the molecular model of the PxB-LPS complex it is known that the linear segment is responsible for several hydrogen bonds necessary for the folding of the molecule and the consequent amphipathic structure key for binding.

It is understandable that the effect of deletions and/or substitutions in the linear segment has been extensively studied. For example, if Dab¹ is removed, no loss in antimicrobial activity is observed, however, if a double (Dab¹-Thr²) or total (Dab¹-Thr²-Dab³) deletion is carried out, an inactive compound is obtained (Sakura, et al., 2004). If the amino acid residues are substituted by neutral or hydrophobic residues (Ala or 2-aminobutyric acid), a decrease in activity is observed (Vaara et al., 2008). On the other hand, by scanning the different positions in the tripeptide segment with substitutions for Ala it can be observed that the Thr² position is more important than

Dab^{1,3}, as the acyl-Ala²-PxB analogue presents lower antimicrobial and binding activity than the analogues with Ala in positions 1 and 3 (Kanazawa et al., 2009). However, if Dab¹ is substituted with Ser, Arg, Phe, Trp and 2,3-diaaminopropionic acid, analogues with activity comparable to PxB are obtained, those analogues with Lys, Ala, Leu or tripeptides (Ala-Ala-Ala, Arg-Arg-Arg and Dab-Dab-Dab) in position 1 display a reduced antimicrobial activity and the substitution with a negatively charged residue, Glu, generates an inactive compound, as expected, due to the electrostatic repulsion with the negatively charged phosphate groups of lipid A (Katsuma et al., 2009).

In the last reported analogue of this kind, NAB739 (Figure 7), developed by Northern Antibiotics Ltd, the tripeptide segment has been substituted by a threonyl-D-serinyl residue, linked to an octanoyl fatty acid thus lacking two of the positive charges (Mingeot-Leclercq, et al., 2012). This modified PxB analogue has proved to be much less nephrotoxic but maintain the high antibiotic potency and is currently in preclinical trials (Vaara & Vaara, 2013; Vaara, et al., 2013).

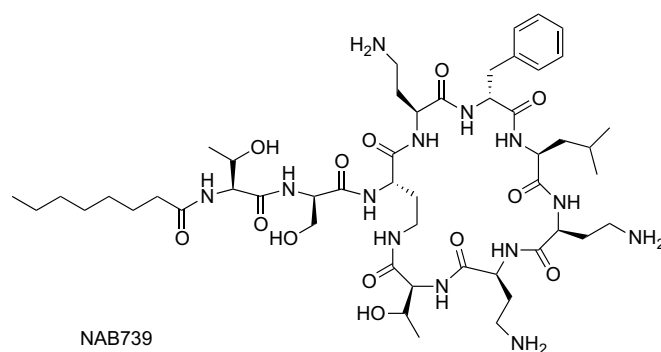


Figure 7: Structure of the last reported analogue (NAB739) with a modified tripeptide segment by deletion of Dab¹ and substitution of Dab³ for a D-Ser.

It is remarkable the presence of naturally occurring polymyxins with amino acid deletions within the tripeptide segment, the octapeptins. These are naturally occurring non-ribosomal peptides that display an almost equal heptapeptide primary sequence as PxB but lack the N-terminal tripeptide segment. Instead, the side chain consists of only one amino acid such as D-Dab or D-Ser covalently bound to a β -hydroxy fatty acid via an acyl group. To date, 17 octapeptins have been extensively described (Kato & Shoji, 1980; Konishi et al., 1983; Meyers, et al., 1973a; Meyers et al., 1973b; Meyers, et al., 1974; Parker & Rathnum, 1973; 1975; Qian et al., 2012; Rosenthal, et al., 1977; Shoji et al., 1980; Sugawara et al., 1983; Terabe, et al., 1979) and categorized into four subgroups (octapeptins A, B, C and D) based on the amino acids in the peptide moiety (Meyers, et al., 1976). Despite their similarities in the structural level, they differ markedly in their antimicrobial spectrum, as octapeptins are active against polymyxin-resistant strains and against Gram-positive bacteria. This can be explained by the fact that the loss of the Dab¹-Thr² segment is compensated by the additional hydrophobic and polar contributions from the longer chain and hydroxyl group of the fatty acid.

Natural PxB heptapeptide, lacking the complete tripeptide segment and fatty acid, has also been described (Kimura, et al., 1992). This peptide has shown to retain the ability to bind to the LPS and increase the permeability of the OM but as expected it is devoid of antibacterial activity. However it can be used as outer-membrane

permeabilizer (Li et al., 1999; Vaara & Vaara, 1983a) and in recent reports, it has been modified by substituting some of the Dab residues present in the cycle by other basic residues such as Orn or diaminopropionic acid obtaining analogues with promising permeabilizing characteristics, which when used in combination with common antibiotics an improvement of the initial activities is observed (Urakawa et al., 2010).

All these results seem to suggest that the tripeptide segment is indispensable for activity, and it does not accept major modifications, only conservative amino acid substitutions or single-deletions, especially in position 1. If partial or complete deletions are carried out, compounds that lack antibacterial activity but retain the activity to permeabilize the OM are obtained and so can be used synergistically with other antibiotics to improve its antibacterial profile.

6) Other modifications.

Other analogues of polymyxin B can be found in the literature, some examples are linear polymyxins (Rustici et al., 1993; Vaara, 1991), synthesized with the objective of lowering the toxicity of the molecule, but so far no active compound has been achieved. The covalent conjugation of PxB molecules (Griffin & Judice, 2002), in order to act as neutralizing agents against the septic effect of LPS, has not rendered especially active compounds. Finally, diverse groups have changed their path to obtain antibiotics by mimicking the physicochemical properties of polymyxins using cyclic amphipathic peptides that consist in alternating cationic (Lys) and non-polar (Val or Phe) residues, based on the structure of PxB, giving place to highly active compounds (Freder, et al., 2004).

A.1.2. Design of novel polymyxin synthetic analogues

The main objective of this thesis was to obtain new antimicrobials, based on the structure of polymyxins, with similar or higher activity against Gram-negative bacteria but with a broader spectrum of activity, active against multidrug-resistant bacteria and with potentially lower toxicity. To do so, the rational design of the molecules should initially maintain the basic characteristics of PxB, key for its activity, as seen in the previous section: The amphipathic character of the molecule, the positive charges and its distribution throughout the molecule, a cycle of 7 amino acids (23-membered ring) which includes a hydrophobic domain in positions 6 and 7, a linear tripeptide and an acylation in the N-terminal side by a medium-sized chain. However, as seen in previous work from the group (Clausell et al., 2006; Clausell, et al., 2004; Clausell et al., 2007; Clausell, et al., 2003) three principal modifications were carried out (Figure 8):

- The isosteric substitution of the lactam bond in the cycle between Dab⁴ and Thr¹⁰ by a disulphide bond between two residues Cys placed in the same positions in order to simplify the chemical synthesis without modifying the size of the cycle, key for activity. Disulphide bridges are common in natural cyclic AMPs, such as bactenecin (from cattle), brevinins (from *Rana brevipoda*), esculentin (from *Rana esculenta*) or the most remarkable ranalexin (from *Rana catesbeiana*), which contains a macrocyclic heptapeptide structure highly similar to that of polymyxin B, as already noted by Zasloff (Clark, et al., 1994). Similarly, Porro et al. (Rustici et al., 1993) described a series of all-L-amino acid heptapeptides cyclized by means of a disulphide bond with activity as LPS binders. These compounds were derived from polymyxin but included several

modifications such as lacking the fatty acyl tail, D-Phe was changed to L-Phe, the C-terminal group was a free carboxylate (therefore anionic at biological pH) and all Dab residues were changed to Lys or Orn. These compounds were able to bind lipid-A with high affinity and detoxify LPS *in-vitro*, but showed no antibiotic activity.

- The C-terminal end of the analogues, where the lateral side chain of Thr¹⁰ is substituted by a carboxamide isostere with similar bonding features. This is crucial for activity as demonstrated by the interaction model between PxB and LPS (Bruch, et al., 1999) where the lateral chain of Thr¹⁰ interacts by hydrogen bonding with the phosphate groups of lipid A.
- The substitution of the (S)-6-methyloctanoic acid by linear acids (octanoic, nonanoic, decanoic or dodecanoic acids), without any stereocentre and commercially available.

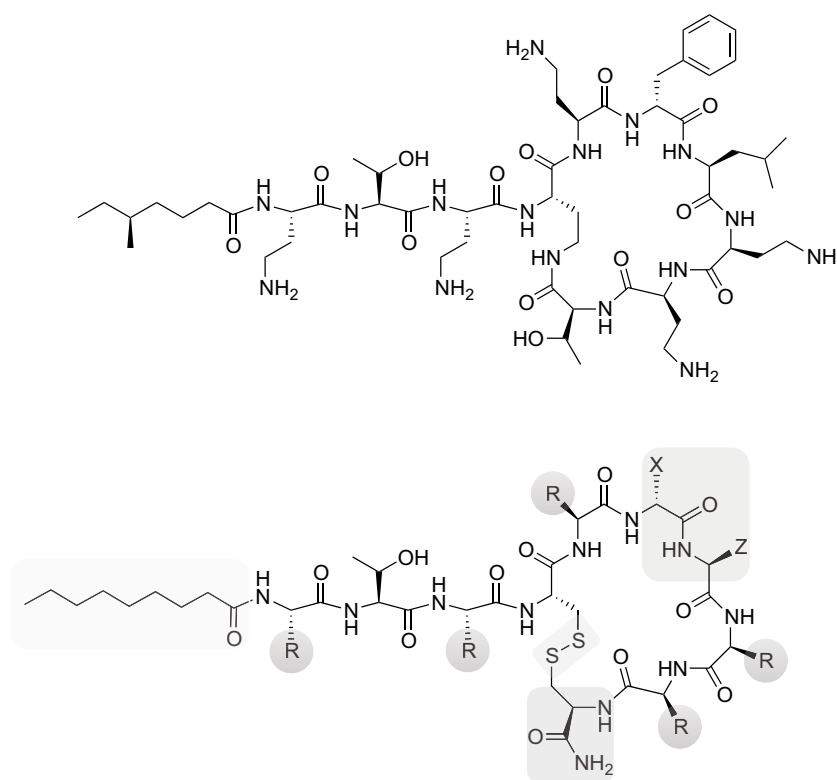


Figure 8: Structure of natural polymyxin B (upper) compared to general structure of the lipopeptide analogues of polymyxin synthesized in our group (lower). The structural and chemical features discussed for the design are highlighted.

In Table 2 the sequence and numeration of the peptides designed and synthesized in this thesis are shown.

Table 2: Sequence of the cyclic lipopeptides displayed in three-letter code, D-amino acids are denoted in italics and underlined residues denote bond formation.

PxB	6-methyl-octanoyl-Dab-Thr-Dab-Dab- <u>Dab</u> -Dab- <i>Phe</i> -Leu-Dab-Dab-Thr
1	nonanoyl-Arg-Thr-Dab- <u>Cys</u> -Dab- <i>Phe</i> -Leu-Arg-Dab- <u>Cys</u>
2	decanoyl-Arg-Thr-Dab- <u>Cys</u> -Dab- <i>Phe</i> -Leu-Arg-Dab- <u>Cys</u>
3	dodecanoyl-Arg-Thr-Dab- <u>Cys</u> -Dab- <i>Phe</i> -Leu-Arg-Dab- <u>Cys</u>
4	nonanoyl-Arg-Thr-Dab- <u>Cys</u> -Dab- <i>Trp</i> -Leu-Arg-Dab- <u>Cys</u>
5	nonanoyl-Dab-Thr-Arg- <u>Cys</u> -Dab- <i>Phe</i> -Leu-Arg-Dab- <u>Cys</u>
6	decanoyl-Dab-Thr-Arg- <u>Cys</u> -Dab- <i>Trp</i> -Leu-Arg-Dab- <u>Cys</u>
7	decanoyl-Arg-Thr-Arg- <u>Cys</u> -Dab- <i>Trp</i> -Nle-Arg-Dab- <u>Cys</u>
8	decanoyl-Dab-Thr-Dab- <u>Cys</u> -Dab- <i>Phe</i> -Nle-Dab-Dab- <u>Cys</u>
9	dodecanoyl-Dab-Thr-Dab- <u>Cys</u> -Dab- <i>Phe</i> -Nle-Dab-Dab- <u>Cys</u>
10	decanoyl-Dab-Thr-Arg- <u>Cys</u> -Dab- <i>Phe</i> -Nle-Arg-Dab- <u>Cys</u>
11	dodecanoyl-Dab-Thr-Arg- <u>Cys</u> -Dab- <i>Phe</i> -Leu-Arg-Dab- <u>Cys</u>
12	decanoyl-Dab-Thr-Dab- <u>Cys</u> -Dab- <i>Leu</i> -Nle-Dab-Dab- <u>Cys</u>
13	nonanoyl-Dab-Thr-Dab- <u>Cys</u> -Dab- <i>Nle</i> -Nle-Dab-Dab- <u>Cys</u>
14	decanoyl-Dab-Thr-Dab- <u>Cys</u> -Dab- <i>Nle</i> -Nle-Dab-Dab- <u>Cys</u>
15	dodecanoyl-Dab-Thr-Dab- <u>Cys</u> -Dab- <i>Nle</i> -Nle-Dab-Dab- <u>Cys</u>
16	nonanoyl-Dab-Thr-Dab- <u>Cys</u> -Dab- <i>Leu</i> -Leu-Dab-Dab- <u>Cys</u>
17	decanoyl-Dab-Thr-Dab- <u>Cys</u> -Dab- <i>Leu</i> -Leu-Dab-Dab- <u>Cys</u>
18	dodecanoyl-Dab-Thr-Dab- <u>Cys</u> -Dab- <i>Leu</i> -Leu-Dab-Dab- <u>Cys</u>
19	nonanoyl-Orn-Thr-Orn- <u>Cys</u> -Orn- <i>Phe</i> -Nle-Orn-Orn- <u>Cys</u>
20	decanoyl-Orn-Thr-Orn- <u>Cys</u> -Orn- <i>Phe</i> -Nle-Orn-Orn- <u>Cys</u>
21	dodecanoyl-Orn-Thr-Orn- <u>Cys</u> -Orn- <i>Phe</i> -Nle-Orn-Orn- <u>Cys</u>
22	nonanoyl-Lys-Thr-Lys- <u>Cys</u> -Lys- <i>Phe</i> -Nle-Lys-Lys- <u>Cys</u>
23	decanoyl-Lys-Thr-Lys- <u>Cys</u> -Lys- <i>Phe</i> -Nle-Lys-Lys- <u>Cys</u>
24	dodecanoyl-Lys-Thr-Lys- <u>Cys</u> -Lys- <i>Phe</i> -Nle-Lys-Lys- <u>Cys</u>

In the first series of peptides synthesized (#1-7), we investigated the effect of the substitution of the charged residues in the molecule by another basic and charged residue, an arginine, while maintaining the overall charge of the molecule. Arginine is known to be a highly membrane active amino acid and is prevalent in many antimicrobial peptide sequences due to its crucial chemical properties. The presence of the guanidine group provides arginine with strong bidentate cationic character and hydrogen-bond forming properties (Fuchs & Raines, 2006). This allows arginine to form cation- π interactions that make the entry into the hydrophobic core of the bilayer energetically more favourable and so facilitate the initial interaction with the OM of the bacteria resulting in an improvement in activity (Arouri, et al., 2009; Chan, et al., 2006; Lättig-Tünnemann et al., 2011).

The use of tryptophan in substitution of phenylalanine was also tested in some of the peptides (#4, 6, 7). This residue has several advantages, it confers the molecule intrinsic fluorescence, very useful to characterize membrane binding by fluorescence techniques

(see Chapter A.3.1) and it favours the interaction with the interfacial region of the lipid membrane (Arouri et al., 2009; Chan et al., 2006).

In addition, in some of the peptides (#1, 5-7) the C-terminal Cys residue was changed to a D-Cys to better mimic the orientation of the polar group of residue Thr¹⁰ in natural PxB. Fatty acids with different lengths were used to find the optimal length needed.

Finally, the introduction of norleucine instead of leucine in position 7 for peptide #7 was studied to increase flexibility in this key hydrophobic residue.

Based on the results obtained by antimicrobial activity testing of the initial peptides, a second series of peptides was designed and synthesized (#8-11). These peptides maintained those structural features that rendered the best results, D-Cys in position 10 and Nle in position 7. However, to fine-tune the sequence that results in the best antimicrobial profile we investigated again the substitution Nle for Leu, Arg for Dab and the length of the fatty acid, while maintaining the rest of the sequence intact.

Given that the residue Nle rendered promising results, we decided to synthesize several colistin analogues in which the hydrophobic domain contained in the cycle was modified (#12-18). The main objective of these modifications was to obtain antimicrobials with potentially lower toxicity than colistin. Although slightly less active than PxB, colistin has proved to have a better toxicological profile (Landman et al., 2008). Colistin has a D-Leu in position 6 instead of the D-Phe in PxB, the idea was to scan which combination of the residues Nle and Leu (substituting positions 6, 7 or both) gave the best results.

Finally, the last series of peptides (#19-24) consists of the replacement of all the Dab residues in compound #8 for Lys and Orn. These charged amino acids present the advantage that they are more commercially convenient making them more suitable for a future large-scale synthesis necessary for clinical and future therapeutical applications.

A.1.3. Chemical synthesis of the polymyxin analogues

The lipopeptides were manually synthesized following a standard Fmoc/tBu procedure. In all cases the resin used was MBHA with Fmoc-Rink amide linker attached in order to obtain the C-terminal side of the peptide as a carboxamide. This bifunctional linker provides higher lability to the linkage with the peptide as it consists of a benzhydrylamine functionalized with two methoxy groups in positions *ortho* and *para*, allowing the cleavage at 95% of TFA.

The protecting groups of the amino acids were the following: Trt for Cys, Boc for Dab, Lys and Orn, tBu for Thr and Pbf for Arg.

The amino acids were incorporated to the resin directly using DIC as activating agent and HOBt as additive to minimize racemization. 3 equivalents of all the reagents were used for 1 hour in DMF. If the coupling was not complete, 1.5 eq. of the reagents were added for 30 more minutes in DMF. Successive cycles of Fmoc-deprotection with 20% piperidine in DMF and Fmoc-protected amino acid coupling to the freshly deprotected N-terminus gave place to the complete protected peptides on resin.

Once the last amino acid was coupled, the Fmoc protecting group was eliminated followed by coupling of the fatty acid (octanoic, nonanoic, decanoic or dodecanoic

acid). 5 equivalents of the acid, DIC and HOBt were used for 1 hour in DMF. In all cases a repetition with 2.5 equivalents and half of the time was carried out.

Cleavage and full deprotection of the linear peptides was carried out by acidolysis with a mixture of TFA/triethylsilane or triisopropylsilane/water for 90 minutes. The filtrate was evaporated to a reduced volume under a gentle stream of nitrogen and the crude product was precipitated with cold diethyl ether.

Cyclization of the crude peptides by disulphide bond formation was carried out by dissolving the peptide in water at a very diluted concentration followed by addition of 5% of DMSO as the mild oxidant (Tam, et al., 1991). This mixture was stirred continuously at RT for 24 to 48 hours and the progress of the cyclization was followed by analytical HPLC (Figure 9). Once the cyclized product was obtained the mixture was directly lyophilized.

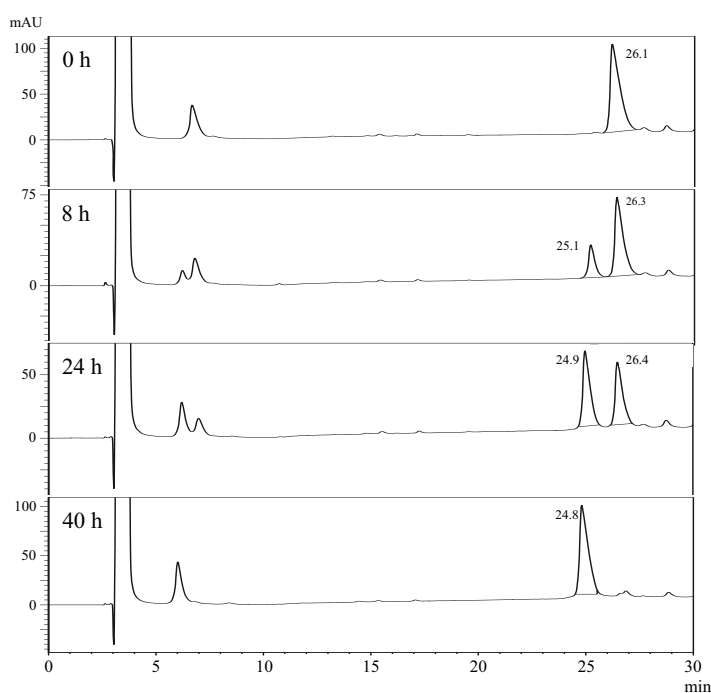


Figure 9: Monitoring by analytical HPLC of the reaction of cyclization in solution using DMSO of peptide #12. Elution conditions of 18% to 40% B in 30 min, solvent A: 0.045% TFA in H₂O and B: 0.036% TFA in ACN.

Finally, the peptides crudes were purified by semi-preparative HPLC and the obtained pure products (purity >95%) were characterized by analytical HPLC, amino acid analysis and MALDI-TOF mass spectrometry. A scheme of the synthetic route is shown in Figure 10.

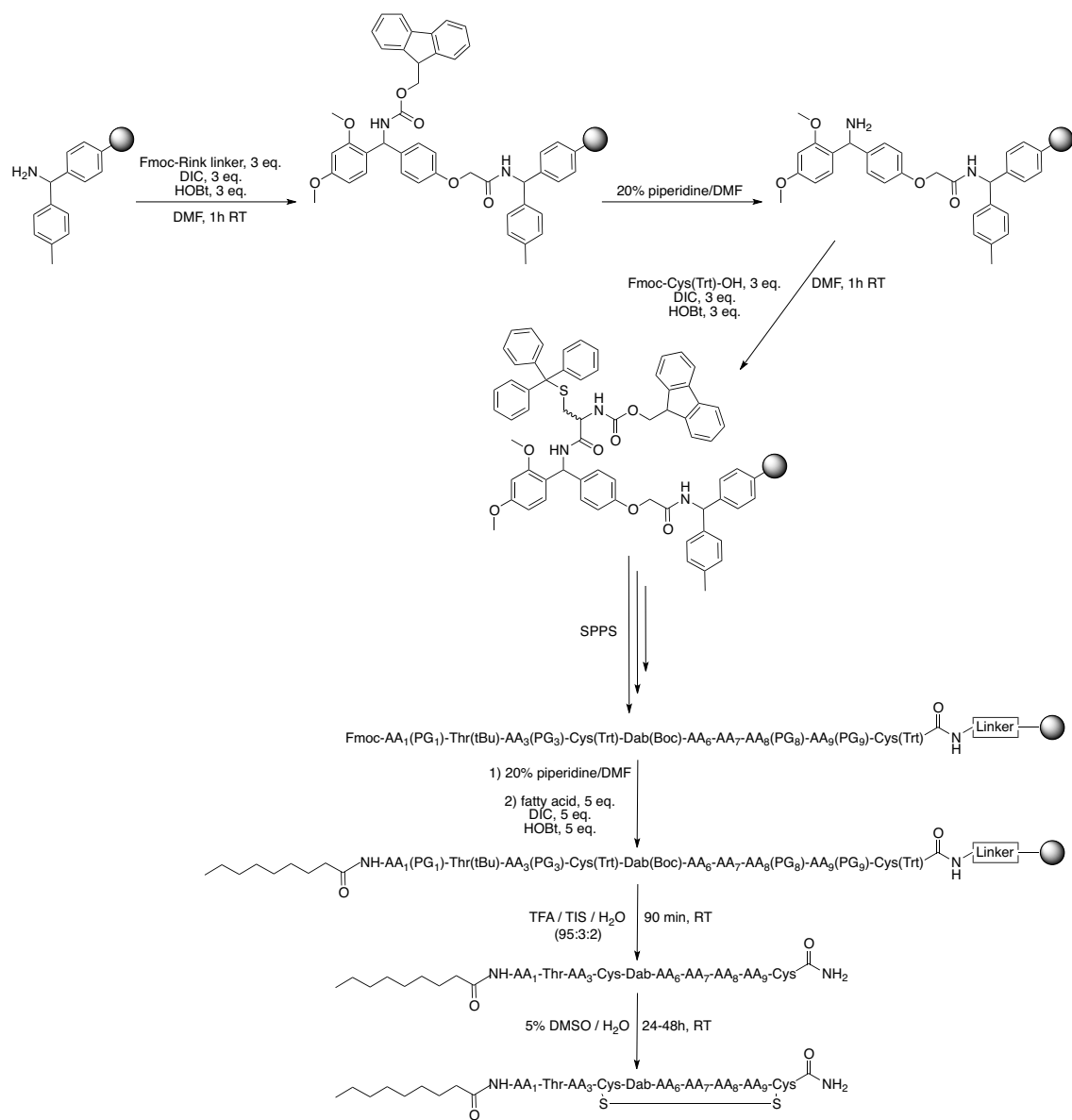


Figure 10: General scheme of the synthetic strategy followed for the analogues of polymyxin. AA_x stands for amino acid and PG_x stands for protecting group, the x indicates the position in the sequence.

A.2. *IN-VITRO* ANTIBACTERIAL ACTIVITY DETERMINATION

A.2.1. Bacterial ATCC Strains

The objective of this part of the thesis was to measure the antibacterial activity of the new polymyxin analogues. This activity was expressed as the minimum inhibitory concentration, which is the lowest concentration of antibacterial agent that inhibits the visible growth of a microorganism in 18-24 h. It was determined using the tube-dilution method (Jorgensen & Ferraro, 2009; Woods, 1995).

The microorganisms used were the following:

- Gram-positive bacteria: *Staphylococcus aureus* (ATTC 29213, ATCC 6538), *Enterococcus faecalis* (ATCC 29212) and *Mycobacterium phlei* (ATCC 41423).
- Gram-negative bacteria: *Escherichia coli* (ATCC 25922 and ATCC 8739), *Pseudomonas aeruginosa* (ATCC 9027), *Acinetobacter sp.* (DSMZ 586) and *Klebsiella pneumoniae* (ATCC 13883).
- Fungi: *Candida albicans* (ATCC 10231).

The microorganisms used in the MIC assay were chosen because they are representative of those microorganisms that nowadays represent a threat for human health:

The ESKAPE pathogens, *Enterococcus faecium*, *Staphylococcus aureus*, *Klebsiella pneumoniae*, *Acinetobacter baumannii*, *Pseudomonas aeruginosa*, and *Enterobacter* species (which include *E. coli*) currently cause the majority of hospital-acquired infections that present resistance to regular antibiotics (Rice, 2008). Some of the microorganisms of choice belong to this ESKAPE pathogens, or have the same genus, therefore possess the same morphological properties but they can be used in a Biosafety Level 2 (BSL-2) laboratory, unlike some of the ESKAPE pathogens which need a BSL-3 laboratory.

A biosafety level is the level of the biocontainment precautions required to isolate dangerous biological agents in an enclosed facility and BSL-2 allows you to work with agents of moderate potential hazard to personnel and environment.

In the case of the genus *Mycobacterium*, the species *Mycobacterium tuberculosis* is the pathogen responsible for tuberculosis. These bacteria can only be used in specially prepared laboratories, but the species *Mycobacterium phlei*, can be used in our laboratory and grows in 48 h using standard broths, whereas *M. tuberculosis* is very difficult to grow (Ogbaini-Emovon, 2009). These features make *M. phlei* a convenient model for *M. tuberculosis* as it also presents the characteristic thick cell wall, containing mycolic acids. This highly hydrophobic wall is very difficult to penetrate by common antibacterial agents, which makes all species of *Mycobacterium* highly difficult to kill.

Finally, in order to investigate if the synthesized peptides were active against fungi, *Candida albicans* was added to our MIC determinations. This fungus causes opportunistic oral and genital infections in humans and has emerged as an important cause of mortality in immunocompromised patients (Calderone & Fonzi, 2001).

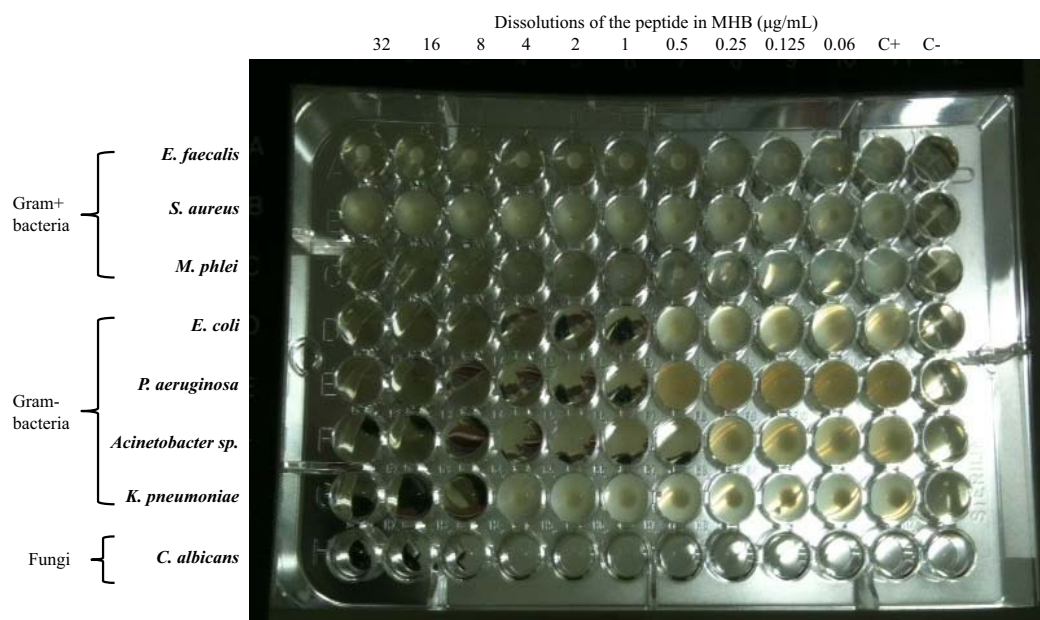


Figure 11: Example of microtiter 96-well plate used in the MIC tests for commercial PxB. The columns 1-10 contain the dissolutions of the peptide tested in MHB (32-0.06 $\mu\text{g/mL}$), and to each row A-H the microorganism is inoculated. Columns 11 and 12 correspond to the positive (no peptide) and negative (no microorganism) control respectively. Observing the plate used as example, rows E and F, which correspond to *E. coli* and *P. aeruginosa* respectively, the MIC value is 0.5 $\mu\text{g/mL}$ (column 7) as the wells with lower concentration of peptide are turbid, which evidences growth of the microorganism. While rows A-C, which correspond to Gram-positive bacteria all present turbidity, therefore the MIC is $>32 \mu\text{g/mL}$.

The MIC values for the synthesized peptides are shown in Table 3. Natural PxB is used as control in each experiment and the MIC is expressed in $\mu\text{g/mL}$. The MIC measures are qualitative as they are based on visual growth of the bacteria, and they are not bactericidal values, as no turbulence does not necessary imply the death of the bacteria.

Table 3: Minimum inhibitory concentration (expressed in µg/mL) of the polymyxin analogues described. Microorganisms not tested for a determinate peptide are expressed as --.

Peptide	GRAM+			GRAM-			FUNGI
	<i>E.faecalis</i>	<i>S.aureus</i>	<i>M.phlei</i>	<i>E.coli</i>	<i>P.aeruginosa</i>	<i>Acinetobacter sp.</i>	<i>C.albicans</i>
PxB	>32	>32	16	1	1	1	>32
1	>32	16	--	4	8	--	--
2	32	16	--	8	8	--	--
3	8	4	--	8	16	--	--
4	32	8	--	4	8	--	--
5	>32	8	--	2	16	--	--
6	32	8	--	8	32	--	--
7	16	4	--	8	>32	--	--
8	32	4-8	2-4	1-2	2	4	16
9	16	4-8	2-4	4-8	4	16	16
10	16-32	4	2	2-4	2	4	16-32
11	16	4	2	4	4	4	16
12	>32	16	4	4-8	1	4	--
13	>32	32	16	4	1-2	2	--
14	>32	8	2-4	2	2-4	2	--
15	8-16	4	1-2	2-4	4	4	--
16	>32	32	>32	4-8	1	4	--
17	>32	8	4	2-4	1-4	8	--
18	16-32	4	2	4	2-4	4-8	--
19	>32	16-32	8	32	>32	>32	>32
20	>32	16	4-8	16	>32	>32	>32
21	8	4	4	16	16	32	16
22	>32	>32	8	32	>32	>32	>32
23	>32	32	16	32	>32	>32	>32
24	16-32	8	8	16	32	8	16

Taking into account the definition of MIC, the lower the value, the higher the antimicrobial activity of the tested peptide. In fact, we consider that a peptide is active when its MIC is 4 µg/mL or less. Some of the values are represented as an interval; this is a result of discrepancy in the different measurements. This might be due to the fact that the MIC values are measured in 2-fold dilutions, so the real value of the MIC could be in between these values. In addition, due to the multiple pipetting steps and in occasions non-homogenous bacterial suspensions, tiny variations in the final value can be expected.

A discussion of the results obtained for the different modifications is detailed below, however it must be noted that the first series of peptides used in this thesis belong to a larger group of more than 100 peptides, synthesized in our group, with several modifications. These analogues (#1-7) were chosen as the most representative of these modifications in order to carry out the biophysical experiments described later (see Chapter A.3.1).

- **Modifications on the configuration of Cys¹⁰:**

In the following table (Table 4), the MIC values of PxB and several analogue peptides are given. **sP-B** was the first peptide synthesized in the group with the canonical application of the design principles (Cys⁴ and Cys¹⁰ and linear nonanoyl fatty acyl group) and proved to retain considerable activity against Gram-negative bacteria, but as PxB itself, it was devoid of activity against Gram-positive bacteria (Claussell et al., 2005). Peptide **sP-2Arg**, not used in this thesis, belongs to the first group of peptides synthesized in the group, and it is analogue to **sP-B** but contains two arginine residues substituting Dab^{1,8}. The substitution of charged residues will be discussed further; we now focus in the replacement of the residue Cys in position 10 for a D-Cys, which yields peptide #1. The objective of this modification was to mimic the configuration of the side chain of Thr¹⁰ present in natural PxB.

If we look at the MIC values for peptide **sP-2Arg** and #1, what we can observe is that the change in configuration of the residue Cys results in a 2-fold increase in activity for *E. coli*, *S. aureus* and *P. aeruginosa*, suggesting that the configuration of the residue in position 10 is important for activity. Due to the favourable results, all future peptides synthesized in the group contained D-Cys in position 10.

Table 4: Antibacterial activity of the polymyxin analogues that contain a Cys in position 10 versus those with a D-Cys. The sequence of the peptides is displayed in three-letter code, the residues in italics are D-isomers, the underlined residues denote bond formation and the MIC values are expressed as µg/mL.

Peptide	Sequence	Gram+		Gram-	
		<i>E.faecalis</i>	<i>S.aureus</i>	<i>E.coli</i>	<i>P.aeruginosa</i>
PxB	6-methyl-octanoyl-Dab-Thr-Dab-Dab-Dab-Phe-Leu-Dab-Dab-Thr	>32	>32	1	1
sP-B	nonanoyl-Dab-Thr-Dab-Cys-Dab-Phe-Leu-Dab-Dab-Cys	>32	>32	4	8
sP-2Arg	nonanoyl-Arg-Thr-Dab-Cys-Dab-Phe-Leu-Arg-Dab-Cys	>32	32	8	16
1	nonanoyl-Arg-Thr-Dab-Cys-Dab-Phe-Leu-Arg-Dab-Cys	>32	16	4	8

- **Modifications on the charged residues:**

In the following table (Table 5), the MIC values of the analogues of polymyxin that contain modifications on the charged residues are represented and compared to PxB and peptide **sP-B**. From previous studies in our group, we know that the substitution of one Dab residue for one Arg residue has little effect in the antibacterial activity; the peptides present approximately the same antibacterial profile as peptide **sP-B** (data not shown). But if we now compare the activity of peptide **sP-B** to that of peptide **#1**, with 2 Arg residues, we can observe that both have the same activity against Gram-negative bacteria but peptide **#1** is more active against *S. aureus*. If we then compare to peptide **#7**, which contains 3 Arg residues, we can observe that the activity against Gram-negative bacteria has dropped considerably while the activity against Gram-positive bacteria has improved, reaching a value of 4 µg/mL for *S. aureus*.

The effect of substituting Dab¹ or Dab³ by Arg can be observed by comparing peptides **#1** and **#5** respectively. The peptide containing an Arg residue in position 3 is relatively more active, especially against *S. aureus* and *E. coli*.

It is clear that the addition of Arg residues to the peptides broadens the spectrum of activity, making them active against Gram-positive strains. However, the drawback is a loss on activity against Gram-negative bacteria, so a compromise should be achieved with both activities by adding none, 1 or maximum 2 Arg residues. The position of the Arg residue in the linear tripeptide seems to be important for activity, as seen in peptide **#5**, being position 1 not so crucial for activity, previously seen in the literature and summarized in Section A.1.1.

Table 5: Antibacterial activity of the polymyxin analogues that contain one or several Dab residues substituted by Arg residues. The residues are displayed in three-letter code and the MIC values are expressed as µg/mL.

Peptide	Position of charged residue					Gram+		Gram-	
	1	3	5	8	9	<i>E.faecalis</i>	<i>S.aureus</i>	<i>E.coli</i>	<i>P.aeruginosa</i>
PxB	Dab	Dab	Dab	Dab	Dab	>32	>32	1	1
sP-B	Dab	Dab	Dab	Dab	Dab	>32	>32	4	8
1	Arg	Dab	Dab	Arg	Dab	>32	16	4	8
5	Dab	Arg	Dab	Arg	Dab	>32	8	2	16
7	Arg	Arg	Dab	Arg	Dab	16	4	8	>32

We next studied the effect of the substitution of all Dab residues of the molecule for Orn or Lys residues (**#19-24**). The idea was to obtain an active compound containing a more accessible residue than Dab. These modifications were based on the sequence of peptide **#8**, the best analogue synthesized in the group so far, which will be commented further.

In Table 6 we can observe the results obtained, where it is clear that the substitution with Orn or Lys residues gave place to almost completely inactive compounds. This can be at first surprising, because the charge is maintained, but it can be explained by the length of the amino acid side chain. The Orn and Lys residues have longer side chains compared to original Dab residues (Figure 12) and as seen in the literature, the substitution with residues with longer or shorter side chains has negative effects on the activity (Tsubery, et al., 2000a; 2000b). If we look at the

model of the PxB-LPS complex, it is the exact length of 2 methylene groups that provides the optimal bridging distance between the N γ -amino side chain groups and the lipid A phosphates

Table 6: Antibacterial activity of the polymyxin analogues that contain all Dab residues substituted by Orn or Lys residues. The residues are displayed in three-letter code and MIC values are expressed as $\mu\text{g/mL}$.

Peptide	Position of charged residue					Gram+		Gram-	
	1	3	5	8	9	<i>E.faecalis</i>	<i>S.aureus</i>	<i>E.coli</i>	<i>P.aeruginosa</i>
PxB	Dab	Dab	Dab	Dab	Dab	>32	>32	1	1
sP-B	Dab	Dab	Dab	Dab	Dab	>32	>32	4	8
8	Dab	Dab	Dab	Dab	Dab	32	4-8	1-2	2
20	Orn	Orn	Orn	Orn	Orn	>32	16	16	>32
23	Lys	Lys	Lys	Lys	Lys	>32	32	32	>32

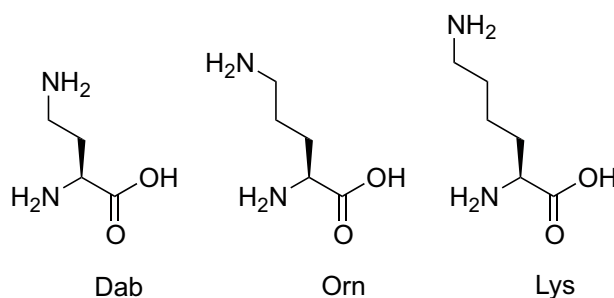


Figure 12: Comparison of the length of the side chain of the different residues Orn and Lys tested for peptides #19-24, compared to Dab.

- Modifications on the hydrophobic section D-Phe⁶-Leu⁷:

The hydrophobic domain composed of residues 6 and 7, contained in the cycle, has been extensively modified in order to find the most promising polymyxin analogues.

The initial modification consisted in the substitution of the residue D-Phe⁶ by D-Trp⁶, maintaining the conformation and hydrophobicity in the domain. As stated previously, this modification had two objectives, firstly, confer the molecule intrinsic fluorescence, and secondly improve the interaction with lipid membranes. If we compare the activities of peptides #1 and #4 (Table 7), we can see that #4 contains an L-Cys instead of a D-Cys, and as seen before, should therefore have a lower activity than peptide #1. Instead, the activity against Gram-positive strains, *E. faecalis* and *S. aureus*, has improved while the activities of both Gram-negative strains remains the same. This improvement of activity in Gram-positive bacteria is due to the substitution with a D-Trp residue in position 6. However, with this substitution not especially active peptides could be obtained, maximum activities reached were 4-8 $\mu\text{g/mL}$, and was only used when fluorescent peptides were needed.

Table 7: Antibacterial activity of the polymyxin analogues that contain D-Trp substituting D-Phe in position 6. The sequence of the peptides is displayed in three-letter code, the residues in italics are D-isomers, the underlined residues denote bond formation and MIC values are expressed as µg/mL

Peptide	Sequence	Gram+		Gram-	
		<i>E.faecalis</i>	<i>S.aureus</i>	<i>E.coli</i>	<i>P.aeruginosa</i>
PxB	6-methyl-octanoyl-Dab-Thr-Dab-Dab-Dab- <i>Phe</i> -Leu-Dab-Dab-Thr	>32	>32	1	1
1	nonanoyl-Arg-Thr-Dab- <u>Cys</u> -Dab- <i>Phe</i> -Leu-Arg-Dab- <u>Cys</u>	>32	16	4	8
4	nonanoyl-Arg-Thr-Dab- <u>Cys</u> -Dab- <i>Trp</i> -Leu-Arg-Dab- <u>Cys</u>	32	8	4	8

Substituting the residue Leu⁷, found in native polymyxin B, for the isomer Nle, with the idea of adding flexibility in this key hydrophobic point had no major effect in our initial analogues. But when placed together with a D-Cys in position 10, gave place to our best analogue, peptide #8.

In Table 8 we compare the activity of #8 with that of peptide #0 (data from our laboratory). This peptide is analogue to sP-B but contains D-Cys¹⁰, and a fatty acid of 10 carbons instead of 9 carbons, and was our starting point for the second round of peptide design. What we can see is that the presence of Nle in position 7 increases 2-fold the activity for all strains except *E. faecalis*, and reaches good values of 1-2 µg/mL in *E. coli* and *P. aeruginosa*.

Table 8: Antibacterial activity of the polymyxin analogues where position 7 is modified. The sequence of the peptides is displayed in three-letter code, the residues in italics are D-isomers, the underlined residues denote bond formation and MIC values are expressed as µg/mL.

Peptide	Sequence	Gram+		Gram-	
		<i>E.faecalis</i>	<i>S.aureus</i>	<i>E.coli</i>	<i>P.aeruginosa</i>
PxB	6-methyl-octanoyl-Dab-Thr-Dab-Dab-Dab- <i>Phe</i> -Leu-Dab-Dab-Thr	>32	>32	1	1
sP-B	nonanoyl-Dab-Thr-Dab- <u>Cys</u> -Dab- <i>Phe</i> -Leu-Dab-Dab- <u>Cys</u>	>32	>32	4	8
0	decanoyl-Dab-Thr-Dab- <u>Cys</u> -Dab- <i>Phe</i> - Leu -Dab-Dab- <u>Cys</u>	32	8	2	4
8	decanoyl-Dab-Thr-Dab- <u>Cys</u> -Dab- <i>Phe</i> - Nle -Dab-Dab- <u>Cys</u>	32	4-8	1-2	2

In a third round of peptide design, based in the sequence of #8, peptides #12-18 were synthesized. The substitution Leu-Nle was further investigated, but this time using colistin as the reference compound, which contains D-Leu in position 6, instead of the residue D-Phe in PxB. The objective was to investigate the effect of substituting Nle in position 6, 7 or both, in order to find a compound with potential lower toxicity.

In Table 9 the results obtained for the different analogues (all containing a 10 carbon fatty acyl unit) are depicted. If we observe the activity of #12, 14 and 17 we can see that they are all active against both Gram-positive and Gram-negative strains, except *E. faecalis*. They have low MIC values of 2 or 4 µg/mL, even reaching 1 µg/mL for #12 against *P. aeruginosa*. However, if we compare the activities to that of #8, we can see that there is not a clear improvement in activity, some peptides have a better activity against one strain but on contrast have a worst activity against others.

Table 9: Antibacterial activity of the polymyxin analogues where position 6 and 7 are studied with the substitution Leu-Nle. The residues are displayed in three-letter code and the MIC values are expressed as µg/mL.

Peptide	Residue		Gram+			Gram-		
	6	7	<i>E.faecalis</i>	<i>S.aureus</i>	<i>M.phlei</i>	<i>E.coli</i>	<i>P.aeruginosa</i>	<i>Acinetobacter sp.</i>
colistin	<i>Leu</i>	Leu	>32	>32	16	1	0.5	>32
PxB	<i>Phe</i>	Leu	>32	>32	16	1	0.5	>32
8	<i>Phe</i>	Nle	32	4-8	2-4	1-2	2	4
12	<i>Leu</i>	Nle	>32	16	4	4-8	1	4
14	<i>Nle</i>	Nle	>32	8	2-4	2	2-4	2
17	<i>Leu</i>	Leu	>32	8	4	2-4	1-4	8

- **Modifications on the length of the fatty acid:**

All our peptides have been synthesized using linear fatty acids, especially of 9, 10 or 12 carbons. The effect of the modification of the length of the fatty acid can be observed in Table 10. If we compare the activity of peptides #16-18, all sharing the same sequence but differing in the length of the fatty acyl moiety, we can see that there is a clear correlation between length and activity. The peptide containing a 12-carbon fatty acid has an improved antibacterial profile, its activity against *E. faecalis* has improved and for *S. aureus* and *M. phlei* good activities are reached, while the analogue with 9 carbons is inactive against all Gram-positive strains. The drawback is a slight decrease in activity for Gram-negative bacteria. This effect has been also seen in the literature, where an increase in fatty acid length has a positive effect in the values for a bacteria but is at the expense of activity against another (O'Dowd et al., 2007).

Table 10: Antibacterial activity of the polymyxin analogues where the length of the fatty acid is modified. Peptides #16-18 have the same sequence but they differ in the length of the fatty acid, the same happens for peptides #8-9. The MIC values are expressed as µg/mL.

	<i>Length of fatty acyl unit</i>	<i>E.faecalis</i>	<i>S.aureus</i>	<i>M.phlei</i>	<i>E.coli</i>	<i>P.aeruginosa</i>	<i>Acinetobacter sp.</i>
PxB	8	>32	>32	16	1	1	0.5
sP-B	9	>32	>32	--	4	8	--
16	9	>32	32	>32	4-8	1	4
17	10	>32	8	4	2-4	2-4	8
18	12	16-32	4	2	4	2-4	4-8
8	10	32	4-8	2-4	2	2	4
9	12	16	4-8	2-4	4-8	4	16

However, in some cases this correlation is not so clear, if we observe peptides #8-9, which have the same sequence but the fatty acids differ in 2-carbons length, we should expect compound #9 to be more active against Gram-positive strains than the analogue with 10 carbons. In this case, the activities remain more or less the same, only for *E. faecalis* we can see an improvement, and as seen before, activities against Gram-negative bacteria decrease. This could be partly due to the fact that these two peptides contain Nle in the hydrophobic segment of the cycle, which contains a longer side chain. It can therefore be hypothesized that adding a long fatty acid together with a longer side chain in position 7, can slightly alter the overall electron density in the molecule causing a slight decrease in activity (Figure 13), due to an incorrect complexation with the LPS and consequently a decreased insertion in the OM.

It can be extracted from our results that when synthesizing polymyxin analogues, different length fatty acids should always be tested as tiny modifications have demonstrated to translate in different antimicrobial behaviour.

In general, we can say that the longer the fatty acid, the more active against Gram-positive strains this peptide becomes, however there is an optimal length of 10-12 carbons as peptides containing too short (< C9) or too long (> C12) fatty acids have proved to be much less active (data from our laboratory not shown in this thesis). The bulkiness or length in the hydrophobic segment (positions 6 and 7) contained in the cycle should be taken into account when modifying the length of the fatty acid.

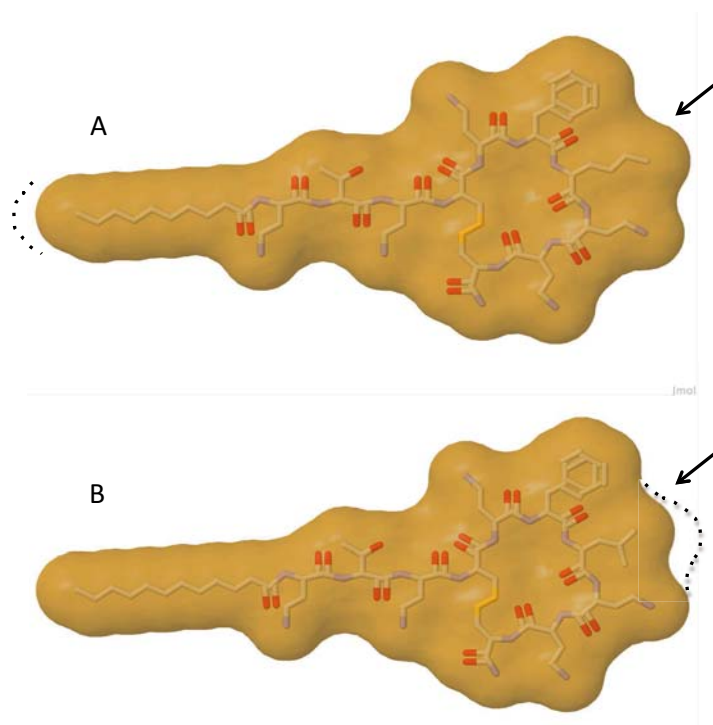


Figure 13: Comparison of the electron distribution of molecules A) containing Nle in position 7 and a fatty acid with 10 carbons, B) Leu in position 7 and a fatty acid of 12 carbons. The dotted lines represent the electron distribution of the longer option. Made using Jmol: www.jmol.org.

A.2.2. Resistant and multidrug-resistant strains

To investigate the potential activity of the most active peptides, MIC assays were carried out in resistant and multidrug-resistant bacteria.

- Gram-positive bacteria:

The MIC assay against a collection strain of methicillin-resistant *Staphylococcus aureus* was carried out in our laboratory and tested with several of the lipopeptides. This strain of bacteria, responsible of many hospital-acquired infections and recently outside hospital infections, is resistant to β -lactam antibiotics and cephalosporins, and is becoming one of the major challenges for worldwide health institutions (Arias & Murray, 2009).

The MIC values are depicted in Table 11, and prove that our peptides #8-11 are active, with values similar to the wild type strain, and even reaching 4 $\mu\text{g}/\text{mL}$ in some cases. For peptides #19-21 (all Orn residues), and #22-24 (all Lys residues), the activities were not so promising, but what is interesting are the values of the peptide with a fatty acid of 12 carbons (#21 and #24) which had an improved activity, respect its short-length analogues, with a MIC of 4-8 $\mu\text{g}/\text{mL}$.

The results obtained are promising because the values against the wild type strain and the resistant strain are almost the same but the synthesized lipopeptides have a very different mechanism of action than β -lactam antibiotics, which are inactive against MRSA, while the polymyxin analogues prove to be active.

Table 11: Antibacterial activity of some of the polymyxin analogues against the wild-type *S. aureus* (left) and methicillin-resistant *S. aureus* (right). Peptides #19-21 and #22-24 have the exact same sequence but only vary on the length of the fatty acyl unit. The MIC values are expressed as µg/mL.

Peptide	Gram-positive <i>S. aureus</i>	
	ATCC 6538	ATCC 43300
	Collection strain	Collection strain resistant to methicillin and oxacillin
8	4-8	8
9	4-8	8
10	4	4-8
11	4	4
19	16-32	>32
20	16	16
21	4	4
22	>32	>32
23	32	>32
24	8	8

- Gram-negative bacteria:

The MIC assays against several resistant and multidrug-resistant Gram-negative clinical isolates was studied in collaboration with Prof. Jordi Vila and carried out by Xavi Vila in the Barcelona Centre for International Health Research in the Hospital Clinic.

Strains of *E. coli* and *P. aeruginosa* with resistance to quinolones, carbapenems and other commonly used antibiotics were tested for several of our most promising compounds (Table 12). The MIC results obtained proved that these compounds were even more active than to regular ATCC bacteria strains, with many MIC values in the submicromolar range (0.5 µg/mL). It is worth mentioning that against an *E. coli* strain containing the enzyme New Delhi Metallo-beta-lactamase-1 (NDM-1) isolated from a traveller to India (Solé et al., 2011), with resistance to all β-lactam antibiotics (penicillins, cephalosporins, monobactams, and carbapenems), aminoglycosides and quinolones, the lipopeptides showed MIC values of <0.5-1 µg/mL.

Table 12: Antibacterial activity of the most promising polymyxin analogues against several resistant and multidrug-resistant Gram-negative strains. The MIC values are expressed as µg/mL.

		Gram-negative bacterial clinical isolates								
Peptide	<i>P. aeruginosa</i>					<i>E. coli</i>				
	ATCC	40b	36a	37a	38a	ATCC	MAC21a	VAL10	VAL5	NDM-1
8	2	4	16	4	0.5	2	0.5	0.5	0.5	0.5
9	1	2	8	0.5	1	4	1	0.5	0.5	0.5
10	4	4	32	4	16	2	2	1	1	1
11	--	--	<0.5	--	8	--	<0.5	<0.5	2	1
14	--	--	<0.5	--	32	--	<0.5	1	2	<0.5
17	--	--	<0.5	--	16	--	<0.5	<0.5	<0.5	<0.5

Resistance profile:
 ATCC: collection strain, 40b: carbapenem-resistant strain
 36a, 38a and NDM: highly-resistant strains, 37a: low-resistant strain,
 MAC21a, VAL10, VAL5: intermediate resistance to quinolones

Finally, the activity against several strains of *Acinetobacter baumannii* was also carried out. These multidrug-resistant bacteria, belonging to the ESKAPE pathogens, are responsible for increasing numbers of nosocomial infections, especially on patients with compromised immune systems (Peleg, et al., 2008). The particularity of the strains used for our peptides is that they are resistant to colistin, the parent compound of the analogues.

The MIC values obtained for the most promising peptides are depicted in Table 13. If we analyse the data, we observe that the peptides have a moderate or even high activity against the wild type strain but what is remarkable is that against two *in-vitro* mutants and several clinical isolates they show much better activities than colistin itself, and even good activities such as MIC values of 4-8 µg/mL.

These results make us think that these antimicrobials might have an alternative mechanism of action; their target might not be just the membrane of bacteria, as they have higher activities than colistin. This is the reason why much effort has been lately devoted in our group to study the mechanism of action of our peptides through different techniques, such as fluorescence, flow cytometry or transmission electron microscopy (Section A.3.).

Table 13: Antibacterial activity of the most promising polymyxin analogues against several strains of colistin-resistant *A. baumannii*. The MIC values are expressed as µg/mL.

Peptide	<i>Acinetobacter baumannii</i> strains								
	ATCC-wt	ATCC	77778	Ab10	Ab19	Ab21R	Ab24	CR49	CR86
Colistin	1	256	256	512	512	32	>256	64	128
8	8	64	256	32	32	--	--	--	--
9	2	16	128	16	16	--	--	--	--
10	4	32	128	8	16	--	--	--	--
11	--	--	--	--	--	8	4	16	8
14	--	--	--	--	--	32	16	64	32
17	--	--	--	--	--	32	128	128	256

Resistance profile:
 ATCC-wt: collection strain, low resistance
 ATCC: *in-vitro* mutant of collection strain with resistance to colistin
 77778: *in-vitro* mutant of a clinical strain with resistance to colistin
 Ab10, Ab19, Ab21R, Ab24, CR49 and CR86: clinical isolates resistant to colistin

A.3. STUDY OF THE MECHANISM OF ACTION

A.3.1. Biological membranes

Membranes are the fundamentals maintaining life through compartmentalization of cells and homeostasis. The membrane tightly controls transport and communication between the two inter- and intracellular spaces and a number of catalytic reactions are only supported in their vicinity.

In animal and bacteria alike, lipids are the primary constituents of membranes. They are amphipathic molecules possessing highly mobile fatty acyl chains and a polar headgroup. In an aqueous solution, hydrophobic forces from the acyl chain and hydrogen bonding with the headgroups often drive the formation of bilayered assemblies which maintain the hydrophobic acyl core between two polar regions at the interface with the aqueous phase.

Membranes are commonly described using the fluid mosaic model of Singer and Nicolson (Singer & Nicolson, 1972) (Figure 14), where proteins and glycoproteins are embedded in this lipid bilayer, either spanning its full width (integral proteins) or bound to the surface (peripheral protein), and where the lipids are in a fluid liquid crystalline state.

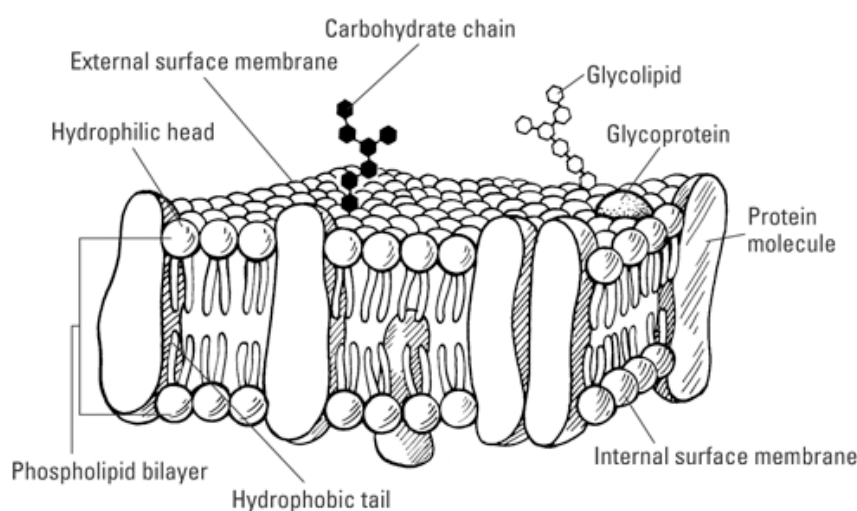


Figure 14: The Nicholson-Singer “fluid mosaic model”. It is the standard conceptualization of membrane architecture. Lipids self-assemble to form bilayers as a matrix in which proteins are embedded (Figure in the public domain).

Membranes differ significantly in their lipid composition as well as in their protein/lipid ratio (Figure 15). The exact composition of a biological membrane depends strongly on its origin, i.e. the organism, the organ or tissue, the type of cell and the type of membrane in a particular cell. Among the various lipid classes in biological membranes the most abundant are glycerophospholipids and sphingolipids (glycolipids). Prokaryotic cytoplasmic membranes contain a high proportion of anionic lipids such as glycerophosphoglycerols (PG), cardiolipins (CL or di-PG), whereas these lipids are hardly found in mammalian cytoplasmic membranes. On the other hand, eukaryotic membranes possess a high proportion of zwitterionic lipids like glycerophosphoethanolamines (PE), glycerophosphocholines (PC), sphingomyelin (SM

or ceramide phosphocholines) and sterols, which are important for the dynamics, and integrity of the lipid layers (de Almeida, et al., 2003; Koronkiewicz & Kalinowski, 2004).

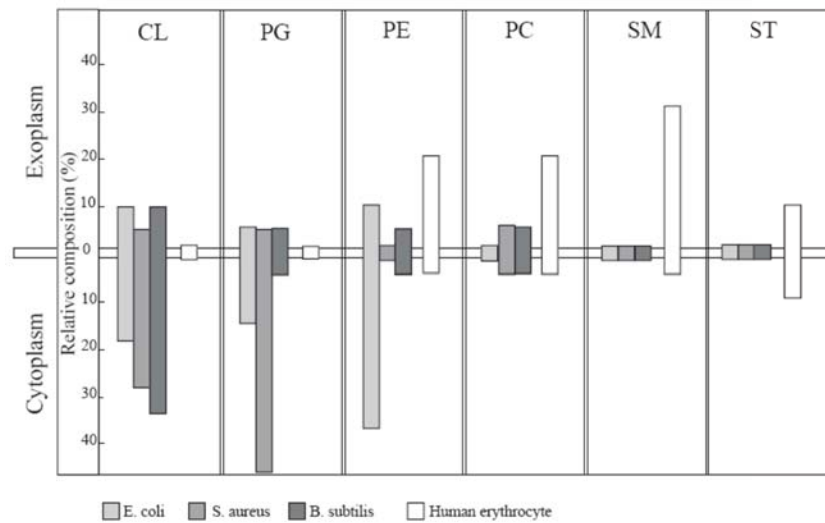


Figure 15: Comparison of the asymmetric lipid composition of cytoplasmic membranes of several bacteria and human erythrocytes. (CL) Cardiolipin, (PG) glycerophosphoglycerol, (PE) glycerophosphoethanolamine, (PC) glycerophosphocholine, (PE) glycerophosphoethanolamine, (SM) sphingomyelin, (ST) sterol. Adapted from: (Yeaman, 2003).

Bacterial membranes are also characterized through a highly asymmetric lipid charge distribution raising the well-known transmembrane potential. This electrical potential is necessary for several energy-dependent catalytic or transport processes. As illustrated in Figure 16, two membrane architectures prevail in bacteria. In Gram-negative bacteria, an outer membrane, rich in PG, lipopolysaccharide and magnesium, followed by a 2 nm thick peptidoglycan wall protects the cytoplasmic membrane. In the case of Gram-positive bacteria, a 20 to 40 nm thick peptidoglycan wall directly surrounds the cytoplasmic membrane.

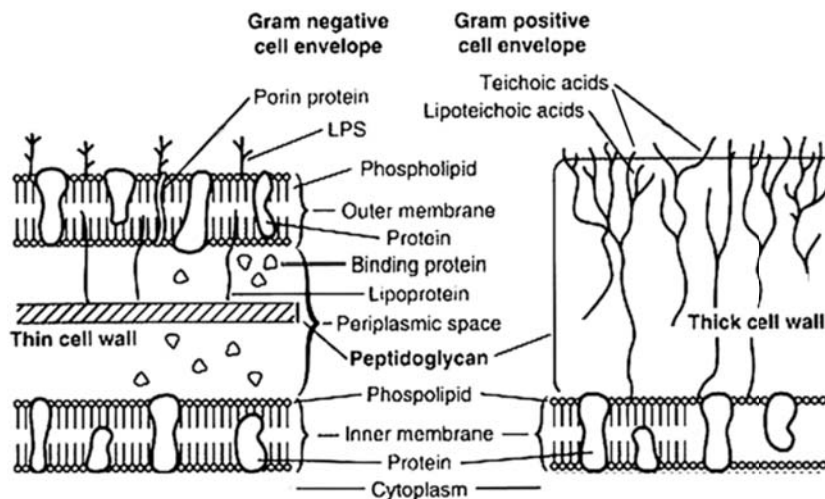


Figure 16: Comparison of the thick cell wall of Gram-positive bacteria (right) with the comparatively thin cell wall of Gram-negative bacteria (left). Adaptation of a figure in the public domain.

A.3.2. Biophysical studies

The mechanism of action of polymyxins and other AMPs is based on the interaction with the lipid component of the bacterial membrane (Zasloff, 2002). In order to study the mechanism of action of polymyxins against bacterial biological membranes, synthetic membrane models are used, as natural membranes have specific characteristics such as composition and asymmetry that difficult its reproduction in the laboratory (Zhang, 2001). With these simplified models the membrane lipid composition can be defined precisely and other factors, such as phase state, curvature and charge, which affect its stability can also be controlled. Therefore, facilitating the differentiation of the steps involved in the mechanism of action of polymyxins. The most extensively studied model membranes are monolayers (Brezesinski & Möhwald, 2003; Jelinek & Kulusheva, 2005; Maget-Dana, 1999; Verger & Pattus, 1982) and liposomes (Kinsky, 1970; Sessa & Weissmann, 1968; Sitaram & Nagaraj, 1999; Szoka & Papahadjopoulos, 1980; Wiese, et al., 2003).

A.3.2.1. Monolayers as model membranes, a tool to study peptide-lipid interactions

The most simple model membranes used to study the specific interactions produced between lipids and peptides or other biologically active molecules, are probably the phospholipid monolayers extended in the air/water interface of aqueous solutions, the thickness of which corresponds to that of a single molecule, and represent half of a cellular membrane (Jelinek & Kulusheva, 2005; Maget-Dana, 1999; Verger & Pattus, 1982).

The main advantage of this model front other more complex systems such as lipid bilayers, lays on the possibility of controlling the order of the molecules, modifying the molecular area and the superficial pressure of the monolayer. The data obtained by modifying these parameters offer valuable information about the interactions lipid-lipid, lipid-subphase or lipid-active molecule and even of the conformation of the studied molecules. Moreover, the lipid composition and exposed area are precisely known (Brockman, 1999).

Two types of monolayers can be distinguished depending on how they are formed (Gaines, 1966):

- **Gibbs adsorption monolayers:** The amphipathic molecules are introduced partially in water, the nonpolar part is in the exterior while the polar part stays in the interior, thus they are adsorbed in the air/water interface. This fact induces a decrease of the superficial tension of the solvent, establishing a dynamic equilibrium between the molecules of the surface and the rest of the solution and a continuous exchange between them.
- **Extension or Langmuir monolayers:** In this case, the amphipathic molecules, such as membrane lipids, insoluble in water, are deposited (solid or dissolved in a volatile solvent) on the surface of a polar liquid, forming a superficial film or extension monolayer. The nonpolar part of the molecule is responsible of the insolubility in the aqueous support and the polar part determines the orientation of the molecule respect the subphase, and is responsible of the extension.

The generally amphipathic character of antimicrobial peptides makes these compounds have superficial activity and, because their biological activity requires the interaction with the interfaces of lipid membranes, monolayers are perfectly suited for the study of their physicochemical and biological properties, as the experiments carried out in the

air/water interface give information about the flexibility and superficial activity of the molecules of study.

To characterize the interaction between the novel polymyxin synthetic analogues with bacterial membranes using lipid monolayers, **kinetics of penetration at constant area** were carried out. This technique is based in the measure of the superficial pressure by the Wilhemy method, which consists in the partial introduction of a platinum plate (Wilhemy plate) in the subphase, linked to an electrobalance that measures the force that the liquid exerts on the plate (Figure 17). The plate experiences gravitational forces, the surface tension towards the water and the counteraction force of floatability displacing the plate upwards from the water. If the dimensions of the plate are known, and the balance is calibrated, the force on the plate can be converted to superficial tension units (mN/m).

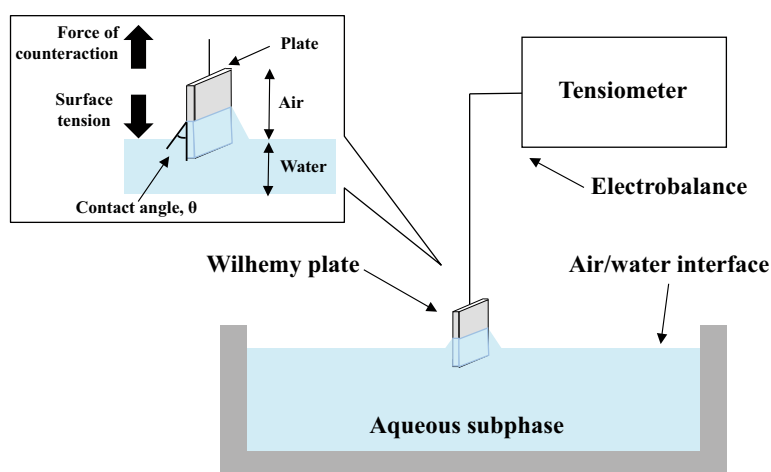


Figure 17: Scheme of the instrument used to measure superficial tension in the air/water interface.

The procedure consists in extending a monolayer using a solution of the lipid in an organic volatile solvent over the surface of a polar liquid. The surface pressure can be manipulated by adding more lipid and therefore modify the degree of packing of the molecules that form the monolayer. Once the monolayer is extended at the desired pressure, a solution of the peptide under study is incorporated in the subphase, to allow its interaction with the molecules forming the monolayer. If the peptide is inserted between the molecules of the monolayer or perturbs the lipid packing, the superficial pressure is modified, which is direct proof of an interaction of the peptide with this particular monolayer. The magnitude of these changes can be used to compare the degree of interaction between different peptides. The tracing of the changes in the surface tension versus interaction time, maintaining the area of the monolayer constant are known as kinetics of penetration at constant area (Figure 18).

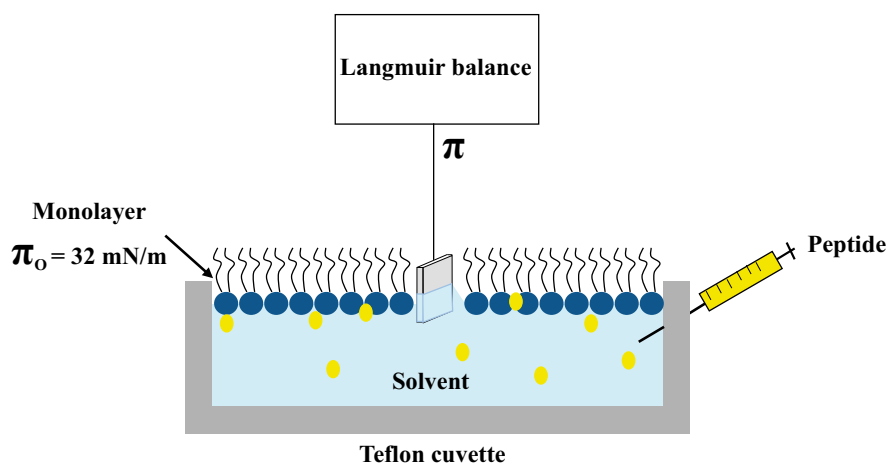


Figure 18: Scheme of the procedure for the measurement of the interaction of active molecules, in our case peptides, with the monolayers at a constant area.

A.3.2.2. Liposomes as model membranes, a tool to study peptide-lipid interactions

Liposomes were described for the first time in 1964 (Bangham & Horne, 1964) and consist in artificially prepared closed vesicles, the size of which varies from 20 nm to some micrometres. They are formed by one or more lipid bilayers, usually phospholipids, encapsulating a region of aqueous solution. Phospholipids are amphipathic molecules that in contact with water spontaneously self-organize forming bilayers, so that the polar part is exposed to the aqueous media while the hydrophobic regions, formed by the nonpolar chains of the fatty acids, are situated in the interior of the bilayer to avoid the contact with the media and therefore form a thermodynamically stable system (Figure 19) (Lasic, 1988; Szoka & Papahadjopoulos, 1980).

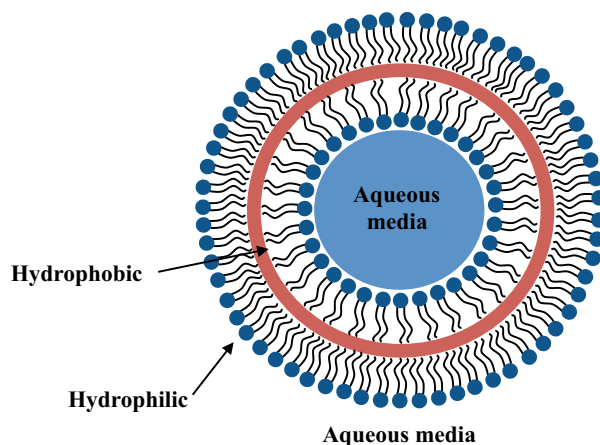


Figure 19: Schematic representation of the structure of a liposome, sphere-shaped vesicles consisting of one or more phospholipid bilayers.

The main biophysical application of liposomes is as model membranes, partially because their physicochemical properties have been largely studied. However, due to their morphology, they can be used to entrap materials such as drugs, either within the central aqueous compartment if they are water soluble, or within the membrane if they are oil soluble without altering the structure of the liposome. For this reason, they have

become an important tool in biological, pharmaceutical and medical research, as effective delivery systems to introduce different agents in the cells. Moreover, liposomal drugs show lower toxicity and by incorporating specific markers in the external monolayer, liposomes can be used to target particular diseased cells (Akbarzadeh et al., 2013).

Liposomes can be classified according to the number of bilayers and their size (Figure 20) (Vance and Vance, 1996, Laouini et al., 2012):

- **Unilamellar vesicles:** Formed by only one lamellae, 2 types can be distinguished:
 - **Giant unilamellar vesicles (GUVs):** The size of these vesicles varies from less than 1 μm to more than 20 μm , thus conferring them similar dimensions to that of bacterial cells.
 - **Large unilamellar vesicles (LUVs):** Their size oscillates between 50 to 500 nm. They have a surface pressure equivalent to that of biological membranes (30-32 mN/m) and present a lipid distribution between internal and external monolayer of approximately 1:1. They are the most studied model membranes to understand the physical, chemical and mechanistic properties of biological membranes. Their intra-vesicular volume is large enough to encapsulate water-soluble substances.
 - **Small unilamellar vesicles (SUVs):** Small-sized liposomes (20 to 100 nm) with a higher membrane curvature than LUVs, consequently less stable.
- **Multilamellar vesicles (MLVs):** Formed by various concentric lamellae (generally 7-19) separated by large aqueous spaces. Their size is very diverse (from 100 to 1000 nm) and they are rapidly obtained in polydisperse populations. Due to their particular structure their use is limited to the physical study of the organization of the bilayer they are not biomimetic models.
- **Multivesicular vesicles (MVVs):** Formed by closely packed non-concentric vesicles.

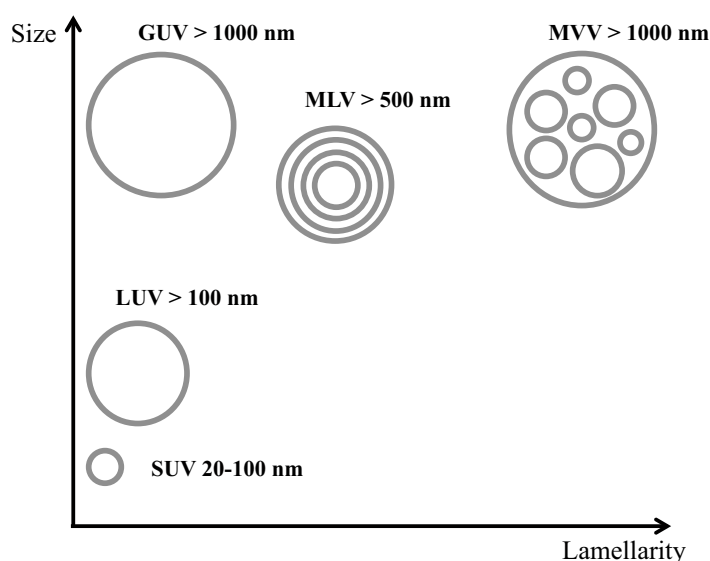


Figure 20: Scheme of the different types of liposomes according to size and lamellarity (SUV=Small unilamellar vesicle, LUV=Large unilamellar vesicle, GUV=Giant unilamellar vesicle, MLV=multilamellar vesicle and MVV=multivesicular vesicle).

Liposomes can be prepared in the laboratory by a great variety of methods, such as sonication (Gregoriadis, 1984), extrusion (Olson, et al., 1979), swelling (Needham & Evans, 1988), electroformation (Angelova & Dimitrov, 1986) or reverse-phase evaporation (Szoka & Papahadjopoulos, 1978), to mention some. All these methods are based in the spontaneous self-organization of the lipids in bilayers, and they all involve four basic steps: evaporation of the organic solvent to obtain a thin lipid film, dispersion of the lipid in aqueous media and mechanical agitation, purification of the resultant liposomes, and characterization of the final product (distribution, size, lipid concentration and/or lamellarity) (Lasic, 1988).

The liposomes used in this thesis are small and large unilamellar vesicles (SUVs and LUVs) obtained by high potency sonication or extrusion with filters of defined diameter pores.

Liposomes are perfect tools to study, in a simplified way, the processes of interest taking place in biological membranes. In the particular case of peptide-lipid interactions, there are many techniques available to characterize how a biologically active peptide exerts its action in the cellular membrane using liposomes, from classical biophysical techniques, to the latest developed techniques such as conical electron tomography (Zampighi et al., 2006) and surface plasmon resonance spectroscopy (Mozsolits & Aguilar, 2002; Papo & Shai, 2003).

In this thesis, to characterize the interaction between the novel polymyxin synthetic analogues with bacterial membranes using liposomes, which mimic the composition of the natural lipid portion of cellular membranes, a series of biophysical techniques were used, based in fluorescence and UV-Vis spectroscopy, which amplify the effect produced by small amounts of peptides in lipid membranes. By combining several of these techniques the effect of the peptides under study on membranes can be determined.

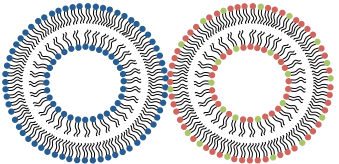
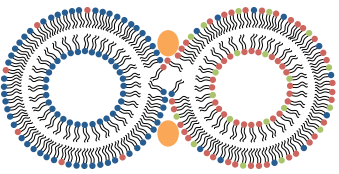
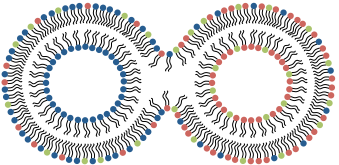
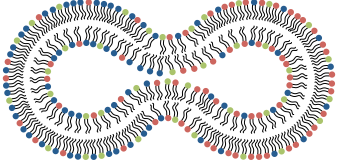
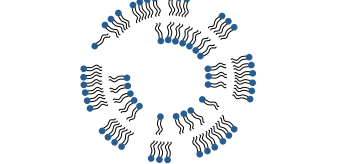
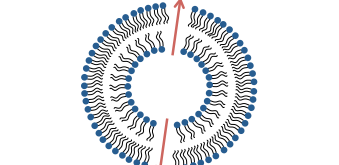
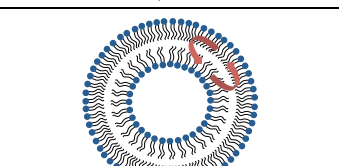
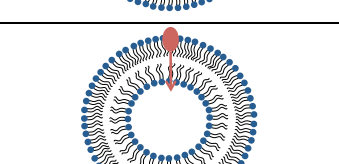
Fluorescence spectroscopy is a very sensible non-destructive technique that can be used to characterize molecules with fluorescence properties and to determine its interactions with other molecules or membrane models. Peptides can contain chromophore groups in their structure, such as the aromatic ring of the residue tryptophan, that absorb certain wavelengths and consequently the molecule is excited to a higher electronic state. When the excited electrons return to their fundamental state, the energy can be transformed into fluorescence. When using fluorescence techniques, 2 types of fluorescent labels or fluorophores can be used: **intrinsic**, the molecules present fluorescent properties, and **extrinsic**, fluorescent substances have to be incorporated to the analysed system. These labels should present the following characteristics: they have to be linked to a defined place in the molecule, the fluorescence should be sensible to the environment conditions and the labels should not affect the characteristics of the molecules that are being studied.

According to the property that has to be studied (Table 14), different techniques have been used, based in fluorescence, to obtain information about the effects of peptide binding on the properties of the lipid membrane:

- Determination of the union affinity of the peptides to the LPS using a displacement assay with dansyl-PxB.
- Properties of fluorescence emission of tryptophan: changes in the wavelength of emission and the intensity of fluorescence to study the incorporation of the

- peptides to the membrane.
- Quenching of Trp fluorescence to determine the insertion of the lipopeptides into the lipid membrane. Leakage and/or mixing of aqueous compartments due to leaky or non-leaky fusion (ANTS/DPX assay).
 - Fluorescence energy transfer to determine and differentiate the exchange processes of phospholipids (fusion, hemifusion or aggregation).
 - Formation of pyrene dimers in the excited state (excimers), to detect the mixing of lipids between membranes.
 - Reduction of fluorescence emission intensity of extrinsic NBD-groups by dithionite to determine the trans-membrane movement of phospholipids (flip-flop).
 - Protocols based in the anisotropy of fluorescence of labels incorporated in the membrane, to determine the influence of peptides in fluidity and transition temperature.

Table 14: Most used biophysical techniques to characterize the effect of a peptide under study on biological membranes. Some of the methods used in this thesis appear underlined.

Process	Scheme	Determination method
Aggregation <ul style="list-style-type: none"> Without lipid mixing Without permeabilization 		<ul style="list-style-type: none"> <u>Light scattering</u> Fluorescence energy transfer (NBD-Rh)
Liposome Mixing <ul style="list-style-type: none"> Selective exchange of external monolayers Without permeabilization Without flip-flop 		<ul style="list-style-type: none"> <u>Pyrene fluorescence</u> Fluorescence energy transfer (NBD-Rh), symmetric and asymmetric vesicles
Hemifusion <ul style="list-style-type: none"> Unspecific exchange of external monolayers Without permeabilization 		<ul style="list-style-type: none"> <u>ANTS/DPX</u> Fluorescence energy transfer (NBD-Rh), symmetric vesicles
Fusion <ul style="list-style-type: none"> Unspecific full mixing With or without permeabilization 		<ul style="list-style-type: none"> <u>ANTS/DPX</u> Fluorescence energy transfer (NBD-Rh)
Lysis <ul style="list-style-type: none"> Detergent effect Permeabilization 		<ul style="list-style-type: none"> <u>ANTS/DPX</u> <u>Light scattering</u> NBD/Dithionite Confocal microscopy
Channel formation <ul style="list-style-type: none"> Permeabilization Without lipid mixing Without aggregation 		<ul style="list-style-type: none"> <u>ANTS/DPX</u> Confocal microscopy (GUVs + calcein) Membrane depolarization
Flip-flop <ul style="list-style-type: none"> Transmembrane movement of phospholipids Without permeabilization Without fusion 		<ul style="list-style-type: none"> NBD/Dithionite
Translocation <ul style="list-style-type: none"> Without permeabilization Without lysis Without flip-flop 		<ul style="list-style-type: none"> Fluorescence energy transfer (Trp/lysoMC), symmetric vesicles Fluorescence confocal microscopy (labelled peptides)

A.3.2.3. Biophysical study of the polymyxin analogues

One of the main objectives of this thesis is to characterize the interaction of PxB and the synthesized polymyxin analogues with the lipid component of bacterial membranes by using membrane models that reproduce its composition.

The novel polymyxin analogues synthesized in this work should have the following characteristics:

- Interact with the model membranes and present a high affinity to LPS.
- Form molecular contacts between membranes, as previously seen for natural PxB (Cajal, et al., 1995), that give place to phospholipid exchange provoking changes in the specific composition of the membrane, necessary to maintain the homeostasis of the cell and therefore compromising the cellular viability.
- Show no lytic effect on model membranes of eukaryotic cells.

The liposomes used in this thesis were SUVs or LUVs prepared by sonication or extrusion, using the following synthetic phospholipid mixtures: pure POPG as a model of Gram-positive bacteria, POPE/POPG (6:4) to model Gram-negative bacteria and pure zwitterionic POPC to mimic the cytoplasmic membrane of eukaryotic cells (Epan, et al., 2008). In the case of monolayers, they were prepared using commercial LPS of the bacteria *Salmonella enterica* serotype Minnesota Re 595 (Re mutant), therefore modelling the external membrane of Gram-negative bacteria.

The sequence and antimicrobial activity against *S. aureus* and *E. coli* of the peptides used for the biophysical experiments are shown in Table 15. As previously reported in section A.2, peptides #1-7 are the most representative of the first series of peptides synthesized in the group. Peptides #8-11 have the best antibacterial activities so far, and have proved to be active even against multidrug-resistant bacteria. As positive control, commercial PxB was used and as negative control, peptides N, NN and 8N were synthesized. Peptide N corresponds to a control of the hydrophobic domain, as it has positions 6 and 7 of the cycle substituted by Gly residues, therefore is devoid of antibacterial activity. Peptide NN is a linear peptide that corresponds to a control of the cyclic structure, the Cys residues are substituted by Ser residues, therefore lacks the cyclic structure and consequently is devoid of antimicrobial activity. Finally, peptide 8N is the nonapeptide of peptide #8, therefore it lacks the fatty acid and Dab¹, it presents no antibacterial activity, but as seen for polymyxin B nonapeptide, we expect 8N to retain the ability to bind to the LPS.

Table 15: Sequence and antibacterial activity (MIC in $\mu\text{g/mL}$) of the peptides used in the biophysical experiments. The sequence of the cyclic lipopeptides is displayed in three-letter code, D-amino acids are denoted in italics and residues underlined denote bond formation.

Peptide	Sequence	Gram+	Gram-
		<i>S.aureus</i>	<i>E.coli</i>
PxB	6-methyl-octanoyl-Dab-Thr-Dab- <u>Dab</u> -Dab- <i>Phe</i> -Leu-Dab-Dab- <u>Thr</u>	>32	1
1	nonanoyl-Arg-Thr-Dab- <u>Cys</u> -Dab- <i>Phe</i> -Leu-Arg-Dab- <u>Cys</u>	16	4
2	decanoyl-Arg-Thr-Dab- <u>Cys</u> -Dab- <i>Phe</i> -Leu-Arg-Dab- <u>Cys</u>	16	8
3	dodecanoyl-Arg-Thr-Dab- <u>Cys</u> -Dab- <i>Phe</i> -Leu-Arg-Dab- <u>Cys</u>	4	8
4	nonanoyl-Arg-Thr-Dab- <u>Cys</u> -Dab- <i>Trp</i> -Leu-Arg-Dab- <u>Cys</u>	8	4
5	nonanoyl-Dab-Thr-Arg- <u>Cys</u> -Dab- <i>Phe</i> -Leu-Arg-Dab- <u>Cys</u>	8	2
6	decanoyl-Dab-Thr-Arg- <u>Cys</u> -Dab- <i>Trp</i> -Leu-Arg-Dab- <u>Cys</u>	8	8
7	decanoyl-Arg-Thr-Arg- <u>Cys</u> -Dab- <i>Trp</i> -Nle-Arg-Dab- <u>Cys</u>	4	8
8	decanoyl-Dab-Thr-Dab- <u>Cys</u> -Dab- <i>Phe</i> -Nle-Dab-Dab- <u>Cys</u>	4-8	1-2
9	dodecanoyl-Dab-Thr-Dab- <u>Cys</u> -Dab- <i>Phe</i> -Nle-Dab-Dab- <u>Cys</u>	4-8	4-8
10	decanoyl-Dab-Thr-Arg- <u>Cys</u> -Dab- <i>Phe</i> -Nle-Arg-Dab- <u>Cys</u>	4	2-4
11	dodecanoyl-Dab-Thr-Arg- <u>Cys</u> -Dab- <i>Phe</i> -Leu-Arg-Dab- <u>Cys</u>	4	4
N	nonanoyl-Arg-Thr-Dab- <u>Cys</u> -Dab-Gly-Gly-Arg-Dab- <u>Cys</u>	>32	>32
NN	nonanoyl-Arg-Thr-Dab-Ser-Dab- <i>Phe</i> -Leu-Arg-Dab-Ser (LINEAR)	>32	>32
8N	Thr-Dab- <u>Cys</u> -Dab- <i>Phe</i> -Nle-Dab-Dab- <u>Cys</u>	>32	>32

A.3.2.3.1. Determination of peptide binding to LPS

Lipid monolayers of LPS at constant area are a good model to study the interaction of the novel polymyxin analogues with the OM of Gram-negative bacteria (Maget-Dana, 1999). Insertion of the antibiotic peptides in the LPS monolayer at the air/water interface packed at around 32 mN/m, a pressure considered to be equivalent to the biological membranes (Marsh, 1996), is monitored as an increase in surface pressure versus time. The experiments were all carried in duplicate at 24 °C on a computer controlled monolayer system KSV5000.

The results obtained for peptides #1-7 are shown in Figure 21. We can observe that all the polymyxin analogues are capable of interacting with LPS, producing important increases on surface pressure, despite the high initial pressure (around 32 mN/m). However, great differences can be observed between the peptides. Peptides #3 and #4, have higher insertion levels than PxB while the rest of the peptides are below the level of natural PxB. Is surprising the response of the negative control N, this inactive peptide has a very high insertion level, much higher than PxB even though it lacks the hydrophobic domain. According to surface increases, the peptides can be ordered as follows: **N** > #4 > #3 > **PxB** > #5 > #1 > #6 > #7 = #2 > **NN**.

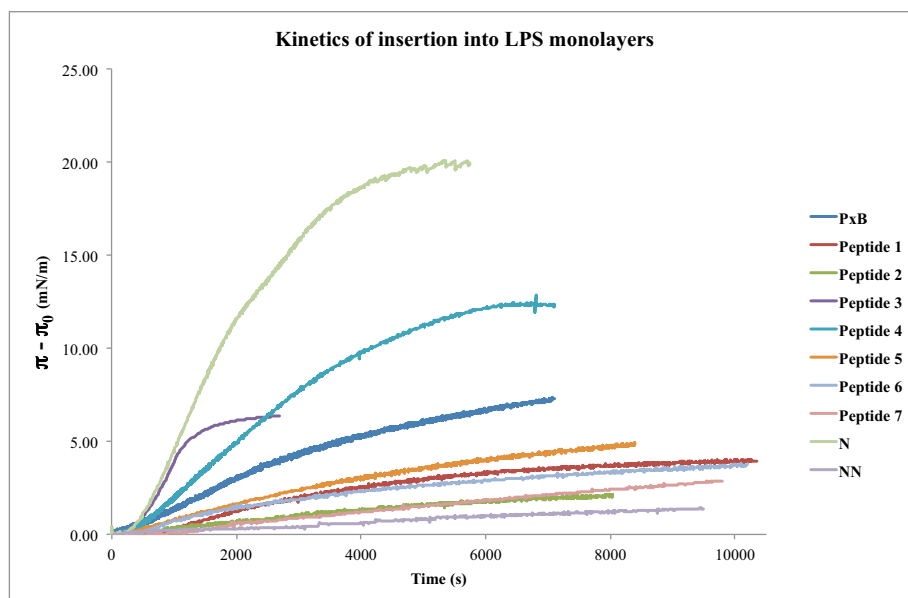


Figure 21: Graphic representation of the changes in surface pressure after the injection of PxB and the novel analogues in the aqueous subphase of a LPS monolayer.

To further investigate the results obtained, the interaction of the synthetic lipopeptides with the bacterial LPS from *S. minnesota* was quantified using the dansyl-polymyxin displacement assay (Fidai, et al., 1997). This method is based on the fact that the dansyl group fluoresces when located within a hydrophobic lipid environment, whereas it undergoes self-quenching in aqueous solution due to the displacement by membrane-bound species, in this case the synthetic lipopeptides added progressively (Figure 22). The results obtained with this assay for the novel polymyxin analogues are plotted in Figure 23 as percentage of inhibition versus peptide concentration (μM).

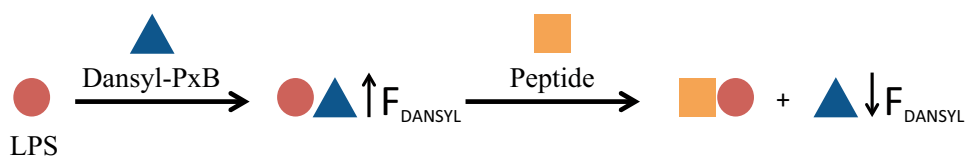


Figure 22: Schematic representation of the dansyl-polymyxin displacement assay, which is used to investigate the affinity of the lipopeptides with LPS.

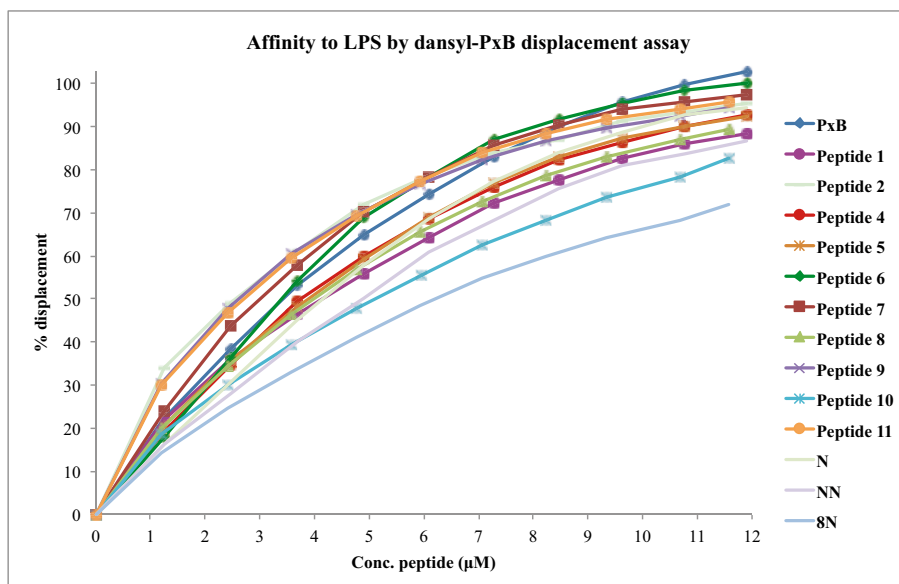


Figure 23: Graphic representation of the percentage of displacement of PxB and the synthesized lipopeptides obtained with the dansyl-polymyxin displacement assay.

In order to analyse the data obtained, the maximum displacement values of dansyl-PxB and the concentration necessary to displace the 50% of the fluorophore were calculated and compared to the values obtained for the increases in surface pressure 60 minutes after peptide injection in LPS monolayers (Table 16). The values obtained for PxB are consistent with those previously described in the literature (Moore, et al., 1986; Patrzykat, et al., 2002). As observed by the displacement values, all the studied analogues present the ability to displace the dansyl-polymyxin previously bound to LPS with similar affinity values. Peptides #2, 6, 7 and 11 demonstrated very high displacement values (> 95%), while the concentration required for 50% displacement were 4 µg/mL or less, making them the best LPS binders. However these don't correlate well with the values for insertion in LPS monolayers, where the peptides present sharp differences between them. As expected, the nonapeptide 8N, although it lacks the fatty acid and Dab¹ retains the ability to bind to LPS reaching a maximal 72 % of displacement.

With the data obtained, we can conclude that all the analogues present high affinity for LPS binding, a necessary first step for antimicrobial action. However, the insertion into monolayers at constant area not only measures the affinity of binding, but also depends on the cross-sectional area of the inserted molecule, which depends on each structure.

Table 16: Ability of PxB and the novel synthesized analogues to bind to LPS (I_{\max} = maximal displacement of dansyl-PxB by the various peptides compared to the displacement caused by non-dansylated PxB which is taken as 100%, IC_{50} = one-half of the peptide concentration required for maximal LPS binding.

Peptide	I_{\max} (%)	IC_{50} ($\mu\text{g/mL}$)	$\Delta\pi$ (mN/m)
PxB	100	4.0	5
1	88.5	4.5	2.5
2	95.2	3.0	1.2
3	--	--	6.4
4	92.7	4.7	9
5	92.3	4.5	3
6	100	4.2	2.1
7	97.4	3.5	1
8	89.4	4.2	--
9	94.2	2.8	--
10	82.6	5.8	--
11	95.8	3.0	--
N	94.2	4.4	18
NN	86.6	5.6	0.6
8N	71.9	5.3	--

A.3.2.3.2. Aggregation of vesicles induced by peptide interaction

In order to determine the interaction of the polymyxin analogues with the cytoplasmic membrane of bacteria, one of the initial stages was to study their capacity to induce vesicle aggregation. This was measured by adding the different cyclic lipopeptides to a mixture containing unilamellar liposomes and recording the increase in light scattering at 90° , a clear indicator that there is an increase in particle size (Zimmerberg, et al., 1993). If there was a lytic (detergent) effect there would be a decrease in turbidity due to destruction of the vesicles and formation of smaller sized particles.

The results obtained for peptides #1-11 with pure POPG liposomes are shown in Figure 24. The results had to be plotted in two different graphs as the experiments were carried out using two different instruments and cannot therefore be directly compared. However, in both cases peptide #7 and PxB were used as a value for comparison. What can be observed is that there is a clear increase in intensity with peptide concentration. The first series of peptides (#1-7) present a higher degree of aggregation than PxB, especially peptide #7, which induces the highest aggregation (in both graphs). In contrast, the second series of peptides (#8-11), present values similar or below to that of natural PxB. No aggregation was observed with liposomes of pure POPC (data not shown), which suggests that the polycationic peptides, like natural PxB, present selectivity towards anionic membranes. This selectivity is important to reduce the toxicity of the synthesized molecules.

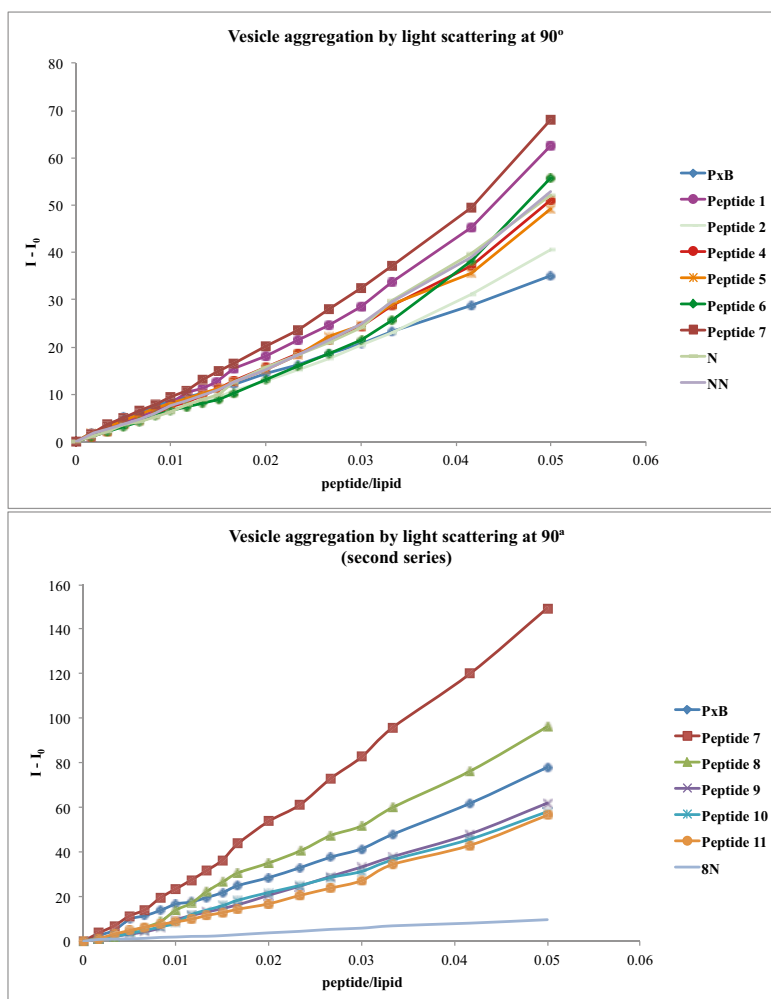
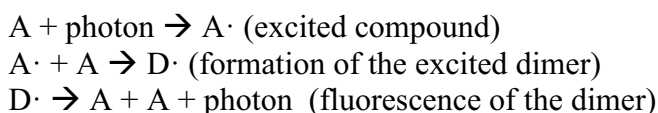


Figure 24: Graphic representation of the intensity of scattered light of the POPG vesicles due to aggregation by the first series of peptides #1-7 (upper graph) and to the second series of peptides #8-11 (lower graph). Peptide #7 and PxB were used in the second series as comparative peptides.

A.3.2.3.3. Lipid mixing between vesicles due to peptide interaction

In some cases an excited molecule can form a complex with another identical non-excited molecule, which can last until the excited molecule emits fluorescence. This complex (D) is denominated excimer and is recognized by the production of a new fluorescence band at a longer wavelength than that of the monomer:



A molecule with the capacity of forming dimers when excited is pyrene, which can be used to monitor lipid mixing. Briefly, the fluorescence intensity of pyrene-labelled phospholipids (donor vesicles) is dominated by the excimer band at 480 nm, on dilution with an excess of unlabelled phospholipids (acceptor vesicles), the intensity of the monomer band, at 395 nm, increases (Figure 25).

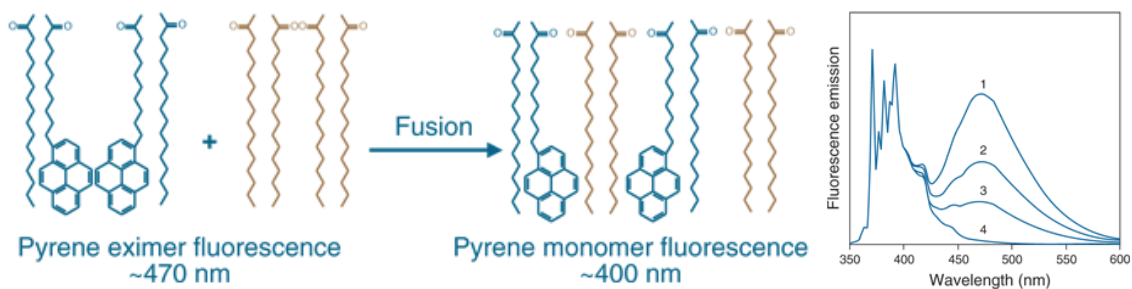


Figure 25: Schematic representation of a lipid-mixing assay based on pyrene excimer formation. The excimer fluorescence is diminished upon fusion of labelled membranes with unlabelled membranes, monitored by following the increase in the ratio of monomer (~400 nm) to excimer (~470 nm) emission, with excitation at about 340 nm. From: www.lifetechnologies.com.

The results obtained for the three lipid compositions, namely POPG, POPE/POPG (6:4) and POPC, are summarized in Figure 26. Both PxB and the synthetic lipopeptides show selectivity for anionic vesicles, inducing fast exchange of pyr-PG in a concentration-dependent manner, whereas none of the peptides induced significant lipid mixing from zwitterionic PC vesicles, even at high peptide concentrations. The extent of lipid mixing for the same peptide concentration is significantly higher in mixed POPE/POPG (6:4) vesicles, a lipid composition that is more representative of the Gram-negative bacterial membranes, than in POPG vesicles. The analogue #7 in both anionic lipid compositions (POPG and POPE/POPG) is the most effective lipopeptide in inducing mixing, probably due to the presence of 3 arginine residues compared to the rest of the lipopeptides only containing 1, 2 or none. As seen for the light scattering experiments, the first series of peptides #1-7, present higher degree of lipid mixing than PxB while the second series #8-11 are below the level of natural PxB. It is interesting that both negative controls N and NN do induce lipid mixing, even if they lack the hydrophobic domain in positions 6 and 7 or the cyclic structure respectively. Contrarily, the nonapeptide analogue (8N) presents low values both in lipid aggregation and exchange.

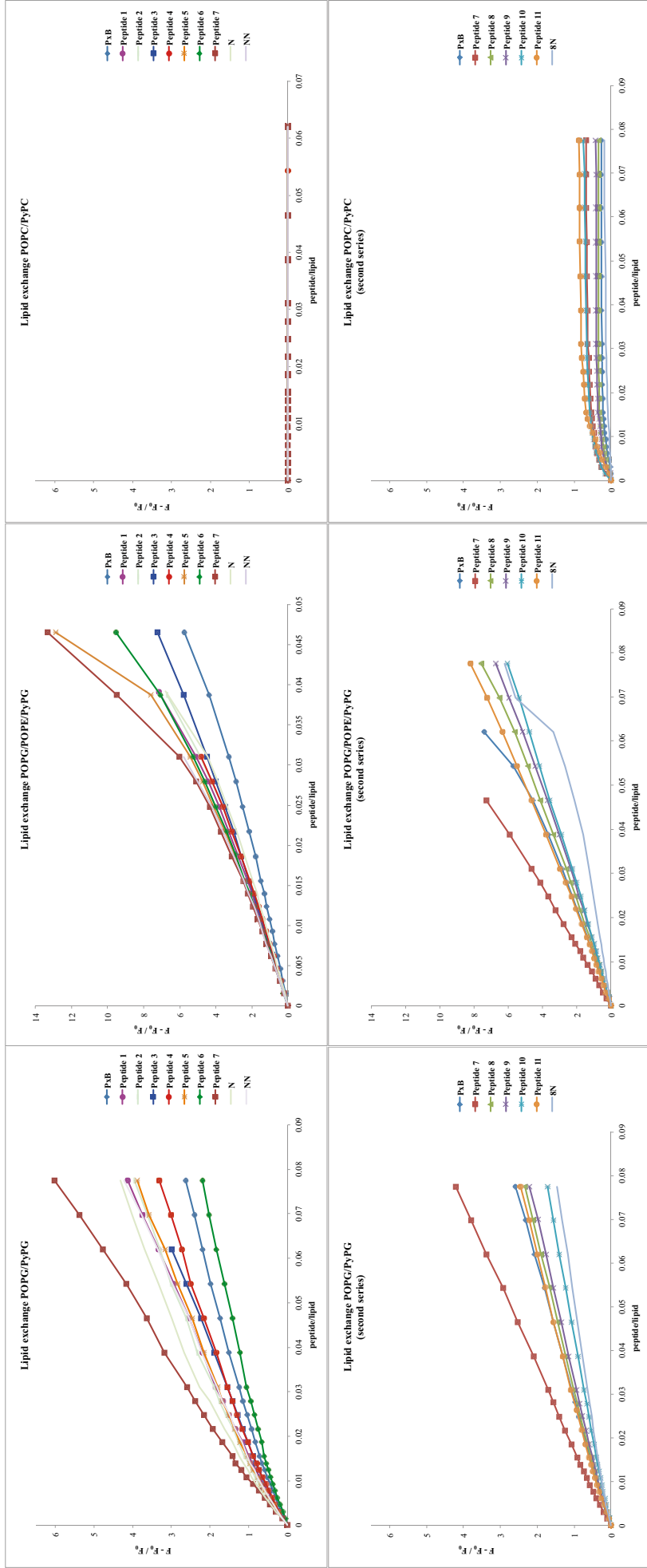


Figure 26: Graphic representation of the mixing of lipids directly monitored as the change in the fluorescence intensity of pyrene-labelled phospholipids on dilution with unlabelled phospholipids.

A.3.2.3.4. Permeabilization of the lipid membrane induced by peptide interaction

Membrane permeability due to lipopeptide binding was assessed by the ANTS/DPX leakage assay. This assay consists in co-encapsulating in liposomes of different lipid composition the aqueous dye ANTS and the cationic quencher DPX. If the peptide is capable of destabilizing the membrane producing the leakage of the probes to the media, dilution of the probes will result in an increase in fluorescence emission of ANTS (Figure 27) (Ellens, et al., 1985).

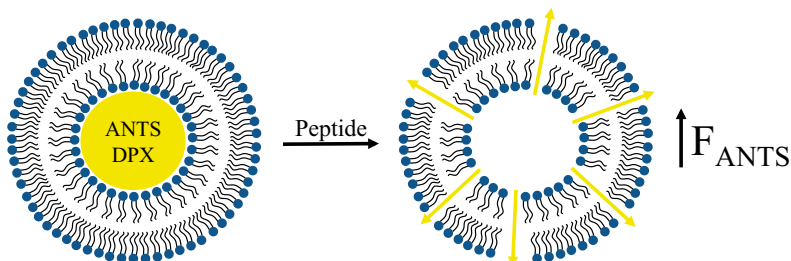


Figure 27: Schematic representation of the ANTS/DPX fusion assay for leakage or mixing of aqueous compartments.

As show in Figure 28, all the lipopeptides induce leakage from anionic vesicles, with efficiencies depending on liposome composition. Peptide #7 induces permeabilization of POPG liposomes from very low peptide/lipid mole ratios (Figure 28, upper). Leakage is very fast upon addition of the peptide and reaches a constant value until a second aliquot is added, thus suggesting that the peptide is irreversibly bound in an all-or-nothing type of permeabilization. In contrast, the other analogues do not induce significant leakage ($< 5\%$) at peptide/lipid ratios below 0.02:1, very similar to PxB. Increasing the peptide concentration results in leakage but always lower than for the same concentration of analogue #7. All lipopeptides are very effective in inducing leakage from mixed POPE/POPG (6:4) liposomes (Figure 28, lower), with a dramatic and almost linear increase in permeability at peptide-to-lipid ratios above 0.03. Leakage from POPC vesicles is very low in all analogues, although there is some detectable permeabilizing effect of less than 10%, that tends to saturate at low peptide/lipid mole ratio (data not shown).

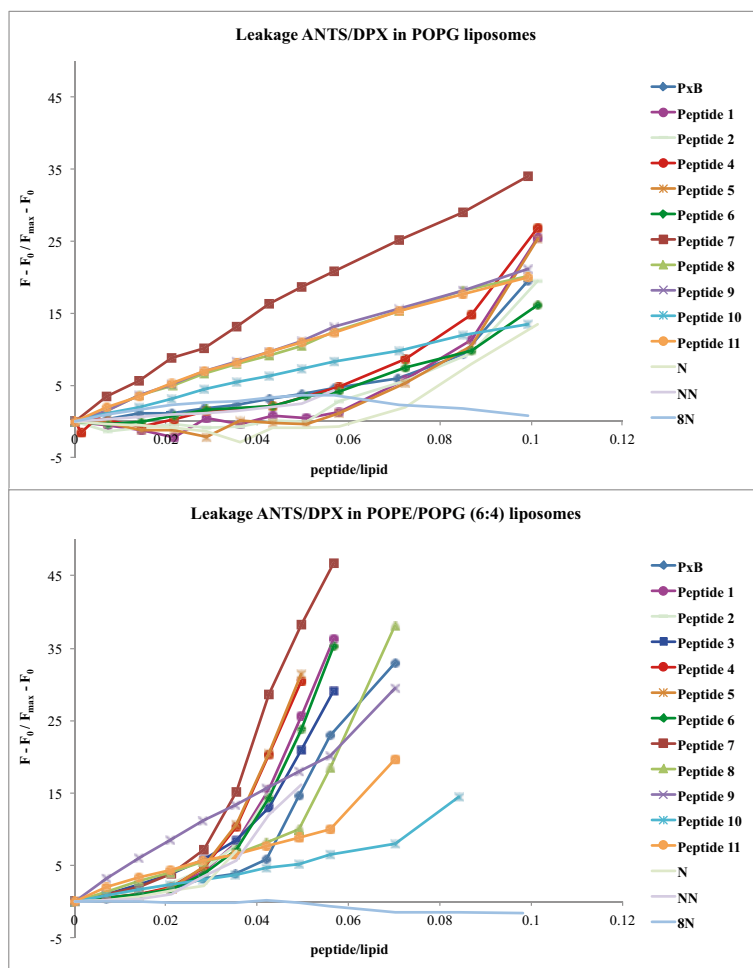


Figure 28: Graphic representation of the leakage of the dye ANTS co-encapsulated in liposomes of POPG (upper) and POPE/POPG 6:4 (lower).

A.3.2.3.5. Determination of the fluidity of the membrane by fluorescence polarization

Polarized light striking a fluorescent molecule results in polarized fluorescence, this polarized emission gradually returns to unpolarized fluorescence depending on rotational diffusion or other factors (Figure 29). Therefore, fluorescence polarization can be used to determine the binding state and microenvironment of fluorophores (Shinitzky & Barenholz, 1978).

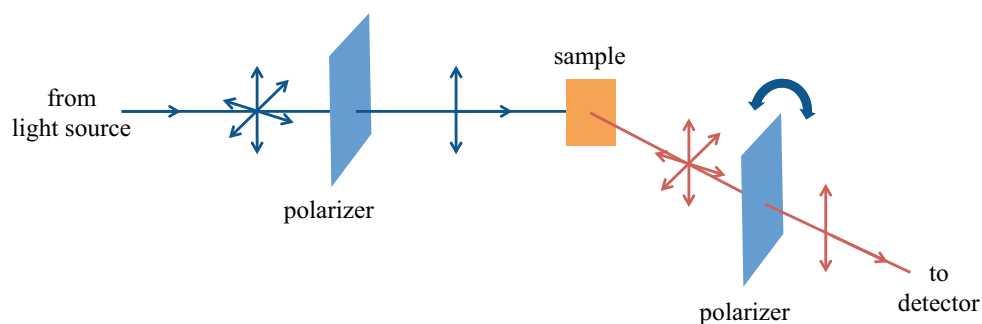


Figure 29: Illustration of the basic principle employed in conventional fluorescence polarization studies.

Fluorescence polarization is defined as follows:

$$P = \frac{I_{Vv} - I_{Vh}}{I_{Vv} + I_{Vh}}$$

where V_v and V_h correspond to the excitation or emission polarizers situated parallelly and perpendicularly to the plane of polarized light respectively. Analysing the data in polarization (P) values can be difficult as these values are not additive, but anisotropy (r) values are, and they are in fact most commonly used in this technique. The relationship between P and r is given by $r = 2P/(3-P)$ and therefore anisotropy can be calculated as follows:

$$r = \frac{I_{Vv} - GI_{Vh}}{I_{Vv} + 2GI_{Vh}}$$

Anisotropy values were corrected automatically using the correction factor G, to avoid the influence of the detection system:

$$G = \frac{I_{Hv}}{I_{Hh}}$$

The fluorophores used to label the liposomes in the polarization studies were: **DPH**, **TMA-DPH** and **NBD-PE** (Figure 30). These compounds are very sensible to the lateral mobility of the membrane where they are situated, and with the exception of NBD-PE, they are practically non-fluorescent in aqueous media while when attached to the lipid membrane they present high fluorescence.

DPH due to its hydrophobic character is situated specifically in the non-polar zone of liposomes, mostly parallel to the fatty acid chains (Kaiser & London, 1998; Lentz, 1993). Therefore, changes in DPH anisotropy reflect changes in the mobility of the hydrocarbon chains of the fatty acids (van Ginkel, et al., 1989), allowing the observation of lipid phase changes. When the bilayer is in a gel phase, the mobility of the phospholipid molecules is lower, therefore DPH has a lower rotational freedom in the excited state, and consequently the fluorescence emission is highly polarized. As the temperature increases, and the liquid crystal state is reached, the lateral mobility of the phospholipids in the membrane and the oscillation of DPH increases and in consequence the polarization diminishes. This decrease is abrupt closer to the transition temperature from gel to liquid crystal (T_m). TMA-DPH is a compound derived from DPH that is anchored to the water/lipid interface due to the presence of a charged group trimethylammonium granting a more polar character to the molecule (Lentz, et al., 1996). Finally, NBD-PE is an indicator of mobility of the hydrophilic region formed by the polar heads of the phospholipids that form the bilayer, as the fluorophore NBD is covalently linked to the polar head of phosphatidylethanolamine (Lentz et al., 1996).

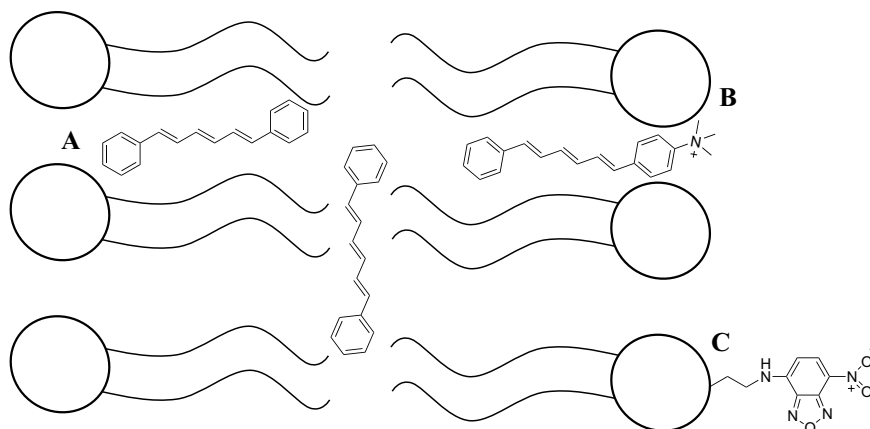


Figure 30: Chemical structure and localization in the lipid bilayer of the probes used in the fluorescence polarization experiments: (A) DPH, (B) TMA-DPH and (C) NBD-PE.

The effect of different concentrations of PxB on the mobility of the phospholipids and the gel-to-liquid crystal phase transition was previously studied in our group by steady-state anisotropy using DPH, TMA-DPH and NBD-PE (Clausell et al., 2003). The results obtained proved that PxB exists in two forms at the interface depending on the concentration. At low peptide concentrations, PxB remains in the outermost part of the membrane and therefore no big changes in microviscosity are observed. While, at high concentrations (over 2 mol%), PxB promotes membrane fusion, inserting deeply in the bilayer and therefore a strong effect on phase properties is observed.

Based in these experiments, we decided to study the effect of the most active polymyxin analogue synthesized in this thesis (#8), on the viscosity of anionic membranes (vesicles of POPG and POPE/POPG) using DPH and TMA-DPH. NBD-PE was not used in these experiments because we already know by previous experiments that these lipopeptides promote vesicle-vesicle contacts and exchange of phospholipids (see Sections A.3.2.3.2 and A.3.2.3.3) but will be used in FRET experiments (see A.3.2.3.6.4.).

Briefly, steady-state anisotropy measurements were conducted in the spectrofluorimeter with L-format polarizers. Labelled vesicles with 1% of the desired probe were mixed with the peptide in 10 mM Tris, and anisotropy was automatically measured by the instrument. For each sample a heating cycle from 10 to 30 °C, at 1 °C intervals allowing for thermal equilibration, was conducted. Additional measurements of vesicles titrated with the peptide at a constant temperature were carried out.

The effect of the binding of peptide #8, our most promising peptide, on the dynamics of the fatty acyl chains in the hydrophobic core region of the bilayers, reported by the DPH probe, is shown in Figures 31 and 32. As shown in Figure 31, DPH anisotropy in the absence of the peptide is relatively high at low temperatures, for example $r = 0.138$ at 15 °C in POPG vesicles, thus suggesting a quite restricted rotation for the probe. Increasing the temperature results in a decrease of anisotropy, due to rotational depolarization as the microviscosity of the membrane decreases and above 27 °C anisotropy has very low values ($r < 0.1$). At P/L = 0.02, a concentration which we have previously seen that there is lipid exchange and the permeability remains relatively low, a slight increase in the r values is observed, especially at high temperatures. For example, at 30 °C, r increased from 0.09084 to 0.1002, thus suggesting that the peptide slightly penetrates in the hydrophobic core of the bilayer. The same experiment was carried out using liposomes of POPE/POPG (6:4, mol/mol), model of Gram-negative

bacteria, and similar results were obtained. When measuring anisotropy in the absence of peptide, high DPH anisotropy values are obtained at low temperatures, while a decrease in anisotropy with temperature is observed. When adding Peptide #8 and PxB to the mixture, at this peptide concentration very small changes in anisotropy were observed. For example, at 30 °C anisotropy values increased from 0.1076 to 0.1153 and 0.1162 for peptide #8 and PxB respectively.

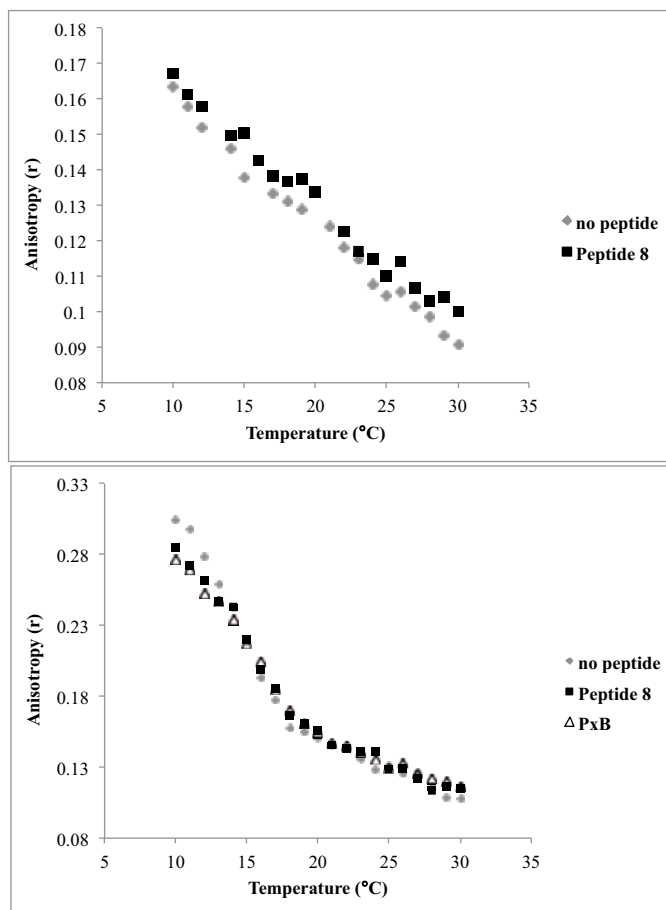


Figure 31: Temperature dependence of the steady-state-fluorescence anisotropy of DPH-labelled vesicles of POPG (upper) and POPE/POPG (lower). Peptides added at a P/L = 0.02, experiments were done in triplicate and the error was lower than 5%.

The change in DPH anisotropy as function of peptide/lipid mole ratio is shown in Figure 32. We can observe that the DPH anisotropy increases above 0.02 peptide/lipid concentration, but no big differences are observed by changing the experiment temperature, only general higher r values at low temperature. In the case of POPE/POPG liposomes, at 30 °C peptide #8 causes an increase in r values, indicating that the peptide inserts in the lipid membrane and reduces the fluidity of the lipid matrix, an effect that is practically non-existing upon PxB binding. In contrast, at 10 °C, a temperature in which the lipid membrane is more tightly packed, the opposite effect is observed, with a pronounced and concentration-dependent decrease in anisotropy, clearly indicating a fluidification of the membrane.

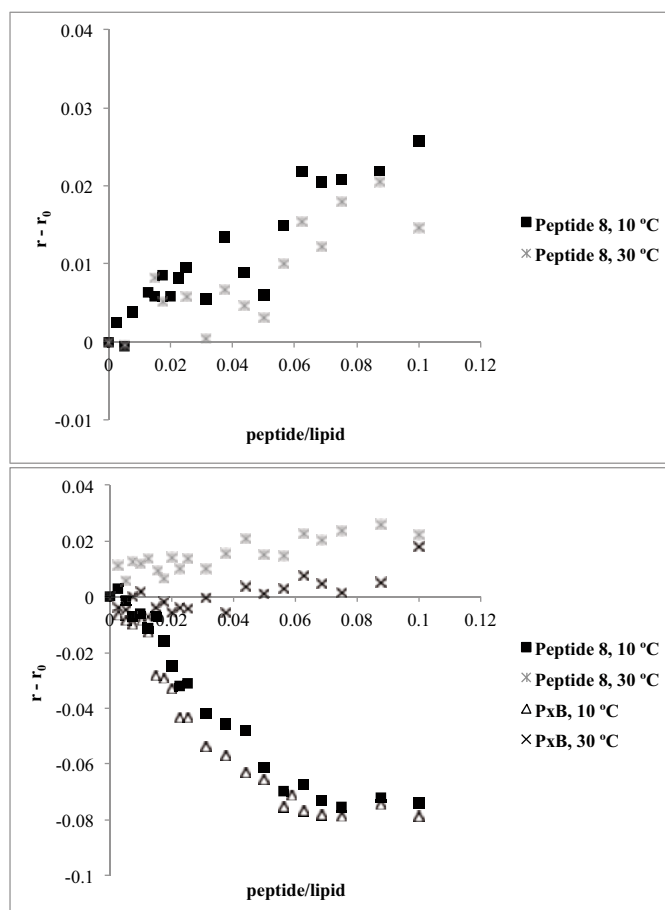


Figure 32: Steady-state fluorescence anisotropy of DPH in POPG (upper) and POPE/POPG (lower) vesicles as a function of peptide/lipid ratio.

These results suggest that peptide #8 has different behaviour depending on the lipid environment and the lipid phase. POPG vesicles (a model of Gram-positive bacterial membranes) have a gel-to-liquid crystal transition temperature at around -5 °C, and so they are in a fluid state at the temperatures of the experiment. Mixed POPG/POPE (4:6) vesicles (a model of Gram-negative bacterial membranes) undergo the main phase transition at 19.4 °C (Pozo Navas et al., 2005), and therefore they are in rigid state at 10 °C, and in a fluid state at 30 °C.

Lipid mobility was reduced in the region closest to the glycerol backbone of the POPG membranes, as deduced from the higher r values of the TMA-DPH probe compared to r values for DPH at the same temperatures (Figure 33). Binding of peptide #8 did not modify lipid order in this region, indicating that, at this concentration, the peptide does not modify the microfluidity of the lipid matrix at this level of the bilayer.

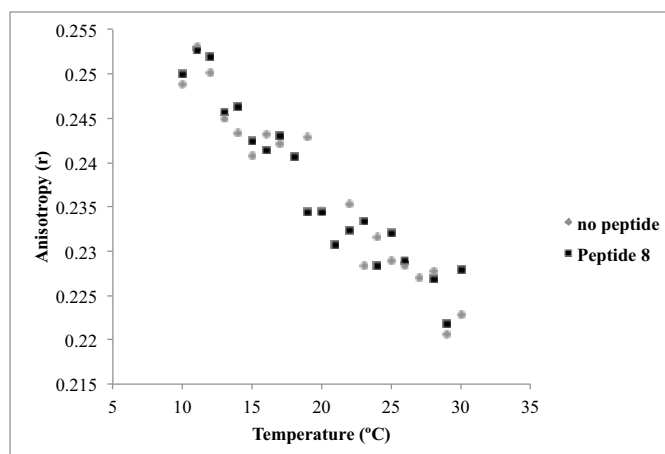


Figure 33: Temperature dependence of the steady-state-fluorescence anisotropy of TMA-DPH-labelled vesicles of POPG. Peptide was added at a P/L = 0.02, experiments were done in triplicate and the error was lower than 5%.

Experiments at a fixed temperature showed that the peptide does not rigidify the chains of the fatty acid, as no increase in the anisotropy values is observed (Figure 34). While in the case of PxB, we can observe a concentration dependent increase in anisotropy, especially at high peptide concentration, from P/L 0.04.

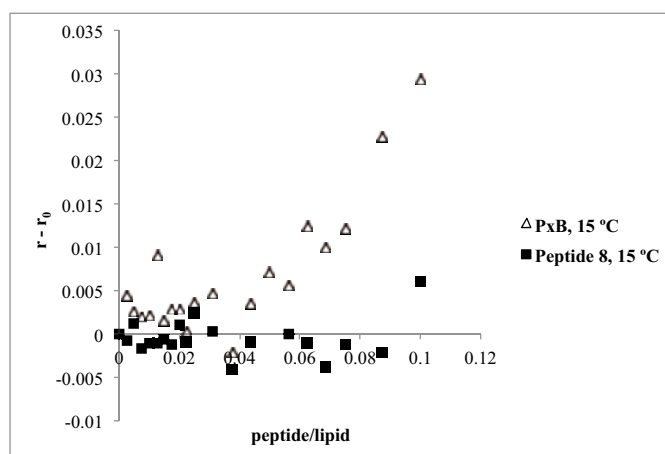


Figure 34: Steady-state fluorescence anisotropy of TMA-DPH in POPG vesicles as a function of peptide/lipid ratio.

These results seem to suggest that peptide #8 insertion in POPG vesicles occurs without significant changes in membrane fluidity, but in mixed POPG/POPE vesicles insertion affects the state of membrane lipids in a way that depends on the lipid phase.

A.3.2.3.6. Tryptophan fluorescence measurements

To further investigate the behaviour of the synthesized peptides, a series of experiments based on the intrinsic fluorescence of the residue tryptophan, were carried out. The sequence of the peptides used, all containing a D-Trp residue in position 7 of the cycle, as well as their activities against representative Gram-negative and Gram-positive bacteria are depicted in Table 17.

Table 17: Sequence and antimicrobial activity (MIC in $\mu\text{g/mL}$) of the peptides used for the experiments based on the fluorescence of Trp. The sequence of the cyclic lipopeptides is displayed in three-letter code, D-amino acids are denoted in italics and residues underlined denote bond formation.

Peptide	Sequence	Gram+	Gram-
		<i>S.aureus</i>	<i>E.coli</i>
PxB	6-methyl-octanoyl-Dab-Thr-Dab- <u>Dab</u> -Dab- <i>Phe</i> -Leu-Dab-Dab- <u>Thr</u>	>32	1
4	nonanoyl-Arg-Thr-Dab- <u>Cys</u> -Dab- <i>Trp</i> -Leu-Arg-Dab- <u>Cys</u>	8	4
6	decanoyl-Dab-Thr-Arg- <u>Cys</u> -Dab- <i>Trp</i> -Leu-Arg-Dab- <u>Cys</u>	8	8
7	decanoyl-Arg-Thr-Arg- <u>Cys</u> -Dab- <i>Trp</i> -Nle-Arg-Dab- <u>Cys</u>	4	8

A.3.2.3.6.1. Modification of the emission spectra of tryptophan due to peptide binding

The fluorescence emission spectra of peptides #4, 6 and 7 in Tris buffer was recorded and a maximum at 350 nm was observed, indicating that the Trp residue is highly exposed to the solvent. When adding liposomes of different lipid composition, alteration of the fluorescence signatures of the lipopeptides was observed, as summarized in Table 18, indicating peptide binding.

Table 18: Tryptophan fluorescence properties of peptides #4, 6 and 7 in the presence of liposomes of POPG, POPE/POPG (7:3) and POPC at two different peptide/lipid molar ratios (0.02 and 0.005). (a) F is the peptide fluorescence intensity in the presence of liposomes at the wavelength of maximum emission, and F_0 is the fluorescence of the free peptide at 350 nm.

Conditions	λ_{max} (nm)			F/ F_0 (a)		
	4	6	7	4	6	7
Free peptide	350	350	350	--	--	--
POPG P/L = 0.02	335	335	336	1.07	1.15	1.64
POPG P/L = 0.005	336	336	337	0.89	0.96	1.45
POPE/POPG P/L = 0.02	336	335	335	1.09	1.19	1.06
POPE/POPG P/L = 0.005	337	337	336	0.96	1.07	0.96
POPC P/L = 0.02	344	343	345	1.06	1.08	1.05
POPC P/L = 0.005	337	338	339	1.21	1.23	1.34

The first important observation is that the three antimicrobial lipopeptides are able to bind to all three membranes, not only the anionic vesicles (POPG and POPE/POPG), but also the zwitterionic (POPC). However, there are important differences depending on the lipid composition, thus reflecting different environment for the Trp residues (Galla, et al., 1985) (representative spectra shown in Figure 35). Binding to anionic vesicles of POPG or POPE/POPG results in a blue shift of 15-16 nm of the emission maximum, indicating that the Trp residue is located in a more hydrophobic environment upon binding to the membrane. The blue shift is the same for the three lipopeptides and independent of the peptide-to-lipid ratio. In contrast, differences are seen in the emission intensity, with an important increase in the case of peptide #7 bound to POPG, whereas less significant increases are seen on binding of #4 and #6 to the anionic vesicles.

When observing the spectral changes of the three lipopeptides in the presence of POPC vesicles, in all cases it can be noticed that they show a gradual blue shift on the emission maximum that depends on the lipid concentration. At very low peptide-to-lipid ratios (0.005), when all the peptide is bound, there is a blue shift of 13, 12 and 11 nm for #4, 6 and 7 respectively, in all cases accompanied by an increase in the intensity of fluorescence emission. Increasing the P/L ratio results in smaller blue shift displacements and less significant changes in fluorescence intensity, probably due to an equilibrium between free and bound peptide forms, as also suggested by the presence of an isosbestic point (Figure 35, bottom).

Increasing the ionic strength by titrating the samples with NaCl (up to 350 mM) resulted in no backshift of the emission maximum, thus indicating that binding was not reversible (data not shown).

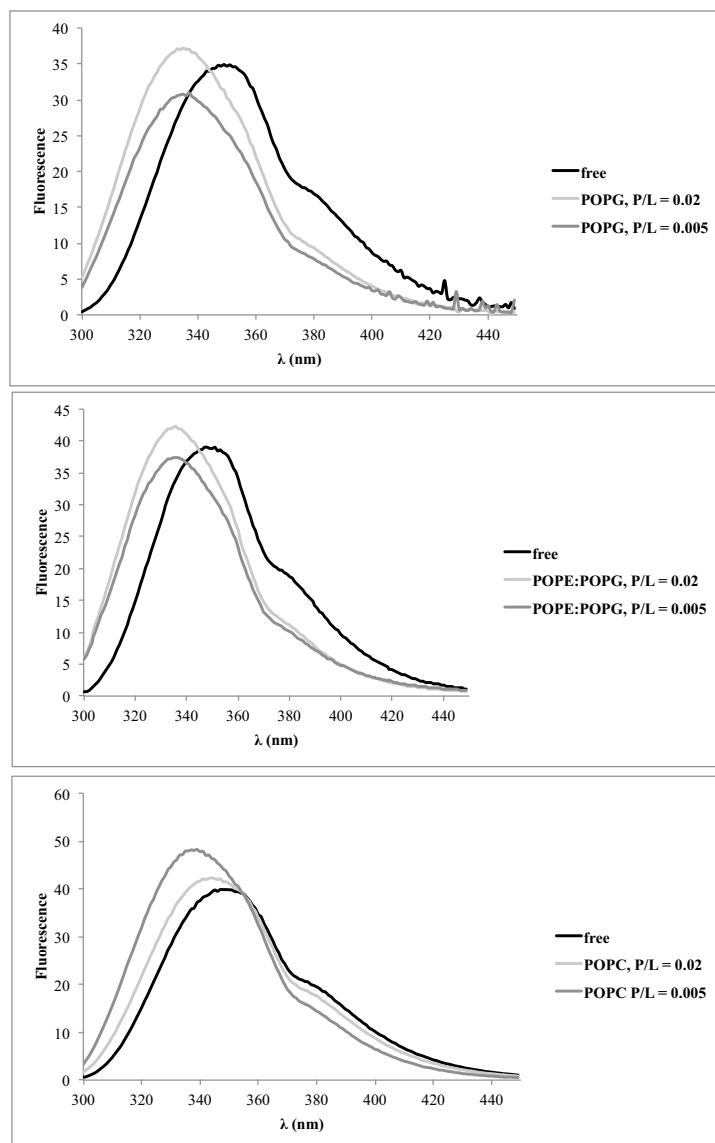


Figure 35: Tryptophan emission spectrum of peptide #4 in 10 mM Tris (pH 8.0) (black trace) and in the presence of liposomes composed of POPG (upper panel), POPE/POPG (7:3, middle panel), or POPC (lower panel). In all cases, the peptide/lipid molar ratios tested were 0.02 (light grey trace) or 0.005 (dark grey trace).

A.3.2.3.6.2. Tryptophan fluorescence anisotropy to determine peptide binding

The previous experiments are indicative that peptides #4, 6 and 7 are able to insert into anionic and zwitterionic lipid vesicles, although in different ways. We next determined the changes in anisotropy of tryptophan fluorescence upon binding (Table 19 and Figure 36).

Briefly, steady-state tryptophan fluorescence anisotropy measurements were carried out at 24 °C in the spectrofluorimeter with L-format polarizers. Each measure was done in duplicate, adding the vesicles to the desired final lipid concentration to a cuvette containing 10 mM Tris buffer (pH 8.0) and the lipopeptide under study. The fluorescence anisotropy (r) was calculated automatically by the software provided with the instrument, according to:

$$r = \frac{I_{Vv} - GI_{Vh}}{I_{Vv} + 2GI_{Vh}}$$

where I_{Vh} and I_{Vv} are the intensities of the emitted polarizer light with the emission polarizer parallel or perpendicular to the excitation polarizer. Anisotropy values were automatically corrected for dependencies in the detection system (G-factor correction, $G=I_{Hv}/I_{Hh}$).

The anisotropy values of the free lipopeptides are very low (Table 19), as expected from a free peptide of this size in solution, where Trp residue has a very high rotational freedom. Binding of the lipopeptides to anionic POPG vesicles results in an important increase in anisotropy, a clear indication that tryptophan is in a more restricted region due to intercalation of the lipopeptides between the phospholipids. The increase in anisotropy is almost complete at a peptide-to-lipid ratio below 0.01, thus suggesting that all the peptide is bound even at low concentrations of lipid. In the case of mixed PE/PG vesicles, results are very similar, with slightly lower values of anisotropy compared to pure POPG vesicles, but the same high efficiency. In the case of POPC vesicles, binding is more gradual, indicating lower binding affinity, although anisotropy values at high lipid concentration, when all the peptide is bound, are in the same range than in anionic vesicles, for example for lipopeptide #7, $r = 0.158$ when bound to POPG vesicles and 0.150 for POPC vesicles at the same peptide concentration (Table 19).

Table 19: Steady-state tryptophan fluorescence anisotropy values of peptides #4, 6 and 7, in the different conditions tested.

Conditions	Anisotropy (r)		
	4	6	7
Free peptide	0.028	0.033	0.033
POPG P/L = 0.02	0.137	0.165	0.126
POPG P/L = 0.005	0.170	0.185	0.158
POPE/POPG P/L = 0.02	0.126	0.126	0.130
POPE/POPG P/L = 0.005	0.132	0.142	0.128
POPC P/L = 0.02	0.114	0.102	0.100
POPC P/L = 0.005	0.135	0.200	0.150

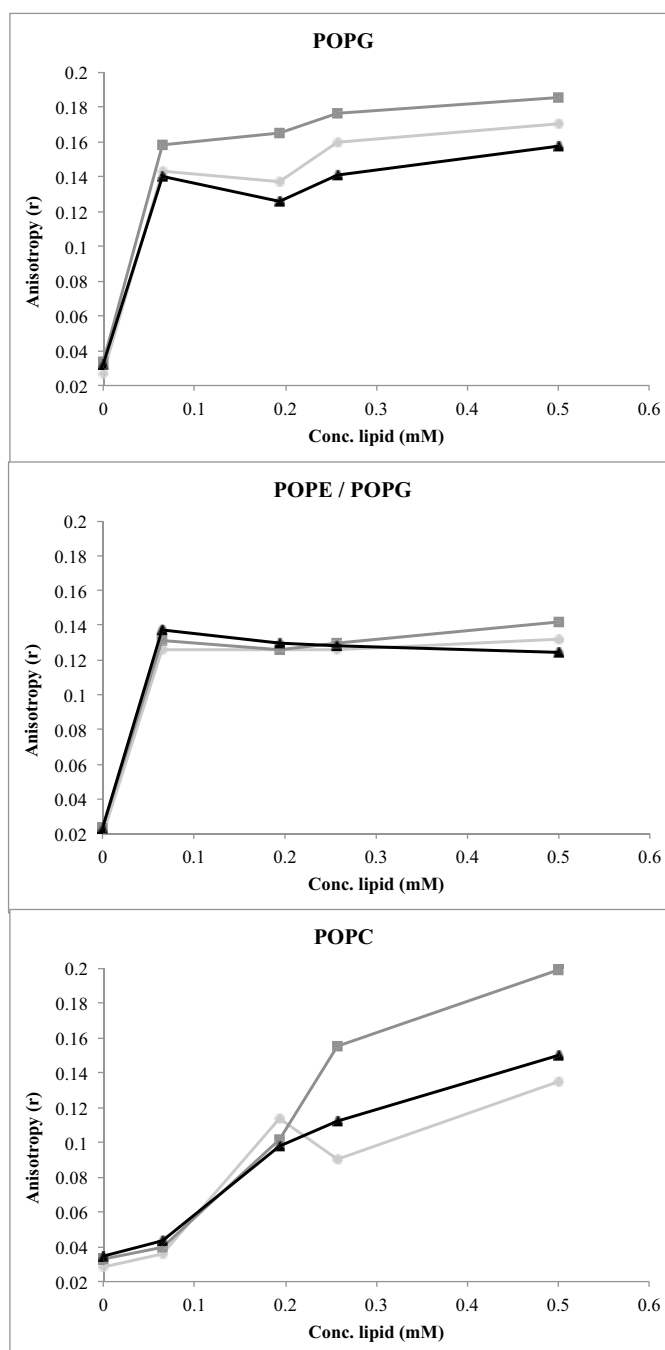


Figure 36: Fluorescence anisotropy change of the lipopeptides, #4 (light grey), #6 (dark grey), #7 (black), as a function of lipid concentration. Titrations were carried out at 24 °C, adding the lipid vesicles to a solution 3 μ M of the desired peptide in 10 mM Tris pH 8.0. Each point corresponds to a separate experiment.

A.3.2.3.6.3. Quenching of tryptophan fluorescence by acrylamide to determine peptide insertion

Results described in the previous section indicate that for peptide #4, 6 and 7, the Trp residue in position 7 intercalates into the hydrophobic part of the membrane. We next investigated to what extent this residue is exposed to the aqueous phase, by using the water-soluble quencher of indole derivatives acrylamide (Eftink & Ghiron, 1977; Rawat, et al., 2004; Zhao & Kinnunen, 2002).

Fluorescence quenching is a non-radiant energy transfer from excited species to other molecules, with a consequent deactivation of the excited state, resulting in a decrease in fluorescence intensity of the fluorescent species. For this experiment, the intrinsic fluorescence of the residue Trp is quenched by adding acrylamide with or without the presence of vesicles of different lipid composition while recording the fluorescence, and therefore analyse to what extent the residue is accessible (representative graph shown in Figure 37).

The Stern-Volmer quenching constants could be calculated with the results obtained by curve fitting using the following modified equation (Eftink & Ghiron, 1977).

$$\frac{F_0}{F e^{V[Q]}} = 1 + K_{SV}[Q]$$

where F_0 and F are the fluorescence intensities in the absence and presence of the quencher, $[Q]$ is the molar concentration of quencher and V and K_{SV} are the static and dynamic quenching constants, respectively.

The calculated constants are depicted in Table 20. We can observe that the free lipopeptides in solution show very high quenching constants, both dynamic and static, indicating that D-Trp is highly accessible to acrylamide. K_{SV} and V values for #4, 6 and 7 are very close, around 12 M^{-1} and 3 M^{-1} respectively. When the lipopeptides are bound to anionic liposomes of POPG, the quenching of Trp fluorescence by acrylamide becomes less efficient, for example for #4 at P/L = 0.005, K_{SV} and V values are 3.439 M^{-1} and 1.330 M^{-1} , and very similar quenching constants are obtained for #6 and 7. In agreement with anisotropy results (Figure 36), the accessibility of Trp for the lipopeptides bound to POPG vesicles is not depending on the peptide-to-lipid ratio. Results obtained with mixed POPE/POPG vesicles are also consistent with a high degree of shielding of the Trp residue from the aqueous solvent due to insertion in the bilayer, without significant differences with the insertion in POPG vesicles. Finally, for POPC vesicles at P/L of 0.02, the higher value of the K_{SV} constant, for example 7.545 M^{-1} for #4 and around 10 M^{-1} for #6 and 7, is indicative of a more exposed tryptophan, or more likely to an equilibrium between free and bound peptide. Increasing the lipid concentration (P/L = 0.005) favours peptide binding, with lower values of the collisional quenching constant.

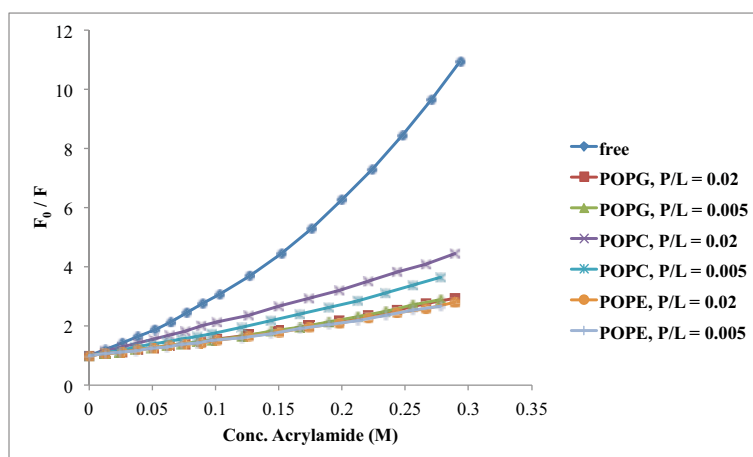


Figure 37: Acrylamide quenching of lipopeptide #7 in 10 mM Tris (pH 8.0).

Table 20: Acrylamide quenching constants (M^{-1}) for antibacterial peptides #4, 6 and 7. K_{sv} and V are the dynamic and static quenching constants respectively. Quenching constants were obtained by fitting of data according to (Eftink & Ghiron, 1977), with r^2 values always above 0.9998.

Conditions		Quenching constants (M^{-1})		
		4	6	7
Free peptide	K_{sv}	12.4	12.46	11.99
	V	2.867	2.878	3.04
POPG P/L = 0.02	K_{sv}	3.317	2.769	3.101
	V	1.396	1.719	1.524
POPG P/L = 0.005	K_{sv}	3.439	3.621	3.298
	V	1.338	1.335	1.477
POPE/POPG P/L = 0.02	K_{sv}	3.245	2.486	3.428
	V	1.283	1.483	1.152
POPE/POPG P/L = 0.005	K_{sv}	3.673	2.209	3.591
	V	1.073	1.283	1.049
POPC P/L = 0.02	K_{sv}	7.545	10.3	10.02
	V	0.7895	0.8885	0.4384
POPC P/L = 0.005	K_{sv}	3.535	6.939	5.69
	V	1.51	1.113	1.237

A.3.2.3.6.4. Fluorescence resonance energy transfer to determine peptide binding

The interaction of peptides with membranes can be monitored by FRET. This method is based on the nonradiative transfer of the excited state energy from a donor to an acceptor molecule. The extent of energy transfer depends mainly on the extent of overlap between emission spectrum of the donor and the absorption spectrum of the acceptor, and on the orientation and distance between them. The efficiency of the transfer decreases proportionally with the increase in distance between donor and acceptor.

The different results in Trp emission fluorescence of #4, 6 and 7 bound to PG vs. PC vesicles (Table 18) can be due to lower peptide binding to the zwitterionic vesicles or to a different form of the bound peptide depending on the charges at the interface. In order to distinguish these two possibilities, the binding of all three lipopeptides to vesicles containing 2.5% of NBD-PE was determined by the increase of fluorescence resonance energy transfer from the Trp donor of the peptide to the NBD acceptor at the interface (Figure 38).

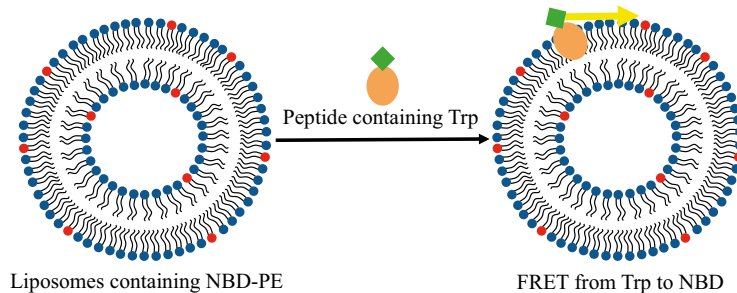


Figure 38: Schematic representation of the FRET from the Trp (donor) contained in the lipopeptides and the NBD (acceptor) in the lipid headgroup of 2.5% of NBD-PE used to prepare liposomes of different composition.

As shown in Figure 39, the FRET intensity at 535 nm increases with the amount of peptide added, and the higher increases correspond to the anionic POPG vesicles, where the FRET signal did not saturate even at very high peptide-to-lipid ratios, indicating a very efficient binding. The presence of POPE results in higher FRET for the same peptide-to-lipid ratio. For example, in #4 at P/L=0.05, the relative increase in fluorescence (δF) is 4.96 for the PE containing vesicles and 3.74 for pure PG vesicles. The synthetic antimicrobial peptides also show binding to POPC vesicles, with a small FRET signal that in this system saturates at P/L around 0.02 (Figure 29, bottom). When POPG-labelled vesicles were added to a premixed sample containing any of the lipopeptides with POPC vesicles, the FRET signal obtained was much lower than the one under the same conditions but without POPC (data not shown). For example, for #7 binding to POPG vesicles (33.3 μM) at P/L 0.02, δF is 1.6, but if the POPG vesicles are added to a mixture of POPC (33.3 μM) with #7 (0.66 μM), a much lower FRET signal is obtained (δF is 0.32), indicating that the lipopeptide is effectively bound to POPC.

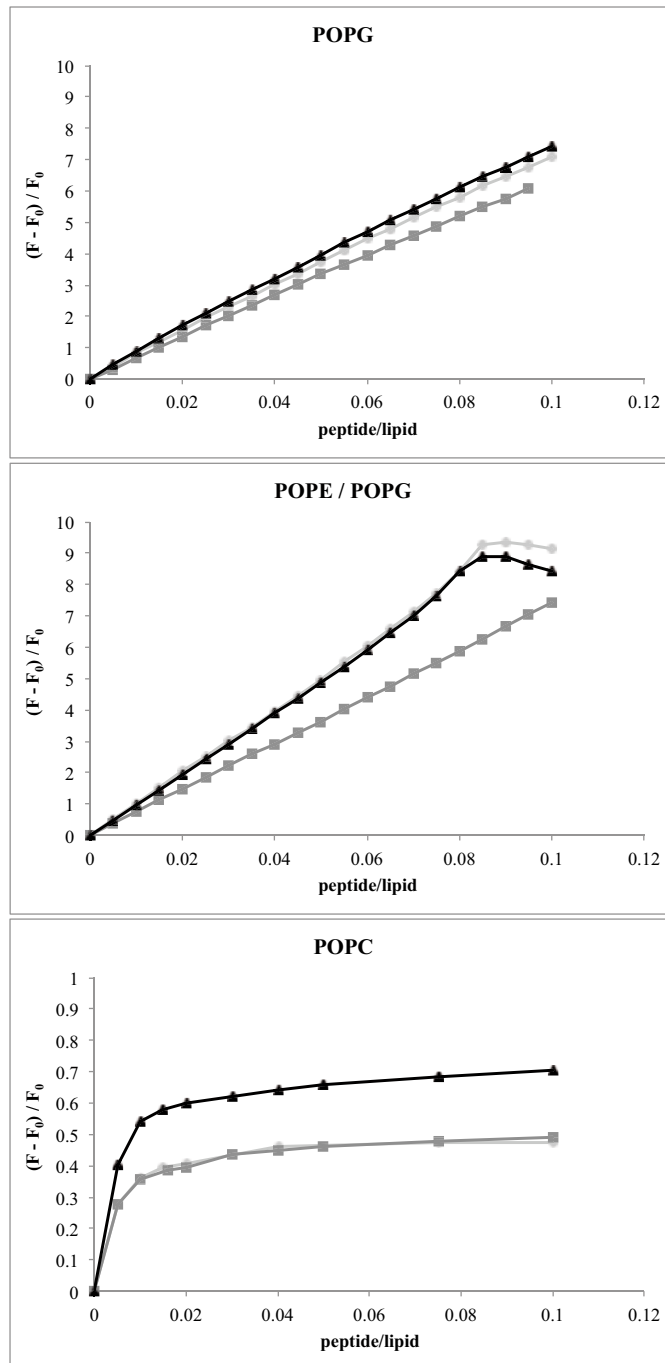


Figure 39: Change in FRET intensity resulting from the addition of lipopeptides to vesicles containing 2.5% NBD-PE. #4 (light grey), #6 (dark grey) and #7 (black).

A.3.3. Flow cytometry as a tool to determine the effect of the novel polymyxin analogues on bacteria

A.3.3.1. Fundamentals of flow cytometry

Flow cytometry is a quantitative analysis technology, which characterizes cell populations at single cell level as cells or particles, suspended in liquid, are illuminated by a laser beam. The intensity of the optical signals generated, which are scattering and/or fluorescence signals (in the case of using fluorescent dyes), is finally correlated to structural and/or functional cell parameters. FC has proved to be very useful for studying the physiological effects of antimicrobial agents on bacterial cells due to their effect on certain metabolic parameters (membrane potential, cell size, and amount of DNA) (Martinez, et al., 1982; Steen et al., 1982).

A simple flow cytometer works as follows: the hydrodynamic focusing gives rise to the formation of a single stream of particles in the flow cell. These cells pass through a laser beam and impact with the laser in a confined site, emitting different signals related to diverse cell parameters (Figure 40). Scattered and fluorescence emissions of each particle are separated by a group of filters and mirrors (optical system) according to certain wavelengths. Signals are collected by the detection system, which is formed by a collection of photodiodes. Finally, signals are sent to a computer obtaining a representation of the distribution of the population with respect to the different parameters.

The key feature of analytical flow cytometers is their ability to measure a very large number of particles (5000 cells per second in common cytometers and even up to 100000 cells per second or more in specialized instruments, although routinely, lower event acquisition rates are used) while measuring multiple cellular parameters on each cell simultaneously. Some flow cytometers are able to physically separate cell subsets (sorting) based on their cytometric characteristics (cell sorters).

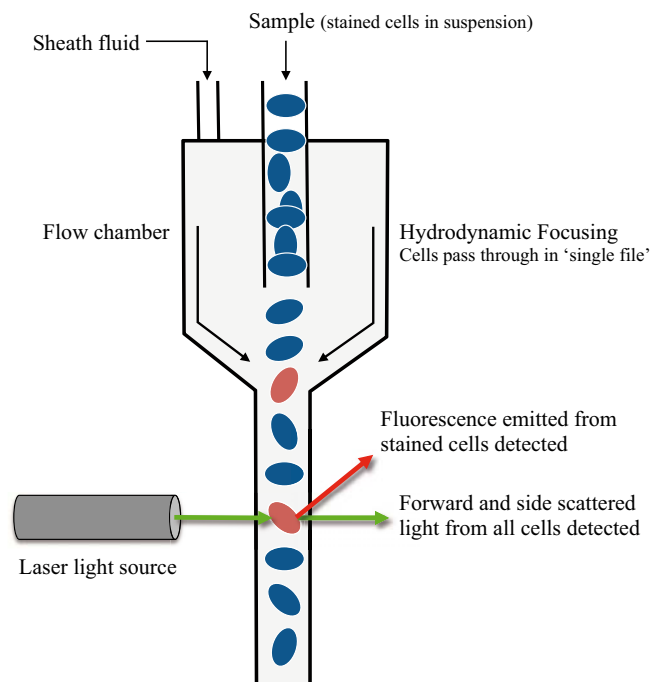


Figure 40: Scheme of a typical flow cytometer chamber.

Light scatter occurs when a particle deflects incident laser light. The extent to which this occurs depends on the physical properties of a particle, namely its size and internal complexity. Factors that affect light scattering are the cell's membrane, nucleus, and any granular material inside the cell. Two types of scattered light are measured in FC experiments (Figure 41):

- Forward-scattered light (FS): is proportional to cell-surface area or size. FS is a measurement of mostly diffracted light and is detected just off the axis of the incident laser beam in the forward direction by a photodiode.
- Side-scattered light (SS): is proportional to cell granularity or internal complexity. SS is a measurement of mostly refracted and reflected light that occurs at any interface within the cell where there is a change in refractive index and is collected at approximately 90 degrees to the laser beam.

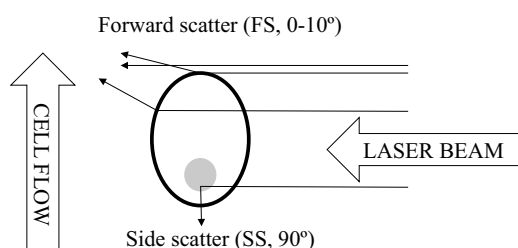


Figure 41: Schematic representation of the scattered light by a single cell in a flow cytometric analysis.

Using fluorochromes in flow cytometric analysis supplies additional information about cell structure or functionality. There are a wide and extensive variety of stains used in combination with FC, but to assess the affectation of the membrane due to peptide interaction two dyes were used in this thesis, a DNA-labelling dye **propidium iodide** and a potential-sensitive dye, **bis-(1,3-dibutylbarbituric acid)-trimethine oxonol** (DiBAC₄ (3)). PI, is a non-permeable fluorochrome that intercalates into double-stranded nucleic acid and is excluded by viable cells, therefore measurement of the loss of viability produced by antimicrobial agents or other compounds is possible (Gant, et al., 1993). BOX is a positively charged dye that accumulates inside the bacterial cell depending on the difference in charge between the two sides of the plasma membrane and therefore differences in membrane potential, due to peptide interaction, can be measured (Comas & Vives-Rego, 1997).

The scattering and fluorescence data acquired in the flow cytometry experiment is represented into histograms or dot plots:

- **One-parameter histograms** (Figure 42, A) represent the number of cells or particles (y-axis) versus the scattering or fluorescence intensity (x-axis). A subclass control is used to determine where the markers will be placed.
- **Dot-plots** (Figure 42, B) provide a two-parameter display of data. A subclass control is used to determine where the quadrant markers will be placed. A quadrant marker divides two-parameter plots into four sections to distinguish populations that are considered negative, single positive, or double positive. The lower-left quadrant (E3) displays events that are negative for both parameters. The upper-left quadrant (E1) contains events that are positive for the y-axis parameter (FL1) but negative for the x-axis (FL3) parameter. The lower-right quadrant (E4) contains events that are positive for the x-axis parameter (FL3) but negative for the y-axis (FL1) parameter. The upper-right quadrant (E2) contains events that are positive for both parameters

(FL1/FL3) or double positive. An alternative way to get statistics is to create regions around the populations instead of using a quadrant marker but a control sample needs to be used previously to establish the unaffected quadrants.

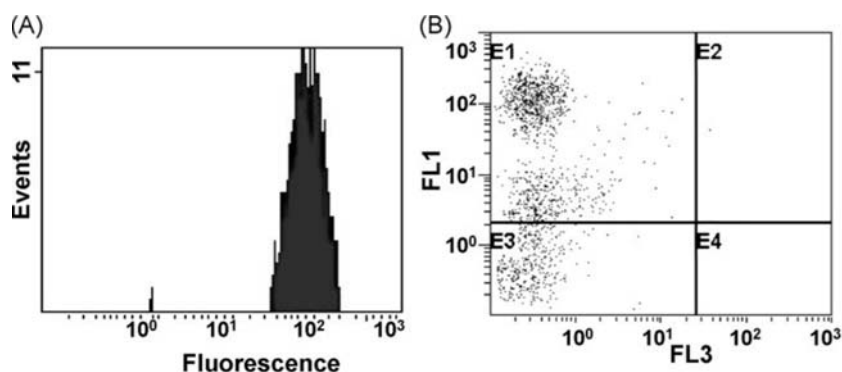


Figure 42: Flow cytometry illustration of (A) Histogram and (B) Dot-plot. From: (Díaz, et al., 2010).

A.3.3.2. Results from FC experiments for the novel polymyxin analogues

The mechanism of action at membrane level of some of the synthesized polymyxin analogues was investigated using flow cytometry. The procedure consisted in incubating at different contact times, *E. coli* and *S. aureus* (as models for Gram-negative and Gram-positive bacteria respectively), with the lipopeptides at the corresponding minimal inhibitory concentration followed by staining of the cells using PI and BOX before flow cytometric analysis. Control samples (non-treated) were always prepared and polymyxin B was used as a control in *E. coli*. Reduction of viability was always performed on parallel by plate count.

The MIC and sequence of the peptides used are shown in Table 21. Peptide #5 was chosen for FC analysis because it is the most active peptide of the first series synthesized in this thesis while #7 was chosen due to its results obtained with the biophysical experiments where it demonstrated high membrane activity. Finally, peptide #8 was investigated as it is the most promising candidate of our group, and showed activity against colistin-resistant strains, therefore flow cytometry could be helpful to give more information in order to study its alternative mechanism of action.

Table 21: Sequence of the peptides used for the flow cytometric experiments and minimum inhibitory concentration against *E.coli* and *S.aureus* in µg/mL at which they were used in these experiments. The sequence is displayed in three-letter code, the residues in italics are D-isomers and underlined residues denote bond formation.

Peptide	Sequence	Gram+	Gram-
		<i>S.aureus</i>	<i>E.coli</i>
PxB	6-methyl-octanoyl-Dab-Thr-Dab- <u>Dab</u> -Dab- <i>Phe</i> -Leu-Dab-Dab- <u>Thr</u>	>32	0.5
PxBN	Thr-Dab- <u>Dab</u> -Dab- <i>Phe</i> -Leu-Dab-Dab- <u>Thr</u>	>32	>32
5	nonanoyl-Dab-Thr-Arg- <u>Cys</u> -Dab- <i>Phe</i> -Leu-Arg-Dab- <u>Cys</u>	8	2
7	decanoyl-Arg-Thr-Arg- <u>Cys</u> -Dab- <i>Trp</i> -Nle-Arg-Dab- <u>Cys</u>	4	8
8	decanoyl-Dab-Thr-Dab-Cys-Dab- <i>Phe</i> -Nle-Dab-Dab- <u>Cys</u>	8	2

The results obtained are shown in Table 22. What can be observed is that PxB induces high amount of permeability (around 70% in 120 min) and to less extent, depolarization. However, depolarization seems to happen at first stages, as samples taken at 5 minutes of contact show 11% of permeability and around 45% of depolarization (data not shown). These results suggest that the first effect due to the presence of PxB in the media is a collapse in membrane potential (depolarization) and later, insertion and disruption of the membrane (permeability).

In order to study to what extent the dye inserts into the bacteria, and thus characterize the insertion of PxB, a control experiment was also carried out with polymyxin B nonapeptide. As previously explained, PxBN is devoid of antibiotic activity but retains the ability to disorganize the outer membrane of Gram-negative bacteria. The working hypothesis was that in the case of bacteria treated with PxBN, PI would not be able to bind the bacterial membrane, as PxBN is only able to disrupt the outer membrane. The results obtained confirmed the hypothesis since no depolarization or permeabilization is detected (only a background 3-6%) after 60 minutes of contact at 5 µg/mL (10 times the MIC of PxB). A staining control consisting of treatment of bacteria cells with a thermal shock (30 min, 70 °C) was also performed.

Table 22: Flow cytometry analysis and reduction of viability (obtained by plate count) of *E. coli* and *S. aureus* treated with PxB, PxBN and peptides #5, 7 and 8.

Peptide	Conc. (µg/mL)	Contact time (min)	<i>E. coli</i>			<i>S. aureus</i>		
			% of stained cells		% viability reduction	% of stained cells		% viability reduction
			PI	BOX		PI	BOX	
Control	-	30	3	5	-	1	5	-
	-	60	3	5	-	1	5	-
	-	120	2	4	-	2	5	-
PxB	0.5	30	68	13	65	-	-	-
	0.5	60	57	23	87	-	-	-
	0.5	120	71	17	98	-	-	-
PxBN	5	30	10	5	0	-	-	-
	5	60	3	6	5	-	-	-
5	MIC	30	52	19	30	1	7	10
	MIC	60	50	25	70	7	5	35
	MIC	120	45	22	80	10	6	65
7	MIC	30	18	29	22	1	10	20
	MIC	60	23	30	69	22	32	58
	MIC	120	46	21	80	23	37	90
8	MIC	30	7	47	20	1	0	15
	MIC	60	23	50	60	3	1	60
	MIC	120	43	47	85	4	4	85
70 °C	-	30	80	11	100	35	25	100

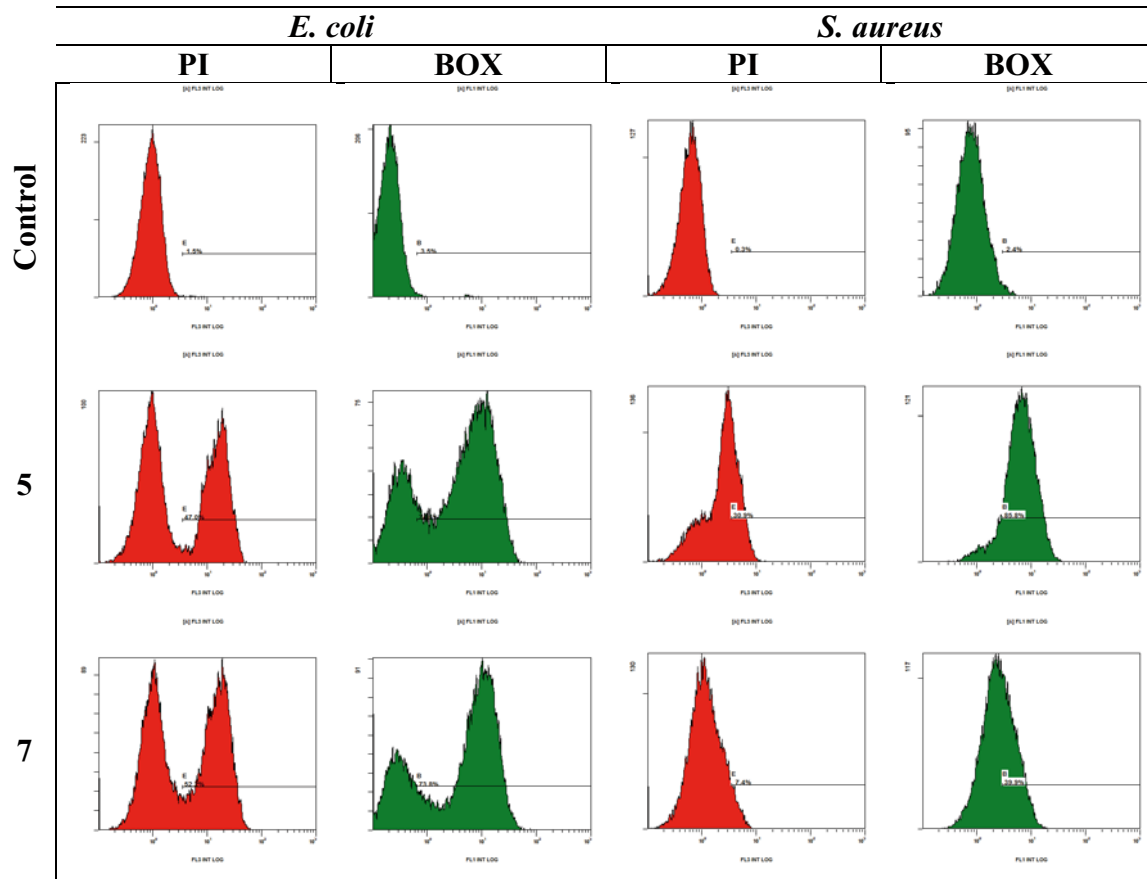
By analysing the values obtained for the synthetic lipopeptides (Table 22), it can be observed that exposure of *E. coli* to the MIC for 30 minutes leads to a loss in membrane potential of 20 % and membrane permeability of 45 % for peptide #5. No substantial modification is observed by increasing contact time. While for *S. aureus*, the permeability and depolarization values are lower (10 and 6 % at 120 min., respectively), although there is significant reduction of viability (65%, 120 min.) (representative histograms are shown in Table 23).

In the case of peptide #7, when treating *E. coli* cells, a gradual uptake of PI can be observed together with a reduction of viability, while the membrane depolarization values only reach 20-30 %. Contrarily, in *S. aureus*, after 30 minutes of exposure a maximum value of permeabilization is reached (20%) as more contact time did not result in a higher PI uptake, while depolarization of the membrane increased gradually with contact time. These results are in agreement with the fluorescence experiments; where in liposomes of POPE/POPG which model Gram-negative bacteria, a clear membrane disrupting effect, together with a permeabilization (ANTS/DPX leakage assay) was observed for this particular lipopeptide.

When *E. coli* is exposed to peptide #8, a progressive and almost complete growth inhibition (85%) can be observed at 2 h, accompanied by a fall of cell membrane potential (47%) and loss of membrane permeability (43%). However, for *S. aureus*, no significant effect is observed on membrane potential (4%) or permeability (4%) whereas cell viability shows an 85% reduction (representative dot-plots shown in Figure 43). The difference between the results obtained by bacterial count and the PI staining indicate the presence of cells that have maintained membrane integrity but are not able to grow, suggesting that the membrane is not the only target of antibacterial action in *S. aureus*.

Altogether, the results obtained seem to suggest that different mechanisms of action may be involved in the activity of lipopeptide #8 depending on the nature of the microorganism studied. The difference observed here between *S. aureus* and *E. coli* might be due to the difference in envelope structure and composition. The cell wall of Gram-positive bacteria contains a thicker peptidoglycan layer than that of Gram-negative cells, providing increased rigidity and could be the cause of not observing a lysis of the membrane although other effects were seen by electron microscopy as explained below.

Table 23: Histograms of the results obtained in the flow cytometry experiments for peptides #5 and 7. The control samples are used to establish the measuring bars. The treated cells are then analysed and the fluorescence band of those cells retaining the dyes (PI or BOX) is displaced to the right and can therefore be measured.



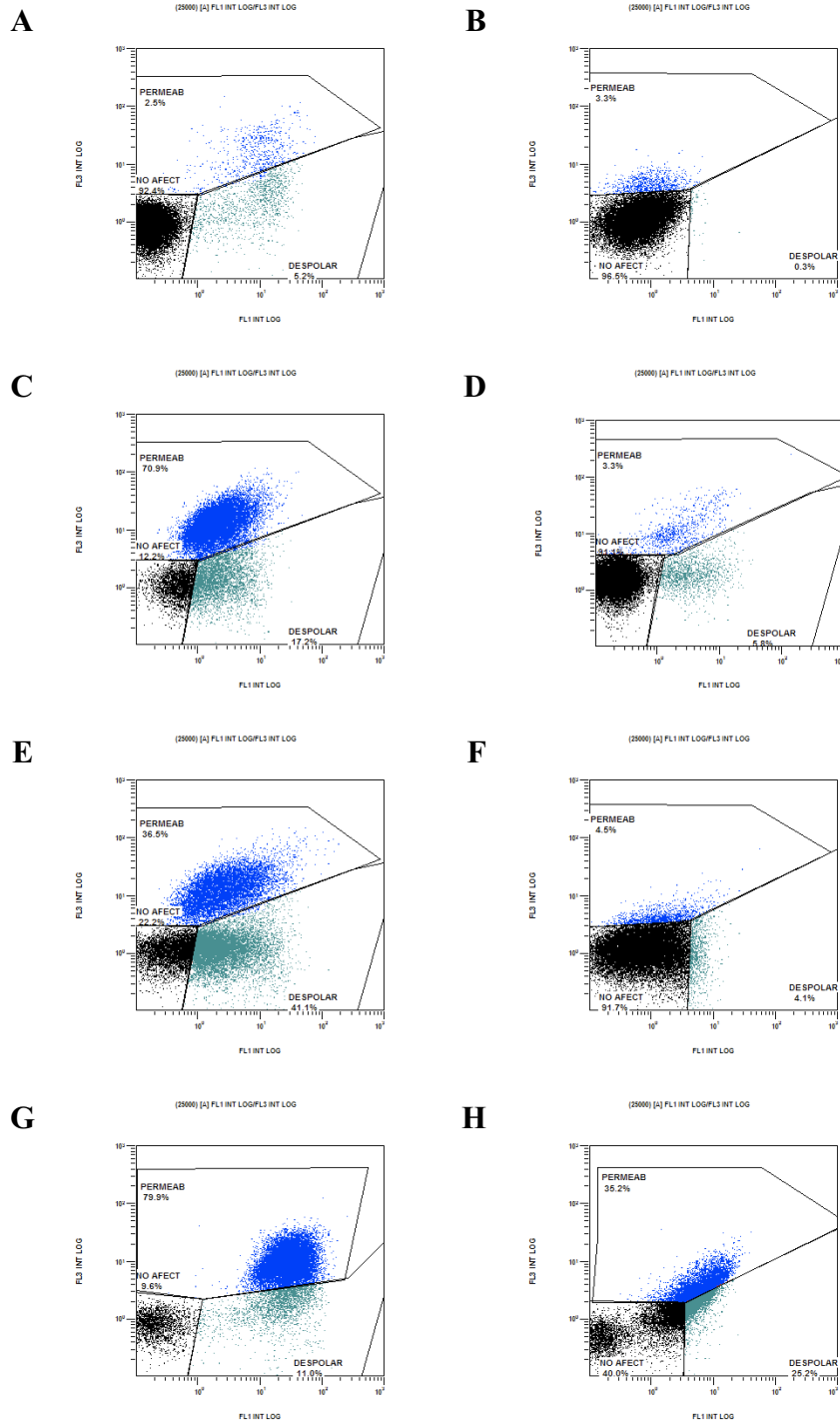


Figure 43: Dot-plots of the results obtained in the flow cytometry experiments for (A, B) untreated control cells of *E. coli* and *S. aureus* respectively, (C, D) *E. coli* cells after exposure to PxB and PxBN respectively, (E, F) *E. coli* and *S. aureus* cells after exposure to peptide #8 respectively, (G, H) *E. coli* and *S. aureus* heated cells. In all cases, the contact time was 2 h except for heated cells (30 min). No affected cells are cells that don't retain the dyes. Depolarized cells (green) are cells with a membrane potential affectation and therefore only retain the dye BOX, while permeabilized cells (blue) have the membrane completely affected and therefore retain both PI and BOX.

A.3.4. Transmission electron microscopy as a tool to determine the effect of the novel polymyxin analogues on bacteria

Transmission electron microscopy is a microscopy technique in which a beam of electrons is transmitted through an ultra-thin specimen. An image is formed from the interaction of the electrons transmitted through the specimen; the image is magnified and focused onto an imaging device. TEM can help clarify the mechanism of cell death due to antimicrobial peptide interaction by observing alterations in bacterial membrane integrity. Increasing number of examples of AMPs investigated ultrastructurally can be found in the literature, such as defensins (Lehrer et al., 1989; Shimoda, et al., 1995) or PGLa (Hartmann et al., 2010).

To further investigate the results obtained by flow cytometry for peptide #8, the effects of the lipopeptide on the cell morphology of *E. coli* and *S. aureus* was also investigated by transmission electron microscopy. PxB was used as a control and to observe the affectation of the membrane due to this widely-used antibacterial. It was surprising that no example of TEM images of bacteria treated with PxB could be found in the literature.

Briefly, the procedure consisted of incubating the bacteria with the peptide at the minimal inhibitory concentration, samples at 2 h contact time were taken and centrifuged followed by fixation, cutting and observation through TEM of the resulting cellular sections. The images obtained are shown in Figure 44 for *E. coli* and Figure 45 for *S. aureus*.

Untreated cells of *E. coli* in standard tryptone water medium show a normal cell shape with an undamaged structure of the inner membrane and an intact, slightly waved outer membrane (Figure 44, A and B). After 2 hours of incubation with PxB at the MIC (0.5 µg/mL), numerous protrusions are found at the outer cell membrane and even completely lysed membranes can be observed (solid arrows) (Figure 44, C and D). In the case of peptide #8, remarkable modifications of bacterial cell membranes are found, with diverse effects observed (Figure 44, E and F). TEM images show membrane abnormal septation, formation of blebs on the bacterial surface, such as the ones observed for PxB (solid arrows), numerous intracellular membranous structures in the polar cell regions (dashed arrows) and the collapsed cytoplasm is evident. Also, the periplasmic space is highly swollen probably due to the leakage of cytoplasm since cellular material can be seen.

Due to the surprising results obtained for both PxB and peptide #8 with *E. coli*, we decided to try another peptide from our group, the initial idea was to investigate peptide #7, which had also been studied in flow cytometry, but due to its highly lytic activity, we finally used peptide #3. We were surprised with the results obtained for this peptide. Treated cells of *E. coli* with 8 µg/mL, showed numerous spherical double-layered mesosome-like structures, most prominent at the periphery of the cells (Figure 44, G and H). By plate count, we know these bacteria are dead therefore these over-production of membrane has an effect on cell viability.

Similarly, control *S. aureus* showed round, compact and proliferating cells with intact cell walls and well-defined membranes (Figure 45, A and B). After treatment with peptide #8 (at 4 and 8 µg/mL), numerous spherical double-layered mesosome-like structures as well as spherical non-membrane-enclosed bodies containing an electron

density similar to that of the septal cell wall layer could be observed in the cytoplasm (Figure 45, C and D).

Mesosomes are intracytoplasmic membrane inclusions. They are indicators of cytoplasmic membrane alteration caused by antibiotic activity. Furthermore, since the cytoplasmic membrane is instrumental in cell wall synthesis and turnover, a perturbation of this membrane may also affect cell wall integrity and autolysin regulation. Accordingly, the very fact that mesosome-like structures are seen in most treated cells is indicative of cytoplasmic-membrane alteration and (possibly) uncoupling of the synthesis and turnover of cell wall polymers (Friedrich, et al., 2000). It has also been hypothesized that the formation of mesosomes in bacteria is a defensive mechanism to protect the bacteria from antibiotic assault. In fact, these invaginations have been detected by the effect of antibiotics as different as amikacin, gentamicin and ciprofloxacin (targeting nucleic acids) (Friedrich et al., 2000), mersacidin and vancomycin (Molitor et al., 1996; Sanyal & Greenwood, 1993) and defensins (Shimoda et al., 1995).

As seen in the flow cytometry assays, various macroscopic effects indicate that this peptide might kill cells in different ways and that these targets, particularly anionic ones such as nucleic acids or some proteins or enzymes, are differentially accessed depending on the type of bacteria.

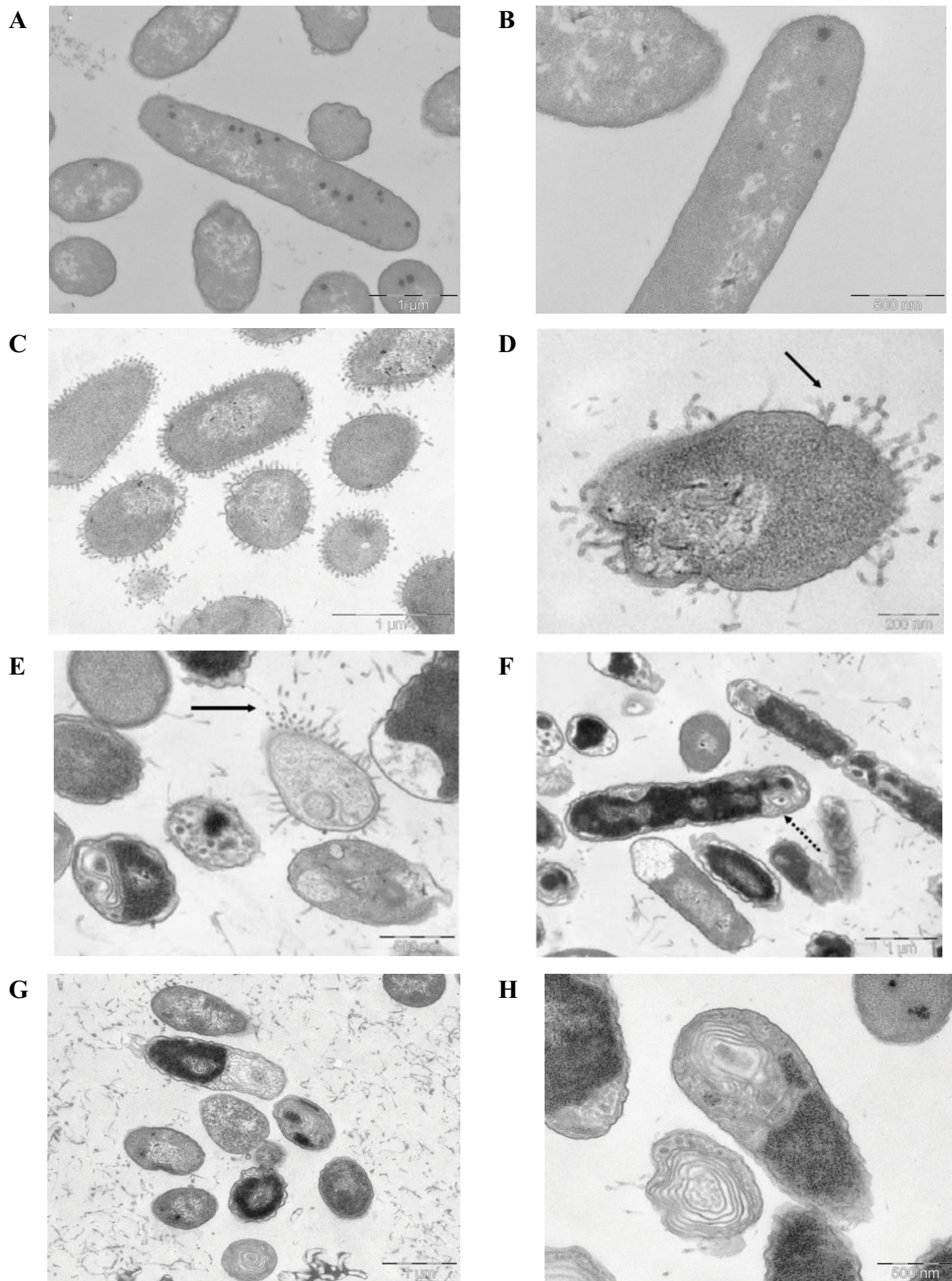


Figure 44: Comparative TEM micrographs of *E. coli*. (A, B) untreated bacteria, (C, D) after treatment with PxB at the MIC (0.5 µg/mL) numerous protrusions (solid arrow) from the cell surface are observed. (E, F) after treatment with peptide #8 (2 µg/mL) the effect is diverse, showing numerous membranous structures, protrusions of the membrane similar to PxB and even swollen periplasmic space (dashed arrow). (G, H) after treatment with peptide #3 (8 µg/mL) numerous membranous structures can be observed.

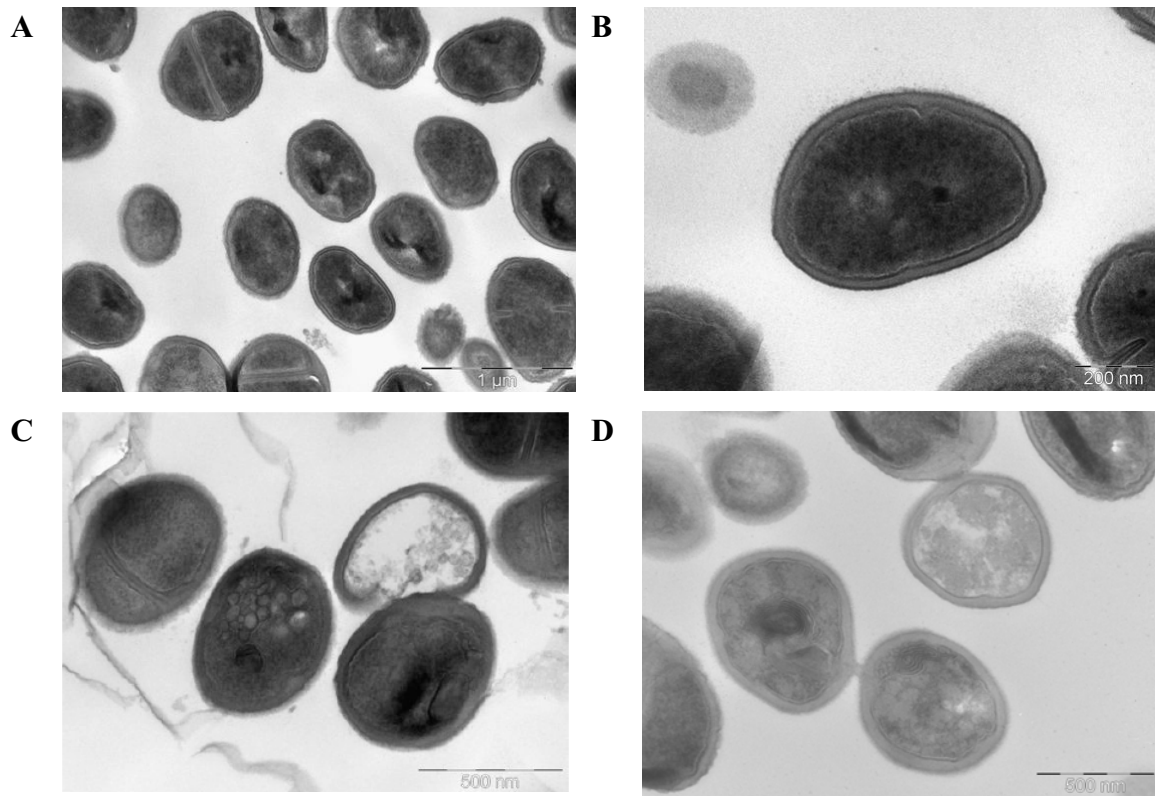


Figure 45: Comparative TEM micrographs of *S. aureus*. (A, B) untreated bacteria, round and intact cells, with a defined cell wall can be observed. (C, D) after treatment with peptide #8 (4 µg/mL) many mesosome-like structures and defects on the cell wall can be observed.

A.4. DISCUSSION SECTION A – New broad-spectrum, cyclic antibacterial lipopeptides with high activity

In an effort to discover new antimicrobial lipopeptides with better therapeutic index, analogues based on the structure of natural polymyxin B have been successfully synthesized and described in this thesis. The head-compound is the synthetic analogue sP-B, which maintains the major putative structural requirements for PxB activity such as the cyclic structure, distribution of charges and hydrophobic domains, but it includes a disulphide bridge between two cysteine residues to simplify the synthetic process. These analogues, which are members of a family of more than 100 peptides synthesized and tested in the group (ES200802626 patent ES2.33.4547: granted, ES201000349 patent ES2.374.779: granted, ES201330519 PCT application; worldwide protection PCT/ES2014/070286), include several modifications that have been discussed in detail in section A.2.1. according to the results obtained in the MIC determination.

As the MIC data show, the synthetic lipopeptides have relatively good antimicrobial activities against both Gram-positive and Gram-negative bacteria, in contrast with the selectivity for Gram-negative bacteria of PxB. In some cases values of 1-2 $\mu\text{g/mL}$ are reached for some of the tested strains, and several of the peptides, especially peptide #8, have proved to be active against multidrug-resistant bacterial strains.

Gram-negative bacteria, such as *E. coli*, have an outer membrane composed mainly of lipopolysaccharide, and LPS binding is a necessary first step for antimicrobial action. Results in table 16 show that **the lipopeptides have a high affinity for LPS, comparable to that of native PxB**, displacing previously bound dansyl-polymyxin from LPS. In addition, all lipopeptides insert into LPS monolayers packed at an initial pressure of $32 \text{ mN}\cdot\text{m}^{-1}$, a lateral pressure that is in the order of the cell membrane, but in this experiment the differences obtained for the different lipopeptides reflect different degrees of insertion into the monolayer rather than different affinities. The highest levels of insertion, even above those obtained by PxB binding, correspond to peptides N, #4 and 3. The N analogue lacks the hydrophobic domain in positions 6-7 of the cycle, and this can facilitate insertion between the LPS molecules due to electrostatic interaction. In the case of #3, the longer acyl chain will probably be responsible for a deeper insertion in the monolayer, whereas in #4, the bulky Trp⁶ can be the reason of the important increase in pressure. As expected, the linear peptide NN has a low capacity to insert into the LPS layer, probably because it cannot adopt the correct amphipathic structure upon binding. According to the molecular model of the LPS-PxB complex (Figure 5) it is evident that it is stabilized by a combination of electrostatic and hydrophobic interactions. The backbone of PxB is folded in an envelope-like fold, separating the polar residues from the hydrophobic components, thus conferring the structure amphiphilicity. The hydrophobic residues D-Phe⁶ and Leu⁷, as well as the N-terminal acyl chain, penetrate into the hydrocarbon portion of LPS, whereas the polar residues are oriented to point into the hydrophilic environment of the OM. The complex is stabilized by electrostatic interactions between the positive charges of the Dab side chains and the phosphates in lipid A. More specifically, two binding sites for anionic phosphoester groups are identified, one is formed by residues Dab¹, Dab³ and Dab⁵, and the second includes Dab⁸, Dab⁹, and Thr¹⁰. Results obtained with the synthetic peptides point towards a similar interaction with LPS, and we can conclude that they will also destabilize the OM by displacing divalent cations that normally function to bridge and stabilize the LPS OM monolayer.

By using several fluorescence spectroscopy experiments, the interaction of the lipopeptides with liposomes that mimic the cytoplasmic membrane of bacteria was studied. Liposomes of pure POPG and mixed POPE/POPG (6:4), were chosen as models, based on the reported membrane composition of different bacterial types (Epanand et al., 2008). In general, cytoplasmic membranes of Gram-positive bacteria, such as *S. aureus*, are mostly composed of anionic lipids, such as PG, whereas high contents of PE are found in Gram-negative bacteria, for example *E. coli*. Finally, vesicles of zwitterionic PC were also prepared as models of the eukaryotic membrane. In general, it was observed that **the peptides show differential binding to POPG, POPE/POPG and POPC model membranes.**

FRET experiments between tryptophan in position 7 as donor and NBD groups at the lipid interface as acceptors, show that antimicrobial lipopeptides #4, 6 and 7 bind with high affinity to anionic vesicles of POPG and POPE/POPG (6:4), with a linear dependence between the intensity of FRET and the peptide concentration. The higher increase in NBD fluorescence observed in POPE/POPG vesicles indicates that the presence of the zwitterionic PE favours peptide binding. Although it is generally accepted that cationic antimicrobial peptides interact with bacterial membranes mainly through electrostatic interactions with the anionic phospholipid head groups of acidic lipids (Dathe, et al., 2001), FRET results shown here demonstrate that zwitterionic PE also plays an important role. As expected, very low increase in FRET was found for NBD-labelled POPC vesicles, thus suggesting a low affinity of the lipopeptides for this zwitterionic lipid, representative of the eukaryotic membrane.

Tryptophan fluorescence emission spectra, anisotropy measurements and quenching experiments were conducted to characterize the membrane bound form of the three lipopeptides. Antimicrobial lipopeptides #4, 6 and 7 showed comparable fluorescence characteristics in buffer, with the fluorescence maxima centred at 350 nm, indicative of Trp residues located in a hydrophilic environment (Burstein, et al., 1973). In addition, similar emission intensities reveal a similar environment for tryptophan. The very low Trp-anisotropy values and high Trp-quenching constants are consistent with the absence of a secondary structure in solution. In the presence of the anionic lipid membranes, modifications in Trp fluorescence properties are a clear indication of membrane binding and insertion of the Trp residue in a more hydrophobic environment. The observed blue-shift of emission maximum of Trp, around 15 nm, and the important increases in anisotropy, are relatively independent on the lipid concentration, and indicate that Trp is in a more hydrophobic region of the bilayer, where it remains relatively immobilized. Acrylamide quenching experiments are consistent with low accessibility to the aqueous phase. From these experiments we can conclude that #4, 6 and 7 bind more efficiently to PE-containing PG vesicles than to pure PG vesicles, but the peptides bind in similar forms with similar spectroscopic characteristics. Binding to POPC vesicles is significantly less efficient, with a lower intensity in the FRET signal that saturates at peptide-to-lipid ratios above 0.02. Spectral signatures in POPC vesicles are also different to the ones in anionic vesicles, and are consistent with a more gradual, concentration-dependent insertion of the lipopeptide in the hydrophobic core of the membrane. The absence of salt effect is indicative of an irreversible binding to the membrane, consistent with the deep insertion of the three lipopeptides. Similar results were obtained for the pore-forming cyclic antimicrobial peptide BPC194 on binding to anionic membranes (Mika, et al., 2011).

Several experiments were used to assess **peptide-induced perturbation of the membrane**, and in general it was observed that it **requires the presence of anionic lipids**.

Even though the synthetic lipopeptides bind to zwitterionic PC membranes, they do not induce significant leakage or fusion from these vesicles, a first indication of selectivity for bacterial cells, and thus suggesting that they will not be toxic in eukaryotic cells. These results also emphasize the importance of choosing the membrane composition to obtain relevant results: although cationic peptide antimicrobial peptides interact with bacterial membranes mainly through electrostatic interactions with the PG head groups, this can not be the only governing factor, because the nature of the additional lipid components also play a role, as demonstrated with aurein 2.2 and derivatives (Cheng, et al., 2011) and plantaricin A (Zhao, et al., 2006).

Leakage experiments show that the lipopeptides are able to permeabilize vesicles of POPE/POPG in a concentration-dependent manner. Peptide #7 and 9 are the more lytic lipopeptides in this model system. Permeabilization shows a biphasic pattern, with higher membrane-permeabilizing effect above P/L = 0.03 and 0.05 respectively. This elevated peptide-to-lipid ratios suggests that possibly these peptides act by the “carpet” mechanism, where a minimum amount of bound peptide is needed before channels are formed (Pouny, et al., 1992). The rest of the lipopeptides are only slightly less permeabilizing at the same P/L ratio.

All the lipopeptides induce mixing of phospholipids between vesicles of POPE/POPG. The efficacy of causing lipid mixing follows the same trend as the ability to induce leakage, with #7 being the most active peptide. Therefore, the lipopeptides cause leaky fusion of POPE/POPG vesicles at concentrations relevant to their antimicrobial activity in *E. coli*, thus suggesting a mechanism of action based on the permeabilization of the cytoplasmic membrane. These results are consistent with the flow cytometry experiments, where a permeabilization of the membrane of *E. coli*, therefore a high PI uptake, is observed. The possibility of an unspecific detergent effect with formation of micelles can be ruled out as demonstrated by a peptide concentration-dependent increase in light scattering of the anionic vesicles, indicative of an increase in particle size by clustering of the vesicles (Figure 24), as is also the case with PxB and sP-B (Clausell et al., 2005; 2006; 2007).

This behaviour is common to other antimicrobial peptides, such as MSI-78 (Hallock, et al., 2003), and can be related to the negative spontaneous curvature imparted by POPE, due to the fact that the polar headgroup has a smaller diameter than the hydrocarbon chain region in the fluid phase, and the increased acyl chain packing induced by this lipid (Poza Navas et al., 2005). Many AMPs are known to induce clustering of anionic lipids, causing lipid segregation and, as a result, leakage of aqueous contents and/or membrane depolarization (Epand & Epand, 2011; Nguyen et al., 2011). The biological significance of membrane fusion is poorly understood, however it is likely that the process enables the translocation of the peptide molecules across the membrane bilayer (Ulvatne, et al., 2001). In contrast, results with PxB are consistent with a different mechanism of action based on the mixing of lipids between the outer and inner membranes and the resulting osmotic imbalance, as reported previously (Daugelavičius, et al., 2000; Mortensen et al., 2009; Oh et al., 1998b).

In pure POPG vesicles, a good model of many Gram-positive membranes, including *S. aureus*, differences among the lipopeptides are more important, with a lower effect of peptides #1-6 on the permeability of the membrane at low peptide concentration, compared to a fast leakage of aqueous contents induced by #7-11, even at low P/L ratios. However, lipid mixing in POPG vesicles occurs in all cases from very low P/L ratio, even at concentrations where leakage is not detected. Lipid mixing without leakage of aqueous contents can be explained if non-leaky fusion is induced by the peptides, or if specific vesicle-vesicle contacts with selective exchange of phospholipids from the outer membranes of the vesicles takes place, as demonstrated for PxB (Cajal et al., 1995; Cajal, et al., 1996b).

In some cases, the results obtained with synthetic vesicles are not fully consistent with those obtained by flow cytometry experiments in viable bacteria. For example, peptide #8 showed no permeabilization in *S. aureus* according to flow cytometry, and high levels of permeabilization in *E. coli*, whereas both in POPG and POPE/POPG liposomes the peptide caused moderate levels of leakage. This can be explained by the fact that liposomes are a simplified model of real bacterial membranes.

In flow cytometry, peptides #5 and 8 gave very low values of permeability from *S. aureus* (although cell death was detected) while peptide #7 had a pronounced effect in this bacterial strain. These permeability values were always comparatively lower than in *E. coli*, although the experiments were always carried at the MIC values. This is probably due to the different morphology and composition of the membrane of both bacterial strains and may point towards a different mechanism of action. A similar result was observed in the anisotropy experiments using DPH and TMA-DPH labelled liposomes, where the insertion of peptide #8 in POPG liposomes caused no significant changes in membrane fluidity, but in mixed POPG/POPE vesicles insertion affected the state of membrane lipids in a way that depends on the lipid phase.

In the TEM experiments, peptide #8 induced important morphological changes on bacterial membranes, with a high level of mesosome formation, which is an indicator of cytoplasmic membrane alteration caused by antibiotic activity. Mesosome formation is considered to be a defensive mechanism of the bacteria to protect it from antibiotic assault.

Although the mode of action of many AMPs involves disruption of the bacterial membrane integrity, other antimicrobial mechanisms have recently been characterized that target key cellular processes such as DNA and protein synthesis, protein folding, enzymatic activity and cell wall synthesis (Nguyen et al., 2011). Some AMPs can even have several targets, a multi-hit strategy that increases their efficiency reducing the possibility of resistance (Peschel & Sahl, 2006). **Looking at the FC and TEM results, it seems that peptide #8 might kill in a multi-hit strategy.**

4. SECTION B – MSI-103 ANALOGUES

B.1. DESIGN AND SYNTHESIS OF MSI-103 ANALOGUES TO STUDY THE EFFECT OF LENGTH ON ACTIVITY

B.1.1. Design of MSI-103 analogues

As previously introduced, MSI-103 is an antimicrobial peptide, with sequence (KIAGKIA)₃-NH₂, that was designed starting from the sequence of PGLa (Blazyk, 2001; Maloy & Kari, 1995). Both peptides have been extensively studied in Anne S. Ulrich's group in the Karlsruhe Institute of Technology (KIT) using different techniques, especially solid-state NMR.

It is known that PGLa, the parent peptide of MSI-103, permeabilizes membranes by forming pores (Matsuzaki et al., 1996; 1998; Matsuzaki, et al., 1995a; Yang, et al., 2000). Such pores are proposed to be formed by peptides in a transmembrane orientation, either with peptides alone forming the walls of the pores, in a so called "barrel-stave pore" found for alamethicin (Qian, et al., 2008), or with lipid headgroups intermixed with peptides in the pore walls, so called "toroidal pores", found for melittin (Lee, et al., 2013).

The initial objective of the project that was going to be carried out in Prof. Anne Ulrich's group in Karlsruhe, was to study if a shorter 14 amino acid version (KIAGKIA)₂-NH₂ was active and its behaviour in lipid membranes. The main reason to use a shorter peptide is the recent observation that even very short antimicrobial peptides can have high activity (Munk et al., 2013; Wadhvani et al., 2014), and as a drug, a shorter peptide would be easier and cheaper to produce. But when (KIAGKIA)₂-NH₂ was tested for antimicrobial activity and solid-state ²H-NMR the results showed that it is completely devoid of activity and only an S-state could be detected by solid-state NMR (data not shown).

Therefore, it was decided to investigate a series of peptides of different length, based on the same repeating units as MSI-103, and called KIAN peptides (where n is the number of amino acids in each peptide) (Table 24). The aim was twofold; to find the optimal length of peptides with a high antimicrobial effect and low haemolysis, and to investigate the **pore formation hypothesis**. If these peptides were to form pores built from transmembrane peptides, a minimum length would be needed for peptides to span the membrane. We could then expect a threshold minimum length needed for activity, which would also vary with the membrane thickness (proposed pore structures are shown in Figure 46). On the other hand, if peptides kill bacteria by permeabilizing the membrane according to the "carpet model" where peptides are bound to the membrane surface (Gazit, et al., 1996; Pouny et al., 1992), or by crossing the membrane and finding intracellular targets, even peptides too short to span the membrane could be active.

Table 24: Sequence, in one-letter code, of the peptides synthesized in this study. The highlighted Ala-10 was labelled with ^{15}N at the backbone amide. (a) Assuming 1.5 Å per residue for an ideal α -helix.

Peptide	Sequence	Length ^a (Å)
KIA14	KIAGKIA KIAGKIA-NH ₂	21
KIA15	KIAGKIA KIAGKIA K-NH ₂	22.5
KIA17	KIAGKIA KIAGKIA KIA-NH ₂	25.5
KIA19	KIAGKIA KIAGKIA KIAGK-NH ₂	28.5
KIA21 (MSI-103)	KIAGKIA KIAGKIA KIAGKIA-NH ₂	31.5
KIA22	KIAGKIA KIAGKIA KIAGKIA K-NH ₂	33
KIA24	KIAGKIA KIAGKIA KIAGKIA KIA-NH ₂	36
KIA26	KIAGKIA KIAGKIA KIAGKIA KIAGK-NH ₂	39
KIA28	KIAGKIA KIAGKIA KIAGKIA KIAGKIA-NH ₂	42

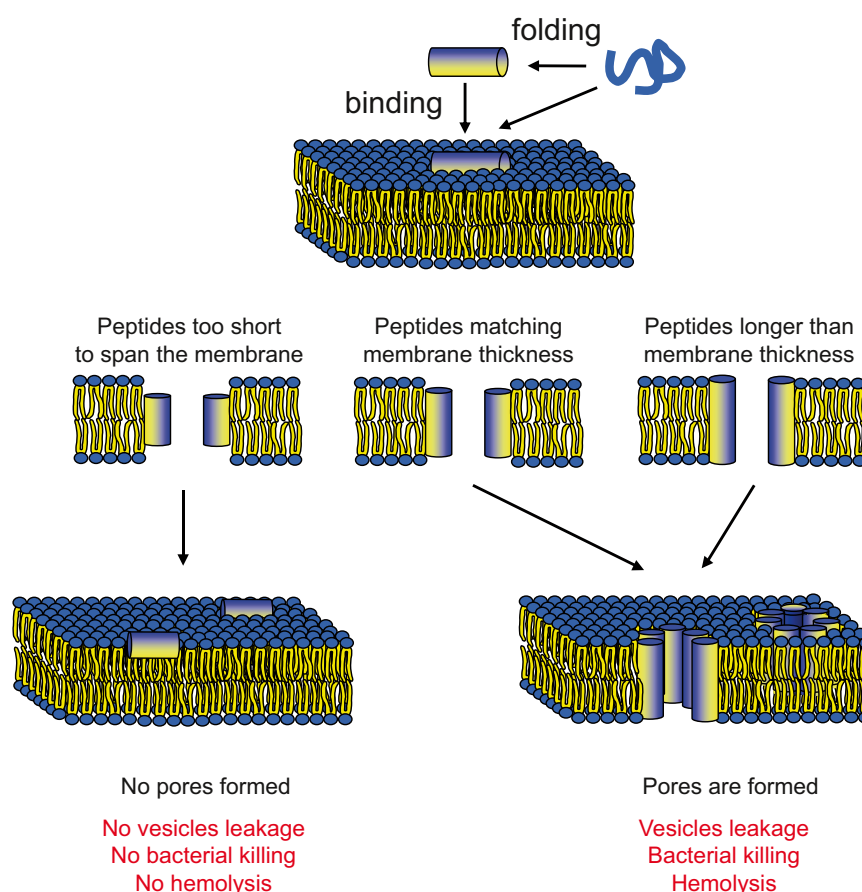


Figure 46: A model of the pore formation proposed to occur for KIA peptides. The peptides are unstructured in solution but form amphipathic α -helices when binding to the membrane. If the peptide is too short to span the membrane, no pores are formed and peptides lie flat on the membrane. If the peptide is at least long enough to span the hydrophobic part of the membrane, a pore can form with peptides in a transmembrane, inserted orientation. If the peptides are too long they may tilt in the membrane (not shown). Pores are depicted as barrel-stave type, but could also be of the toroidal wormhole type with lipid headgroups lining the pore.

B.1.2. Chemical synthesis of MSI-103 analogues

The peptides of the KIA series with lengths of 14-28 amino acids were synthesized on an automated peptide synthesizer Syro II (from Multisynthtech GmbH), with and without ^{15}N -label, using standard solid phase Fmoc protocols. A scheme of the synthetic strategy is shown in Figure 47. Rink amide MBHA resin was used, and the protecting group of the amino acid Lys was Boc.

The Fmoc-protected amino acids were incorporated to the resin directly using a mixture of HBTU/HOBt/DIEA. Each amino acid was coupled twice on the automated peptide synthesizer for 30 min before the next cycle was repeated. Successive cycles of Fmoc-deprotection with 20% piperidine in DMF and Fmoc-protected amino acid coupling to the freshly deprotected N-terminus gave the desired protected peptides on resin.

For structure analysis using solid-state ^{15}N -NMR spectroscopy isotope labels were incorporated manually using Fmoc protected Ala with a ^{15}N -label at the backbone amide as described above but with half the quantity of the reagents. Each coupling here was performed twice for 60 min.

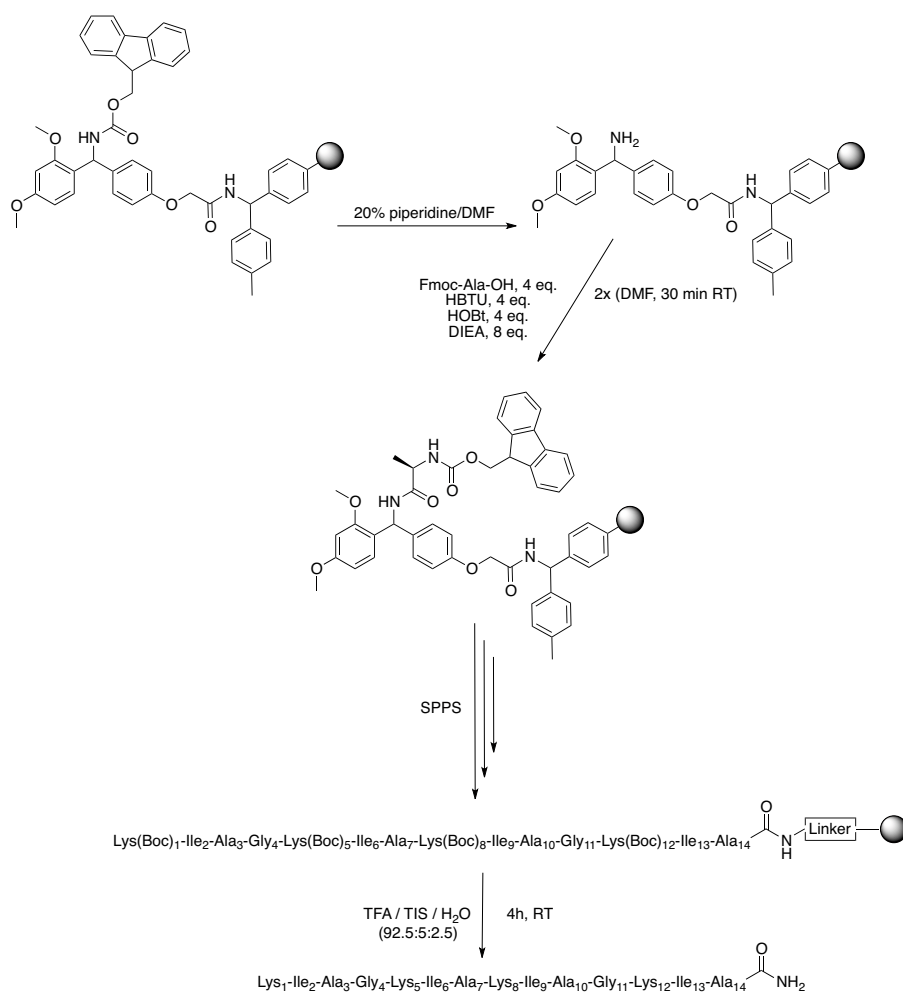


Figure 47: General scheme of the synthetic strategy followed for the KIA peptides.

Cleavage and full deprotection of the peptides was carried out by acidolysis with a mixture of TFA/triisopropylsilane/water for 4 h with occasional gentle shaking. The

filtrate was evaporated to a reduced volume under a gentle stream of nitrogen and the crude product was precipitated with cold diethyl ether.

The crude material was purified by high-pressure liquid chromatography on a Vydac C-18 column using an acetonitrile/water gradient. The identity of the products was confirmed by analytical HPLC combined with ESI-mass spectrometry, and all peptides were shown to be over 95% pure.

B.2. *IN-VITRO* ANTIBACTERIAL AND HAEMOLYTIC ACTIVITY DETERMINATION

B.2.1. Antibacterial activity

To investigate the pore formation hypothesis and determine the optimal length needed, the antibacterial activity of the different length peptides had to be determined. This activity was expressed as the minimum inhibitory concentration, which is the lowest concentration of antibacterial agent that inhibits the visible growth of a microorganism after overnight culture (18-24 h). It was determined using a standard broth dilution assay (Wiegand, et al., 2008).

The microorganisms used were the following:

- Gram-positive bacteria: *Staphylococcus aureus* (DSM 1104) and *Enterococcus faecalis* (DSM 2570).
- Gram-negative bacteria: *Escherichia coli* (DSM 1103) and *Pseudomonas aeruginosa* (DSM 1117).

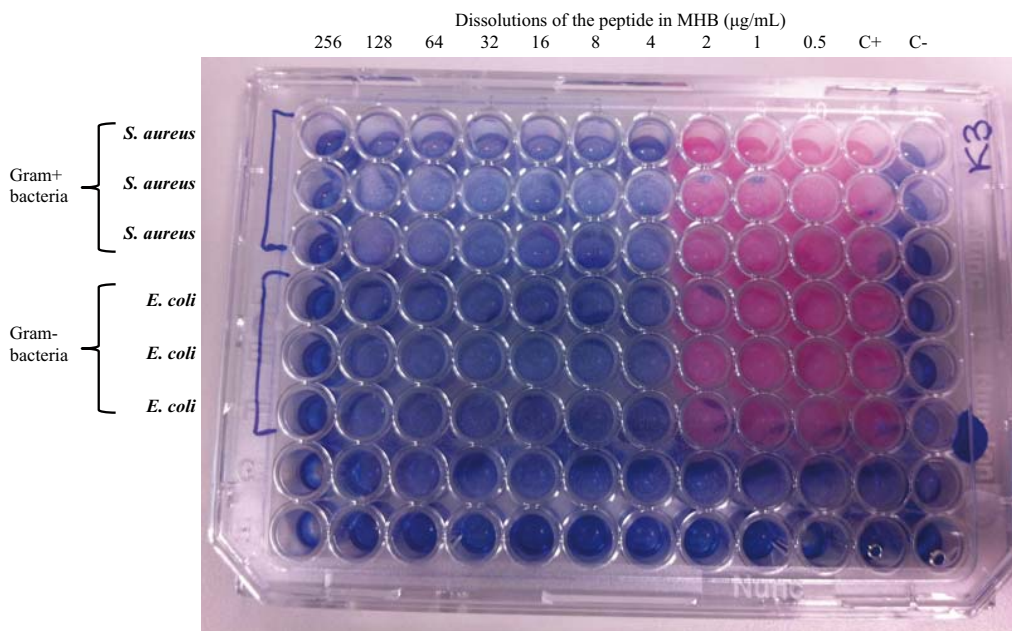


Figure 48: Example of microtiter 96-well plate used in the MIC tests. The columns 1-10 contain the dissolutions of the peptide tested in MHB (256-0.5 µg/mL), and to each row A-H the microorganism is inoculated. Columns 11 and 12 correspond to the positive (no peptide) and negative (no microorganism) control respectively. Observing the plate used as example, we can see that the activity was measured by triplicate directly in the plate. Rasazurin was added to evaluate growth by respiration activity of bacteria. This blue dye is reduced to the pink resorufin by bacteria still capable of respiration. Therefore, for this peptide, rows A-C are blue till column 7, so the MIC for *S. aureus* is 4 µg/mL.

The bacteria used belong to the DSM collection and therefore are standard reference microorganisms for research and the most representative bacteria for antibacterial activity testing.

The MIC values for the synthesized peptides are shown in Table 25. The experiments were done by triplicate and repeated in different days to avoid environmental effects; PGLa was used as control in each experiment and the MIC expressed in $\mu\text{g/mL}$.

Table 25: MIC values (expressed in $\mu\text{g/mL}$) for the KIA peptides in four bacterial strains. Inactive peptides for each strain are marked in grey.

Peptide	GRAM-		GRAM+	
	<i>E. coli</i>	<i>P. aeruginosa</i>	<i>S. aureus</i>	<i>E. faecalis</i>
KIA14	>256	>256	>256	>1024
KIA15	>256	>256	>256	>1024
KIA17	32	256	256	>1024
KIA19	32	256	>256	>1024
KIA21	4	64	8	1024
KIA22	4	32	16	1024
KIA24	4	16	4	64
KIA26	4	16	8	64
KIA28	8	16	8	16
PGLa	32	256	64	>1024

When observing the MIC values, it can be immediately noticed that there is a clear correlation between peptide length and activity, and the threshold length is different for different bacterial strains. In *E. coli*, KIA14 and KIA15 are inactive, KIA17 and KIA19 show some activity, and KIA21 and longer peptides show high activity. In *P. aeruginosa*, KIA19 and shorter analogues are inactive, KIA21 and KIA22 are relatively active, but for full activity 24 or more amino acids are needed. In *S. aureus*, the threshold is more distinct; KIA19 and shorter peptide are inactive while KIA21 and longer peptides are highly active. In *E. faecalis*, hardly any activity is found for KIA22 and shorter peptides, KIA24 and KIA26 show some activity (much higher than shorter peptides), and KIA28 is more active than the shorter peptides. We can also note that the control peptide PGLa (with 21 amino acids), shows an activity similar to that of KIA17 or KIA19.

In summary, in most cases there is a clear threshold length, with peptides shorter than the threshold having much lower activity than peptides longer than the threshold. This is in contrast to a gradual change of activity with length.

B.2.2. Haemolytic activity

Haemolysis is the rupturing of erythrocytes (red blood cells) and the release of their contents into the surrounding fluid. A good antibacterial agent should have low MIC values and maintain low haemolytic activity, a measure of toxicity. Therefore, the next step was to measure the haemolytic activity of the KIA peptides.

The haemolytic activity was examined with a serial 2-fold dilution assay (Strandberg et al., 2007), using citrate phosphate dextrose-stabilized blood bags with erythrocyte suspensions from healthy donors obtained from the blood bank of the local municipal hospital (Städtisches Klinikum, Karlsruhe, Germany). Briefly, the erythrocytes were incubated with the peptides at 37 °C for 30 min. The samples were then centrifuged and the absorbance of the supernatant containing haemoglobin was measured (the coloured fluids obtained are shown in Figure 49). The percentage of haemolysis was then calculated relative to 100% lysis by 1% Triton X-100. All the measurements were done by duplicate and to avoid environmental effects repeated in different days.

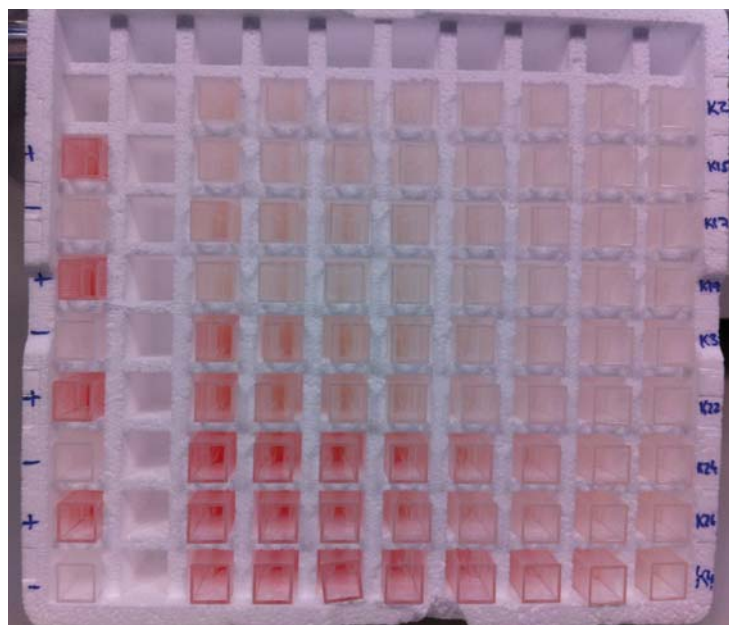


Figure 49: Supernatant obtained after 30 min incubation of the human erythrocytes with the peptide followed by centrifugation and absorbance measurement. A clear correlation between length and haemolysis can already be visually detected, the samples are ordered from KIA14 (top) to KIA28 (bottom) and from lower concentration (right) to higher concentration (left). The longer peptides gave rise to darker samples, due to a higher release of the erythrocyte content, therefore they are more haemolytic.

The results obtained are shown in Table 26. It can be observed that short peptides, KIA14 to KIA19, gave very low haemolysis even at a high peptide concentration of 512 $\mu\text{g}/\text{mL}$ (marked in grey in Table 26). KIA21 and KIA22 showed considerable activity at or above 128 $\mu\text{g}/\text{mL}$, while KIA24 and longer peptides already at 8 $\mu\text{g}/\text{mL}$ gave considerable haemolysis and at the highest concentration, about 100% haemolysis.

In the haemolysis assay there is, like in the MIC assay, some thresholds, with stepwise higher activity between 19 and 21 amino acids, and between 22 and 24 amino acids, but there is also a monotonous increase in haemolysis with peptide length and concentration.

Table 26: Haemolytic activity of the KIA peptides at different peptide concentration. Peptides showing small effects even at the highest tested concentration are marked in grey.

Peptide	% haemolysis			
	8 µg/mL	32 µg/mL	128 µg/mL	512 µg/mL
KIA14	5	3	2	3
KIA15	2	2	1	7
KIA17	2	2	2	8
KIA19	4	5	3	9
KIA21	3	7	15	38
KIA22	5	8	19	59
KIA24	15	34	67	96
KIA26	12	23	52	94
KIA28	41	64	86	100

B.3. STUDY OF THE MECHANISM OF ACTION – Investigation of the pore formation hypothesis

B.3.1. Circular dichroism spectroscopy

B.3.1.1. Fundamentals of circular dichroism spectroscopy

Circular dichroism spectroscopy is a form of light absorption spectroscopy that measures the difference in absorbance of right- and left-circularly polarized light by a substance. Briefly, a beam of light has time dependent electric and magnetic fields associated with it. If the light is polarized by passing through suitable prisms or filters its electric field, E , will oscillate sinusoidally in a single plane. When viewed from the front, the sinusoidal wave can be visualized as the resultant of two vectors of equal length, which trace out circles, one which rotates clockwise (E_R) and the other which rotates counter-clockwise (E_L). The two circularly polarized waves have physical existence. The waves are 90 degrees out of phase with each other and can be separated using a variety of prisms or electronic devices that utilize Pockel's effect (Velluz, et al., 1965). When asymmetric molecules interact with light, they may absorb right- and left-handed circularly polarized light to different extents (hence the term circular dichroism) and also have different indices of refraction for the two waves. The result is that the plane of the light wave is rotated and that the addition of the E_R and E_L vectors results in a vector that traces out an ellipse and the light is said to be elliptically polarized (Figure 50). CD is reported either in units of ΔE , the difference in absorbance of E_R and E_L by an asymmetric molecule, or in degrees ellipticity, which is defined as the angle whose tangent is the ratio of the minor to the major axis of the ellipse. $[\theta]$, the molar ellipticity in $\text{deg.} \cdot \text{cm}^2/\text{dmol} = 3298\Delta E$ (Kelly, et al., 2005).

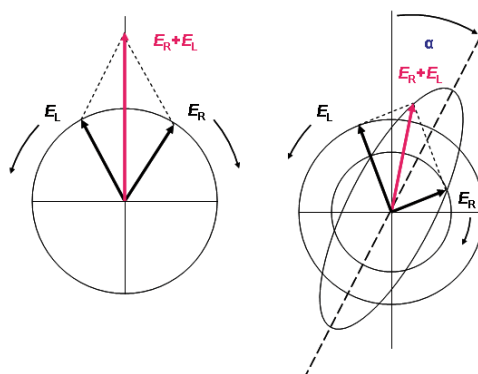


Figure 50: (left) Linear polarized light can be viewed as a superposition of opposite circular polarized light of equal amplitude and phase. (right) Different absorption of the left- and right-hand polarized component leads to ellipticity.

CD is an excellent tool for rapid determination of the secondary structure and folding properties of peptides and proteins. When the chromophores of the amides of the polypeptide backbone of proteins are aligned in arrays, their optical transitions are shifted or split into multiple transitions due to “exciton” interactions. The result is that different structural elements have characteristic CD spectra (Figure 51). For example, α -helical proteins have negative bands at 222 nm and 208 nm and a positive band at 193 nm. Proteins with well-defined antiparallel β -sheets have negative bands at 218 nm and positive bands at 195 nm, while disordered proteins have very low ellipticity above 210 nm and negative bands near 195 nm (Kelly & Price, 2000).

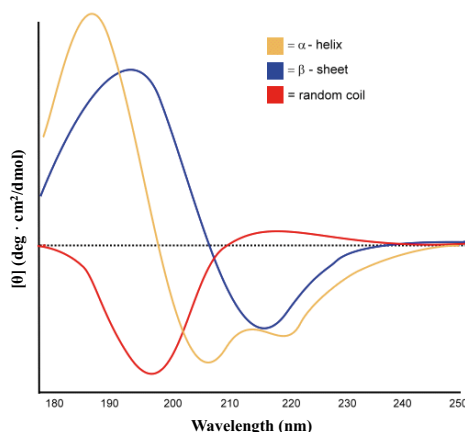


Figure 51: CD spectra associated with various types of secondary structure: (yellow) α -helix; (blue) β -sheet and (red) random coil.

B.3.1.2. Results from CD experiments for KIA peptides

In order to determine the secondary structure of the synthesized KIA peptides, CD spectra both in phosphate buffer and in a lipid environment were recorded. The results are shown in Figure 52.

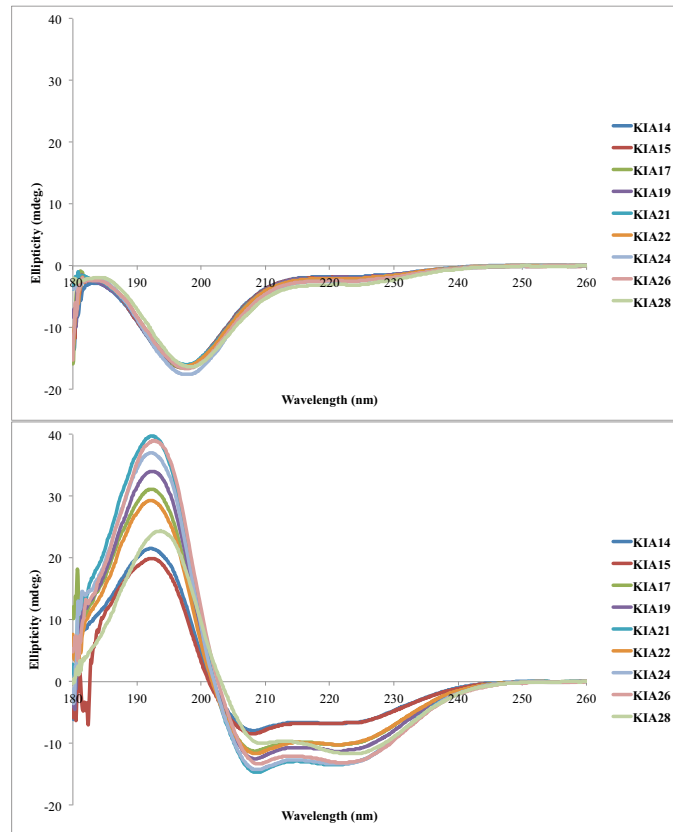


Figure 52: Circular dichroism spectra of KIA peptides. In 10 mM phosphate buffer (upper) and in presence of DMPC/DMPG (3:1) vesicles (lower).

It can be observed that all KIA peptides show random coil spectra in phosphate buffer (Figure 52, upper panel). But when the measurements were done in DMPC/DMPG (3:1) vesicles, a mixture that mimics microbial membranes, all peptides gave very similar CD spectra, typical of α -helical peptides (Figure 52, lower panel). This shows that the peptides are unstructured in solution but form helices when bound to the membrane (models of the KIA helices shown in Figure 53) as suggested in the first step of the pore formation hypothesis (Figure 46). A deconvolution of CD data to determine quantitative amounts of different secondary structure elements could not be done, due to uncertainties in the peptide concentrations.

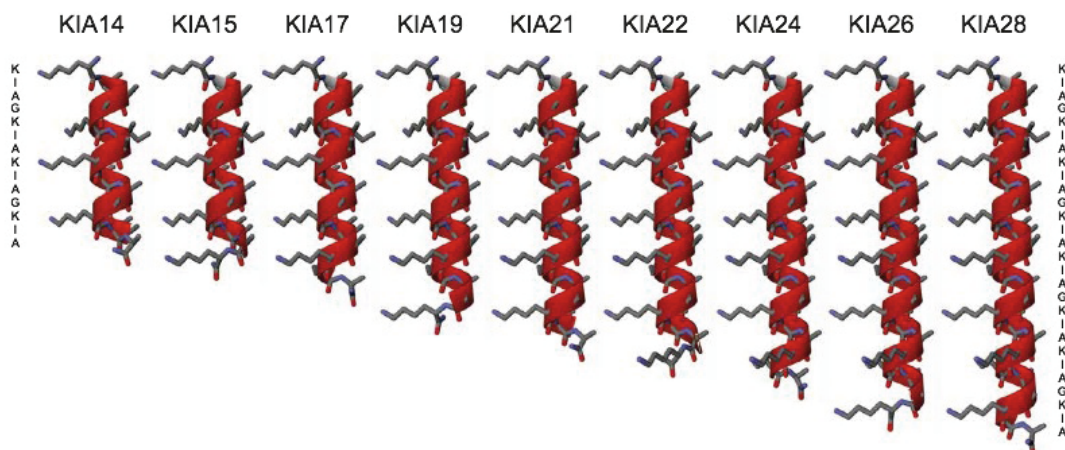


Figure 53: Models of the KIA peptides in their α -helical conformation when bound to the lipid membrane.

B.3.2. Biophysics experiments – Vesicle leakage

Membrane permeability due to peptide binding was assessed by the ANTS/DPX leakage assay. This assay consists in co-encapsulating in liposomes of different lipid composition (with defined chain length) the aqueous dye ANTS and the cationic quencher DPX. If the peptide is capable of forming pores producing the leakage of the probes to the media, an increase in fluorescence emission of ANTS can be detected due to an un-effective quenching (Ellens et al., 1985).

The idea behind the leakage experiments was to study the effect of **membrane thickness**. If the peptide is shorter than the lipid membrane it should not be able to form pores, and no leakage should be observed, while if the peptide matches or is longer than the lipid membrane, leakage of the dye should be detected. Therefore synthetic lipids with a well-defined chain length had to be used to prepare the vesicles. In all cases, a 1:1 (mol/mol) mixture of zwitterionic PC lipids and negatively charged PG lipids were used (Table 27), since electrostatic effects are essential to bind the water-soluble, positively charged peptides to the vesicles. In the case of the short-sized lipid system, the initial idea was to use a mixture DLPC/DLPG with an acyl chain of 12:0, but no encapsulation of the dyes was detected. A mixture DMPC/DMPG (acyl chain 14:0) was then tried, in this case some encapsulation was achieved but continuous leaking of the dye was detected and the vesicles could not therefore be used. It seemed that short, saturated chains were not suitable for these leakage experiment. The shortest commercial lipid available with unsaturated chains was DMOPC but the corresponding PG lipid was not available so the final mixture used was DMOPC:DOPG.

Table 27: Lipid mixtures used in the leakage experiments. The lipid numbers (number of carbons :number of insaturations) and hydrophobic thickness of lipid bilayers are also given.

Lipid system	Acyl chain	Length (Å)	Comment
DMoPC	14:1	19.2	Short size
DOPG	18:1	26.8	
POPC	16:0/18:1	28.3	Medium size
POPG	16:0/18:1	28.3	
DEPC	22:1	34.4	Long size
DEPG	22:1	34.4	
POPC	16:0/18:1	28.3	Mixed
DEPG	22:1	34.4	
DEPC	22:1	34.4	Mixed
POPG	16:0/18:1	28.3	

Leakage curves were measured at different P/L ratios, over 10 minutes after addition of vesicle solutions to the peptide solution in the cuvette. At low peptide concentration only partial leakage was observed, but with a higher P/L of 1:25 or higher, there was in almost all cases either no leakage (10% or less) or total leakage (85% or more), as shown in Figure 54 for POPC/POPG. A clear length-dependent effect was observed,

where leakage was found only when peptides were long enough to span the hydrophobic part of the membrane, or longer.

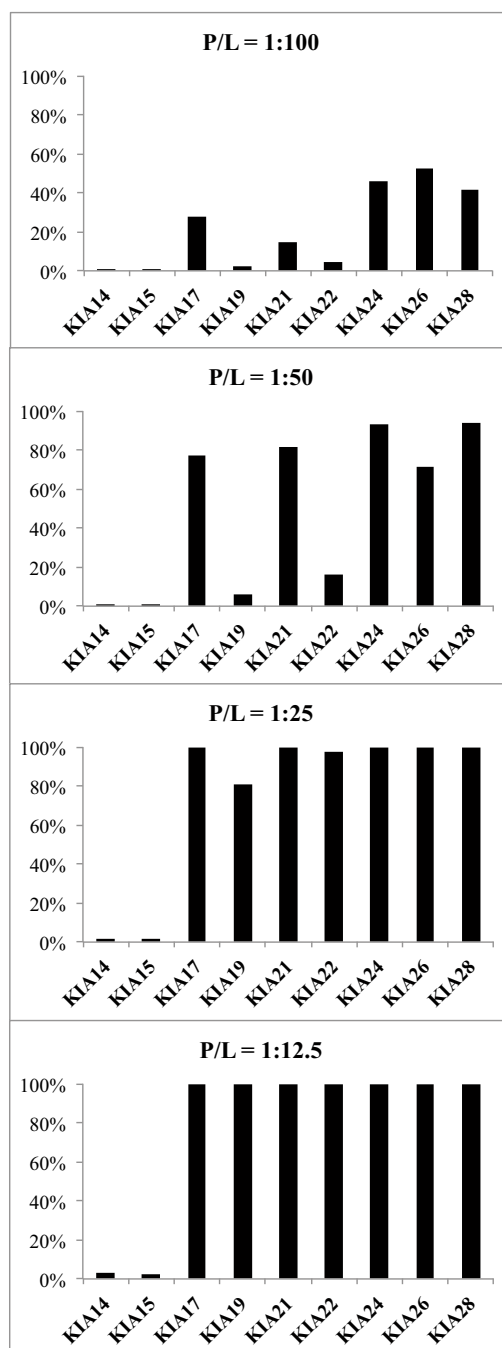


Figure 54: Leakage of POPC/POPG (1:1) vesicles at different peptide-to-lipid molar ratios (P/L) of KIA peptides, after 10 minutes. At high peptide concentration the shortest peptides give no leakage, but KIA17 and longer peptides give 100% leakage.

The results at P/L = 1:12.5 are given in Table 28. It can be observed that in POPC/POPG, no leakage was detected for KIA14 and KIA15, but with KIA17 or longer peptides, almost complete leakage was observed. In DEPC/DEPG, there was also a threshold, but in these longer chain lipids, only KIA24 and longer peptides gave rise to leakage. Interestingly, when PC and PG lipids of different length were mixed, the

threshold length of the peptides was mainly determined by the acyl chain length of the charged PG lipids. In DMoPC/DOPG and DEPC/POPG, the behaviour was identical to that of POPC/POPG, so that KIA17 or longer peptides gave total leakage, even if the PC lipids were much shorter and longer than POPC, respectively. However, in POPC/DEPG, the threshold was in between that of POPC/POPG and DEPC/DEPG; here 21 residues long peptides were needed for leakage.

Table 28: Leakage induced by KIA peptides in vesicles of different lipid composition. Leakage is given after 10 minutes at P/L=1:12.5, as percentage of leakage after addition of Triton X-100 (defined as 100% leakage). The length of peptides and hydrophobic thickness of lipid bilayers are also given. Inactive peptides for the different lipid systems are marked in grey.

Peptide		Lipids				
		DMoPC/DOPG	POPC/POPG	DEPC/POPG	DEPC/DEPG	POPC/DEPG
	Length (Å)	19.2 / 26.8	28.3 / 28.3	34.4 / 28.3	34.4 / 34.4	28.3 / 34.4
KIA14	21	8	3	5	1	2
KIA15	22.5	3	2	3	0	2
KIA17	25.5	100	100	84	1	17
KIA19	28.5	100	100	30	2	4
KIA21	31.5	100	100	98	4	82
KIA22	33	100	100	85	6	26
KIA24	36	100	100	100	89	100
KIA26	39	100	100	100	10	97
KIA28	42	100	100	100	84	100

In some cases, longer peptides were less active than shorter ones (for example KIA19 is less active than KIA17 in DEPC/POPG, and KIA26 is less active than KIA24 in DEPC/DEPG). In these cases, a detailed analysis shows there is leakage also for the longer peptide, but at a lower rate (example in Figure 55). It can be noted that the more active peptides all end with Ile-Ala, while the longer, less active peptides all end with Lys.

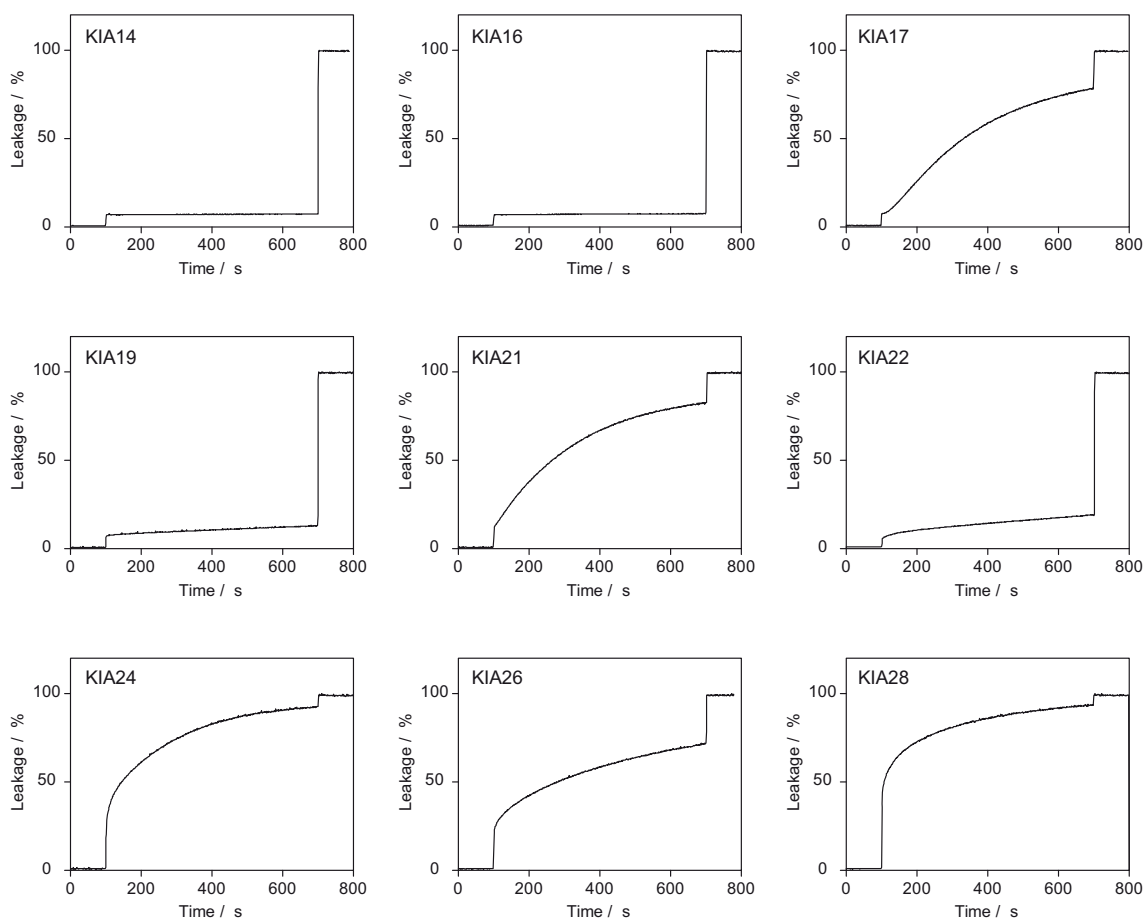


Figure 55: Time dependent leakage of KIA peptides in POPC/POPG (1:1) vesicles at P/L = 1:50. Vesicles are added after 100 s to the cuvette containing the peptide solution. After 700 s triton-X is added, giving complete (100%) leakage of the vesicles. KIA14 and KIA15 give no leakage. KIA17 and longer peptides give leakage, but with very different rates. KIA17, KIA21, KIA24 and KIA28 all end the amino acid sequence with Ile-Ala, and the rate is higher for longer peptides. KIA19, KIA22 and KIA26 all end the amino acid sequence with Lys, and also within this group, the rate is higher for longer peptides, but these peptides have a rate that is lower than the next shorter peptide.

B.3.3. Solid-state nuclear magnetic resonance spectroscopy

B.3.3.1. Fundamentals of NMR spectroscopy

NMR employs an intrinsic property of atomic nuclei, their **nuclear spin**. Only nuclei with spin $I > 0$ are suited for this method. Placing the nuclei in an external magnetic field gives rise to different energy for different spin states. Application of electromagnetic radiation in the radio frequency range, enables transitions between different energy states (resonance) to be measured, resulting in the NMR spectrum.

In solid-state NMR spectroscopy the orientational dependence of internal interactions, i.e. interactions between nuclear spins of a sample, can be detected. In solution these interactions are averaged out due to fast isotropic motions of the molecules and cannot be observed directly.

The spin of an atomic nucleus is composed of the spins of its protons and neutrons, each having a spin $I = 1/2$. The resulting nuclear spin is described by its spin quantum number I , being an integer multiple of $1/2$. A selection of nuclear isotopes along with their properties is shown in Table 29.

Table 29: A selection of isotopes and their properties.

Isotope	Spin quantum number I	Gyromagnetic ratio γ ($\text{T}^{-1} \text{s}^{-1}$)	Natural abundance (%)	Sensitivity (relative to ^1H)
^1H	$\frac{1}{2}$	$2.675 \cdot 10^8$	99.98	1.0
^2H	1	$4.11 \cdot 10^7$	0.015	0.0096
^{12}C	0	--	98.9	--
^{13}C	$\frac{1}{2}$	$6.73 \cdot 10^7$	1.1	0.0159
^{14}N	1	$1.93 \cdot 10^7$	99.6	0.00101
^{15}N	$\frac{1}{2}$	$-2.71 \cdot 10^7$	0.36	0.00104
^{19}F	$\frac{1}{2}$	$2.517 \cdot 10^8$	100	0.833
^{31}P	$\frac{1}{2}$	$1.083 \cdot 10^8$	100	0.0663
^{32}S	0	--	99.26	--

Due to its nuclear spin the nucleus has a magnetic moment $\bar{\mu}$. This is proportional to the spin vector \bar{I} and to the gyromagnetic ratio γ , a constant for each nucleus, according to $\bar{\mu} = \gamma \cdot \bar{I}$. When no magnetic field is present, the magnetic moments of nuclei can be aligned randomly in any direction. The energies of all nuclei are identical, i.e. they exhibit Zeeman degeneracy. When these nuclei are placed in a magnetic field B_0 , they exhibit Zeeman splitting, i.e. they adopt different discrete energy states proportional to their magnetic moment μ and the applied magnetic field (Figure 56). The number of possible energy states they can adopt, depends on their spin quantum number I .

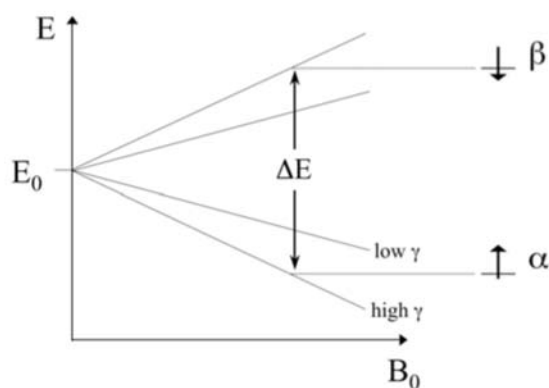


Figure 56: Zeeman splitting for nuclei with $I=1/2$ results in the two different spin states β (higher) and α (lower). ΔE between the energy levels of both spin states is linearly dependent on the external magnetic field B_0 and on the gyromagnetic ratio γ of a particular type of nucleus.

Nuclei ^{31}P and ^{15}N with $I=1/2$ were used in this study. They exhibit two energy states, α and β . The projection of a nuclear spin magnetic moment along the direction of the magnetic field B_0 , is either parallel or antiparallel to B_0 , with the parallel orientation being the lower energy state. The extent to which nuclear spins favour the low-energy state over the high-energy state at equilibrium is described by the Boltzmann equation.

The slight excess of nuclear spins in the lower energy state at equilibrium results in a net magnetic field (vector) of a sample along the direction of the applied magnetic field, i.e. the z-axis. That is called the bulk equilibrium magnetization.

The different energy levels give rise to the NMR spectrum, as the nuclear spins can undergo a transition between both energy states upon absorption of electromagnetic radiation matching this energy difference (resonance). At magnetic field strengths used in NMR experiments, the frequencies necessary to fulfill that condition are in the RF range, i.e. in the range of tens to hundreds of MHz.

B.3.3.2. Single-pulse experiment

In a single-pulse experiment (Figure 57) an RF pulse of appropriate frequency and duration is applied from the (sample/receiver) coil along the x-axis. That 90°_x -pulse rotates the magnetization vector M_0 away from its equilibrium position along the z-axis around the x-axis onto the y-axis. The magnetization vector rotates around the external magnetic field vector in the xy-plane at its Larmor frequency $\omega = -\gamma \cdot B_0$. The Larmor frequency corresponds to the difference between the two energy states and for a given external static magnetic field is proportional to the gyromagnetic ratio γ of a nucleus; hence it is a characteristic for each isotope. The rotation of the magnetization vector around the z-axis induces an oscillating current in the (sample/receiver) coil along the x-axis, the free induction signal. This is the NMR-signal. Relaxation processes cause this x-magnetization to decay away to zero over time, returning to equilibrium. The signal is also called free induction decay. Fourier transformation converts the time domain signal, the FID, into a frequency domain signal, the NMR spectrum.

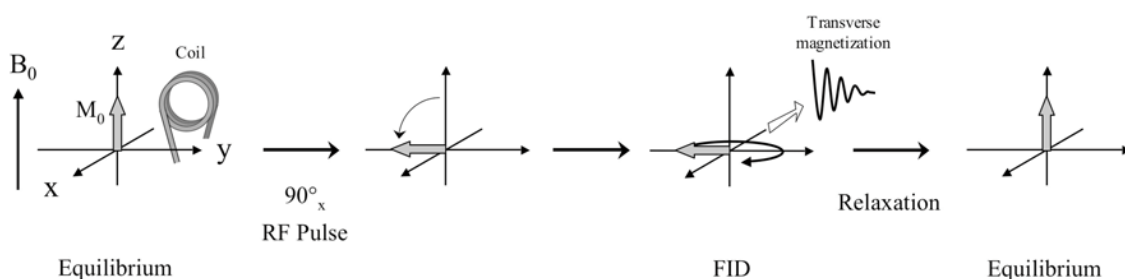


Figure 57: Basic principle of a single-pulse experiment as described in the text.

B.3.3.3. Spin interactions

Spin interactions can be grouped into external and internal interactions. External interactions are the above-described Zeeman interaction with the external static magnetic field B_0 and the interaction with the applied B_1 -field (RF). From the above description one should expect the same frequency signal for identical isotopes in a particular NMR experiment. However, the exact resonance frequency is slightly

changed due to several internal interactions of the nuclear spins, i.e. due to their environment in the sample. These internal interactions modulate the energy states and the transitions between them. That is the main source of the information NMR spectroscopy can give, including the local structural information. Internal interactions are chemical shielding, J-coupling, dipolar coupling and quadrupolar coupling. They depend on the chemical environment of a nucleus.

Only one of these essential internal interactions will be used in this work and will be described in brief below, i.e. the chemical shielding, resulting in shifts of signals in the spectrum.

B.3.3.3.1. Chemical shielding

The effective magnetic field that a nucleus encounters depends on its electronic environment, as the surrounding electrons may enhance or reduce the applied external magnetic field, by generating a secondary magnetic field. Depending on the chemical surrounding, the resonance frequency of a nucleus is slightly shifted. Values for the chemical shift are very small compared to the Larmor frequency and are given in parts per million. The chemical shift has a time-averaged (isotropic) value in solutions, where molecular tumbling is in the range of up to 10^3 GHz. That results in a particular resonance shift for nuclei in a particular type of chemical surrounding, e.g. for a certain chemical group.

However, the electron distribution around a nucleus is not spherically symmetric, but depends on the shape of its molecular orbital. In solids, where the motion of molecules is restricted, the chemical shift hence depends on the orientation of a molecule within the applied external magnetic field. This effect is called chemical shift anisotropy. Every orientation of a molecule with regard to the magnetic field contributes to the overall spectrum by a single line of a particular frequency.

In a single crystal, all molecules have the same orientation and a single signal is obtained, varying with the orientation of the crystal. In a powder, where all orientations of molecules are present, the resulting spectrum is called a “powder spectrum”.

The orientational dependence (anisotropy) of the chemical shift can be mathematically described by a CSA tensor (3 x 3 matrix) and can be visualized as an asymmetric ellipsoid, in the most general case with three different main tensor components. Transformed into its own principal axes system by diagonalization, the three main tensor elements coincide with the three coordinate axes of the PAS. The PAS is characteristic for each nucleus in its specific chemical environment and the applied external magnetic field is not necessarily aligned along the external B_0 field (z-axis) anymore. A general tensor with three different principal axes is shown in Figure 58. The order of shielding magnitude of the tensor elements is defined as $\sigma_{11} \leq \sigma_{22} \leq \sigma_{33}$ with σ_{11} representing the least shielded element, resulting in the highest field resonance, and σ_{33} the most shielded element, resulting in the lowest field resonance (Figure 59, upper three pictures). The orientation of the external magnetic field B_0 vector in the PAS system is described by the angles θ and Φ between B_0 and the PAS z-axis, i.e. σ_{33} (Figure 58).

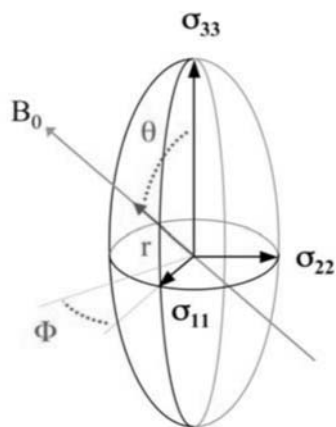


Figure 58: Graphical presentation of a CSA tensor with three different principle axes. The tensor represents the orientation dependence of the chemical shielding. The length of a vector along B_0 from centre to surface (r) of the ellipsoid defines the frequency in the NMR spectrum.

In an un-oriented powder, all orientations of a molecule are present with equal probability. However, except for the outermost tensor values, several combinations of the polar angles deliver the same values for r , resulting in a characteristic powder pattern or tensor line shape (Figure 59, lower).

In solutions of low viscosity, where the molecules move rapidly along all three axes, the electronic environment is averaged out to a spherical distribution, giving an isotropic value for the CSA tensor and hence for the chemical shift, as mentioned above, according to $\sigma_{\text{ISO}} = (\sigma_{11} + \sigma_{22} + \sigma_{33}) / 3$.

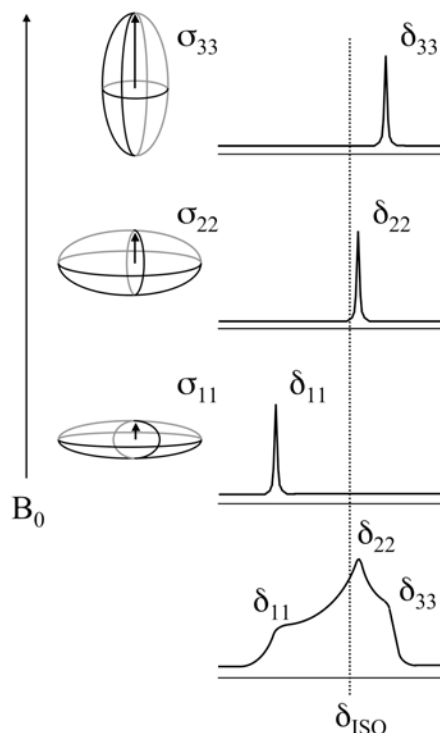


Figure 59: CSA anisotropy for a tensor with three different principle axes. The tensor ellipsoid (left) is depicted aligned with its principal axes along the magnetic field, resulting in the characteristic frequencies (right three, upper) of the powder spectrum (right, lower), which is the sum of single frequencies of multiple randomly aligned tensors in a sample, i.e. molecules with different orientations.

B.3.3.4. ^{31}P -ssNMR as a tool to study phospholipids

Phospholipids in a membrane environment under physiological conditions can rotate freely along their longitudinal axis, but are restricted in their tilt. Hence, the three-component ^{31}P CSA tensor of the phospholipid head group is averaged to an axially symmetric CSA tensor, with two of three axes being identical. In the fluid lamellar bilayer phase the axis of rotation of a phospholipid is aligned parallel to the local membrane normal, so is the least shielded element σ_{\parallel} (0° edge) of the averaged ^{31}P CSA tensor, resulting in the highest chemical shift. The most shielded perpendicular CSA element σ_{\perp} (90° edge) results in the lowest chemical shift.

Therefore, when lipid bilayers are macroscopically aligned, i.e. the molecular orientation is fixed with regard to the magnetic field, the resulting spectrum shows one narrow line. The exact position under a particular alignment is characteristic for a particular lipid. Oriented DMPC lipid bilayers, for example, at 0° alignment of their membrane normal with regard to the magnetic field, show a signal at about +30 ppm corresponding to σ_{\parallel} . Badly oriented lipid bilayers give rise to additional signals along the whole CSA range, in case of DMPC bilayers from approximately +30 up to about -15 ppm (σ_{\perp}). Upon integration and comparison of signals at the 0° edge with the whole CSA range, the degree of the orientation of a sample can be determined.

Multilamellar vesicles are concentric spheres up to about $1\ \mu\text{m}$ in diameter. Suspensions of phospholipid vesicles due to spherical distribution of lipids, result in a characteristic shape of the spectrum with more lipids contributing to σ_{\perp} than to σ_{\parallel} (Figure 60).

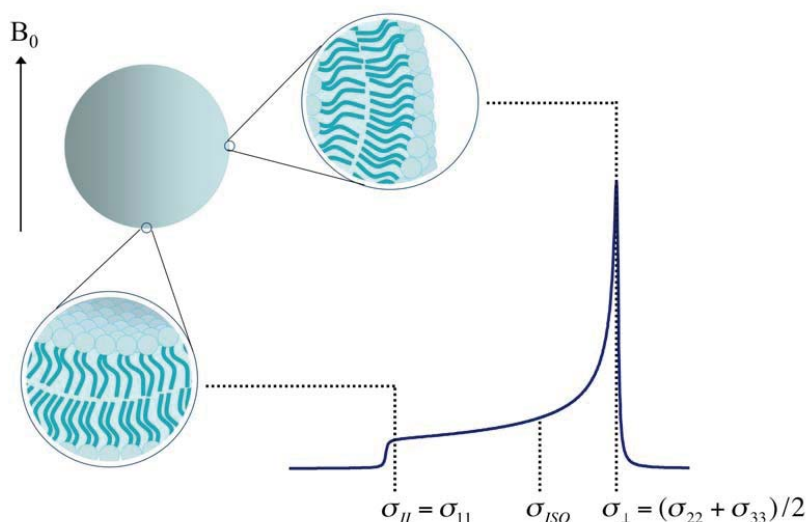


Figure 60: Simulated solid-state ^{31}P -NMR spectrum of phospholipids in fluid lamellar bilayers in vesicles. The CSA tensor is axially symmetric due to rotation of lipids around the membrane normal.

B.3.3.5. ^{15}N -ssNMR as a tool to study peptide orientation in lipid membranes

The most common label for ssNMR studies of membrane-bound peptides is ^{15}N in the backbone. When the peptide forms an α -helix, the NH bond vector will lie almost parallel to the helical long axis. The σ_{33} element of the CSA tensor of ^{15}N is aligned roughly along the NH bond and, thus, also more or less parallel to the helix axis. It is, therefore, possible to estimate the peptide orientation simply by looking at the narrow chemical shift signal of a single labelled position, as illustrated in Figure 61.

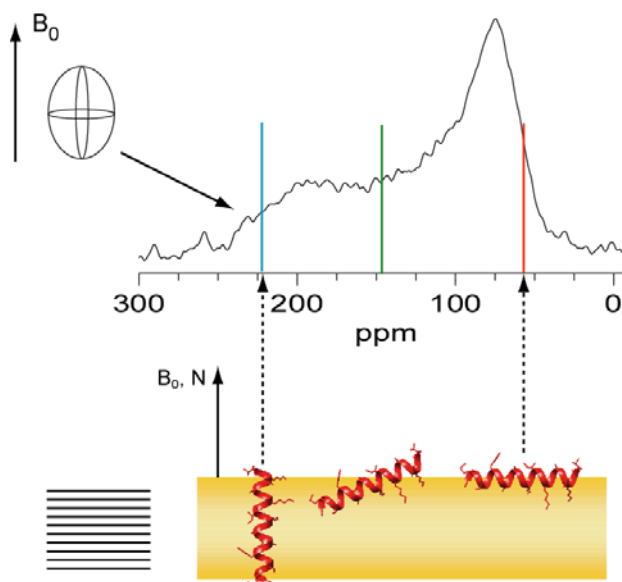


Figure 61: The orientation of an α -helical peptide in a lipid bilayer can be determined by visual inspection of the anisotropic chemical shift of a single ^{15}N labelled amide group, when measured in an oriented membrane sample. This approach is relatively straightforward because the ^{15}N CSA tensor is almost axially symmetrical and aligned almost parallel to the helical axis. A helical peptide in a transmembrane orientation gives a chemical shift close to 220 ppm (blue). A peptide lying flat on the bilayer surface gives a chemical shift close to 50 ppm (red). Tilted peptides give chemical shifts in between these values (green).

This one-dimensional ^{15}N -ssNMR experiment has to be performed on macroscopically oriented samples that are aligned with their normal parallel to the static magnetic field. By tilting the sample at a right angle, it is furthermore possible to find out whether a peptide is undergoing fast long-axial rotation about the membrane normal. A narrow line is indicative of such motion, whereas a broadening up to the static CSA width indicates a static alignment in the membrane. The line width of an oriented ^{15}N signal can be on the order of 10 ppm, while the chemical shift range of the static powder sample of the dry peptide is approximately 200 ppm. The helix tilt angle cannot be defined very accurately from a single label (there will be a range of possible tilts, varying up to 30° depending on the chemical shift value), but it is easy to distinguish between a transmembrane orientation and a peptide lying flat on the membrane surface.

Since ^{15}N has a very low sensitivity in NMR, usually a cross-polarization sequence is used. The principle is to transfer the magnetization from ^1H , which has a much higher polarization, to the attached ^{15}N nucleus.

B.3.3.6. ^{31}P - and ^{15}N -ssNMR to study the orientation of the KIA peptides in lipid membranes

The last step of this study was to use solid-state NMR to analyse the orientation of the KIA peptides in different lipid systems, to investigate whether there is a length dependent reorientation of these amphipathic peptides in membranes. To do so, all KIA peptides had to be synthesized with a ^{15}N -amide at Ala-10, in order to perform ^{15}N -ssNMR experiments in several lipid systems.

The macroscopically oriented NMR samples were prepared by co-dissolving the peptides and the lipids in a mixture of methanol/chloroform (1:1, v/v) and spreading it onto thin glass plates. Once the plates were dry, they were stacked and placed into a hydration chamber for 18-24 h and finally wrapped in parafilm and plastic foil for the measurements. These oriented samples were placed in the flat-coil probe such that the lipid bilayer normal was usually aligned parallel to the magnetic field, but additional experiments were carried out in a perpendicular alignment to find out if the peptides were rotating around the bilayer normal (example of a sample preparation sequence in Figure 62).



Figure 62: Preparation of samples for ssNMR. From left to right: (1) Sample preparation, (2) Sample wrapping (3) The samples are placed in the flat-coil probe and (4) The probe is introduced in the NMR spectrometer for the measurements.

^{31}P -ssNMR measurements were always performed before and after the ^{15}N -ssNMR to check the quality of the lipid orientation in the samples. Considering the different length of the peptides, the concentration was varied such that the number of amino acid residues per lipid was kept constant, with a peptide-to-lipid molar ratio of 1:50 for KIA21 as a starting point.

It can be observed that in DOPC (Figure 63) and DEPC/DEPG (1:1) (Figure 64), all peptides gave a sharp peak close to 90 ppm, indicating that peptides were oriented on the surface of the membrane, with the peptide long axis parallel to the membrane plane.

In DMPC/lyso-MPC (2:1) (Figure 65), a much larger chemical shift was found for all peptides, which also varied with the peptide length. This indicates a more inserted state, with peptides having a more upright orientation in the membrane, with the helical axis close to parallel with the membrane normal. The shortest peptide, KIA14, gave a signal at 167 ppm, and longer peptides gradually had a smaller chemical shift down to 134 ppm for KIA28. This indicates that the shortest peptides are almost upright in the membrane, while longer peptides have a smaller tilt, which would be expected for transmembrane peptides where a larger tilt for longer peptides would be needed to avoid hydrophobic mismatch (Strandberg, et al., 2012a).

In DMPC (Figure 66), peptides were also found to lie more or less flat on the membrane surface. Here, samples were also made with a higher peptide concentration, P/L=1:20 for all the peptides (Figure 67). In this case, a peptide length dependent orientation was observed. KIA14 and KIA15 had signals indicating a surface orientation, but KIA17 and KIA19 had a chemical shift of around 150 ppm, indicating a more inserted state. KIA21 and KIA22 gave broad line shapes with signals both at 90 ppm and 150 ppm, where the 150 ppm signal is probably due to large aggregates. KIA24 had a signal around 90 ppm, but both KIA24 and KIA26 had a bad orientation in the membrane, as seen from the ^{31}P spectra, and KIA26 gave powder spectra both for ^{31}P and ^{15}N , indicating that these peptides at such a high P/L ratio form immobilized aggregates which disturbed the membranes and destroyed the membrane orientation.

Finally, some of the samples, both short and long peptides, were also measured at a 90° tilt (Figure 68), that is with the membrane normal perpendicular to the magnetic field (not all samples were measured as each measurement takes about 24 h long). In all cases, it was found that the peptides rotate fast around the bilayer normal, which is detected as a shift in the signal from one side of the isotropic chemical shift to the other side. In the case of DOPC and DEPC/DEPG bilayers, the chemical shift at 0° tilt was around 90 ppm (blue line), but when the measurements were done at 90° tilt, the value changed to around 140 ppm (red line). While for DMPC/lyso-MPC, which as previously commented, the peptides are inserted in the membrane, at 0° tilt the chemical shift was in the range of 140-170 ppm but it shifted to lower values of around 100 ppm when measuring at 90° tilt.

KIAGKIA / DOPC (1.2 mg peptide / 20 mg lipid)

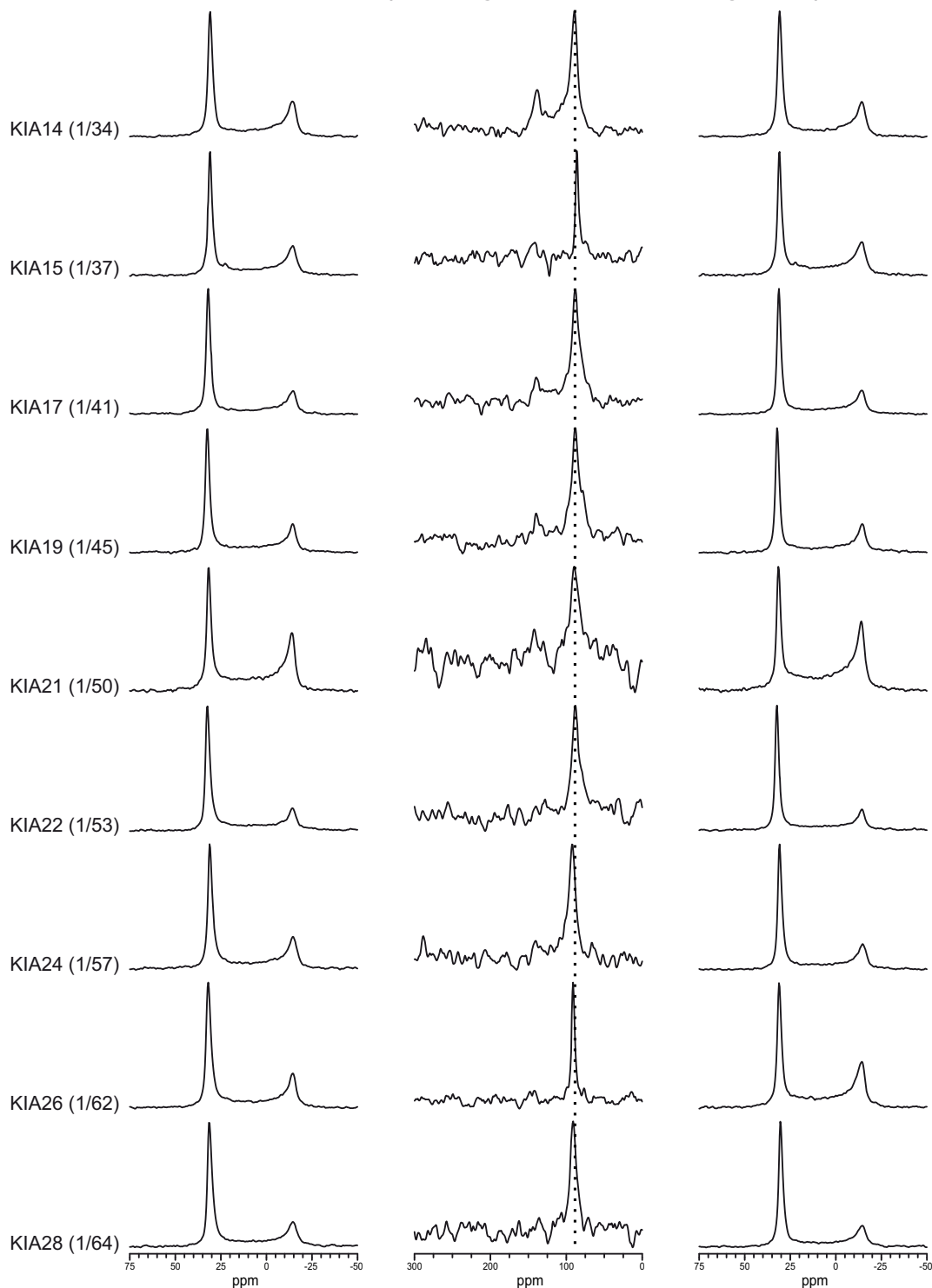


Figure 63: ^{15}N -ssNMR spectra (middle column) of KIA peptides in DOPC at a constant mass ratio of approximately 1.2 mg peptide and 20 mg lipid. The P/L value of each sample is given in the figure. ^{31}P -ssNMR spectra before (left) and after (right) ^{15}N -ssNMR are also shown. All peptides give a signal close to 90 ppm, indicating a surface-bound orientation. The shortest peptides also show some powder lineshape with a peak around 140 ppm.

KIAGKIA / DEPC:DEPG (1:1) (1.2 mg P / 10 mg:10 mg L)

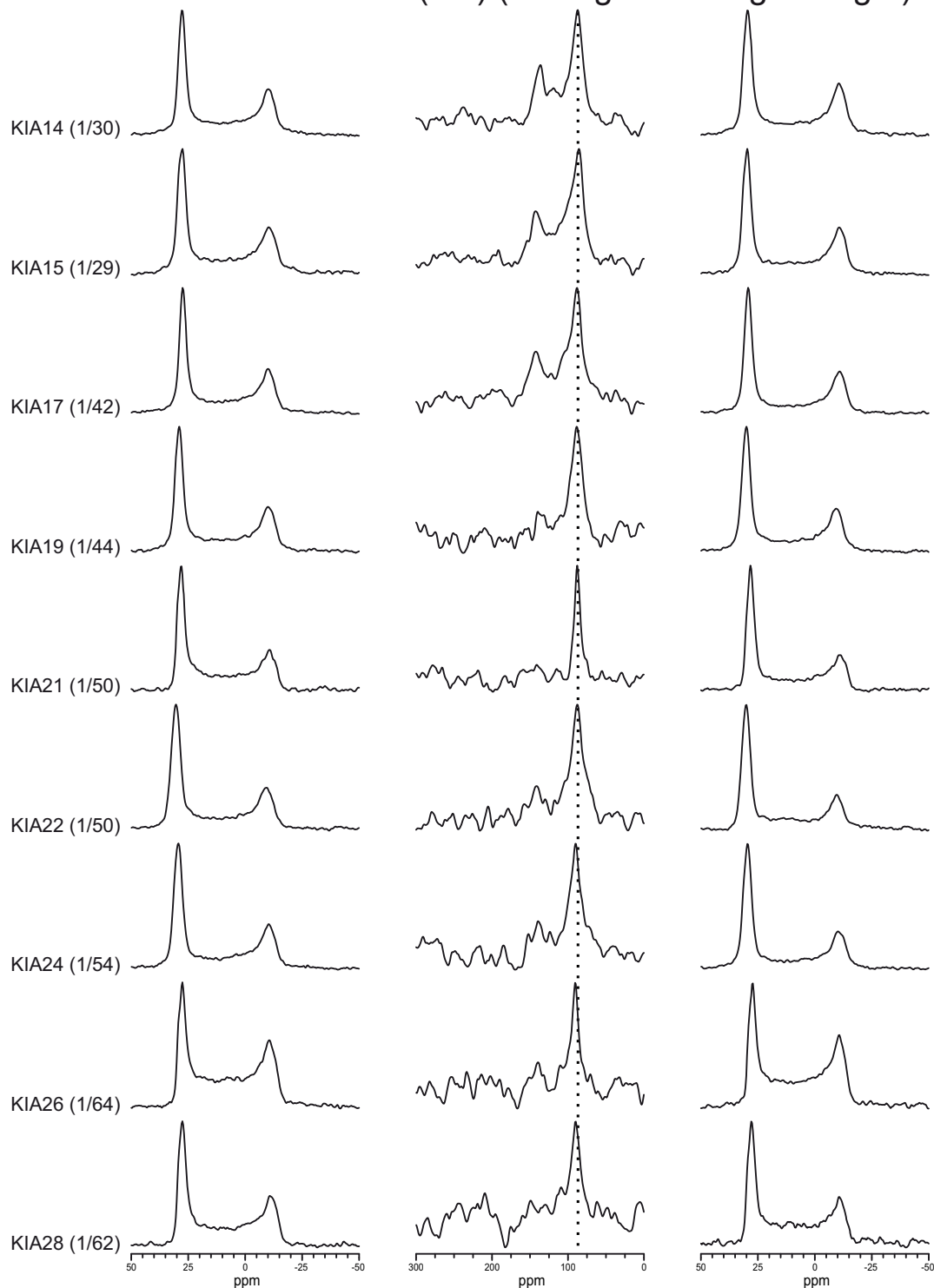


Figure 64: ^{15}N -ssNMR spectra (middle column) of KIA peptides in DEPC/DEPG (1:1) at a constant mass ratio of approximately 1.2 mg peptide and 20 mg lipid. The P/L value of each sample is given in the figure. ^{31}P -ssNMR spectra before (left) and after (right) ^{15}N -ssNMR are also shown. All peptides give a signal close to 90 ppm, indicating a surface-bound orientation. The shortest peptides also show some powder lineshape.

KIAGKIA / DMPC lysoMPC (2:1) (1.2 mg P / 12 mg:5 mg L)

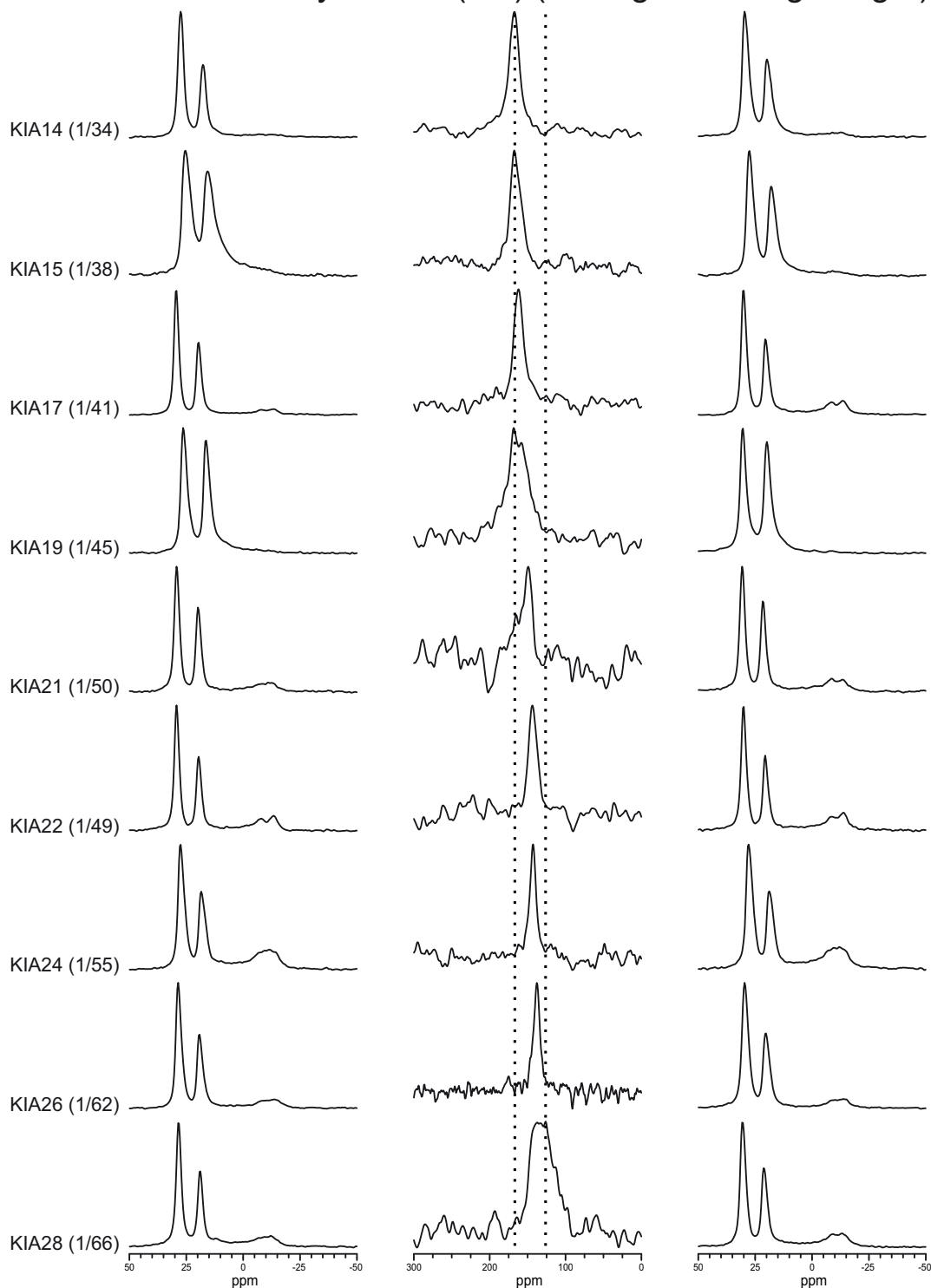


Figure 65: ^{15}N -ssNMR spectra (middle column) of KIA peptides in DMPC/lyso-MPC (2:1) at a constant mass ratio of approximately 1.2 mg peptide and 17 mg lipid. The P/L value of each sample is given in the figure. ^{31}P -ssNMR spectra before (left) and after (right) ^{15}N -ssNMR are also shown. The chemical shift of KIA14 is 167 ppm, indicating an almost upright orientation. Longer peptides have smaller chemical shifts indicating that they are less tilted.

KIAGKIA / DMPC (1.1 mg peptide / 15 mg lipid)

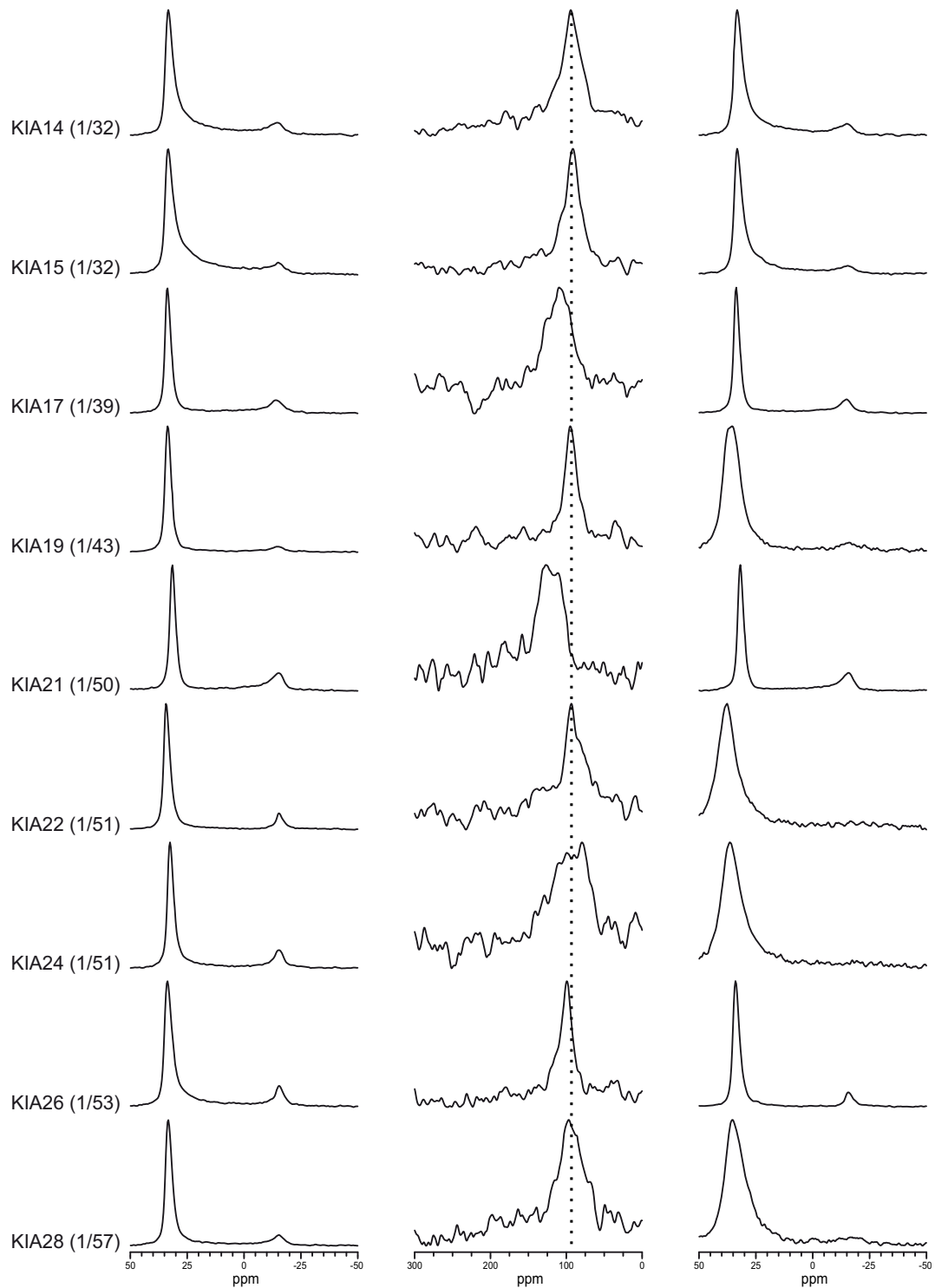


Figure 66: ^{15}N -ssNMR spectra (middle column) of KIA peptides in DMPC at a constant mass ratio of approximately 1.1 mg peptide and 15 mg lipid. The P/L value of each sample is given in the figure. ^{31}P -ssNMR spectra before (left) and after (right) ^{15}N -ssNMR are also shown. Peptides are mostly flat on the membrane, but KIA17, KIA21, KIA24 and KIA28 (which correspond to those peptides that end with Ile-Ala) give broader lines and KIA17 and KIA21 seem to be more tilted

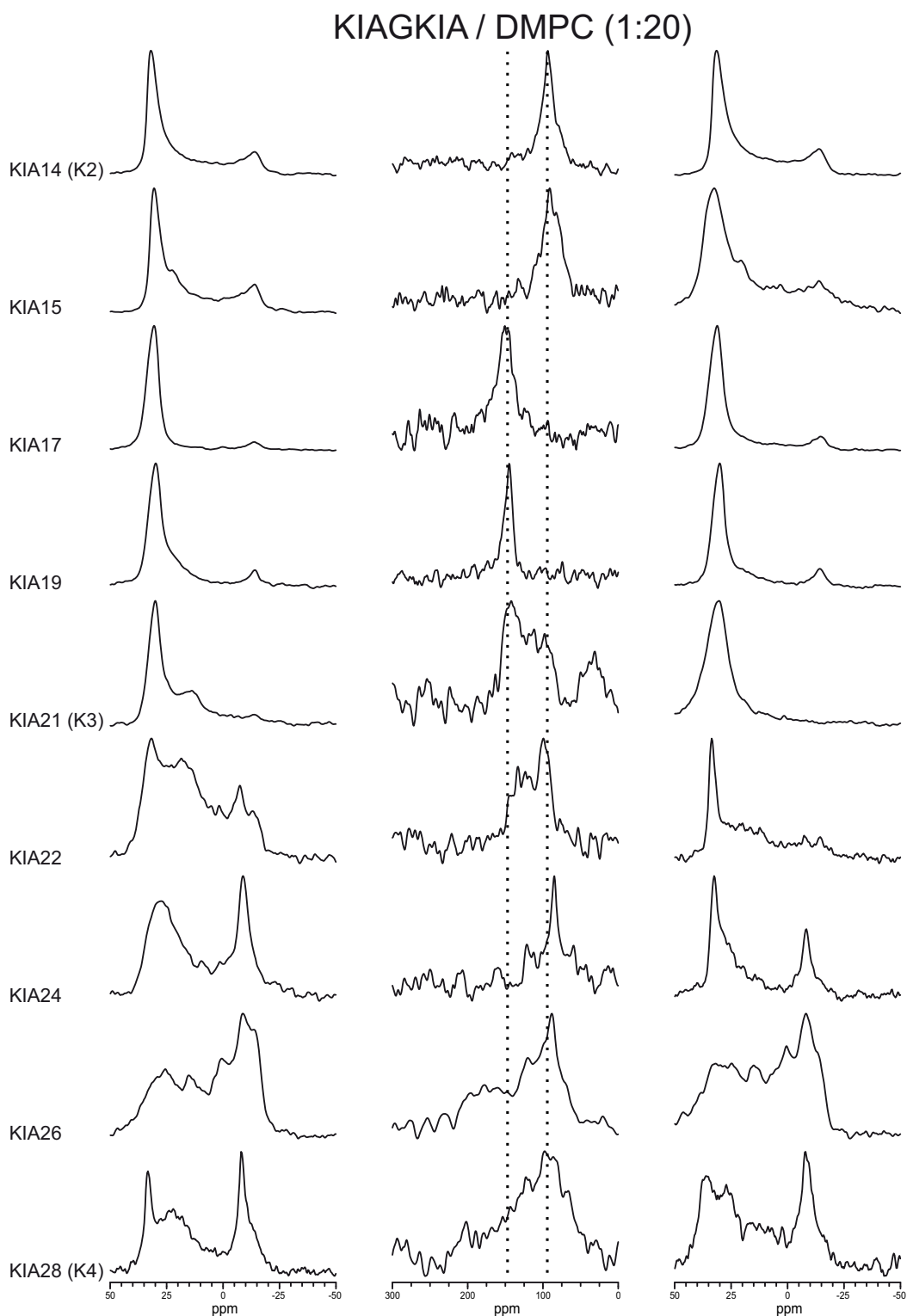


Figure 67: ^{15}N -ssNMR spectra (middle column) of KIA peptides in DMPC at P/L = 1:20. ^{31}P -ssNMR spectra before (left) and after (right) ^{15}N -ssNMR are also shown. There is a shift in the ^{15}N -ssNMR peak from around 90 ppm, typical of S-state, in KIA14 and KIA15, to a peak around 150 ppm, indicating a more tilted, inserted state for KIA17 and longer peptides. For KIA21 and longer peptides the ^{31}P -ssNMR spectra show disturbed lipids and powder-like lineshapes are then seen in the ^{15}N -ssNMR spectra.

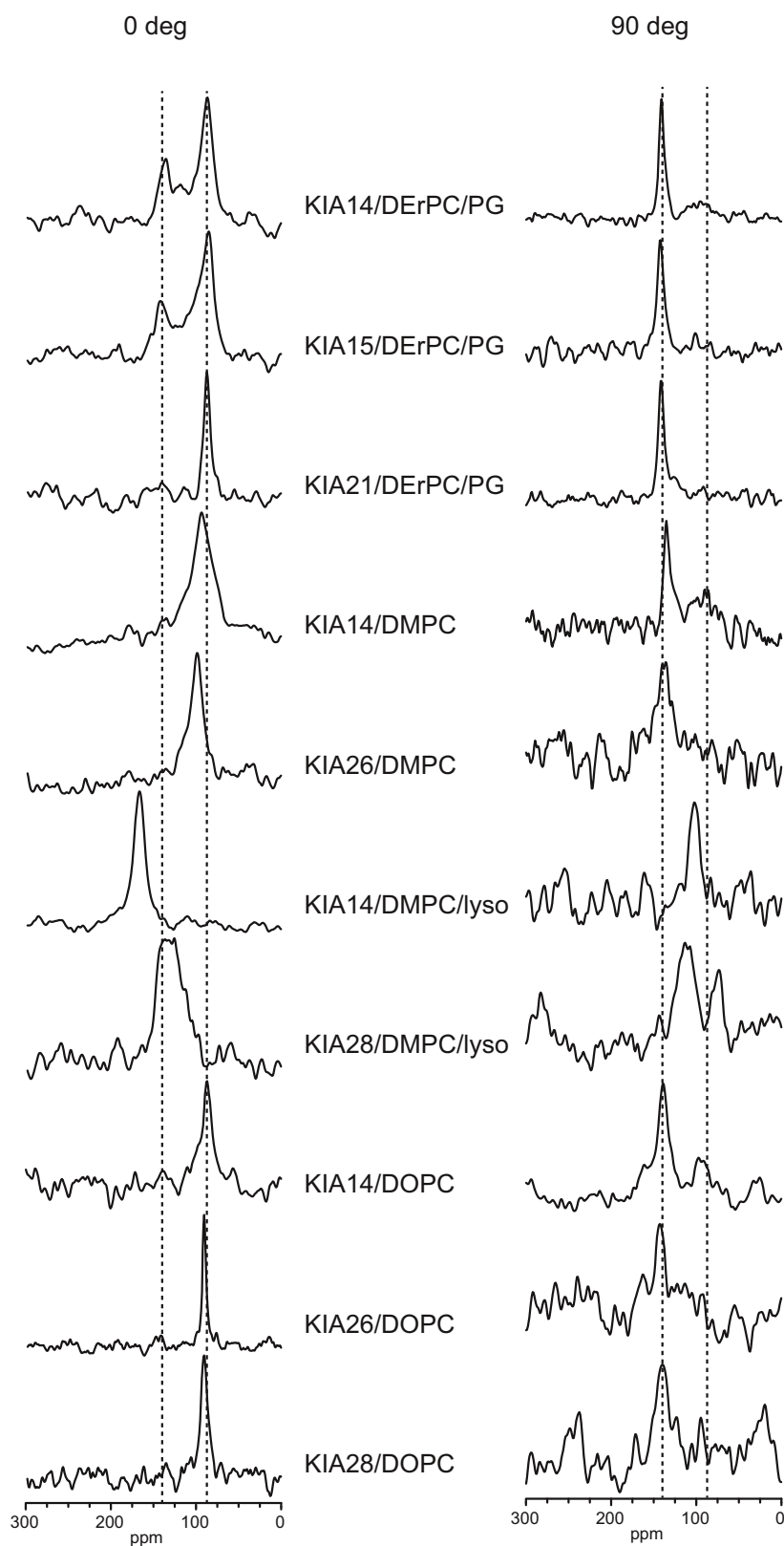


Figure 68: ^{15}N -ssNMR spectra of several KIA peptides in different lipid systems at 0° tilt, that is with the lipid bilayer normal aligned parallel to the magnetic field (left), and at 90° tilt, in this case the lipid bilayer normal is perpendicular to the magnetic field (right). It can be observed that the peptides rotate fast around the bilayer normal as detected by a shift in the signals.

B.4. DISCUSSION SECTION B – Length dependent activity of α -helical amphipathic membrane bound peptides

In this part of the thesis, by using model peptides with repeats of the basic sequence KIAGKIA with 14 to 28 amino acids it was found that the antimicrobial effect has a threshold length, with a different minimum length in different bacterial strains. The leakage experiments using vesicles of different composition also showed that a threshold length was needed for the dye to leak. In the case of the haemolysis assay, a stepwise increase with peptide length was detected, but no clear threshold length was found.

All these results are consistent with the hypothesis that peptides form pores through the membrane with a transmembrane orientation of peptides, as shown in Figure 46. Such pores can only form if the peptide is long enough to span the membrane; shorter peptides will stay on the membrane surface and are inactive.

Using the formulae from a study by Marsh (Marsh, 2008) the membrane thickness can be estimated as the lipid acyl chain is known, and the length of α -helical peptides can be estimated as 1.5 Å per residue, therefore a quantitative analysis can be done. In Table 28 the peptide lengths and hydrophobic thicknesses of lipid bilayers are depicted, and the results for the leakage experiments at this particular P/L ratio. For DEPC/DEPG, there is a very clear correlation, so that only peptides longer than the hydrophobic thickness of 34.4 Å give any leakage, but longer peptides give full leakage. In POPC/POPG, KIA17 with a length of 25.5 Å gives leakage, even though it is slightly too short compared to the lipids (28.3 Å), and all longer peptides also give leakage. Given these results, it can be concluded that **only peptides long enough to span the membrane can form pores that are responsible for leakage**. The peptide length needed to span the membrane is approximately given by the length of the corresponding ideal α -helix, with 1.5 Å per residue, but this is a simplified model. It is known that close to the termini helices can unwind, which could slightly change the length. It is interesting that those peptides with Ile-Ala at the C-terminus were often more active in the leakage assay, than the next longer peptide with Lys at the terminal, indicating that subtle length effects can be due to the exact residues at the end of the helix. One reason could be that the addition of a Lys makes the peptide more charged and less hydrophobic (helical wheels of KIA14, KIA21 and KIA28 are shown in Figure 69), and therefore it has less affinity to bind to the membrane as seen with the slower dynamics of these peptides (Figure 55) in the leakage assay.

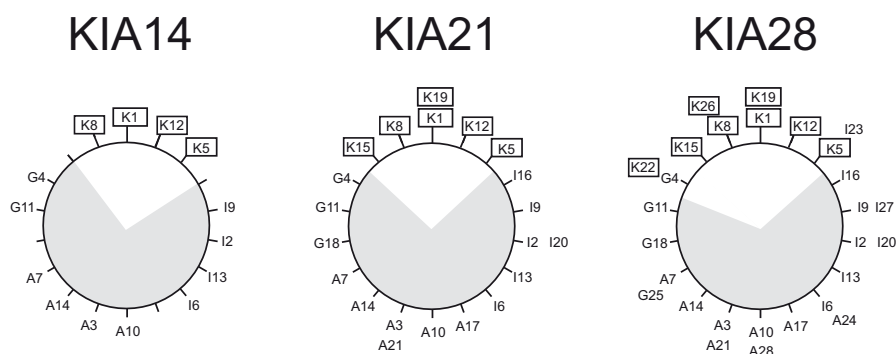


Figure 69: Helical wheel projections of the amphiphilic α -helical peptides KIA14 ((KIAGKIA)₂-NH₂), KIA21 ((KIAGKIA)₃-NH₂) and KIA28 ((KIAGKIA)₄-NH₂). Charged residues are marked by rectangles and the hydrophobic sector is shaded.

When using lipid systems with different length PC and PG lipids (DEPC/POPG and POPC/DEPG), it is clear that **the threshold length of the peptides is determined mostly by the length of the PG acyl chains**. DMoPC/DOPG and DEPC/POPG have the same threshold as POPC/POPG, even though the PC lipids have very different length acyl chains; DMoPC (Di-14:1-PC) only 19.2 Å and DEPC (Di-22:1-PC) as much as 34.4 Å, but DOPG has a length (26.8 Å) comparable to that of POPG (28.3 Å). On the other hand, POPC/DEPG has a threshold in between POPC/POPG and DEPC/DEPG. These observations lead to the conclusion that **the positively charged KIA peptides will bind to the membrane surface and attract negatively charged PG lipids, forming a PG-rich domain. The peptide must then be long enough to span this domain in order to form pores.**

In order to determine the orientation of the peptides in different lipid bilayers, solid-state ^{15}N -NMR was performed. In DOPC and DEPC/DEPG (1:1) all the peptides were found to lie flat on the membrane surface. This was no surprise, since it has been previously seen for other AMPs and for MSI-103 that amphipathic helices always prefer this orientation in lipids with unsaturated chains, which has been shown to be related to the negative spontaneous curvature of these lipids (Strandberg, et al., 2012b; Strandberg, et al., 2013). On the other hand, in DMPC/lyso-MPC (2:1) membranes, which due to the lyso-lipids have a positive spontaneous curvature, all peptides get into a more inserted, probably transmembrane orientation, also in agreement with previous studies (Strandberg et al., 2013; Strandberg, et al., 2012b). In DMPC at high peptide concentrations (P/L=1:20), a peptide length dependent orientation was observed, and in this case the peptides started to get inserted when the peptide length (i.e. 25.5 Å for KIA17) reached the bilayer hydrophobic thickness (i.e. 25.4 Å for DMPC). Even if the chemical shift of 150 ppm of KIA17 in DMPC is not as high as the chemical shifts found in DMPC/lyso-MPC, and may not correspond to completely upright peptides, this indicates that **the peptides start getting inserted when they are long enough to span the membrane.**

The orientation found in ^{15}N -ssNMR does not correlate well with the membrane leakage, but can still be reconciled with the activity. Leakage is found when pores are formed, but it may be enough to have a small population of peptides in these possibly transient and short-lived pores to get considerable amount of leakage. On the other hand, ^{15}N -ssNMR gives a steady-state picture of all peptides. If only a small fraction of peptides are in the transmembrane, pore-forming state at a given time, this will hardly be seen in the NMR-spectra. **That a large population of inserted peptides was observed in DMPC and especially in DMPC/lyso-MPC membranes indicates that in these lipid systems, peptides are more likely to insert into stable pores, and in DMPC at high concentration the insertion also fits with the peptide length.**

As previously commented, leakage could not be determined in DMPC/DMPG (1:1) bilayers, only when using unsaturated lipids, stable vesicles were formed. The fact that in such lipids, ^{15}N -ssNMR did not show any inserted peptides, seems to mean that leakage can occur with only a small fraction of peptides forming pores at any given time, but the strong length dependence in leakage indicate that only peptides long enough to span the membrane can form pores at all.

In the leakage experiments synthetic lipids with known acyl chain length were used, while in the biological assays the biomembranes consist of a variety of lipids with

different chains and headgroups, and also other components like membrane proteins and cholesterol. Therefore, in the bacterial assays the membrane thickness is unknown. But assuming that bacteria are killed by pores, formed in the same way as in the leakage experiments in vesicles, we can now use the KIA peptides as a **molecular ruler** to get information about bacterial membrane thickness:

- In *E. coli*, we note that the shortest peptide able to kill bacteria is KIA17, which is able to induce leakage in POPC/POPG membranes. Thus, the *E. coli* **membrane thickness should be similar to POPC/POPG, or around 27 Å.**
- In *S. aureus* and *P. aeruginosa* KIA21, but not shorter peptides, can kill the bacteria and thus **the membranes should be around 30 Å thick.**
- *E. faecalis* was only killed by KIA24 or longer peptides, which were also needed to induce leakage in DEPC/DEPG, so **the membrane thickness of *E. faecalis* should be similar as in DEPC/DEPG, around 34 Å.**
- For **erythrocytes**, there was no clear threshold, but only KIA21 or longer peptides showed a large effect at high concentration, so these **membranes may be similar in thickness to those of *S. aureus* and *P. aeruginosa*, around 30 Å.**

5. CONCLUSIONS

The conclusions reached in this thesis are the following:

- Several **new lipopeptides analogues to the polymyxins have been successfully synthesized** according to the design principles established in the group. These novel compounds have demonstrated a high to very high activity, especially against multi-drug resistant bacteria and a broad spectrum of activity, as they are active against both Gram-positive and Gram-negative bacteria (while polymyxins are only active against the latter).
- Some of the peptides' behaviour against model membranes has been studied using fluorescence, where it has been demonstrated that **they are all able to bind to LPS with high affinity and they are all membrane-active peptides but with different rates depending on the sequence** (causing aggregation, mixing, etc.).
- Finally, some of our most active peptide, especially #8, were also studied using flow cytometry and TEM, where it was observed that **these peptides probably kill bacteria using several mechanisms of action** ('multi-hit') and the effect seems to be different on Gram-negative and Gram-positive bacteria according to their different membrane morphology.
- By synthesizing a series of KIA peptides with length varying from 14 amino acid residues to 28, it has been possible to determine **that length has a drastic effect on both antibacterial and haemolytic activity**. Long peptides have a lower MIC, therefore they are more active but the side effect is that they cause complete haemolysis of erythrocytes. Shorter peptides are less active but also less haemolytic, therefore a compromise between both activities should be achieved.
- **The formation of pores by these peptides has been demonstrated** by using different techniques. In the determination of the antibacterial activity a clear threshold for each tested strain was detected. In the leakage experiments, as different length lipid were used, a clear threshold depending on membrane thickness was also observed. In the case of the ssNMR experiments, in some lipid systems an inserted state could be detected demonstrating that the peptides are capable of inserting in the lipid bilayer by forming pores, and that these pores are only formed when the peptide is long enough to span the membrane.
- As a result of all these experiments, the KIA peptides were used as **membrane rulers** to determine the approximate thickness of the membranes of bacteria and erythrocytes.

6. EXPERIMENTAL PART

6.1. MATERIALS AND METHODS

6.1.1. SECTION A

6.1.1.1. Chemical synthesis of the polymyxin analogues

6.1.1.1.1. Solvents

All solvents used were reagent grade quality unless stated otherwise and used without further purification. DMF was kept over molecular sieves of 4Å, and a N₂ stream was bubbled before use. The Et₂O was dried and conserved over Na. Milli-Q water was obtained by filtrating purified water using a Milli-Q Plus system (Millipore) to obtain water with a resistivity superior to 18 MΩ/cm.

Solvent	Brand
Acetone	Scharlau
ACN quality HPLC	VWR
CHCl ₃	Scharlau
DCM	Scharlau or SDS
DMF peptide synthesis quality	SDS
Et ₂ O	Scharlau
EtOH	Panreac
H ₂ O (Milli-Q)	Millipore
MeOH quality HPLC	VWR

6.1.1.1.2. Reagents

All reagents used were of the maximum purity possible.

Reagent	Brand
MBHA	
Rink linker	Iris Biotech, Polypeptide Laboratories or Sigma-Aldrich
Amino acid residues	
Decanoic acid	Sigma-Aldrich
DIEA	Sigma-Aldrich
DIC	Sigma-Aldrich
DMSO	Acros Organics
Dodecanoic acid	Sigma-Aldrich
HCl 37%	Scharlau
HOBt	Sigma-Aldrich

Ninhydrin	Merck
Nonanoic acid	Sigma-Aldrich
Octanoic acid	Sigma-Aldrich
Piperidine	Fisher Scientific
TES	Sigma-Aldrich
TFA	Sigma-Aldrich
TIS	Sigma-Aldrich

6.1.1.1.3. Instruments

Instrument	Brand and Model
Centrifuge	Hettich <i>ROTOFIX 32 A</i>
Evaporator	BÜCHI <i>R-200</i>
Lyophilizer	Labconco <i>Freezone 6</i>
Mass spectrometry	<i>4800 Plus MALDI TOF/TOF</i> , ABSciex 1) Analytical: <i>Shimadzu Series 20 Prominence</i> , with two <i>LC-20AD</i> pumps, automatic <i>SIL-20A</i> injector, controller <i>CBM-20A</i> and detector <i>SPD-M20A</i> .
RP-HPLC	2) Semi-preparative: <i>Waters Delta Prep 3000</i> , with a <i>Waters 600E</i> pump and controller, manual <i>Waters 712</i> injector, detector <i>Waters 484</i> and a data recorder <i>Pharmacia Biotech RED 101</i> .
Weighing scale	Mettler <i>PJ360 DeltaRange</i> Mettler Toledo <i>AB204-S</i>

6.1.1.1.4. Methods

6.1.1.1.4.1. Qualitative ninhydrin assay

This assay allows the qualitative evaluation of the efficiency of the couplings of the amino acid residues in solid phase peptide synthesis, by means of the colorimetric detection of the free amino groups in the N-terminal side of the growing peptide chain. In the assay two different reagent dissolutions are used:

- Reagent A: phenol (40 g) is dissolved in warm absolute EtOH (10 mL). Parallely, KCN (65 mg) is dissolved in H₂O (100 mL) and 2 mL of this resulting dissolution are added to 100 mL of freshly distilled pyridine. The two obtained dissolutions are separately agitated with 4 g of Amberlite MB-3 resin for 45 minutes, filtered and the filtrates mixed.
- Reagent B: ninhydrin (2.5 g) is dissolved in absolute EtOH (50 mL), and the dissolution is carefully kept protected from light.

The assay is carried out by introducing in a tiny glass tube some clean and dry beads of the elongating peptide. Then, 6 drops of Reagent A and 2 of reagent B are added, and the mixture is heated at 110 °C for 3 minutes. The blue colour of the dissolution and the resin indicates the presence of free primary amino groups (positive assay), therefore the coupling is incomplete, while a yellow colour indicates the absence of free primary amino groups (negative assay) (reaction in Figure 70).

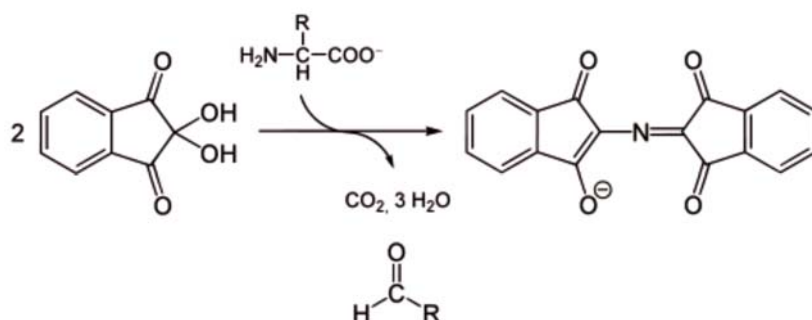


Figure 70: Reaction taking place between the free primary amino group and the ninhydrin, giving place to a blue compound (positive assay).

6.1.1.1.4.2. Hydrolysis and amino acid analysis

This method allows for the determination of the amino acid composition of a peptide sample and the quantification of the quantity of peptide synthesized.

A known quantity of dissolution of the lipopeptides in water was hydrolysed in 6M HCl at 110 °C overnight in a sealed tube (70 x 150 mm) containing a known volume of internal standard 2-aminobutyric acid (2.5 mM). The obtained residue was dried after repeated evaporation and re-dissolved in 20 mM of HCl to a final concentration of 0.1 mM. The amino acids were then analysed by HPLC using the AccQTag pre-column derivatization method from Waters (Cohen & Michaud, 1993), in the Centres científics i tecnològics of the University of Barcelona (CCiTUB) in the Parc Científic of Barcelona. Reaction of the amino acids with 6-aminoquinolyl-N-hydroxysuccinimidyl carbamate yields derivatives that are detected at 254 nm. The analysis was performed on a Nova-Pak C18 column (3.9 x 150 mm) at a flow rate of 1 mL/min at 37 °C attached to a Delta 600 chromatographic system with a 2478 Dual Absorbance detector and a 717plus autosampler (Waters Corporation, Massachusetts, USA).

6.1.1.1.4.3. SPPS

The lipopeptides were manually synthesized following standard Fmoc/tBu procedure using polypropylene syringes (of variable volume according to the quantity of resin used) equipped with a polyethylene filter. The mixture was manually stirred using a Teflon rod. After every reaction cycle, the excess of reagents and solvents were eliminated by filtration under vacuum. In all cases the resin used was MBHA (f = 0.69 mmol/g) with Fmoc-Rink amide linker attached in order to obtain the C-terminal side of the peptide as a carboxamide.

The MBHA resin was previously treated in order to solvate it and eliminate possible impurities (Table 30):

Table 30: Protocol used for the treatment of the MBHA resin prior to the coupling of the residues (the times given are relative).

Step	Reagent	Operation	Time
1	DCM	Wash	5 x 0,5 min
2	40% TFA in DCM	Wash	1 x 1 min
3	40% TFA in DCM	Wash	2 x 10 min
4	DCM	Wash	5 x 0,5 min
5	5% DIEA in DCM	Neutralization	3 x 2 min
6	DCM	Wash	5 x 0,5 min
7	DMF	Wash	5 x 0,5 min

The Rink linker and the amino acid residues were incorporated to the resin directly using DIC as activating agent and HOBt as additive to minimize racemization (followed protocol shown in Table 31). 3 equivalents of all the reagents were used for 1 hour in DMF. If the coupling was not complete, 1.5 eq. of the reagents were added for 30 more minutes in DMF. Successive cycles of Fmoc-deprotection with 20% piperidine in DMF and Fmoc-protected amino acid coupling to the freshly deprotected N-terminus gave place to the protected peptides on resin.

Table 31: Protocol of elongation of the peptide chain in a Fmoc/tBu strategy (the times given are relative).

Step	Reagent	Operation	Time
1	DMF	Wash	5 x 0,5 min
2	20% Piperidine in DMF	Deprotection	1 x 1 min
3	20% Piperidine in DMF	Deprotection	2 x 10 min
4	DMF	Wash	5 x 0,5 min
5	Fmoc-AA-OH, 3 eq. DIC, 3 eq. HOBt, 3 eq.	Coupling	60 min
6	DMF	Wash	5 x 0,5 min
7	DCM	Wash	5 x 0,5 min
8	Ninhydrin assay	Control	3 min

Once the last amino acid was coupled, the Fmoc protecting group was eliminated with 20% piperidine in DMF, followed by coupling of the fatty acid (octanoic, nonanoic, decanoic or dodecanoic acid) using 5 eq. of the acid, 5 eq. of DIC and 5 eq. of HOBt for 1 hour in DMF. In all cases a repetition with half equivalents and half of the time was carried out.

6.1.1.1.4.4. Cleavage, deprotection and cyclization of the lipopeptides

Cleavage and full deprotection of the lineal peptides was carried out by acidolysis with

a mixture TFA/triethylsilane or triisopropylsilane/water (95:3:2, v/v) for 90 minutes. In all cases, a previous test was carried out with an aliquot of the peptide and analysed with analytical HPLC to determine the optimal conditions. For the cleavage the resin was filtered off and washed with pure TFA. The combined filtrates were evaporated to a reduced volume under a gentle stream of nitrogen. The crude product was precipitated with cold diethyl ether, centrifuged and separated from the supernatant by decantation. In all cases the crude product was used in the next step without purification but in some cases the crude product was taken up in acetonitrile/water (1:1) and lyophilised before cyclization.

Cyclization of the crude peptides by disulphide bond formation was carried out by dissolving the peptide in water at a very diluted concentration (0.5 mg of peptide/mL of dissolution) followed by addition of 5% of DMSO as the mild oxidant (Tam et al., 1991). This mixture was agitated continuously at RT for 24 to 48 hours and the progress of the cyclization was followed by analytical HPLC. Once the cyclized product was obtained the mixture was directly lyophilized.

6.1.1.1.4.5. RP-HPLC

The peptides were purified by semi-preparative RP-HPLC. The column used was a Phenomenex C18 (1 x 25 cm) of 5 µm diameter of particle, the instrument used is specified in 6.1.1.1.3 and the detection was carried out at 220 nm. The samples were eluted at a flow rate of 3 mL/min using lineal gradients of the following solvents:

A: H₂O – 0,1% TFA

B: ACN – 0,1% TFA

The peptides were characterized by analytical RP-HPLC. The column used was a Nucleosil C18 (0,4 x 25 cm) with an octadecyl matrix of 5 µm diameter particle and 120 Å pore size, the instrument used is specified in 6.1.1.1.3 and the detection was carried out at 220 nm. The samples were eluted at a flow rate of 1 mL/min using lineal gradients of the following solvents:

A: H₂O – 0,045% TFA

B: ACN – 0,036% TFA

6.1.1.1.4.6. Mass spectrometry MALDI-TOF

The peptides were also characterized by MALDI-TOF mass spectrometry. The analysis was made by mixing 1 µL of a dissolution of the peptide with 1 µL of the matrix α -cyano-4-hydroxycinnamic acid. This matrix had been previously prepared by dissolving 10 mg of CHCA in 1 mL of H₂O/ACN (1:1) containing 0,1% TFA. The mixture was directly placed in the MALDI metallic plaque and the solvent has to evaporate at room temperature before measurement. All the mass spectra were recorded in positive mode using the instrument specified in 6.1.1.1.3.

6.1.1.2. Evaluation of the biological activity, minimum inhibitory concentration determination

6.1.1.2.1. Material used

All the material used in the microbiological assays was previously sterilized using an autoclave with the following conditions: 1 atm, 120 °C for 20 minutes. All the liquid and solid mediums used were prepared according to the fabricator instructions. The isotonic

solution Ringer ¼ was prepared dissolving a quarter part of the quantities recommended in the fabricator instructions in distilled water.

Material	Brand
Bacterial strains	American Type Culture Collection or Deutsche Sammlung von Mikroorganismen und Zellkulturen
MHB	Oxoid
Polymyxin B sulphate salt	Sigma-Aldrich
Ringer powder	Oxoid
Tryptone water	Oxoid
TSB	Oxoid
TSA	Pronadisa
96-well sterile microtiter plates	Corning Costar 3598

6.1.1.2.2. Methods

Antimicrobial activity was measured by a tube dilution method, carried out with Gram-positive *S. aureus* (ATTC 29213 and ATCC 6538), *E. faecalis* (ATCC 29212) and *M. phlei* (ATCC 41423) and with Gram-negative *E. coli* (ATCC 25922 and ATCC 8739), *P. aeruginosa* (ATCC 9027), *Acinetobacter sp.* (DSMZ 586) and *K. pneumoniae* (ATCC 13883) and in some cases with the fungi *C. albicans* (ATCC 10231).

The microorganism strains are maintained frozen at -80 °C in cryoballs, when needed they are grown overnight in TSB liquid medium, followed by overnight culture in a TSA plate until colony growth. The day before the MIC determination, the strains that are going to be used are cultured in test tubes containing MHB.

The procedure of MIC determination involves preparing an initial dissolution of the peptides in water (0.636 mg/mL), previously quantified by amino acid analysis, followed by two-fold dilutions of the antibiotics (from 0.06 to 32 µg/mL, Figure 71) in liquid growth medium Mueller-Hinton broth in test tubes. The peptides were then added to 96-well polypropylene microtiter plates (final volume 200 µL) and inoculated with a bacterial suspension in MHB of 10⁷-10⁸ CFU/mL (the suspensions were previously standardized by optical density and plate count for each bacterial strain used). The final concentration of bacteria in each well was 10⁵-10⁶ CFU/mL. Following overnight incubation at 35 °C, the plates were examined for visible bacterial growth as evidenced by turbidity. The lowest concentration of antibiotic that prevented growth represents the minimal inhibitory concentration. Each determination was done by duplicate and the two final rows of each plate remained without peptide, so that the penultimate data point served as positive control (drug-free) and the final one as negative control (microorganism-free). Commercial PxB was every time tested as a control of the technique.

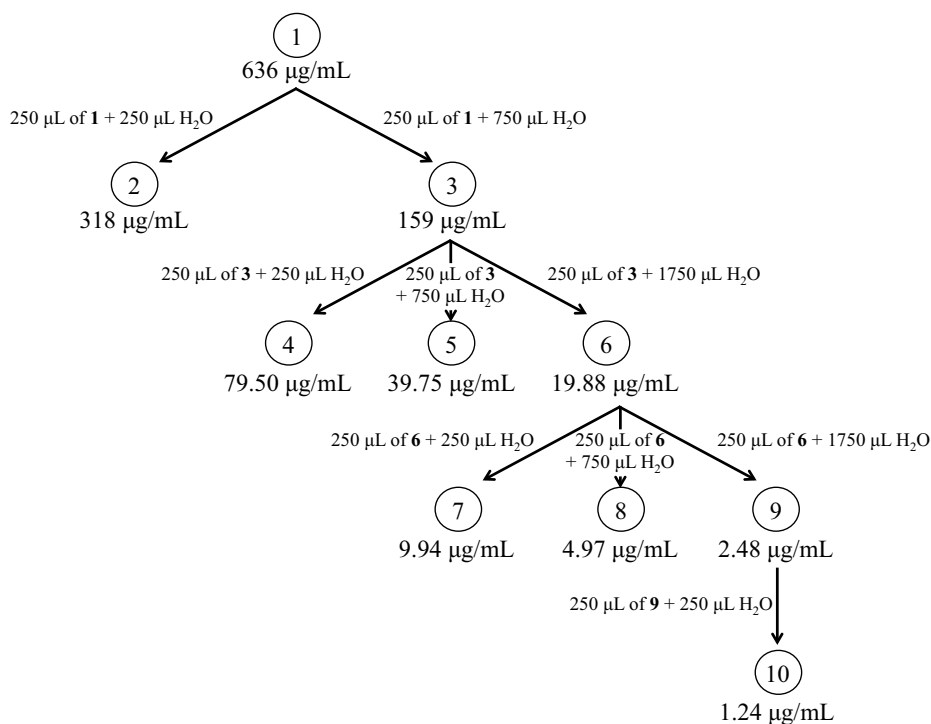


Figure 71: Serial dilution of the peptides in water from an initial dissolution quantified by amino acid analysis.

6.1.1.3. Study of the mechanism of action

6.1.1.3.1. Solvents

All solvents used were HPLC grade quality unless stated otherwise and used without further purification. Milli-Q water was obtained by filtrating purified water using a Milli-Q Plus system (Millipore) to obtain water with a resistivity superior to 18 MΩ/cm.

Solvent	Brand
CHCl ₃	Fisher Scientific
H ₂ O (Milli-Q)	Millipore
MeOH	Fisher Scientific

6.1.1.3.2. Reagents

All reagents used were of the maximum quality possible.

Reagents	Brand
Acrylamide	Sigma-Aldrich
ANTS	Invitrogen Molecular Probes
BOX	Sigma-Aldrich
Dansyl-Polymyxin B	Invitrogen Molecular Probes

DPX	Invitrogen Molecular Probes
LPS from <i>Salmonella enterica</i> serotype minnesota Re 595 (Re mutant)	Sigma-Aldrich
NaCl	Sigma-Aldrich
MHB	Oxoid
Polymyxin B sulphate salt	Sigma-Aldrich
PI	Invitrogen Molecular Probes
Ringer powder	Oxoid
Sephadex G-50	Sigma-Aldrich
TMA	Invitrogen Molecular Probes
TMA-DPH	Invitrogen Molecular Probes
Tris	Sigma-Aldrich
Tryptone water	Oxoid
TSB	Oxoid
TSA	Pronadisa
POPC	Avanti Polar Lipids
POPE	
POPG	
py-PC	Invitrogen Molecular Probes
NBD-PE	
py-PG	

6.1.1.3.3. Instruments

Instrument	Brand and Model
Electron microscope	Jeol, <i>JEM-1010</i>
Evaporator	Heidolph Laborota 4000
Extruder	Northern Lipids Inc. <i>LIPEX</i>
Flow cytometer	Beckman Coulter, Inc <i>Gallios multi-color flow cytometer</i>
Monolayer system	<i>KSV5000</i>
Osmometer	Advanced Instruments Inc. <i>3320 Osmometer</i>
pH-meter	Crison <i>pH & ION-Meter GLP 22+</i>
Particle Size Distribution Analyser	Malvern <i>Autosizer IIC</i>
Sonicator	Lab Supplies <i>G112SPIT</i>
Spectrofluorimeter	1) AMINCO-Bowman Series 2 <i>SLM-Aminco</i> , with a temperature controller

6.1.1.3.4. Methods

6.1.1.3.4.1. Preparation of liposomes

Unilamellar vesicles of POPG, POPE/POPG (6:4) or POPC, alone or with the fluorescently labelled phospholipids: pyPG, pyPC or NBD-PE or with the fluorescent probes DPH or TMA-DPH, were prepared by evaporation of a mixture of the lipids and probes in CHCl₃/CH₃OH (2:1 v/v). The dried film was hydrated for a final lipid concentration of 10 mM, and then sonicated in a bath type sonicator until a clear dispersion was obtained (typically 2-4 minutes).

For the ANTS/DPX fusion assay, the dried lipid films were dispersed in 12.5 mM ANTS, 45 mM DPX and 10 mM Tris buffer at pH 8.0 and subjected to 10 freeze-thaw cycles prior to extrusion 10 times through a 0.1 µm polycarbonate membrane at 250 psi N₂ pressure. The unencapsulated material was separated by gel-filtration on a Sephadex G-50 column eluted with 10 mM Tris buffer and 80 mM NaCl. Osmolarities were adjusted with NaCl and measured in an osmometer. Lipid concentration was determined by the Stewart-Marshall assay, a colorimetric method based on the formation of a complex between phospholipids and ammonium ferrothiocyanate (Stewart, 1980). These vesicles were used within 24 h.

Vesicle size was measured by dynamic light scattering with a particle analyser, typically obtaining a mean diameter of 80 nm and 105 nm for sonicated and extruded respectively, and a narrow size distribution (polydispersity < 0.1).

6.1.1.3.4.2. Kinetics of insertion into monolayers of LPS

Insertion experiments at constant area were conducted at 24 °C on a computer-controlled monolayer system. To avoid carryover of lipid and peptides, the polytetrafluoroethylene (PTFE, Teflon) trough and the Wilhelmy platinum plate were thoroughly cleaned with hot double-distilled water at >75 °C. Kinetics of insertion at constant area were monitored as an increase in the surface pressure by use of a cylindrical trough (5 cm diameter or 19.6 cm² area) containing stirred aqueous phase (30 mL) with 10 mM Tris at pH 8.0. The peptide was added without disturbance of the monolayer via an inlet port in the trough, and the surface pressure was continuously recorded by the KSV balance.

6.1.1.3.4.3. Dansyl-PxB binding and displacement assay

The fluorescence of dansyl-polymyxin bound to LPS was measured by using a PTI QM4 spectrofluorimeter set at an excitation wavelength of 340 nm and an emission wavelength of 485 nm. The saturation of LPS was determined by recording the fluorescence after the addition of portions of dansyl-polymyxin to a 1 mL cuvette containing 3 µg/mL of LPS in 10 mM Tris buffer (pH 8.0). The background fluorescence of dansyl-polymyxin was determined repeating the same experiment in the absence of LPS. The decrease in fluorescence due to dansyl polymyxin B displacement was recorded upon the progressive addition of aliquots of 5 µL of each of the peptides into a 1 mL cuvette containing 3 µg/mL of LPS and 2.9 µM dansyl-polymyxin (corresponding to 85-90 % of saturation of the LPS) in Tris buffer. The data was plotted

as percentage inhibition *versus* the concentration of peptide (μM), and IC_{50} values were obtained from these plots.

6.1.1.3.4.4. Aggregation of liposomes measured as light scattering at 90°

Vesicle aggregation induced by the different peptides was determined by the increase in turbidity of a liposome preparation (lipid concentration $106 \mu\text{M}$). The experiments were carried out in the spectrofluorimeter set at an excitation and emission wavelength of 360 nm (slit-widths 1 nm), to determine the light scattering as a function of the peptide concentration.

6.1.1.3.4.5. Fluorescence assay for lipid mixing.

The transfer of pyrene-labelled phospholipids as donor vesicles ($0.83 \mu\text{M}$) to an excess of unlabelled phospholipid vesicles ($106 \mu\text{M}$) as acceptors was measured. Emission from vesicles containing 30% pyrene-phospholipid is dominated by the excimer band at 480 nm , and the intensity of the monomer band, at 395 nm , increases as the probe is diluted due to exchange with excess unlabelled vesicles in contact. Experiments were carried out at $24 \text{ }^\circ\text{C}$ in 1.5 mL of 10 mM Tris buffer at $\text{pH } 8.0$ on a PTI QM4 spectrofluorimeter with constant stirring. Peptide was added from a stock solution 0.25 mM in water to the cuvette containing vesicles of the desired composition (lipid concentration $107 \mu\text{M}$). Fluorescence emission was monitored at 395 nm (with excitation at 346 nm) corresponding to the monomer emission. The slit widths were kept at 2 nm each. Unilamellar lipid vesicles used for the exchange experiments were prepared with POPG, POPE/POPG (6:4 mol:mol) or POPC unlabelled or with 30% pyPG or pyPC.

6.1.1.3.4.6. ANTS/DPX fusion assay for leakage or mixing of aqueous compartments

Dequenching of coencapsulated ANTS and DPX fluorescence resulting from dilution was measured to assess leakage of aqueous contents (Ellens et al., 1985). Fluorescence measurements were performed at $24 \text{ }^\circ\text{C}$ in 1.5 mL of 10 mM Tris buffer at $\text{pH } 8.0$ on a PTI QM4 spectrofluorimeter with constant stirring by measuring ANTS emission at 530 nm with an excitation at 350 nm . Peptide was added from a stock solution 0.25 mM in water to the cuvette containing vesicles of the desired composition (lipid concentration $115 \mu\text{M}$). The 0% leakage corresponded to the fluorescence of the vesicle at time zero while 100% leakage was the fluorescence value obtained after addition of Triton X-100 (10% v/v).

6.1.1.3.4.7. Polarization

Steady-state anisotropy measurements were conducted on an Aminco AB-2 spectrofluorimeter using L-format fluorescence polarizers. The dynamics of lipid in liposome membranes in the presence of the lipopeptides were determined by measuring the degree of depolarization of the fluorescence emitted from the probes DPH and TMA-DPH. The excitation and emission wavelength for both probes were $356/425 \text{ nm}$ (slit-widths 4 nm). Labelled vesicles with 1% of the desired probe ($133 \mu\text{M}$ lipid) were mixed with the peptide in 10 mM Tris $\text{pH } 8.0$, and anisotropy was measured automatically by the software provided with the instrument. For each sample a heating cycle from 10 to $30 \text{ }^\circ\text{C}$, at $1 \text{ }^\circ\text{C}$ intervals allowing for thermal equilibration, was conducted. Additional measurements of vesicles titrated with the peptide at a constant

temperature were carried out. All solutions were stirred continuously during the measurements.

6.1.1.3.4.8. Modification of the emission spectra of tryptophan

Tryptophan fluorescence spectra were recorded with an excitation wavelength of 285 nm over an emission range 300-450 nm, with 4 nm slit widths. The peptide was added from a stock solution in water to a final concentration of 3 μ M, and vesicles were added to the desired lipid concentration. Titration of the peptide with vesicles was avoided due to the disruption of the vesicles (fusion and leakage) that occurs at high peptide-to-lipid ratios. The contribution from scattering due to vesicles was subtracted using the same concentration of peptide analogues without tryptophan that induced the same changes in light scattering (control experiments, not shown). In some cases, samples were titrated with NaCl to a final concentration of 350 mM, to determine the influence of increasing ionic strength.

6.1.1.3.4.9. Tryptophan fluorescence anisotropy

Steady-state tryptophan fluorescence anisotropy measurements were carried out at 24 °C on an Aminco AB-2 spectrofluorimeter with L-format polarizers. The excitation wavelength was set at 285 nm, and the emission at 340 nm with excitation and emission slit widths at 4 nm. Each measure was done in duplicate, independently (no sequential addition of lipid in the same cuvette), adding the vesicles to the desired final lipid concentration to a cuvette containing 1.5 mL of 10 mM Tris buffer (pH 8.0), and 3 μ M lipopeptide. All solutions were stirred continuously during the measurements. The fluorescence anisotropy (r) was calculated automatically by the software provided with the instrument.

6.1.1.3.4.10. Quenching of tryptophan fluorescence by acrylamide

Quenching of tryptophan fluorescence of the peptides by acrylamide was recorded at 340 nm (excitation 285 nm). Appropriate amounts of POPG, POPE/POPG (6:4) or POPC vesicles, were added to a solution of 3 μ M peptide, and aliquots of quencher were added with continuous stirring. Acrylamide was added from a 4 M stock solution in Tris buffer up to a final quencher concentration of 0.3 M. The Stern-Volmer quenching constants were evaluated by curve fitting using the modified equation (Eftink & Ghiron, 1976) described in the results section.

6.1.1.3.4.11. Fluorescence resonance energy transfer

Binding of the lipopeptides to vesicles of different composition containing 2.5% of NBD-PE was determined as the increase in the FRET signal from Trp in the peptide to the labelled phospholipid in the interface at 535 nm (excitation 285 nm). Vesicles in buffer (33.3 μ M lipid) were titrated with peptide from a stock solution 0.25 mM in water, and the relative change in fluorescence (δF) was obtained. δF is defined as $(F - F_0)/F_0$, where F_0 and F are the intensities without and with peptide, respectively. Due to the low lipid concentration used in this experiment, the contribution from light scattering is negligible.

6.1.1.3.4.12. Flow cytometry

- Bacteria, growth conditions and antimicrobial treatment: An overnight culture (12 to 16 h) of *S. aureus* (ATCC 29213) or *E. coli* (ATCC 25922) in TSB was grown at 37 °C and 400 µL were added in 50 mL of tryptone water (~10⁷ bacteria/mL). The bacterial suspension was split into aliquots of 4-5 mL and treated with the peptides (at the MIC) for different contact times at room temperature. Cells were collected by centrifugation (10000 rpm, 20 min) and resuspended in 1 mL of filtered Ringer's solution.
- Staining procedure: A stock solution of PI (1 mg/mL) and BOX (250 µM) was prepared in distilled water. Portions (10 µL and 2 µL, respectively) were added to aliquots of cells (100 µL of each sample in 1 mL of Ringer's solution) to give a final concentration of 10 µg of PI per mL and 0.5 µM for BOX.
- Analysis: Flow cytometric measurements were performed on a Gallios multi-color flow cytometer instrument (Beckman Coulter, Inc, Fullerton, CA) set up with the 3-lasers 10 colours standard configuration. Excitation was done using a blue (488 nm) laser. Forward scatter (FS), side scatter (SS), green fluorescence (525/40 nm) from BOX and red fluorescence (620/30 nm) emitted by PI were collected using logarithmic scales. FS was used as the discriminating parameter. The single-cell bacterial population was selected on a forward-side scatter scattergram. Fluorescence was presented in a dot plot of BOX vs. PI. Three regions were defined on this graph according to the controls: depolarized, permeabilized and non-affected cells. Control cells (non-stained and single stained populations) were used to define these regions. 25000 cells defined according to their scatter parameters were counted in each sample.

6.1.1.3.4.13. Transmission electron microscopy

- Bacteria, growth conditions and antimicrobial treatment: An overnight culture (12 to 16 h) of *S. aureus* (ATCC 29213) or *E. coli* (ATCC 25922) in TSB was grown at 37 °C and 500 µL were added in 50 mL of tryptone water (~10⁸ bacteria/mL). The bacterial suspension was split into aliquots of 10 mL and treated with the peptides (at the MIC) for 120 minutes at room temperature. Cells were collected by centrifugation (10000 rpm, 20 min).
- Transmission electron microscopy preparation and observation: The preparation of the samples was carried out by the specialized technicians in the Centres científics i tecnològics of the University of Barcelona (CCiTUB) in the Parc Científic of Barcelona as follows; the samples were fixed with 2.5% glutaraldehyde in phosphate buffer for 2 h at 4 °C, then washed with the same buffer and post fixed with 1% osmium tetroxide in buffer containing 0.8% potassium ferricyanide at 4 °C. The samples were then dehydrated for 1 hour in acetone and infiltrated in a graded series of Epon resin (Ted pella, Inc, USA) during 2 days, and finally embedded in fresh Epon resin and polymerised at 60 °C during 48 hours. Ultrathin sections were obtained using a Leica Ultracut UCT ultramicrotome (Leica, Vienna) and mounted on Formvar-coated copper grids. Sections were stained with 2% aqueous uranyl acetate and lead citrate and examined in a JEM-1010 electron microscope (Jeol, Japan).

6.1.2. SECTION B

6.1.2.1. Chemical synthesis of the MSI-103 analogues

6.1.2.1.1. Solvents

All solvents used were reagent grade quality unless stated otherwise, and used without further purification. They were all purchased from Merck (Darmstadt, Germany). Milli-Q water was obtained by filtrating purified water using a Milli-Q Plus system (Millipore) to obtain water with a resistivity superior to 18 MΩ/cm.

6.1.2.1.2. Reagents

All reagents used were of the maximum quality possible.

Reagent	Brand
Rink amide MBHA resin	Novabiochem (Merck Chemicals) or Iris Biotech
Amino acid residues	
¹⁵ N-labelled amino acid residues	Cambridge Isotope Laboratories
DIEA	Sigma-Aldrich
HOBt	Biosolve
HBTU	Biosolve
Piperidine	Sigma-Aldrich
TIS	Sigma-Aldrich
TFA	Sigma-Aldrich

6.1.2.1.3. Instruments

Instrument	Brand and Model
Centrifuge	Sigma, 3-18K
Lyophilizator	Christ
HPLC	Jasco, MD-2087 Plus Intelligent Multiwavelength Detector, PU-2087 Plus Intelligent Pump and a Column Oven
HPLC-MS	Agilent LC-System, 1100 Series with a Bruker Daltonics ESI-microTOF Spectrometer
Peptide synthesizer	Multisyntech, Syro II

6.1.2.1.4. Methods

6.1.2.1.4.1. SPPS

The peptides of the KIA series with lengths of 14-28 amino acids were automatically synthesized, as C-terminal amides, on an automated peptide synthesizer, with and without ¹⁵N-label, using standard solid phase Fmoc protocols. All synthesis were performed on 100 μM scale. The resin used was Rink amide MBHA resin (f = 0.60 mmol/g). The protecting group of the amino acid Lys was Boc.

Fmoc deprotection was carried out for 20 min using piperidine (20-25% v/v in DMF), and amino acids were coupled in DMF using a mixture of Fmoc-amino acid/HBTU/HOBt/DIEA in a molar ratio of 4:4:4:8 respectively. Each amino acid was coupled twice on the automated peptide synthesizer for 30 min before the next cycle was repeated. Successive cycles of Fmoc-deprotection with piperidine and Fmoc-protected amino acid coupling to the freshly deprotected N-terminus gave the desired protected peptides on resin.

For structure analysis using solid-state ¹⁵N-NMR spectroscopy isotope labels were incorporated manually using Fmoc protected Ala with a ¹⁵N-label at the backbone amide as described above but in a molar ratio of 2:2:2:4. Each coupling here was performed twice for 60 min.

6.1.2.1.4.2. Cleavage and deprotection of the peptides

Cleavage and full deprotection of the peptides was carried out by acidolysis with a mixture TFA (92.5%, v/v)/TIS (5%, v/v)/water (2.5%, v/v) for 4 h with occasional gentle shaking. In all cases, a previous test cleavage was carried out with an aliquot of the peptide for 1 h, and analysed with analytical HPLC to determine the optimal conditions. For the cleavage the resin was filtered off and washed with pure TFA. The combined filtrates were evaporated to a reduced volume under a gentle stream of nitrogen. The crude product was precipitated with cold diethyl ether, centrifuged and separated from the supernatant by decantation. The crude product was taken up in acetonitrile/water (1:1) and lyophilised.

6.1.2.1.4.2. RP-HPLC

The peptides were purified by semi-preparative RP-HPLC. The column used was a Vydac C18 (10 x 250 mm) and was always kept at 35 °C. The instrument used is specified in 6.1.2.1.3. and the detection was carried out at 220 nm. The samples were eluted at a flow rate of 10 mL/min using lineal gradients of the following solvents:

A: 90% H₂O – 10% ACN and 5 mM HCl

B: 90% ACN – 10% H₂O and 5 mM HCl

The peptides were characterized by analytical RP-HPLC combined with ESI-mass spectrometry. An analytical LC column was used at 35 °C with the instrument specified in 6.1.2.1.3. The samples were eluted at a flow rate of 0.3 mL/min using a linear gradient of 10-90% B containing 5 mM TFA, in 25 min. All the peptides showed to be over 95% pure and could be used for the biological and biophysical experiments.

6.1.2.2. Evaluation of the biological activity, antibacterial and haemolytic activity determination

6.1.2.2.1. Material used

All the material used in the microbiological assays was previously sterilized using an autoclave with the following conditions: 1 atm, 120 °C for 20 minutes. All the liquid and solid mediums used were prepared according to the fabricator instructions.

Material	Brand
Bacterial strains	Deutsche Sammlung von Mikroorganismen und Zellkulturen
Centrifuge	Sigma
LB Agar	Roth
MHB	Becton (Dickinson and Co)
Spectrophotometer	SmartSpec Plus BIORAD
96-well sterile microtiter plates	Thermo Scientific Nunc Plates

6.1.2.2.2. Methods

6.1.2.2.2.1. MIC assay

Antimicrobial activity was measured by a standard minimal inhibitory concentration assay, carried out with Gram-positive *S. aureus* (DSM 1104) and *E. faecalis* (DSM 2570) and with Gram-negative *E. coli* (DSM 1103) and *P. aeruginosa* (DSM 1117).

The microorganism strains are maintained frozen at -80 °C in cryoballs, when needed they are grown overnight in MHB liquid medium, followed by overnight culture in a LB agar plate until colony growth.

Bacteria were grown in Mueller-Hinton medium at 37 °C overnight (OD = 0.02). Microtiter plates (96 wells of 100 µL) were filled with 50 µL of MHB, and serial 2-fold dilutions of peptides were arranged in quadruple. The two final rows of each plate remained without peptide, so that the penultimate data point served as the positive control (no peptide) and the final one as the negative control (not inoculated). 50 µL of bacterial suspension (OD = 0.2) was added to the wells (except for the final row of each plate) to give a final concentration of 10⁶ CFU/mL. The plates were incubated at 37 °C for 20 h, and the MIC was determined visually on the basis of turbidity as the lowest peptide concentration inhibiting bacterial growth.

6.1.2.2.2.2. Haemolysis assay

Haemolytic activity was examined with a serial 2-fold dilution assay. Citrate phosphate dextrose-stabilized blood bags with erythrocyte suspensions of healthy donors were obtained from the blood bank of the local municipal hospital (Städtisches Klinikum, Karlsruhe, Germany). The erythrocytes, previously washed, were incubated with peptide solutions at 37 °C for 30 min with gentle shaking. The tubes were centrifuged at 13000 rpm for 10 min to pellet the cells, and the absorbance at 540 nm was recorded

against a negative control (autohaemolysis, cells without peptide). The percentage of lysis was then calculated relative to 100% lysis by 1% Triton X-100. The absorbance measurements were repeated three times, and the averaged values were used.

6.1.2.3. Study of the mechanism of action

6.1.2.3.1. Solvents

All solvents used were UV-grade quality and used without further purification. Milli-Q water was obtained by filtrating purified water using a Milli-Q Plus system (Millipore) to obtain water with a resistivity superior to 18 M Ω /cm.

Solvent	Brand
CHCl ₃	VWR
H ₂ O (Milli-Q)	Millipore
MeOH	VWR

6.1.2.3.2. Reagents

All reagents used were of the maximum quality possible.

Reagents	Brand
ANTS DPX	Molecular Probes
DEPC DEPG	NOF Corporation
DMPC DMPG DMoPC DOPG Lyso-MPC POPC POPG	Avanti Polar Lipids
HEPES	Sigma
NaCl	Fluka

6.1.2.3.3. Instruments

Instrument	Brand and Model
Extruder	Avanti Polar Lipids, <i>Mini Extruder</i>
Fine scale	Sartorius
Sonicator	Hielscher Ultrasonics, <i>UTR200</i>

Spectropolarimeter	Jasco, <i>J-815</i>
Spectrometer	Bruker Avance 500 or 600
Spectrophotometer	HORIBAJobin Yvon, FluoroMax2

6.1.2.3.4. Methods

6.1.2.3.4.1. Circular dichroism spectroscopy

CD samples were prepared by co-solubilizing DMPC and DMPG (3:1 mol/mol) in chloroform/methanol 3:1 (v/v). After drying, the lipid film was dispersed in phosphate buffer (10 mM, pH 7) and homogenised by vortexing. Small unilamellar vesicles (SUVs) for CD samples were generated by sonication. CD spectra were recorded on a J-815 spectropolarimeter between 260 and 185 nm at 0.1-nm intervals using 1-mm quartz-glass cells (Suprasil; Hellma USA) at 20 °C, as reported previously (Glaser et al. 2004). The peptides were measured at 20 °C in 10 mM sodium phosphate buffer (pH 7.0) and in lipid vesicles composed of DMPC/DMPG (3:1). An averaged baseline of the pure solvent was subtracted. Typical peptide concentration of the final samples was 0.1 mg/mL and a peptide to lipid molar ratio (P/L) of 1:50 was used.

6.1.2.3.4.2. Vesicle leakage assay

For the leakage experiments (Duzgunes et al. 1993), a buffer containing 12.5 mM ANTS, 45 mM DPX and 50 mM NaCl in 10 mM HEPES was prepared at pH 7.5. Liposomes were prepared by codissolving PC/PG 1:1 (mol/mol) mixtures of the lipids with different chain length in CHCl₃/MeOH (3:1 v/v), together with 2-3 μL of rhodamine. The mixture was dried under N₂ (g) and left to dry under vacuum overnight. The obtained thin film was then resuspended in the combined dye buffer by vortexing, followed by 10 freeze-thaw cycles using 50 °C warm water (Mayer et al. 1986). A uniform population of large unilamellar vesicles (LUVs) was obtained by repeated high-pressure extrusion of the liposomes through a polycarbonate Unipore membrane (pore size, 100 nm; Millipore) at a temperature above the gel-to-liquid crystal phase transition. To remove unencapsulated dye, the vesicles were washed right before the experiment by gel filtration on a Sephacryl 100-HR (Sigma-Aldrich, St. Louis, MO) column using a 150 mM HEPES/10 mM NaCl elution buffer, which balances the internal vesicle osmolarity.

The release of aqueous contents from the vesicles was monitored by the fluorescence dequenching of ANTS by DPX, both entrapped in the vesicles as described above. Fluorescence measurements were performed in a thermostated cuvette, with constant stirring, at 30 °C (above the transition temperature for all the lipids used) in 10 mM HEPES buffer containing 150 mM NaCl at pH 7.5 on a FluoroMax2 spectrofluorimeter by setting the ANTS emission at 515 nm (5 nm slit) and the excitation at 422 nm (5 nm slit). The vesicles of the desired composition were added to the cuvette containing the peptide at the P/L ratio to be tested (stock solution 1 mM in water). The 0% leakage corresponded to the fluorescence of the vesicle at time zero while 100% leakage was the fluorescence value obtained after addition of 0.5 vol% Triton X-100 (10% v/v) after 12 min.

6.1.2.3.4.3. Solid-state NMR

Macroscopically oriented NMR samples were prepared by codissolving appropriate amounts of peptides and lipids in 400 μl of methanol/ CHCl_3 1:1 (v/v) and spread onto 23 thin glass plates of dimensions 18 mm \times 7.5 mm \times 0.08 mm (Marienfeld Laboratory Glassware, Lauda-Königshofen, Germany). The plates were dried in air for 1 h, followed by drying under vacuum overnight. They were stacked and placed into a hydration chamber with 96% relative humidity at 48 °C for 18–24 h, before wrapping the stack in parafilm and plastic foil for the ssNMR measurements.

All ssNMR measurements were carried out on a Bruker Avance 500 or 600 MHz spectrometer at 308 K. ^{31}P -NMR was used to check the quality of the lipid orientation in the samples, using a Hahn echo sequence with phase cycling (Rance et al. 1983). ^2H -ssNMR experiments were performed using a quadrupole echo sequence (Davis et al. 1976) with a 90° pulse of 4.5 μs , an echo delay of 70 μs , a 100 ms relaxation delay time, a 500 kHz spectral width, and 2048 data points. Between 100000 and 1000000 scans were collected and processed by zero filling to 16384 data points and a 400 Hz exponential multiplication, followed by Fourier transformation. ^1H - ^{15}N cross polarization experiments using a CP-MOIST pulse sequence (Levitt et al. 1986) were performed using a double-tuned probe with a low-E flat-coil resonator (3 mm \times 9 mm cross section), employing a ^1H and ^{15}N radiofrequency field strength of 65 kHz during the cross polarization, and 36 kHz ^1H SPINAL16 (Fung et al. 2000) decoupling during acquisition. A mixing time of 500 μs was used, and between 10000 and 30000 scans were accumulated. The acquisition time was 10 ms and the recycle time 4 s. The ^{15}N chemical shift was referenced using the signal of an ammonium sulphate sample, of which the chemical shift was set to 26.8 ppm. The oriented samples were placed in the flat-coil probe such that the lipid bilayer normal was usually aligned parallel to the magnetic field, and additional experiments were carried out in a perpendicular alignment.

6.2. EXPERIMENTAL SECTION A

The polymyxin analogues were synthesized as explained in 6.1.1.1. Some of the peptides (#1-11, N and NN) were already available in our laboratory and are therefore not included in the first table, however all peptides were analysed prior to its use in the biological and biophysical experiments (Table 33).

The peptides synthesized in our laboratory were usually synthesized starting with 150 mg of MBHA resin. As the functionalization of the resin is 0.69 mmol AC/g resin, this can be translated as a 104 μ M scale. The reagent quantities used for all the couplings were: 311 μ mol Fmoc-AA-OH (168 mg Fmoc-Rink linker, 182 mg Fmoc-Cys(Trt)-OH, 136.8 mg Fmoc-Dab(Boc)-OH, 123.4 mg Fmoc-Thr(tBu)-OH, 109.7 mg Fmoc-Leu/Nle-OH, 120.3 mg Fmoc-Phe-OH, 145.5 mg Fmoc-Lys(Boc)-OH, 141 mg Fmoc-Orn(Boc)-OH): 311 μ mol HOBt (42 mg): 311 μ mol DIC (48 μ L).

The coupling of the acyl moiety for peptide #12 took place with the following reagent quantities: 518 μ mol fatty acid (89 mg decanoic acid): 518 μ mol HOBt (70 mg): 518 μ mol DIC (80 μ L). For peptides #13-15, #16-18, #19-21 and #22-24 before the coupling of the fatty acid the resin was divided into three equal batches in order to make individual couplings of nonanoic, decanoic and dodecanoic acid. If we suppose 50 mg of dry resin for each of the couplings, the quantities of reagents used are the following: 173 μ mol fatty acid (30 μ L nonanoic acid, 30 mg decanoic acid or 34.6 mg dodecanoic acid): 173 μ mol HOBt (23 mg): 173 μ mol DIC (27 μ L). In all cases, the coupling of the fatty acid was repeated with half of the reagent quantities.

In the following tables all the information regarding the synthesis and purification of each peptide is depicted.

Table 32: Obtained quantities and synthetic yield of the polymyxin analogues manually synthesized for this thesis. Some of the yields are given as 100% because the obtained quantity after the cleavage is higher than the theoretical quantity, which is calculated according to 50 mg of dry resin. However, not always an exact division of the resin is accomplished and therefore changes in the experimental quantities obtained occur, however, the coupling are always done with an excess of reagent and repeated to ensure a complete coupling.

Peptide	Crude peptide (mg)	Synthesis yield (%)	Cyclized crude peptide (mg)	Cyclization yield (%)	Pure peptide (mg)	Purification yield (%)	TOTAL YIELD (%)
12	87.5	68	73.3	84	23	31	18
13	22.1	45	18.2	82	9.4	52	19
14	30.8	67	35	~100	17.7	51	34
15	59	~100	38.1	65	25	66	43
16	28.3	63	24.3	86	14	58	31
17	33.1	69	31.4	95	20.5	65	43
18	41	88	33	81	19	58	41
19	43.9	75	33.1	76	21.2	64	37
20	53.7	91	46.7	87	15.9	34	27
21	52	85	50.8	98	17.7	35	29
22	64.7	~100	50	77	20.4	41	32
23	62.4	~100	49.9	80	14.3	29	23
24	64	~100	50	78	15.8	32	25

Table 33: Purification characteristics and masses of all the pure polymyxin analogues used in this thesis. For those peptides containing an * in the HPLC gradient, the solvents used were A: 0.05% TFA + 2% ACN and B: 0.05% TFA + 90% ACN. For the amino acid analysis results, only those residues that were quantified are listed, in some cases Nle was quantified because the reference used contained this uncommon residue. Some of the amino acid residues undergo specific hydrolysis under these conditions and therefore the values obtained were not used for the purity calculation.

Peptide	HPLC gradient	Retention time (min)	EM MALDI-TOF (m/z)	Amino acid analysis	
				[experimental (calculated)]	Purity (%)
1	15-45% B in 30 min*	10.8	$[M+H]^+ = 1336.7$	Thr 0.53 (1) Cys 0.23 (2) Arg 1.16 (2) Leu 0.54 (1) Phe 0.55 (1)	45
2	15-45% B in 30 min*	9.9	$[M+H]^+ = 1350.2$	Thr 0.91 (1) Cys 0.79 (2) Arg 1.99 (2) Leu 0.91 (1) Phe 0.94 (1)	64
3	20-50% B in 30 min*	21.8	$[M+H]^+ = 1378.4$	Thr 0.68 (1) Arg 1.53 (2) Leu 0.76 (1)	63
4	15-45% B in 30 min*	18.1	$[M+H]^+ = 1375.1$ $[M+Na]^+ = 1397.7$ $[M+K]^+ = 1413.4$	Thr 0.95 (1) Cys 1.45 (2) Arg 1.95 (2) Leu 0.94 (1)	66
5	32-47% B in 15 min*	4.2	$[M+H]^+ = 1336.8$	Thr 0.87 (1) Cys 0.73 (2) Arg 1.82 (2) Leu 0.80 (1) Phe 0.87 (1)	64
6	32-47% B in 15 min*	7.6	$[M+H]^+ = 1389.6$	Thr 0.88 (1) Cys 1.58 (2) Arg 1.84 (2) Leu 0.73 (1)	67
7	5-95% B in 30 min 25-40% B in 30 min	16.8 18.8	$[M+H]^+ = 1445.0$ $[M+Na]^+ = 1466.9$ $[M+K]^+ = 1482.9$	Thr 0.70 (1) Cys 1.06 (2) Arg 2.18 (3)	52
8	5-95% B in 30 min	16.9	$[M-H_2O]^+ = 1219.9$ $[M+H]^+ = 1237.9$ $[M+Na]^+ = 1259.7$ $[M+K]^+ = 1275.7$	Thr 2.25 (2) Cys 1.23 (4) Nle 2.33 (2) Phe 2.41 (2)	71
9	5-95% B in 30 min	17.9	$[M-H_2O]^+ = 1247.8$ $[M+H]^+ = 1265.9$ $[M+Na]^+ = 1287.8$ $[M+K]^+ = 1303.7$	Thr 2.08 (2) Cys 2.00 (4) Nle 2.16 (2) Phe 2.23 (2)	74
10	25-45% B in 20 min*	10.6	$[M-H_2O]^+ = 1332.8$ $[M+H]^+ = 1349.9$ $[M+Na]^+ = 1371.8$ $[M+K]^+ = 1387.7$	Thr 1.69 (2) Arg 3.54 (4) Phe 1.70 (2)	80

11	32-47% B in 30 min	12.4	$[M+H]^+ = 1377.8$ $[M+Na]^+ = 1399.8$	Thr 1.74 (2) Arg 3.87 (4) Leu 1.93 (2) Phe 1.87 (2)	76
12	20-45% B in 25 min	19.6	$[M-H_2O]^+ = 1185.7$ $[M+H]^+ = 1203.6$ $[M+Na]^+ = 1225.6$ $[M+K]^+ = 1241.6$	Thr 1.11 (1) Cys 1.93 (2) Leu 1.19 (1)	67
13	25-40% B in 30 min	12.7	$[M-H_2O]^+ = 1171.8$ $[M+H]^+ = 1189.8$ $[M+Na]^+ = 1211.8$ $[M+K]^+ = 1227.7$	Thr 1.39 (1) Cys 1.68 (2)	77
14	25-40% B in 30 min	17.3	$[M-H_2O]^+ = 1185.7$ $[M+H]^+ = 1203.7$ $[M+Na]^+ = 1225.7$ $[M+K]^+ = 1241.6$	Thr 1.08 (1) Cys 1.50 (2)	61
15	25-40% B in 30 min	29.9	$[M-H_2O]^+ = 1213.7$ $[M+H]^+ = 1231.6$ $[M+Na]^+ = 1253.6$	Thr 1.18 (1) Cys 1.85 (2)	66
16	25-40% B in 30 min	11.9	$[M+H]^+ = 1189.6$ $[M+Na]^+ = 1211.6$ $[M+K]^+ = 1227.6$	Thr 1.45 (1.5) Cys 2.53 (3) Leu 3.01 (3)	68
17	25-40% B in 30 min	20.5	$[M+H]^+ = 1203.7$ $[M+Na]^+ = 1225.7$	Thr 0.88 (1) Cys 1.31 (2) Leu 1.87 (2)	55
18	25-40% B in 30 min	28.9	$[M-H_2O]^+ = 1213.7$ $[M+H]^+ = 1231.7$ $[M+Na]^+ = 1253.7$	Thr 1.07 (1) Cys 0.90 (2) Leu 2.31 (2)	61
19	30-45% B in 30 min	21	$[M+H]^+ = 1293.7$ $[M+Na]^+ = 1315.7$ $[M+K]^+ = 1331.7$	Thr 1.50 (1.5) Nle 1.56 (1.5) Phe 1.63 (1.5)	72
20	30-45% B in 30 min	17	$[M+H]^+ = 1307.7$ $[M+Na]^+ = 1329.7$ $[M+K]^+ = 1345.7$	Thr 1.73 (1.5) Cys 0.97 (3) Nle 1.80 (1.5) Phe 1.86 (1.5)	72
21	30-45% B in 30 min	14.7	$[M+H]^+ = 1335.8$ $[M+Na]^+ = 1358.7$ $[M+K]^+ = 1373.7$	Thr 1.51 (1.5) Cys 1.73 (3) Nle 1.59 (1.5) Phe 1.62 (1.5)	70
22	25-40% B in 30 min	14	$[M+H]^+ = 1363.8$ $[M+Na]^+ = 1385.7$	Thr 1.23 (1.5) Nle 1.28 (1.5) Phe 1.33 (1.5) Lys 6.73 (7.5)	64
23	30-45% B in 30 min	21.2	$[M+H]^+ = 1377.8$ $[M+Na]^+ = 1400.8$	Thr 1.36 (1.5) Nle 1.40 (1.5) Phe 1.46 (1.5) Lys 7.39 (7.5)	68
24	30-45% B in 30 min	16	$[M+H]^+ = 1406.0$ $[M+Na]^+ = 1428.0$ $[M+K]^+ = 1444.0$	Thr 1.50 (1.5) Nle 1.62 (1.5) Phe 1.61 (1.5) Lys 8.18 (7.5)	69

N	0-30% B in 30 min*	20.5	$[M+H]^+ = 1191.9$ $[M+Na]^+ = 1213.9$	Thr 0.76 (1) Cys 0.79 (2) Arg 1.61 (2) Gly 1.68 (2)	48
NN	15-45% B in 30 min*	15.4	$[M+H]^+ = 1307.0$ $[M+Na]^+ = 1329.3$	Thr 0.48 (1) Arg 1.31 (2) Leu 0.58 (1) Phe 0.53 (1) Ser 0.97 (2)	54
8N	5-95% B in 30 min 15-45% B in 30 min	12.3 10.4	$[M+H]^+ = 983.5$ $[M+Na]^+ = 1005.5$ $[M+K]^+ = 1021.5$	Thr 0.73 (1) Nle 0.74 (1) Phe 0.79 (1)	47

6.3. EXPERIMENTAL SECTION B

The KIA peptides were synthesized as explained in 6.1.2.1. All the peptides were synthesized in a 100 μ M scale. Because the functionalization of the resin used is 0.6 mmol AC/g resin, this can be translated as 166.67 mg of resin used for all of the peptides. The reagent quantities used for all the couplings were: 400 μ mol Fmoc-AA-OH (187.4 mg Fmoc-Lys(Boc)-OH, 141.4 mg Fmoc-Ile-OH, 124.5 mg Fmoc-Ala-OH, 118.9 mg Fmoc-Gly-OH): 400 μ mol HBTU (151.7 mg): 400 μ mol HOBt (67.8 mg): 800 μ mol DIEA (139 μ L).

In the case of the labelled peptides, the reagent quantities used for the manual coupling were: 200 μ mol Fmoc-AA-OH (62.5 mg Fmoc-Ala(¹⁵N)-OH): 200 μ mol HBTU (75.9 mg): 200 μ mol HOBt (33.8 mg): 400 μ mol DIEA (70 μ L).

In the following tables all the information regarding the synthesis and purification of each peptide is depicted.

Table 34: Obtained quantities and synthetic yield of the KIA peptides. Some of the peptides are common in the group and were therefore already synthesized; they are marked in the table as ... The peptide KIA14-¹⁵N was synthesized in a big scale and a smaller batch of the crude peptide was used in this thesis, therefore the synthetic yield could not be calculated and is marked as * in the table.

Peptide	Crude peptide (mg)	Synthesis yield (%)	Pure peptide (mg)	Purification yield (%)	TOTAL YIELD (%)
KIA14 wt
KIA15 wt	127	84	40,3	32	27
KIA17 wt	128,9	76	81,7	63	48
KIA19 wt	149,9	80	69	46	37
KIA21 wt
KIA22 wt	171,5	78	94,4	55	43
KIA24 wt	178,9	75	90,2	50	38
KIA26 wt	211,2	83	100	47	39
KIA28 wt	235,7	86	92,5	39	34
KIA14- ¹⁵ N	138,8	*	42,1	30	*
KIA15- ¹⁵ N	102,9	68	45,5	44	30
KIA17- ¹⁵ N	123	73	49	40	29
KIA19- ¹⁵ N	146,5	78	78,8	54	42
KIA21- ¹⁵ N	145,6	71	79,8	55	39
KIA22- ¹⁵ N	149,5	68	69,9	47	32
KIA24- ¹⁵ N	172,9	73	75,7	44	32
KIA26- ¹⁵ N	161,1	63	72	45	28
KIA28- ¹⁵ N	204,1	74	90,2	44	33

Table 35: Purification characteristics and masses of the obtained pure KIA peptides. Some of the peptides are common in the group and were therefore already synthesized, they are marked in the table as ...

Peptide	HPLC gradient	Retention time (min)	EM ESI (m/z)
KIA14 wt
KIA15 wt	0-50% B in 20 min	11-12	[M+3H] ³⁺ = 503.5 [M+2H] ²⁺ = 754.8 [M+H] ⁺ = 1508.8
KIA17 wt	0-50% B in 20 min	12-13	[M+3H] ³⁺ = 564.9 [M+2H] ²⁺ = 846.9 [M+H] ⁺ = 1694.0
KIA19 wt	0-50% B in 20 min	12-13	[M+3H] ³⁺ = 626.9 [M+2H] ²⁺ = 940.0 [M+H] ⁺ = 1879.1
KIA21 wt
KIA22 wt	0-50% B in 20 min	13-14	[M+4H] ⁴⁺ = 548.5 [M+3H] ³⁺ = 731.0 [M+2H] ²⁺ = 1096.1
KIA24 wt	10-60% B in 20 min	12-13	[M+4H] ⁴⁺ = 594.5 [M+3H] ³⁺ = 792.4 [M+2H] ²⁺ = 1188.1
KIA26 wt	10-60% B in 20 min	12-13	[M+4H] ⁴⁺ = 640.8 [M+3H] ³⁺ = 854.1 [M+2H] ²⁺ = 1280.7
KIA28 wt	10-60% B in 20 min	13-14	[M+3H] ³⁺ = 915.5 [M+2H] ²⁺ = 1372.7
KIA14- ¹⁵ N	0-50% B in 20 min	11-12	[M+2H] ²⁺ = 691.3 [M+H] ⁺ = 1381.8
KIA15- ¹⁵ N	0-50% B in 20 min	11-12	[M+2H] ²⁺ = 755.4 [M+H] ⁺ = 1509.9
KIA17- ¹⁵ N	0-50% B in 20 min	12-13	[M+3H] ³⁺ = 565.3 [M+2H] ²⁺ = 847.4 [M+H] ⁺ = 1695.0
KIA19- ¹⁵ N	0-50% B in 20 min	12-13	[M+3H] ³⁺ = 627.3 [M+2H] ²⁺ = 940.5 [M+H] ⁺ = 1880.1
KIA21- ¹⁵ N	0-50% B in 20 min	14-15	[M+3H] ³⁺ = 688.6 [M+2H] ²⁺ = 1032.5 [M+H] ⁺ = 2064.2
KIA22- ¹⁵ N	0-50% B in 20 min	14-15	[M+3H] ³⁺ = 731.3 [M+2H] ²⁺ = 1096.6
KIA24- ¹⁵ N	10-60% B in 20 min	12-13	[M+3H] ³⁺ = 792.7 [M+2H] ²⁺ = 1188.7 [M+H] ⁺ = 2376.5
KIA26- ¹⁵ N	10-60% B in 20 min	12-13	[M+3H] ³⁺ = 854.4 [M+2H] ²⁺ = 1281.2
KIA28- ¹⁵ N	10-60% B in 20 min	13-14	[M+3H] ³⁺ = 915.8 [M+2H] ²⁺ = 1373.3

7. SUMMARY OF THE THESIS IN CATALAN

7.1. INTRODUCCIÓ

7.1.1. Resistència bacteriana, la crisi dels antibiòtics i els pèptids antimicrobians

7.1.2. Pèptids antimicrobians emprats en aquesta tesi

7.1.2.1. Les polimixines

7.1.2.2. Peptidil-glicina-leucina-carboxamida (PGLa) i el seu derivat MSI-103

7.2. OBJECTIUS

7.3. SECCIÓ A – ANÀLEGS DE LES POLIMIXINES

7.3.1. DISSENY I SÍNTESI DELS ANÀLEGS

7.3.1.1. Disseny de nous anàlegs de polimixina

7.3.1.2. Síntesi química dels anàlegs de polimixina

7.3.2. DETERMINACIÓ *IN-VITRO* DE L'ACTIVITAT ANTIBACTERIANA

7.3.2.1. Soques bacterianes de tipus ATCC

7.3.2.2. Soques bacterianes resistents i multiresistents

7.3.3. ESTUDI DEL MECANISME D'ACCIÓ

7.3.3.1. Estudi biofísic, de citometria de flux i microscòpia electrònica de transmissió dels nous anàlegs de polimixina

7.3.3.2. Breu discussió sobre els resultats obtinguts per a l'estudi del mecanisme d'acció dels nous anàlegs de polimixina

7.4. SECCIÓ B – ANÀLEGS DE MSI-103

7.4.1. DISSENY I SÍNTESI DELS ANÀLEGS DE MSI-103 PER ESTUDIAR L'EFECTE DE LA LONGITUD DE LA CADENA PEPTÍDICA EN L'ACTIVITAT

7.4.1.1. Disseny dels anàlegs de MSI-103

7.4.1.2. Síntesi química dels anàlegs de MSI-103

7.4.2. DETERMINACIÓ *IN-VITRO* DE L'ACTIVITAT ANTIBACTERIANA I HEMOLÍTICA

7.4.2.1. Activitat antibacteriana

7.4.2.2. Activitat hemolítica

7.4.3. ESTUDI DEL MECANISME D'ACCIÓ – Investigació de la hipòtesi de la formació de porus

7.4.3.1. Dicroïsmes circulars

7.4.3.2. Experiments biofísics – Permeabilització de vesícules

7.4.3.3. Ressonància magnètica nuclear de fases condensades de ³¹P i ¹⁵N per estudiar l'orientació dels pèptids KIA en membranes lipídiques

7.4.3.4. Breu discussió sobre els resultats obtinguts per a la investigació de la hipòtesi de la formació de porus

7.5. CONCLUSIONS

7.1. INTRODUCCIÓ

7.1.1. Resistència bacteriana, la crisi dels antibiòtics i els pèptids antimicrobians

L'aparició i propagació mundial de bacteris resistents a múltiples fàrmacs (definites com resistents a tres o més classes de fàrmacs antibacterians) s'ha convertit en un problema clínic molt important. Alguns dels factors que han contribuït al desenvolupament de la resistència bacteriana inclouen l'ús inadequat d'antibiòtics, com l'ús excessiu dels antibiòtics d'ampli espectre, la presència d'antibiòtics en la indústria alimentària/ramaderia i la inclusió d'antimicrobians en productes per a la llar (Aiello & Larson, 2003; Arnold, 2007). No obstant això, el nombre de nous antimicrobians que es troben en les últimes etapes de desenvolupament és molt baix, de fet, els patògens ESKAPE (*Enterococcus faecium*, *Staphylococcus aureus*, *Klebsiella pneumoniae*, *Acinetobacter baumannii*, *Pseudomonas aeruginosa* i espècies *Enterobacter*) causen infeccions que no responen a cap dels antibiòtics existents (Boucher et al., 2009; Rice, 2008). El nombre d'agents antimicrobians aprovats per la Food and Drug Administration dels Estats Units (FDA) i l'Agència Europea de Medicaments (EMA) ha disminuït dràsticament en els últims 25 anys.

En aquest context, ara hi ha un renovat interès en la recerca de fàrmacs que tenen més d'una diana terapèutica en la cèl·lula bacteriana, en lloc d'actuar sobre un receptor quiral específic o enzim, amb especial atenció en tractaments amb mecanismes menys susceptibles de promoure resistència. Els pèptids antimicrobians són una classe d'antibiòtics que ha despertat gran interès en els últims anys pel fet que poques vegades estimulen el desenvolupament d'organismes genèticament resistents. Són un grup divers de molècules que comparteixen algunes característiques comunes, com ser curts (típicament 10-50 aminoàcids), generalment catiónics i adopten estructures amfipàtiques, però el més important és que la seva diana terapèutica és principalment la membrana bacteriana. En els últims anys però, nous estudis han demostrat que els AMPs poden tenir dianes intracel·lulars, com per exemple l'ADN o la síntesi de proteïnes, tot i que en qualsevol cas la interacció amb la membrana és un pas necessari.

7.1.2. Pèptids antimicrobians emprats en aquesta tesi

7.1.2.1. Les polimixines

L'aparició de patògens bacterians amb resistència adquirida a gairebé tots els antibiòtics disponibles, és una preocupació mèdica cada vegada més gran en l'àmbit hospitalari i d'atenció mèdica. En conseqüència, hi ha hagut un ressorgiment d'antibiòtics abandonats, com les polimixines, descobertes al 1947 (Ainsworth et al., 1947), com a fàrmacs d'últim recurs per al tractament d'infeccions causades per patògens Gram-negatius multiresistents, malgrat la seva toxicitat (nefrotoxicitat i neurotoxicitat) i la manca de dades d'eficàcia clínica (Landman et al., 2008; Pogue et al., 2011).

Polimixina B (PxB) i colistina (PxE) són dos lipopèptids cíclics no ribosòmics produïts pel bacteri del sòl *Bacillus polymyxa*, i són les dues polimixines utilitzades clínicament. Totes dues són específiques i altament potents contra bacteris Gram-negatius. Comparteixen una seqüència primària comuna, amb cinc càrregues positives a causa del àcid L- α,γ -diaminobutíric (Dab), l'única diferència es troba en la posició 6, que està ocupada per D-Phe en PxB i D-Leu en colistina (Figura 1).

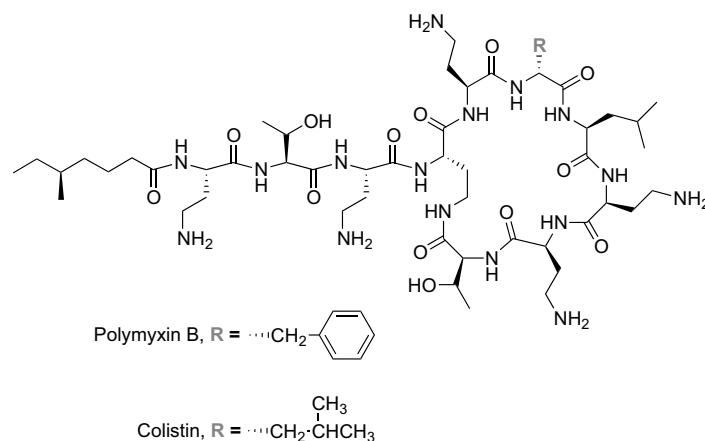


Figura 1: Estructura de Polimixina B i colistina, usades en aquesta tesi.

El mecanisme d'acció de les polimixines ha sigut estudiat en detall (Cajal et al., 1995; 1996b; Cajal, et al., 1996a; Velkov et al., 2010), i està basat principalment en la interacció de les molècules catióniques amb el LPS, component de càrrega negativa que forma la membrana externa, i la posterior interacció amb la membrana citoplasmàtica, rica també en fosfolípids aniónics.

7.1.2.2. Peptidil-glicina-leucina-carboxamida (PGLa) i el seu derivat MSI-103

En els últims anys s'han fet grans esforços per dissenyar i sintetitzar nous pèptids d'elevada activitat, ja sigui nous dissenys o basats en seqüències naturals. Un exemple d'aquestes pèptids dissenyats és el MSI-103, amb seqüència $(\text{KIAGKIA})_3\text{-NH}_2$, que va ser dissenyat a partir de la seqüència del pèptid PGLa, membre de la família de les magainines trobat a la pell de la granota africana *Xenopus laevis* (Hoffmann, et al., 1983; Richter, et al., 1985). La seqüència de MSI-103 es va optimitzar per simplificació utilitzant només quatre aminoàcids diferents en un heptàmer repetit augmentant per tant la càrrega positiva però mantenint el caràcter amfipàtic global del pèptid inicial (Blazyk, 2001; Maloy & Kari, 1995). Es va trobar que l'anàleg sintètic presentava una activitat més gran que PGLa amb efectes secundaris hemolítics baixos (Blazyk, 2001; Strandberg et al., 2007) i una major taxa de fusió (Wadhvani et al., 2012).

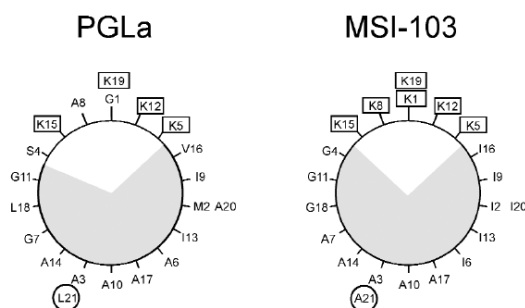


Figura 2: Projeccions de les rodes helicoïdals dels pèptids α -helicoïdals amfifílics PGLa i MSI-103. Els residus carregats estan marcats per rectangles, i el aminoàcid C-terminal per un cercle. El sector hidrofòbic es troba ombrejat.

MSI-103, ha sigut àmpliament estudiat usant ressonància magnètica nuclear (RMN) en fases condensades o experiments biofísics però el seu mecanisme d'acció no ha sigut encara establert tot i que es creu que està basat en la permeabilització de les bacteries per formació de porus com en el cas del pèptid original, PGLa.

7.2. OBJECTIUS

Els principals objectius d'aquesta tesi van ser els següents:

- Dissenyar i sintetitzar nous lipopèptids basats en l'estructura de les polimixines per tal d'obtenir nous compostos antimicrobians amb ampli espectre d'activitat i actius contra bacteris resistents. A més, el disseny hauria de facilitar la síntesi química i futura síntesi en gran escala dels anàlegs.
- Investigar el mecanisme d'acció d'aquests pèptids utilitzant diferents tècniques, com ara les biofísiques basades en la fluorescència utilitzant liposomes i monocapes com a membranes model, i citometria de flux i microscòpia electrònica de transmissió utilitzant bacteris.
- Estudiar l'efecte de la longitud de la cadena peptídica en l'activitat (antibacteriana i hemolítica) mitjançant la síntesi d'una sèrie de pèptids de diferent longitud (de 14 a 28 aminoàcids) basat en les mateixes unitats repetitives del pèptid MSI-103.
- Estudiar si els pèptids MSI-103 formen porus en una orientació transmembrana com el pèptid original PGLa, mitjançant l'ús de tècniques biofísiques com la RMN de fases condensades, i si aquest fos el cas, determinar la longitud mínima dels pèptids necessària per travessar la membrana. Per tant un llindar de longitud mínima seria necessari per a observar activitat, que també variaria segons el gruix de la membrana.

7.3. SECCIÓ A – ANÀLEGS DE LES POLIMIXINES

7.3.1. DISSENY I SÍNTESI DELS ANÀLEGS

7.3.1.1. Disseny de nous anàlegs de polimixina

Per tal d'obtenir anàlegs de polimixina, amb activitat semblant o superior contra els bacteris Gram-negatius, però amb un espectre d'activitat més ampli, actiu contra els bacteris resistents i potencialment amb menor toxicitat, el disseny racional de les molècules ha de mantenir inicialment les característiques bàsiques de la PxB, clau per a la seva activitat, que són: El caràcter amfipàtic de la molècula, les càrregues positives i la seva distribució al llarg de la molècula, un cicle de 7 aminoàcids (anell de 23 membres) que inclou un domini hidrofòbic en les posicions 6 i 7, un tripèptid lineal i una acilació en l'extrem N-terminal per una cadena de mida mitjana. No obstant això, com s'ha mostrat en treballs anteriors del grup (Clauell et al., 2003; 2004; 2006; 2007), es van dur a terme tres modificacions principals (Figura 3):

- La substitució isostèrica de l'enllaç lactàmic en el cicle entre Dab⁴ i Thr¹⁰ per un enllaç disulfur entre dos residus de Cys col·locats en les mateixes posicions per tal de simplificar la síntesi química sense modificar la mida del cicle, clau per a l'activitat. La presència de ponts disulfur no és estranya en pèptids antimicrobians natural cíclics, com la ranalexina (de *Rana catesbeiana*), que conté una estructura de heptapèptid macrocíclic altament similar a la de polimixina B, com ja va destacar Zasloff (Clark et al., 1994).
- L'extrem C-terminal dels anàlegs, on la cadena lateral de Thr¹⁰ es troba substituïda per un isòster carboxàmid amb característiques d'unió similars. Això és crucial per a l'activitat com es demostra pel model d'interacció entre

- PxB i LPS (Bruch et al., 1999) on la cadena lateral del Thr¹⁰ interactua per enllaços d'hidrogen amb els grups fosfat del lípid A.
- La substitució del àcid (S)-6-metiloctanoic per àcids lineals (àcid octanoic, nonanoic, decanoic o dodecanoic), sense cap estereocentre i disponibles comercialment.

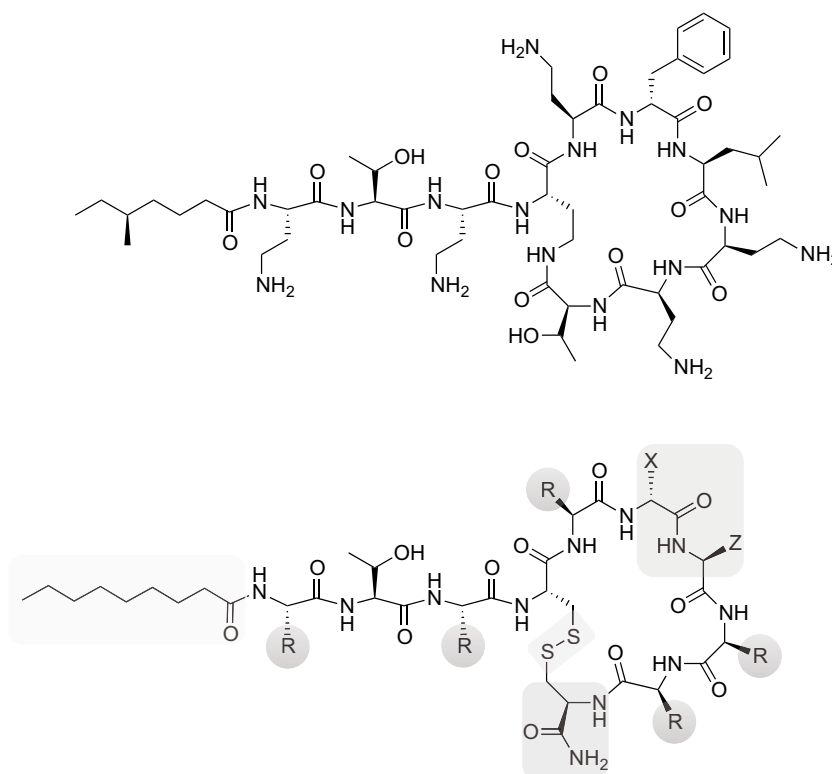


Figura 3: Estructura de polimixina B natural (superior) en comparació amb l'estructura general dels lipopeptids anàlegs de polimixina sintetitzats en el nostre grup (inferior). Les característiques estructurals i químiques analitzades per al disseny dels anàlegs es troben destacades.

En la Taula 1 es mostren la seqüència i numeració dels pèptids dissenyats i sintetitzats en aquesta tesi.

Taula 1: Seqüència dels lipopèptids cíclics en codi de tres lletres, els D-aminoàcids s'indiquen en cursiva i els residus subratllats indiquen la formació d'un enllaç.

PxB	6-metil-octanoïl-Dab-Thr-Dab-Dab-Phe-Leu-Dab-Dab-Thr
1	nonanoïl-Arg-Thr-Dab-Cys-Dab-Phe-Leu-Arg-Dab-Cys
2	decanoïl-Arg-Thr-Dab-Cys-Dab-Phe-Leu-Arg-Dab-Cys
3	dodecanoïl-Arg-Thr-Dab-Cys-Dab-Phe-Leu-Arg-Dab-Cys
4	nonanoïl-Arg-Thr-Dab-Cys-Dab-Trp-Leu-Arg-Dab-Cys
5	nonanoïl-Dab-Thr-Arg-Cys-Dab-Phe-Leu-Arg-Dab-Cys
6	decanoïl-Dab-Thr-Arg-Cys-Dab-Trp-Leu-Arg-Dab-Cys
7	decanoïl-Arg-Thr-Arg-Cys-Dab-Trp-Nle-Arg-Dab-Cys
8	decanoïl-Dab-Thr-Dab-Cys-Dab-Phe-Nle-Dab-Dab-Cys
9	dodecanoïl-Dab-Thr-Dab-Cys-Dab-Phe-Nle-Dab-Dab-Cys
10	decanoïl-Dab-Thr-Arg-Cys-Dab-Phe-Nle-Arg-Dab-Cys
11	dodecanoïl-Dab-Thr-Arg-Cys-Dab-Phe-Leu-Arg-Dab-Cys
12	decanoïl-Dab-Thr-Dab-Cys-Dab-Leu-Nle-Dab-Dab-Cys
13	nonanoïl-Dab-Thr-Dab-Cys-Dab-Nle-Nle-Dab-Dab-Cys
14	decanoïl-Dab-Thr-Dab-Cys-Dab-Nle-Nle-Dab-Dab-Cys
15	dodecanoïl-Dab-Thr-Dab-Cys-Dab-Nle-Nle-Dab-Dab-Cys
16	nonanoïl-Dab-Thr-Dab-Cys-Dab-Leu-Leu-Dab-Dab-Cys
17	decanoïl-Dab-Thr-Dab-Cys-Dab-Leu-Leu-Dab-Dab-Cys
18	dodecanoïl-Dab-Thr-Dab-Cys-Dab-Leu-Leu-Dab-Dab-Cys
19	nonanoïl-Orn-Thr-Orn-Cys-Orn-Phe-Nle-Orn-Orn-Cys
20	decanoïl-Orn-Thr-Orn-Cys-Orn-Phe-Nle-Orn-Orn-Cys
21	dodecanoïl-Orn-Thr-Orn-Cys-Orn-Phe-Nle-Orn-Orn-Cys
22	nonanoïl-Lys-Thr-Lys-Cys-Lys-Phe-Nle-Lys-Lys-Cys
23	decanoïl-Lys-Thr-Lys-Cys-Lys-Phe-Nle-Lys-Lys-Cys
24	dodecanoïl-Lys-Thr-Lys-Cys-Lys-Phe-Nle-Lys-Lys-Cys

7.3.1.2. Síntesi química dels anàlegs de polimixina

Els lipopèptids es van sintetitzar manualment seguint un procediment Fmoc/tBu estàndard. En tots els casos la resina utilitzada va ser MBHA amb un espaiador bifuncional Fmoc-Rink amida. Els grups protectors dels aminoàcids van ser els següents: Trt per Cys, Boc per Dab, Lys i Orn, tBu per Thr i Pbf per Arg.

Els aminoàcids es van incorporar directament a la resina utilitzant DIC com a agent activant i HOBt com a additiu per minimitzar la racemització. Tres equivalents de tots els reactius es van barrejar durant 1 hora en DMF. Cicles successius de desprotecció amb piperidina al 20% en DMF i acoblament dels aminoàcids protegits van donar lloc als pèptids desitjats. Després de l'últim acoblament, i eliminació del grup protector Fmoc, es va dur a terme l'acoblament de l'àcid gras (àcid octanoic, nonanoic, decanoic o dodecanoic) utilitzant 5 equivalents d'àcid, DIC i HOBt durant 1 hora en DMF.

L'escissió i desprotecció completa dels pèptids lineals es va dur a terme mitjançant acidòlisi amb una barreja de TFA/trietilsilà o triisopropilsilà/aigua durant 90 minuts. El filtrat es va evaporar fins a un volum reduït sota un corrent suau de nitrogen i el cru es va precipitar amb èter dietílic fred.

La ciclació dels crús peptídics per formació d'enllaços disulfur es va dur a terme dissolent el pèptid en aigua a una concentració molt diluïda seguit per l'addició de 5% de DMSO com a oxidant suau (Tam et al., 1991).

Finalment, els crús peptídics es van purificar per HPLC semi-preparatiu i els productes purs obtinguts (puresa >95%) van ser caracteritzats mitjançant HPLC analític, anàlisi d'aminoàcids i espectrometria de masses MALDI-TOF (esquema de la ruta sintètica a la Figura 4).

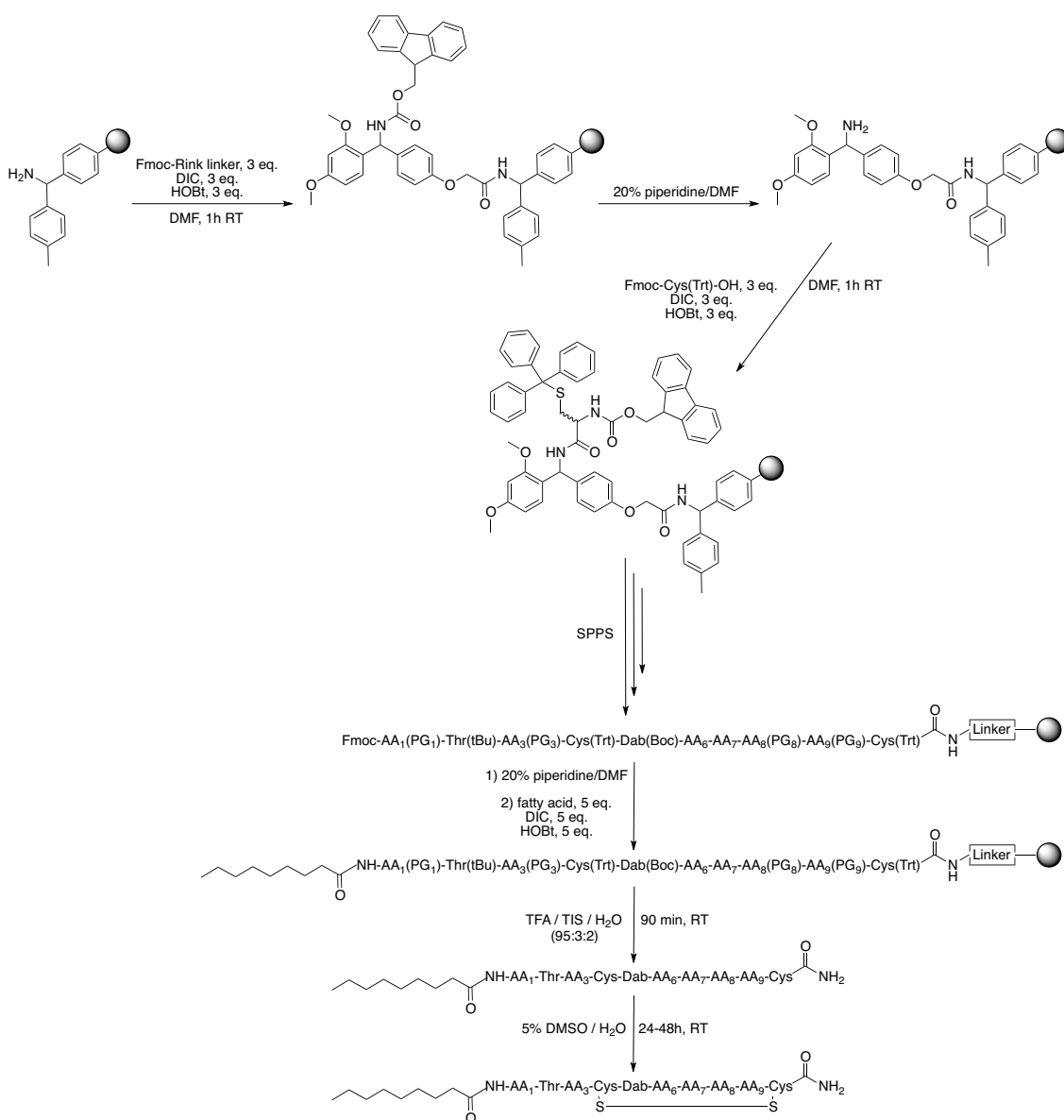


Figura 4: Esquema general de l'estratègia de síntesi seguida pels anàlegs de polimixina. AA_x fa referència a aminoàcid i PG_x grup protector, la x indica la posició en la seqüència.

7.3.2. DETERMINACIÓ *IN-VITRO* DE L'ACTIVITAT ANTIBACTERIANA

7.3.2.1. Soques bacterianes de tipus ATCC

L'objectiu d'aquesta part de la tesi va ser mesurar l'activitat antibacteriana dels nous anàlegs de polimixina. Aquesta activitat es va expressar com a concentració mínima inhibidora (CMI), que és la concentració més baixa d'agent antibacterià que inhibeix el creixement visible d'un microorganisme en 18-24 h. Es va determinar pel mètode de dilució amb tubs (Jorgensen & Ferraro, 2009; Woods, 1995). Els valors de CMI per als pèptids sintetitzats es mostren a la Taula 2. PxB natural es va utilitzar com a control en cada experiment.

Taula 2: La concentració mínima inhibidora (expressada en µg/mL) dels anàlegs de polimixina descrits. Els microorganismes que no han estat avaluats per un pèptid determinat s'expressen com --.

Pèptid	GRAM+			GRAM-			FONG
	<i>E.faecalis</i>	<i>S.aureus</i>	<i>M.phlei</i>	<i>E.coli</i>	<i>P.aeruginosa</i>	<i>Acinetobacter sp.</i>	<i>C.albicans</i>
PxB	>32	>32	16	1	1	1	>32
1	>32	16	--	4	8	--	--
2	32	16	--	8	8	--	--
3	8	4	--	8	16	--	--
4	32	8	--	4	8	--	--
5	>32	8	--	2	16	--	--
6	32	8	--	8	32	--	--
7	16	4	--	8	>32	--	--
8	32	4-8	2-4	1-2	2	4	16
9	16	4-8	2-4	4-8	4	16	16
10	16-32	4	2	2-4	2	4	16-32
11	16	4	2	4	4	4	16
12	>32	16	4	4-8	1	4	--
13	>32	32	16	4	1-2	2	--
14	>32	8	2-4	2	2-4	2	--
15	8-16	4	1-2	2-4	4	4	--
16	>32	32	>32	4-8	1	4	--
17	>32	8	4	2-4	1-4	8	--
18	16-32	4	2	4	2-4	4-8	--
19	>32	16-32	8	32	>32	>32	>32
20	>32	16	4-8	16	>32	>32	>32
21	8	4	4	16	16	32	16
22	>32	>32	8	32	>32	>32	>32
23	>32	32	16	32	>32	>32	>32
24	16-32	8	8	16	32	8	16

En la primera sèrie de pèptids sintetitzats (#1-7), es va investigar l'efecte de la substitució dels residus carregats en la molècula (Dab) per un altre residu bàsic carregat, l'arginina, mentre es mantenia la càrrega total de la molècula. L'arginina és coneguda per ser un aminoàcid altament actiu en la membrana i és prevalent en moltes seqüències de pèptids antimicrobians per les seves propietats químiques que afavoreixen la interacció amb la membrana bacteriana. La presència del grup guanidini proporciona a l'arginina d'un fort caràcter catiònic bidentat i l'habilitat de formar enllaços d'hidrogen (Fuchs & Raines, 2006). Això permet que l'arginina formi interaccions π -catiòniques que fan l'entrada al nucli hidrofòbic de la bicapa energèticament més favorable, afavorint així la interacció inicial amb la membrana externa (ME) dels bacteris resultant en una millora en l'activitat (Arouri et al., 2009; Chan et al., 2006; Lättig-Tünnemann et al., 2011).

L'ús de triptòfan en substitució de fenilalanina també va ser provat en alguns dels pèptids (#4, 6, 7). Aquest residu presenta diversos avantatges, per exemple confereix la molècula de fluorescència intrínseca, molt útil per caracteritzar la unió a la membrana per tècniques de fluorescència (vegeu el capítol 7.3.3) i afavoreix la interacció amb la regió interfacial de la membrana lipídica (Arouri et al., 2009; Chan et al., 2006).

A més, en alguns dels pèptids (#1, 5-7) el residu C-terminal Cys es va canviar a un D-Cys per a reproduir millor l'orientació del grup polar del residu Thr¹⁰ en la PxB natural. Addicionalment, es van utilitzar àcids grassos de diferent longitud per trobar la longitud òptima necessària.

Finalment, es va estudiar la introducció de norleucina en lloc de leucina en posició 7 per al pèptid #7 per tal d'augmentar la flexibilitat en aquest residu hidrofòbic clau.

Basant-se en els resultats obtinguts per les proves d'activitat antimicrobiana dels pèptids inicials, una segona sèrie de pèptids es va dissenyar i sintetitzar (#8-11). Aquests pèptids mantenen les característiques estructurals que van obtenir els millors resultats, D-Cys en la posició 10 i Nle en posició 7. No obstant, per posar a punt la seqüència que resulti en el millor perfil antimicrobià, es va dur a terme novament la substitució Nle per Leu, Arg per Dab i la longitud de l'àcid gras, mentre es mantenia la resta de la seqüència intacta. Es va poder observar que l'addició d'Arg en la seqüència ampliava l'espectre d'acció dels pèptids, fent-los actius front soques Gram-positives però l'efecte secundari era una reducció d'activitat front les soques Gram-negatives. En el cas de la longitud de l'àcid gras els resultats van ser semblants, a major llargada de la cadena millor activitat front *S. aureus*, però a expenses d'una certa pèrdua d'activitat en altres soques. En qualsevol cas es va poder establir que la llargada òptima de la cadena acílica era de 9-12 carbonis.

Atès que el residu Nle va donar lloc a resultats prometedors, es va decidir sintetitzar diversos anàlegs de colistina en què es va modificar el domini hidrofòbic que hi ha en el cicle (#12-18). Cal recordar que la colistina té un residu de D-Leu en la posició 6, mentre que la PxB té un residu de D-Phe en aquesta posició. L'objectiu principal d'aquestes modificacions era obtenir antimicrobians amb potencialment menor toxicitat ja que la colistina, encara que lleugerament menys activa que la PxB, ha demostrat tenir un millor perfil toxicològic (Landman et al., 2008). La idea era explorar quina combinació dels residus de Nle i Leu (substituent posicions 6, 7 o ambdues) donaven els millors resultats. Els pèptids obtinguts no van presentar millores d'activitat front altres pèptids del grup.

Finalment, l'última sèrie de pèptids (#19-24) consisteix en la substitució de tots els

residus de Dab en el compost #8 per Lys i Orn. Aquests aminoàcids carregats presenten l'avantatge de ser més convenients comercialment, més adequat per a una futura síntesi a gran escala necessària per a futures aplicacions terapèutiques clíniques. Però els resultats mostren que els pèptids obtinguts no presenten una millora respecte als anteriors pèptids del grup.

7.3.2.2. Soques bacterianes resistents i multiresistents

Degut al potencial dels pèptids més actius, es va determinar la seva activitat en bacteris resistents i multiresistents. En el nostre laboratori es va estudiar la activitat front el *Staphylococcus aureus* resistent a la meticil·lina, obtenint millors resultats que front la soca de col·lecció, un resultat prometedor ja que aquests antibacterians presenten un mecanisme d'acció diferent que els antibiòtics β -lactàmics, inactius front el MRSA.

Més destacables són els resultats obtinguts en col·laboració amb el Professor Jordi Vila i duts a terme per en Xavi Vila a l'Hospital Clínic de Barcelona, front diferents aïllats clínics de bacteris Gram-negatius. Els pèptids estudiats van presentar millors activitats front diferents soques de *E. coli* i *P. aeruginosa* altament resistents que front les soques de col·lecció, arribant en alguns casos a valors de CMI de 0.5 $\mu\text{g}/\text{mL}$.

Finalment, la activitat contra soques d'*Acinetobacter baumannii* resistent a colistina es va determinar per als millors compostos. Els valors de CMI es mostren a la Taula 3, on es pot veure que els pèptids mostren activitats moderades i en alguns casos una activitat superior que la pròpia colistina (la molècula de partida dels nostres anàlegs). Aquests resultats suggereixen que potser els nostres compostos tenen un mecanisme d'acció alternatiu, és a dir no actuen només en la membrana. És per això que en aquesta tesi gran esforç s'ha destinat a estudiar el mecanisme d'acció dels pèptids mitjançant diferents tècniques, com és la fluorescència, citometria de flux o microscòpia electrònica de transmissió (Secció 7.3.3.).

Taula 3: Activitat antibacteriana dels anàlegs de polimixina més prometedors contra diverses soques de *A. baumannii* resistents a colistina. Els valors de CMI s'expressen en $\mu\text{g}/\text{mL}$.

Pèptid	Soques d' <i>Acinetobacter baumannii</i>								
	ATCC-wt	ATCC	77778	Ab10	Ab19	Ab21R	Ab24	CR49	CR86
Colistina	1	256	256	512	512	32	>256	64	128
8	8	64	256	32	32	--	--	--	--
9	2	16	128	16	16	--	--	--	--
10	4	32	128	8	16	--	--	--	--
11	--	--	--	--	--	8	4	16	8
14	--	--	--	--	--	32	16	64	32
17	--	--	--	--	--	32	128	128	256

Perfil de resistència:
 ATCC-wt: soca de col·lecció, resistència baixa
 ATCC: mutant *in-vitro* de la soca de col·lecció amb resistència a colistina
 77778: mutant *in-vitro* d'una soca clínica amb resistència a colistina
 Ab10, Ab19, Ab21R, Ab24, CR49 i CR86: aïllats clínics resistents a colistina

7.3.3. ESTUDI DEL MECANISME D'ACCIÓ

7.3.3.1. Estudi biofísic, de citometria de flux i microscòpia electrònica de transmissió dels nous anàlegs de polimixina

Un dels principals objectius d'aquesta tesi és caracteritzar la interacció de la PxB i els anàlegs sintetitzats amb el component lipídic de les membranes bacterianes mitjançant l'ús de models de membrana que reproduïen la seva composició.

Els nous anàlegs de polimixina sintetitzats en aquest treball han de tenir les següents característiques:

- Interactuar amb les membranes model i presentar una alta afinitat pel LPS.
- Formar contactes moleculars entre les membranes, com es va veure anteriorment per la PxB natural (Cajal et al., 1995), que donen lloc al intercanvi de fosfolípids provocant canvis en la composició específica de la membrana, necessàries per mantenir l'homeòstasi de la cèl·lula i per tant comprometre la viabilitat cel·lular.
- No mostrar efecte lític sobre membranes model de les cèl·lules eucariotes.

Per dur a terme aquests experiments es van usar liposomes i monocapes com a models de membrana. Els liposomes utilitzats en aquesta tesi són SUVs o LUVs preparats per sonicació o extrusió, utilitzant les següents barreges de fosfolípids sintètics: POPG com a model dels bacteris Gram-positius, POPE/POPG (6:4) per modelar els bacteris Gram-negatius i POPC zwitteriònic per imitar la membrana citoplasmàtica de les cèl·lules eucariotes (Epanand et al., 2008). En el cas de les monocapes, aquestes es van preparar utilitzant LPS comercial del bacteri *Salmonella enterica* serotip Minnesota Re 595 (Re mutant), per tant, model de la membrana externa dels bacteris Gram-negatius.

Alguns dels assajos complementaris que s'han utilitzat es resumeixen a continuació:

- Contingut aquós: Barreja o permeabilització induïda pels pèptids
- Agregació de membrana / lisi mesurat per dispersió de llum
- Barreja de lípids: formació de contactes, hemifusió o fusió de vesícules
- Flip-flop dels fosfolípids
- Alteracions en la fluïdesa de la membrana
- Fluorescència del triptòfan i la seva modificació degut a la interacció dels pèptids

Complementàriament, s'han dut a terme experiments de citometria de flux i microscòpia electrònica de transmissió en els Centres científics i tecnològics de la Universitat de Barcelona (CCiTUB), mitjançant els quals s'ha pogut estudiar els efectes del pèptid directament sobre bacteris Gram-positius i Gram-negatius. En el cas de citometria de flux, usant dues sondes, iodur de propidi i bis-(àcid 1,3-dibutylbarbituric)-trimethine oxonol s'ha pogut estudiar la permeabilització i despolarització respectivament de la membrana bacteriana. Amb l'ús de la microscòpia electrònica de transmissió s'han pogut observar els efectes morfològics causats per la exposició de les bacteries als anàlegs de polimixina.

7.3.3.2. Breu discussió sobre els resultats obtinguts per a l'estudi del mecanisme d'acció dels nous anàlegs de polimixina

Els diferents pèptids estudiats van mostrar les següents característiques:

- **Gran afinitat pel LPS**, comparable a la de la PxB natural, i capacitat d'inserció en monocapes de LPS però amb valors molt diferents segons l'estructura de cada pèptid.
- **Afinitat d'unió a la membrana lipídica que depèn de la composició de la mateixa** (POPG, POPE/POPG o POPC). Mitjançant diversos experiments, com FRET o per tres dels pèptids fluorescència del Trp, es va poder concloure que els pèptids s'uneixen de manera més eficient a vesícules que contenen PE que PG pur, però s'uneixen de forma similar amb característiques espectroscòpiques similars. En canvi, la unió a vesícules de POPC és significativament menys eficient, i consistent amb una inserció més gradual.
- **La pertorbació de la membrana induïda pels pèptids requereix la presència de lípids aniònics**. Mitjançant múltiples experiments es va poder establir que tot i que els pèptids són capaços de unir-se a liposomes de POPC, no indueixen permeabilització o fusió destacable en aquestes vesícules. En canvi, els pèptids mostren elevada capacitat d'inducció de la barreja dels fosfolípids en vesícules de POPE/POPG, i a elevades concentracions, permeabilització. En el cas de liposomes de POPG (model de bacteries Gram-positives), els pèptids #1-6 són poc actius a concentracions baixes mentre que els pèptids #7-11 indueixen una ràpida permeabilització fins i tot a baixes concentracions de pèptid.
- **L'afectació en la membrana és molt diferent en *S. aureus* i *E. coli* segons els experiments de citometria de flux**, probablement degut a la diferent composició de les membranes Gram-positives i Gram-negatives. Per exemple, el pèptid #8, un dels lipopèptids més prometedors de la sèrie ja que presenta elevada activitat fins i tot contra soques multiresistents, no causa permeabilitat de la membrana de *S. aureus* però sí en la de *E. coli*.
- **Elevada afectació en la membrana observada en els experiments de microscòpia**. El pèptid #8 indueix la formació de mesosomes, que són considerats un mecanisme defensiu de les bacteries per protegir-les de l'assalt antibiòtic.
- Tots aquests resultats semblen indicar que **els pèptids actuen a nivell de la membrana i en concret el pèptid #8 probablement mata les bacteries mitjançant una estratègia *multi-hit***, és a dir el seu mecanisme d'acció no és únicament la pertorbació de la membrana bacteriana.

7.4. SECCIÓ B – ANÀLEGS DE MSI-103

7.4.1. DISSENY I SÍNTESI DELS ANÀLEGS DE MSI-103 PER ESTUDIAR L'EFECTE DE LA LONGITUD DE LA CADENA PEPTÍDICA EN L'ACTIVITAT

7.4.1.1. Disseny dels anàlegs de MSI-103

Com ja s'ha comentat a l'apartat d'introducció, el MSI-103 és un pèptid antimicrobià, de seqüència (KIAGKIA)₃-NH₂, que va ser dissenyat a partir de la seqüència del PGLa (Blazyk, 2001; Maloy & Kari, 1995). Tots dos pèptids s'han estudiat àmpliament en el grup de la professora Anne S. Ulrich al Karlsruhe Institute of Technology (KIT) emprant diferents tècniques, especialment la RMN en fases condensades (ssNMR).

L'objectiu inicial del projecte que s'havia de dur a terme en el grup de la Dra. Anne Ulrich a Karlsruhe, era estudiar si una versió més curta de 14 aminoàcids (KIAGKIA)₂-NH₂ era actiu i determinar el seu comportament en les membranes lipídiques. La raó principal per utilitzar un pèptid més curt és la recent observació que els pèptids antimicrobians, fins i tot molt curts poden tenir alta activitat (Munk et al., 2013; Wadhvani et al., 2014), i com a fàrmac, un pèptid més curt seria més fàcil i més barat de produir. Però quan es va determinar la seva activitat antibacteriana i es va estudiar el comportament per ²H-RMN en fases condensades, es va trobar que (KIAGKIA)₂-NH₂ està completament desproveït d'activitat i només un estat superficial (estat-S) es va poder detectar per RMN (dades no mostrades).

Per tant, es va decidir investigar una sèrie de pèptids de diferent longitud, basat en les mateixes unitats repetitives que MSI-103, anomenats pèptids KIAN (on n és el nombre d'aminoàcids en cada pèptid) (Taula 4). L'objectiu era doble: trobar la longitud òptima de la seqüència peptídica amb un alt efecte antimicrobià i una baixa activitat hemolítica, i investigar la hipòtesi de la **formació de porus**. Si aquests pèptids formen porus transmembrana, caldria una longitud mínima dels pèptids per travessar la membrana. Podríem llavors esperar una longitud mínima llindar necessària per a l'activitat, que també variaria amb el gruix de la membrana (les estructures de porus proposades es mostren a la Figura 5). D'altra banda, si els pèptids maten els bacteris per permeabilització de la membrana d'acord amb el "carpet model" on els pèptids s'uneixen a la superfície de la membrana (Gazit et al., 1996; Pouny et al., 1992), o creuant la membrana a la recerca de dianes intracel·lulars, fins i tot pèptids massa curts per travessar la membrana podrien ser actius.

Taula 4: Seqüència, en codi d'una lletra, dels pèptids sintetitzats en aquest estudi. El aminoàcid Ala-10 es va marcar amb ^{15}N a l'amida de l'eix central. (a) Suposant 1,5 Å per residu d'un α -hèlix ideal.

Pèptid	Seqüència	Llargada ^a (Å)
KIA14	KIAGKIA KIAGKIA-NH ₂	21
KIA15	KIAGKIA KIAGKIA K-NH ₂	22.5
KIA17	KIAGKIA KIAGKIA KIA-NH ₂	25.5
KIA19	KIAGKIA KIAGKIA KIAGK-NH ₂	28.5
KIA21 (MSI-103)	KIAGKIA KIAGKIA KIAGKIA-NH ₂	31.5
KIA22	KIAGKIA KIAGKIA KIAGKIA K-NH ₂	33
KIA24	KIAGKIA KIAGKIA KIAGKIA KIA-NH ₂	36
KIA26	KIAGKIA KIAGKIA KIAGKIA KIAGK-NH ₂	39
KIA28	KIAGKIA KIAGKIA KIAGKIA KIAGKIA-NH ₂	42

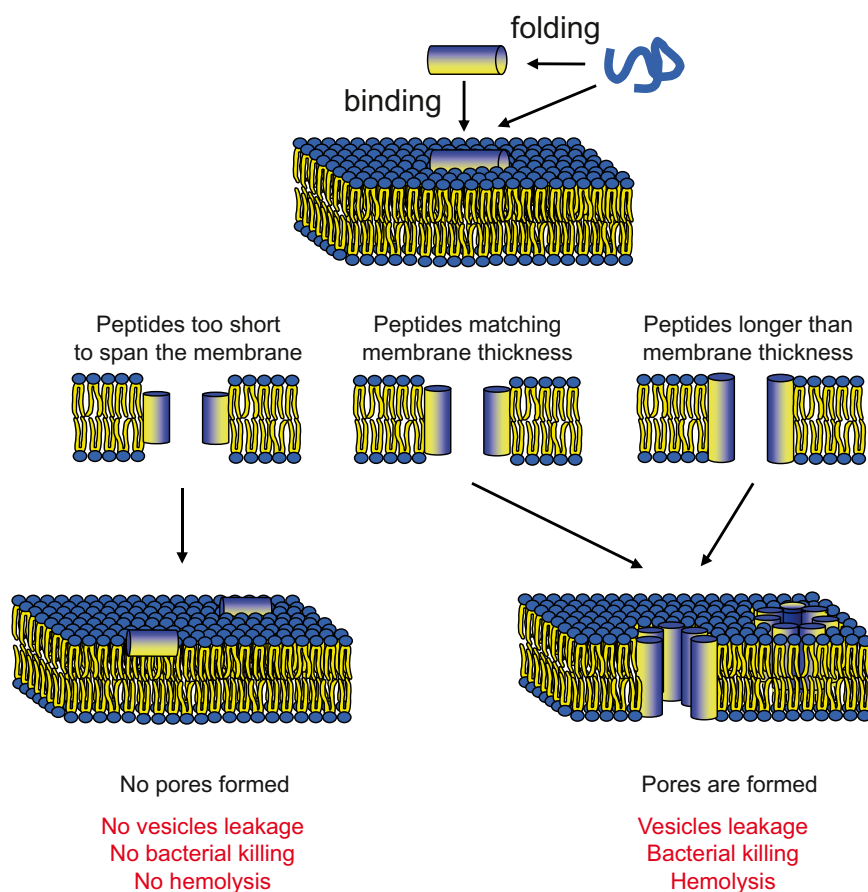


Figura 5: Model proposat de la formació de porus per als pèptids KIA. Els pèptids es troben desestructurats en solució però formen α -hèlixs amfipàtiques quan s'uneixen a la membrana. Si el pèptid és massa curt per travessar la membrana, no es formen porus i els pèptids es col·loquen paral·lels al pla de la membrana. Si el pèptid és prou llarg per travessar la part hidrofòbica de la membrana, pot formar un porus amb els pèptids en una orientació transmembrana inserida. Si els pèptids són massa llargs es poden inclinar en la membrana (no mostrat). Els porus es representen com a tipus 'barrel-stave', però també podrien ser del tipus 'toroidal wormhole' amb els caps polars dels lípids recobrint el porus.

7.4.1.2. Síntesi química dels anàlegs de MSI-103

Els pèptids de la sèrie KIA es van sintetitzar en un sintetitzador automàtic de pèptids Syro II (Multisynthtech GmbH), amb i sense ^{15}N , utilitzant protocols estàndards de síntesi en fase sòlida de tipus Fmoc (esquema de la estratègia sintètica a la Figura 6). La resina que es va utilitzar en tots els casos va ser Rink amida MBHA i el grup protector de l'aminoàcid Lys va ser Boc.

Els aminoàcids protegits amb Fmoc es van incorporar a la resina directament utilitzant una barreja de HBTU/HOBt/DIEA. Cada aminoàcid es va acoblar durant 30 minuts per duplicat. Per els experiments amb ^{15}N -RMN de fases condensades, les sondes marcades es van incorporar manualment utilitzant Fmoc-Ala marcada en la amida de l'esquelet peptídic tal i com s'ha descrit anteriorment però utilitzant la meitat dels reactius, durant 60 minuts i per duplicat.

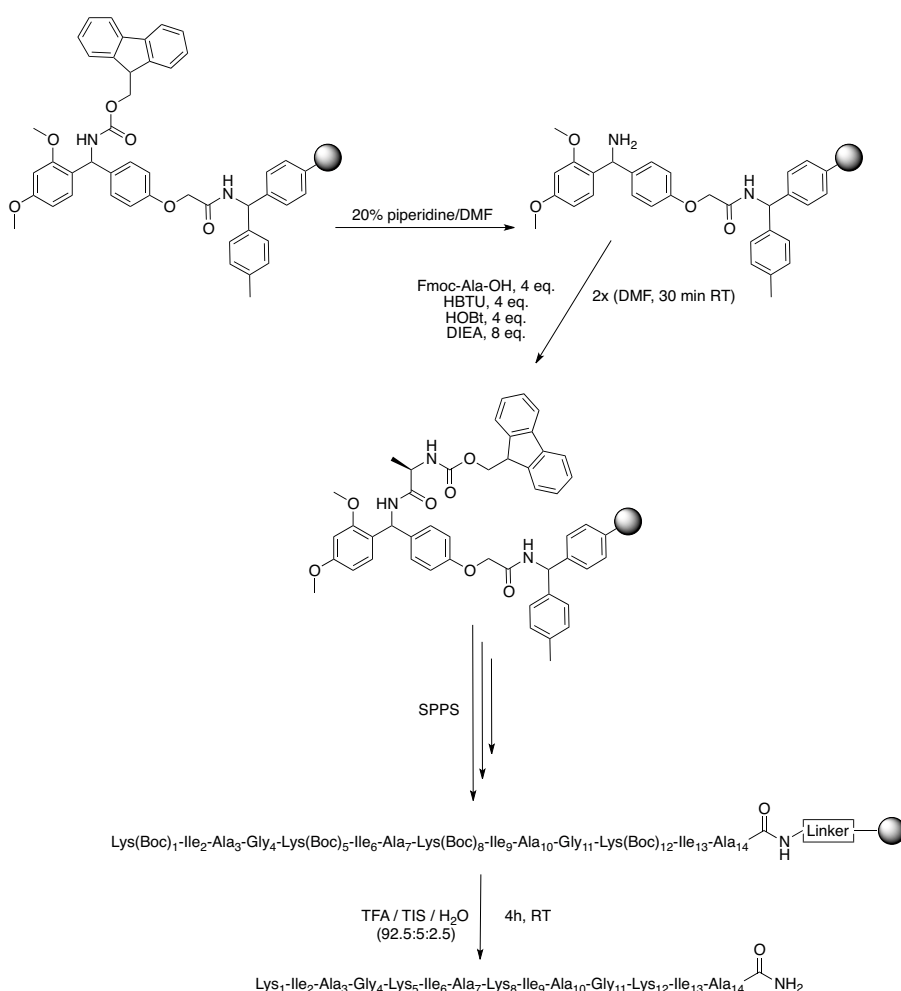


Figura 6: Esquema general de la estratègia sintètica emprada per els pèptids KIA.

L'escissió i desprotecció completa dels pèptids lineals es va dur a terme mitjançant acidòlisi amb una barreja de TFA/triisopropilsilà/aigua durant 4 hores amb agitació suau. El filtrat es va evaporar fins a un volum reduït sota un corrent suau de nitrogen i el cru es va precipitar amb èter dietílic fred.

Finalment, els crus peptídics es van purificar per HPLC semi-preparatiu i els productes purs obtinguts es van caracteritzar mitjançant HPLC analític combinat amb

espectrometria de masses ESI, i tots els pèptids van mostrar una puresa superior a 95%.

7.4.2. DETERMINACIÓ *IN-VITRO* DE L'ACTIVITAT ANTIBACTERIANA I HEMOLÍTICA

7.4.2.1. Activitat antibacteriana

Per tal d'investigar la hipòtesi de la formació de porus i esbrinar la longitud òptima necessària, es va determinar l'activitat antibacteriana dels diferents pèptids expressada com a concentració mínima inhibidora. Es va determinar utilitzant un assaig estàndard de dilució en brou (Wiegand et al., 2008).

Els bacteris utilitzats pertanyen a la col·lecció del DSM i per tant són els microorganismes estàndard de referència per a la investigació i els bacteris més representatius per a les proves d'activitat antibacteriana. Els valors de CMI per als pèptids sintetitzats es mostren a la Taula 5. Els experiments es van realitzar per triplicat i es van repetir en diferents dies per evitar els efectes ambientals. PGLa es va utilitzar com a control en cada experiment.

Taula 5: Valors de CMI (expressada en µg/mL) per als pèptids KIA en quatre soques bacterianes. Els pèptids inactius per a cada soca es troben marcats en gris.

Pèptid	GRAM-		GRAM+	
	<i>E. coli</i>	<i>P. aeruginosa</i>	<i>S. aureus</i>	<i>E. faecalis</i>
KIA14	>256	>256	>256	>1024
KIA15	>256	>256	>256	>1024
KIA17	32	256	256	>1024
KIA19	32	256	>256	>1024
KIA21	4	64	8	1024
KIA22	4	32	16	1024
KIA24	4	16	4	64
KIA26	4	16	8	64
KIA28	8	16	8	16
PGLa	32	256	64	>1024

En observar els valors de CMI, es pot observar immediatament que hi ha una clara correlació entre la longitud i l'activitat del pèptid, i la longitud llindar és diferent per a cada soca bacteriana. En *E. coli*, KIA14 i KIA15 són inactius, KIA17 i KIA19 mostren certa activitat, i KIA21 i pèptids més llargs mostren elevada activitat. En *S. aureus*, el llindar és més clar; KIA19 i el pèptids més curts són inactius mentre KIA21 i els pèptids més llargs són molt actius. En *P. aeruginosa*, KIA19 i anàlegs més curts són inactius, KIA21 i KIA22 són relativament actius, però per a obtenir activitat completa es necessiten 24 o més aminoàcids. En *E. faecalis*, gairebé cap activitat es troba per KIA22 i pèptids més curts, KIA24 i KIA26 mostren certa activitat (molt més gran que els pèptids més curts), i KIA28 és més actiu que els pèptids més curts. També podem observar que el pèptid de control PGLa (amb 21 aminoàcids), mostra una activitat similar a la de KIA17 o KIA19.

En resum, en la majoria dels casos hi ha una longitud llindar clarament definida, on aquells pèptids més curts que el llindar tenen una activitat molt més baixa que els pèptids més llargs que el llindar. Això contrasta amb un canvi gradual de l'activitat amb la longitud.

7.4.2.2. Activitat hemolítica

L'hemòlisi és la ruptura dels eritròcits (glòbuls vermells) i l'alliberament del seu contingut en el líquid circumdant. Un bon agent antibacterià ha de tenir una CMI el més baixa possible alhora que manté una baixa activitat hemolítica, el que es considera una primera indicació de baixa toxicitat. Per tant, el següent pas va ser mesurar l'activitat hemolítica dels pèptids KIA.

L'activitat hemolítica es va examinar usant un mètode estàndard (Strandberg et al., 2007) utilitzant sang de donants sans del banc de sang de l'hospital municipal local (Städtisches Klinikum, Karlsruhe, Alemanya).

Els resultats obtinguts es mostren a la Taula 6. Es pot observar que els pèptids curts, KIA14 a KIA19, van donar baixa hemòlisi fins i tot a una concentració de pèptid alta (marcat en gris a la Taula 6). KIA21 i KIA22 van mostrar una activitat hemolítica considerable a concentracions de 128 µg/mL o superior, mentre que KIA24 i pèptids més llargs ja a 8 µg/mL van induir una considerable hemòlisi, arribant al 100% a la concentració més alta assajada.

En l'assaig d'hemòlisi, com també passa en l'assaig de CMI, es poden observar alguns llindars, amb paulatins increments en la activitat entre 19-21 aminoàcids i 22-24 aminoàcids, però també hi ha un increment gradual en l'hemòlisi amb la longitud i la concentració de pèptid.

Taula 6: Activitat hemolítica dels pèptids KIA a diferents concentracions de pèptid. Els pèptids que mostren efectes baixos fins i tot a la concentració més alta assajada estan marcats en gris.

Pèptid	% hemòlisi			
	8 µg/mL	32 µg/mL	128 µg/mL	512 µg/mL
KIA14	5	3	2	3
KIA15	2	2	1	7
KIA17	2	2	2	8
KIA19	4	5	3	9
KIA21	3	7	15	38
KIA22	5	8	19	59
KIA24	15	34	67	96
KIA26	12	23	52	94
KIA28	41	64	86	100

7.4.3. ESTUDI DEL MECANISME D'ACCIÓ – Investigació de la hipòtesi de la formació de porus

7.4.3.1. Dicroïsme circular

El dicroïsme circular és una eina excel·lent per a la determinació ràpida de l'estructura secundària i plegament de pèptids i proteïnes. Els diferents elements estructurals tenen espectres de CD característics (Figura 7). Per exemple, les proteïnes α -helicoidals tenen bandes negatives a 222 nm i 208 nm i una banda positiva a 193 nm mentre que les proteïnes desestructurades tenen el·lípticitat molt baixa per sobre de 210 nm i bandes negatives prop de 195 nm (Kelly & Price, 2000).

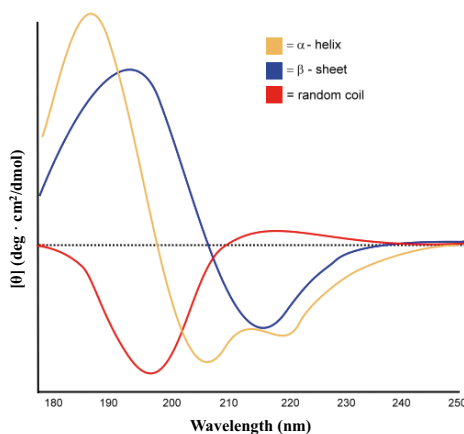


Figura 7: Espectres de CD associats amb diversos tipus d'estructura secundària: (groc) α -hèlix; (blau) β -full i (vermell) desestructurats.

Per tal de determinar l'estructura secundària dels pèptids KIA sintetitzats, es van enregistrar els espectres de CD tant en tampó de fosfat com en un entorn lipídic. Els resultats es mostren a la Figura 8.

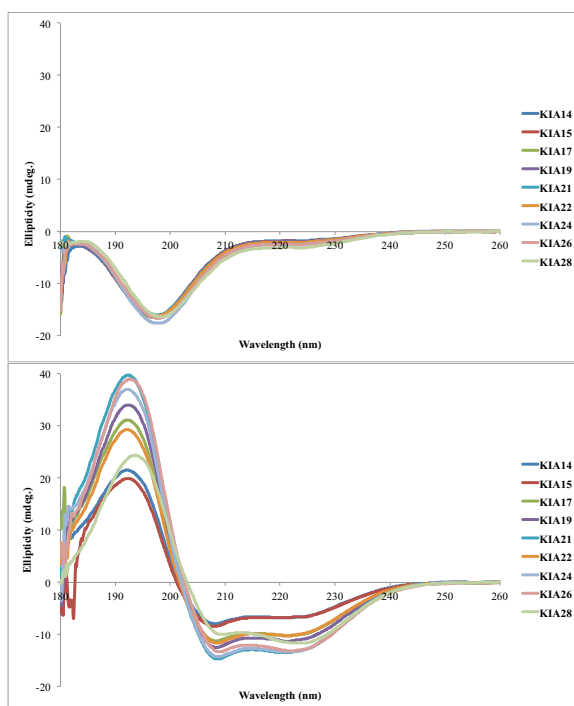


Figura 8: Espectres de dicroïsme circular dels pèptids KIA. En tampó fosfat 10 mM (superior) i en presència de vesícules de DMPC/DMPG (3:1) (inferior).

Es pot observar que tots els pèptids van mostrar una estructura desestructurada en tampó fosfat (Figura 8, superior), però quan les mesures es van fer amb vesícules de DMPC/DMPG (3:1), tots els pèptids van donar espectres similars, típics de pèptids α -helicoidals (Figura 8, inferior). Això mostra que els pèptids es troben desestructurats en solució però formen hèlices quan s'uneixen a la membrana com suggereix el primer pas de la hipòtesi de la formació de porus (Figura 5).

7.4.3.2. Experiments biofísics – Permeabilització de vesícules

La permeabilitat de la membrana a causa de la unió del pèptid es va avaluar per l'assaig de permeabilització d'ANTS/DPX. Aquest assaig consisteix en la co-encapsulació en liposomes de diferent composició (amb lípids de longitud de cadena definida) la sonda aquosa ANTS i l'inhibidor de la fluorescència DPX. Si el pèptid és capaç de formar porus que produeixen la fugida de les sondes al medi, es pot detectar un augment en l'emissió de fluorescència d'ANTS (Ellens et al., 1985).

La idea darrere dels experiments de permeabilització era estudiar l'efecte del **gruix de la membrana**. Si el pèptid és més curt que la membrana lipídica, no s'hauria d'observar cap fuga, mentre que si el pèptid és igual o més llarg que la membrana lipídica la fuga de la sonda ANTS s'hauria de detectar. Per tant es van usar lípids sintètics amb una longitud de cadena ben definida per preparar les vesícules. En tots els casos es va utilitzar una barreja 1:1 (mol/mol) de lípids zwitteriònics (PC) i lípids carregats negativament (PG) (Taula 7), ja que el component electrostàtic és essencial per garantir la unió a la membrana dels pèptids, tots ells solubles en aigua i amb càrrega neta positiva.

Taula 7: Barreges de lípids utilitzades en els experiments de permeabilització. (a) relació 1:1; (b) tipus d'àcid gras en posicions 1 i 2 del fosfolípid, indicant nombre d'àtoms de carboni : nombre d'insaturacions; (c) gruix hidrofòbic de les bicapes lipídiques.

Sistema lipídic ^a	Cadena ^b	Llargada ^c (Å)	Comentaris
DMoPC	14:1	19.2	Mida curta
DOPG	18:1	26.8	
POPC	16:0/18:1	28.3	Mida mitjana
POPG	16:0/18:1	28.3	
DEPC	22:1	34.4	Mida llarga
DEPG	22:1	34.4	
POPC	16:0/18:1	28.3	Barreja
DEPG	22:1	34.4	
DEPC	22:1	34.4	Barreja
POPG	16:0/18:1	28.3	

Les corbes de permeabilització es van mesurar a diferents relacions molars P/L, durant 10 minuts després de l'addició de vesícules a la solució de pèptid dins la cubeta. A baixa concentració de pèptid només es va observar permeabilització parcial, però a una relació P/L de 1:25 o superior, en gairebé tots els casos es va observar o bé cap

permeabilització (10% o menys) o permeabilització total (85% o més), com es mostra a la Figura 9 per POPC/POPG. Clarament es pot observar un efecte dependent de la longitud, on només quan els pèptids són prou llargs per abastar la part hidròfoba de la membrana es pot observar la fuga de la sonda.

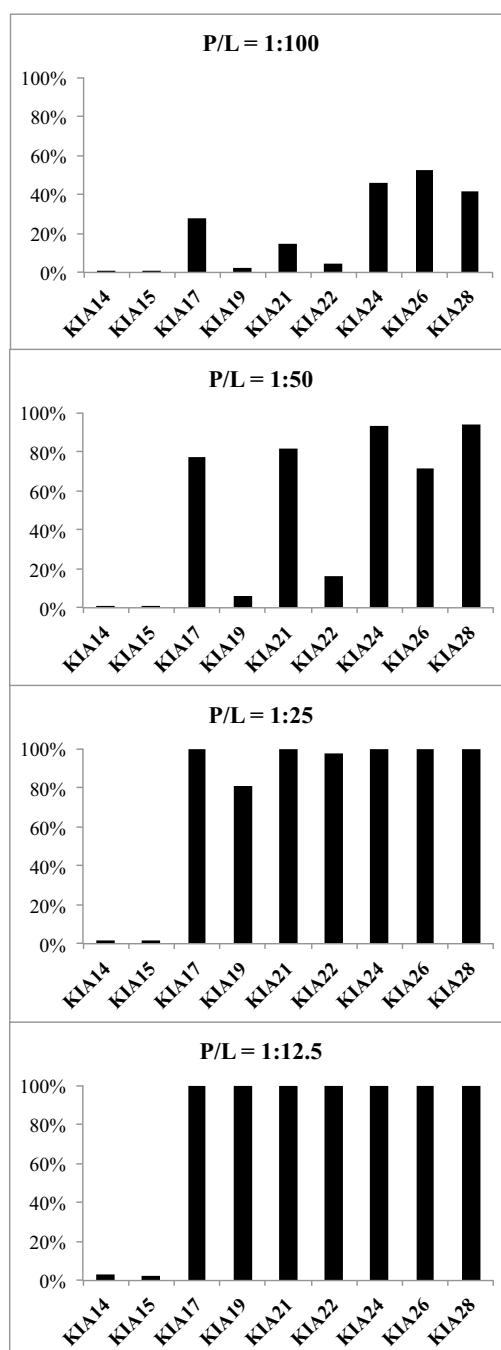


Figura 9: Permeabilització de liposomes de POPC/POPG (1:1) a diferents relacions molars de pèptid-lípid (P/L) dels pèptids KIA, després de 10 minuts. A alta concentració de pèptid, els pèptids més curts no permeabilitzen la membrana, però els pèptids KIA17 i més llargs donen 100% permeabilització.

Els resultats obtinguts per a tots els lípids a P/L=1:12.5 es donen en la Taula 8. Es pot observar que en POPC/POPG, no es va detectar permeabilització per KIA14 i KIA15,

però a partir de KIA17 i pèptids més llargs, es va observar permeabilització gairebé completa. En DEPC/DEPG, també hi va haver un llindar, però en aquests lípids de cadena més llarga, només KIA24 i pèptids més llargs van donar lloc a permeabilització. Curiosament, quan es van barrejar els lípids de diferent longitud de PC i PG, la longitud de llindar dels pèptids es va determinar principalment per la longitud de la cadena d'acil dels lípids de PG carregats negativament. En DMOPC/DOPG i DEPC/POPG, el comportament era idèntic que en POPC/POPG, de manera que KIA17 o pèptids més llargs donen permeabilització total, encara que el lípid DMOPC és molt més curt i el DEPC molt més llarg que POPC. No obstant això, en POPC/DEPG, el llindar es troba entre POPC/POPG i DEPC/DEPG; en aquest cas, una llargada de 21 residus eren necessaris per a observar permeabilització.

En alguns casos, els pèptids més llargs eren menys actius que els més curts (per exemple KIA19 és menys actiu que KIA17 en DEPC/POPG, i KIA26 és menys actiu que KIA24 en DEPC/DEPG). En aquests casos, una anàlisi detallada mostra que hi ha permeabilització també per al pèptid més llarg, però aquesta és més lenta (dades no mostrades). Es pot observar que els pèptids més actius tots acaben amb Ile-Ala, mentre que els pèptids que mostren menys permeabilització, però són més llargs, tots acaben amb Lys.

Taula 8: Permeabilització induïda pels pèptids KIA en vesícules de diferent composició. La permeabilització es dona després de 10 minuts a P/L=1:12.5, com a percentatge de permeabilització després de l'addició de Tritó X-100 (definit com a 100% de fuga). La longitud dels pèptids i gruix de les bicapes lipídiques es troba indicat en la taula. Aquells pèptids inactius per als diferents sistemes lipídics estan marcats en gris.

Pèptid		Lípids				
		DMoPC/DOPG	POPC/POPG	DEPC/POPG	DEPC/DEPG	POPC/DEPG
	Llargada (Å)	19.2 / 26.8	28.3 / 28.3	34.4 / 28.3	34.4 / 34.4	28.3 / 34.4
KIA14	21	8	3	5	1	2
KIA15	22.5	3	2	3	0	2
KIA17	25.5	100	100	84	1	17
KIA19	28.5	100	100	30	2	4
KIA21	31.5	100	100	98	4	82
KIA22	33	100	100	85	6	26
KIA24	36	100	100	100	89	100
KIA26	39	100	100	100	10	97
KIA28	42	100	100	100	84	100

7.4.3.3. Ressonància magnètica nuclear de fases condensades de ^{31}P i ^{15}N per estudiar l'orientació dels pèptids KIA en membranes lipídiques

L'últim pas d'aquest estudi va ser l'ús de RMN de fases condensades per analitzar l'orientació dels pèptids KIA en diferents sistemes lipídics, per tal d'investigar si hi ha una reorientació dels pèptids en les membranes depenent de la longitud de la cadena peptídica. El isòtop més comú per a estudis de RMN de fases condensades de pèptids units a la membrana és ^{15}N a l'esquelet peptídic, ja que és possible estimar l'orientació del pèptid simplement mirant el senyal de desplaçament químic estreta d'una sola posició, com s'il·lustra a la Figura 10. Per això, tots els pèptids KIA van haver de ser

sintetitzats amb ^{15}N en el residu Ala-10. Aquest experiment unidimensional s'ha de realitzar en mostres orientades macroscòpicament.

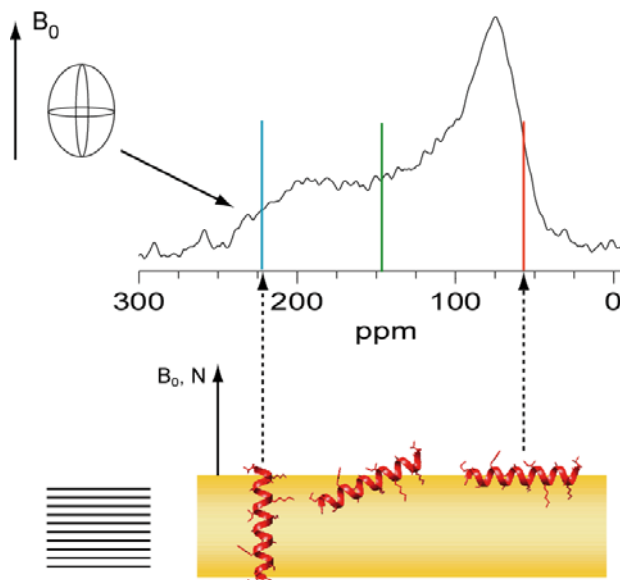


Figura 10: L'orientació d'un pèptid α -helicoidal en una bicapa lipídica es pot determinar pel desplaçament químic anisotròpic d'un sol grup amida marcat amb ^{15}N , quan es mesura en una mostra orientada. Un pèptid helicoidal en una orientació transmembrana dona un desplaçament químic prop de 220 ppm (blau). Un pèptid situat paral·lel al pla de la bicapa dona un desplaçament químic prop de 50 ppm (vermell). Pèptids inclinats donen desplaçaments químics entre aquests valors (verd).

Les mostres de RMN orientades macroscòpicament es van preparar codissolvent els pèptids i els lípids en una barreja de metanol/cloroform (1:1, v/v) i estenent la barreja sobre plaques de vidre primes. Una vegada que les plaques eren seques, es van apilar i col·locar en una cambra d'hidratació durant 18-24 h i finalment es van embolicar en parafilm i film transparent per a les mesures. Aquestes mostres orientades es van col·locar a la sonda de bobina plana de tal forma que la normal de la bicapa lipídica es trobés alineada en paral·lel al camp magnètic, però experiments addicionals es van dur a terme en una alineació perpendicular per esbrinar si els pèptids presentaven rotació al voltant de la normal de la bicapa (exemple d'una seqüència de preparació de la mostra a la Figura 11).



Figura 11: Preparació de mostres per RMN de fases condensades. D'esquerra a dreta: (1) Preparació de la mostra, (2) embolcall de la mostra, (3) les mostres es col·loquen a la sonda de bobina plana i (4) la sonda s'introdueix en l'espectròmetre de RMN per efectuar les mesures.

Es van realitzar sempre mesures de ^{31}P -ssRMN abans i després de ^{15}N -ssRMN per comprovar la qualitat de l'orientació dels lípids en les mostres. Tenint en compte la diferent longitud dels pèptids, la concentració es va variar de manera que el nombre de residus d'aminoàcids per lípids es va mantenir constant, amb una relació molar de pèptid a lípid de 1:50 per KIA21 com a punt de partida.

Es va observar que en DOPC i DEPC/DEPG (1:1) (dades no mostrades), tots els pèptids van donar un pic agut prop de 90 ppm, la qual cosa indica que els pèptids es troben orientats a la superfície de la membrana, amb l'eix llarg del pèptid paral·lel al pla de la membrana.

En DMPC/lyso-MPC (2:1) (Figura 12, panell esquerra), es va trobar per a tots els pèptids un desplaçament químic molt més gran, que també varia amb la longitud del pèptid. Això indica un estat més inserit, amb els pèptids mostrant una orientació més vertical a la membrana, amb l'eix de l'hèlix casi paral·lel amb la normal de la membrana. El pèptid més curt, KIA14, va donar un senyal a 167 ppm, i a mida que augmentava la llargada dels pèptids el desplaçament químic era gradualment menor fins els 134 ppm per KIA28. Això indica que els pèptids curts són gairebé en posició vertical a la membrana, mentre que els pèptids més llargs tenen una inclinació menor, el que s'esperaria per pèptids transmembrana on una inclinació més gran pels pèptids més llargs es necessària per evitar repulsions hidrofòbiques (Strandberg, et al., 2012a).

En DMPC, també es va trobar que els pèptids es mantenen més o menys horitzontals sobre la superfície de la membrana. No obstant, les mostres també es van fer amb una concentració més alta de pèptid, P/L=1:20 (Figura 12, panell dret). En aquest cas, es va observar que l'orientació depenia de la longitud del pèptid. KIA14 i KIA15 van presentar senyals que indiquen una orientació en la superfície, però KIA17 i KIA19 tenien un desplaçament químic al voltant de 150 ppm, el que indica un estat més inserit a la membrana. KIA21 i KIA22 van donar bandes amples amb senyals tant a 90 ppm i 150 ppm, on el senyal de 150 ppm és probablement degut a la formació d'agregats. KIA24 va donar un senyal al voltant de 90 ppm, però tots dos KIA24 i KIA26 van mostrar una mala orientació a la membrana, com es veu a partir dels espectres de ^{31}P , i KIA26 va donar espectres irregulars i amples ('*powder*') tant per ^{31}P i ^{15}N , el que indica que aquests pèptids a tant alta relació P/L formen agregats immòbils que van pertorbar les membranes i van destruir l'estructura de la bicapa.

Finalment, algunes de les mostres, tant pèptids curts com llargs, es van mesurar amb una inclinació de 90° (dades no mostrades), és a dir, amb la normal de la membrana perpendicular al camp magnètic. En tots els casos, es va trobar que els pèptids giren ràpidament al voltant de la normal de la bicapa, fet que es detecta com un canvi en el senyal d'un costat del desplaçament químic isotròpic a l'altre costat.

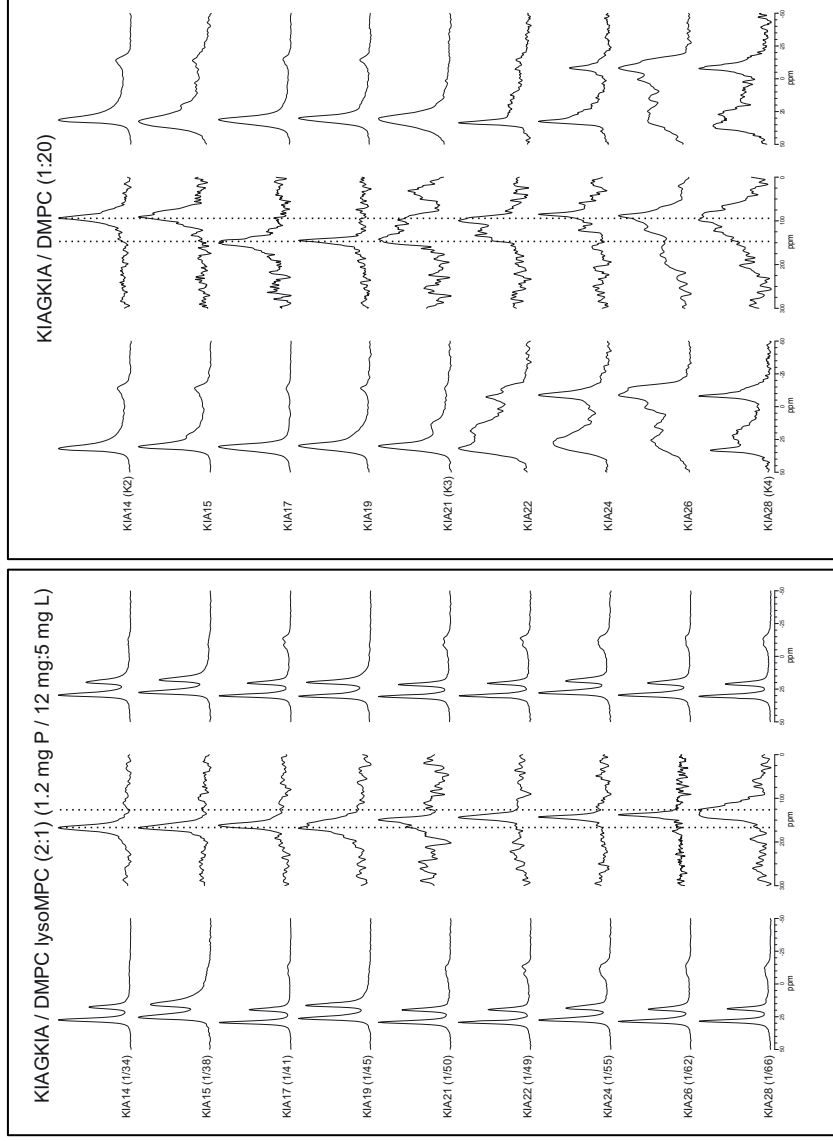


Figura 12: Espectres de ^{15}N -RMN (columna central de cada panel) dels pèptids KIA. També es mostren els espectres de ^{31}P -NMR abans (columna esquerra en cada panel) i després (columna dreta en cada panel) de ^{15}N -RMN. (esquerra) En DMPC/lyso-MPC (2:1) en una relació de massa constant d'aproximadament 1.2 mg de pèptid i 17 mg de lípid. El valor de P/L de cada mostra es dona a la figura. El desplaçament químic de KIA14 és de 167 ppm, el que indica una orientació gairebé vertical. Els pèptids més llargs tenen desplaçaments químics més petits que indiquen que es troben menys inclinats. (dreta) En DMPC a P/L=1:20. Hi ha un canvi en el pic de ^{15}N -RMN a partir de al voltant de 90 ppm, típic d'un estat superficial, en KIA14 i KIA15, a un pic al voltant de 150 ppm, el que indica un estat inserit més inclinat per KIA17 i pèptids més llargs. Per KIA21 i pèptids més llargs, els espectres de ^{31}P mostren una perturbació de l'estructura de bicapa i per tant els espectres de ^{15}N mostren senyals amples (*powder*).

7.4.3.4. Breu discussió sobre els resultats obtinguts per a la investigació de la hipòtesi de la formació de porus

Mitjançant la síntesi i estudi d'una sèrie de pèptids de diferent llargada, els pèptids KIA, s'ha pogut determinar el següent:

- **Tots els resultats obtinguts són consistents amb la hipòtesi de que aquests pèptids formen porus a la membrana amb una orientació transmembrana com indica la Figura 5.** Aquests porus només es formen si el pèptid es prou llarg per travessar la membrana, pèptids massa curts es queden a la superfície i són inactius. En el cas dels experiments de permeabilització, es va poder fer un anàlisi quantitativa (Taula 8), suposant 1.5 Å per residu en una α -hèlix i usant les formules de Marsh (Marsh, 2008) per estimar el gruix de les membranes. En DEPC/DEPG, hi ha una correlació clara on només aquells pèptids més llargs que el gruix hidrofòbic de 34.4 Å donen permeabilització. En POPC/POPG, a partir de KIA17 (25.5 Å) hi ha permeabilització, tot i que és una mica més curt que els lípids (28.3 Å), però pot ser degut a que prop dels extrems les hèlices es relaxen.
- Mitjançant RMN de fases condensades s'ha pogut observar també que **els pèptids s'insereixen quan són prou llargs per travessar la membrana.** Els resultats de permeabilització de liposomes no correlacionen perfectament amb els de ^{15}N -RMN, però es poden reconciliar amb l'activitat. La fuga de la sonda és detectable quan es formen porus, però és suficient tenir una petita població de pèptids en aquest estat transitori per tenir considerable permeabilització de la sonda. Mentre que, la tècnica de ^{15}N -RMN ens dona una imatge d'estat estacionari dels pèptids. Si només una petita fracció dels pèptids es troben en el estat transmembrana de formació de porus en un moment donat, això difícilment es veurà en el espectre de RMN. Per tant, el fet que una elevada proporció de pèptids inserits es pugui observar en DMPC i especialment en DMPC/lyso-MPC, ens indica que en aquests sistemes lipídics els pèptids s'insereixen de manera estable i en DMPC a elevada concentració la inserció també correlaciona amb la llargada del pèptid.
- En els experiments de permeabilització de liposomes, es van usar lípids sintètics on la llargada de la cadena és coneguda amb exactitud, mentre que en els assaigs biològics, les biomembranes consisteixen en una varietat de lípids amb diferents cadenes i caps polars, a més d'altres components com proteïnes de membrana i colesterol. És per això que en els assaigs bacterians el gruix de la membrana és desconegut. Però si assumim que les bacteries moren per la formació dels porus, com hem vist en els experiments de permeabilització de les vesícules, podem doncs usar els pèptids KIA com a **regles moleculars**:
 - A *E. coli*, el pèptid més curt capaç de matar les bacteries és KIA17, que és capaç de induir permeabilització en POPC/POPG. Per tant, **el gruix de la membrana de *E. coli* hauria de ser similar a POPC/POPG, és a dir al voltant de 27 Å.**
 - En *S. aureus* i *P. aeruginosa* KIA21, però no els pèptids més curts, pot matar les bacteries i per tant **les membranes haurien de ser al voltant de 30 Å.**
 - *E. faecalis* només era afectat per KIA24 o pèptids més llargs, que també eren necessaris per induir permeabilització en DEPC/DEPG, per tant el gruix de la membrana de *E. faecalis* **hauria de ser similar a DEPC/DEPG, al voltant de 34 Å.**

- Per els **eritròcits**, no hi havia un llindar clar, però només KIA21 o pèptids més llargs mostraven un gran efecte a elevada concentració, per tant aquestes membranes haurien de tenir un gruix similar a *S. aureus* i *P. aeruginosa*, de al voltant de 30 Å.

7.5. CONCLUSIONS

Les conclusions assolides en aquesta tesi són les següents:

- Diversos **nous lipopèptids anàlegs a les polimixines s'han sintetitzat amb èxit** d'acord amb els principis de disseny establerts en el grup. Aquests nous compostos han demostrat una alta activitat, especialment contra bacteris resistents a múltiples fàrmacs i un ampli espectre d'activitat, ja que són actius contra bacteris tant Gram-positius com Gram-negatius (mentre les polimixines són actives només contra aquests últims).
- El comportament amb membranes model d'alguns d'aquests pèptids ha estat estudiat utilitzant fluorescència, on s'ha demostrat que **tots ells són capaços d'unir-se al LPS amb alta afinitat i tots els pèptids són actius a la membrana, però amb diferents efectes en funció de la seqüència i de la composició de la membrana.**
- Finalment, alguns dels pèptids més actius, especialment el pèptid #8, es van estudiar per citometria de flux i microscòpia electrònica de transmissió, on es va observar que **aquests pèptids probablement causen la mort dels bacteris mitjançant més d'un mecanisme d'acció** ('pèptids bruts') i l'efecte sembla ser diferent en els bacteris Gram-negatius i Gram-positius degut a la diferent morfologia de la membrana.
- Mitjançant la síntesi d'una sèrie de pèptids KIA amb una llargada que varia de 14 a 28 amino àcids, ha sigut possible determinar que **la llargada té un efecte dràstic tant en la activitat antibacteriana com hemolítica.** Pèptids llargs tenen una CMI més baixa, per tant són més actius però l'efecte secundari és que causen la hemòlisi completa dels eritròcits. Pèptids més curts són menys actius però també menys hemolítics, per tant s'ha d'aconseguir un compromís entre les dues activitats.
- **S'ha demostrat la formació de porus per aquests pèptids** mitjançant l'ús de diferents tècniques. En la determinació de l'activitat antibacteriana es va detectar un llindar clar per a cada soca assajada. En els experiments de permeabilització, com es van utilitzar lípids de diferent longitud, també es va observar un llindar clar depenent del gruix de la membrana. En el cas dels experiments de RMN, en alguns sistemes lipídics un estat inserit va poder ser detectat el que demostra que els pèptids són capaços d'inserir-se en la bicapa lipídica mitjançant la formació de porus, i que aquests porus només es formen quan el pèptid és prou llarg per abastar la membrana .
- Com a resultat de tots aquests experiments, els pèptids KIA es proposen com a **regles de membrana** per determinar el gruix aproximat de les membranes dels bacteris i els eritròcits.

8. REFERENCES

- Aiello, A. E., & Larson, E. (2003). Antibacterial cleaning and hygiene products as an emerging risk factor for antibiotic resistance in the community. *The Lancet Infectious Diseases*, 3(8), 501–506.
- Ainsworth, G. C., Brown, A. M., & Brownlee, G. (1947). “Aerosporin,” an Antibiotic Produced by *Bacillus aerosporus* Greer. *Nature*, 160(4060), 263–263.
- Akbarzadeh, A., Rezaei-Sadabady, R., Davaran, S., Joo, S. W., Zarghami, N., Hanifehpour, Y., et al. (2013). Liposome: classification, preparation, and applications. *Nanoscale Research Letters*, 8(1), 1–9.
- Alvarez-Barrientos, A., Arroyo, J., Canton, R., Nombela, C., & Sanchez-Perez, M. (2000). Applications of Flow Cytometry to Clinical Microbiology. *Clinical Microbiology Reviews*, 13(2), 167–195.
- Angelova, M. I., & Dimitrov, D. S. (1986). Liposome electroformation. *Faraday Discuss Chem Soc*, 81, 303–311.
- Arias, C. A., & Murray, B. E. (2009). Antibiotic-Resistant Bugs in the 21st Century — A Clinical Super-Challenge. *New England Journal of Medicine*, 360(5), 439–443.
- Arnold, S. R. (2007). Revenge of the killer microbe. *CMAJ : Canadian Medical Association Journal = Journal De l'Association Medicale Canadienne*, 177(8), 895–896.
- Arouri, A., Dathe, M., & Blume, A. (2009). Peptide induced demixing in PG/PE lipid mixtures: a mechanism for the specificity of antimicrobial peptides towards bacterial membranes? *Biochimica Et Biophysica Acta*, 1788(3), 650–659.
- Bangham, A. D., & Horne, R. W. (1964). Negative staining of phospholipids and their structural modification by surface-active agents as observed in the electron microscope. *Journal of Molecular Biology*, 8, 660–668.
- Barnett, M., Bushby, S., & Wilkinson, S. (1964). Sodium sulphomethyl derivatives of polymyxins. *British Journal of Pharmacology and Chemotherapy*, 23(3), 552–574.
- Bechinger, B. (1999). The structure, dynamics and orientation of antimicrobial peptides in membranes by multidimensional solid-state NMR spectroscopy. *Biochimica Et Biophysica Acta*, 1462(1-2), 157–183.
- Bechinger, B., & Lohner, K. (2006). Detergent-like actions of linear amphipathic cationic antimicrobial peptides. *Biochimica Et Biophysica Acta*, 1758(9), 1529–1539.
- Blazyk, J. (2001). A Novel Linear Amphipathic beta -Sheet Cationic Antimicrobial Peptide with Enhanced Selectivity for Bacterial Lipids. *Journal of Biological Chemistry*, 276(30), 27899–27906.
- Boucher, H. W., Talbot, G. H., Bradley, J. S., Edwards, J. E., Gilbert, D., Rice, L. B., et al. (2009). Bad Bugs, No Drugs: No ESKAPE! An Update from the Infectious Diseases Society of America. *Clinical Infectious Diseases*, 48(1), 1–12.
- Brezesinski, G., & Möhwald, H. (2003). Langmuir monolayers to study interactions at model membrane surfaces. *Advances in Colloid and Interface Science*, 100-102, 563–584.
- Brockman, H. (1999). Lipid monolayers: why use half a membrane to characterize protein-membrane interactions? *Current Opinion in Structural Biology*, 9(4), 438–443.
- Brogden, K. A. (2005). Antimicrobial peptides: pore formers or metabolic inhibitors in bacteria? *Nature Reviews Microbiology*, 3(3), 238–250.
- Brown, K. L., & Hancock, R. E. (2006). Cationic host defense (antimicrobial) peptides. *Current Opinion in Immunology*, 18(1), 24–30.
- Bruch, M. D., Cajal, Y., Koh, J. T., & Jain, M. K. (1999). Higher-Order Structure of Polymyxin B: The Functional Significance of Topological Flexibility. *Journal of*

- the American Chemical Society*, 121(51), 11993–12004.
- Burstein, E. A., Vedenkina, N. S., & Ivkova, M. N. (1973). Fluorescence and the location of tryptophan residues in protein molecules. *Photochemistry and Photobiology*, 18(4), 263–279.
- Butler, M. S., Blaskovich, M. A., & Cooper, M. A. (2013). Antibiotics in the clinical pipeline in 2013. *The Journal of Antibiotics*, 66(10), 571–591.
- Bürck, J., Roth, S., Wadhvani, P., Afonin, S., Kanithasen, N., Strandberg, E., & Ulrich, A. S. (2008). Conformation and membrane orientation of amphiphilic helical peptides by oriented circular dichroism. *Biophysical Journal*, 95(8), 3872–3881.
- Cajal, Y., Berg, O. G., & Jain, M. K. (1995). Direct vesicle-vesicle exchange of phospholipids mediated by polymyxin B. *Biochemical and Biophysical Research Communications*, 210(3), 746–752.
- Cajal, Y., Ghanta, J., Easwaran, K., Surolia, A., & Jain, M. K. (1996a). Specificity for the exchange of phospholipids through polymyxin B mediated intermembrane molecular contacts. *Biochemistry*, 35(18), 5684–5695.
- Cajal, Y., Rogers, J., Berg, O. G., & Jain, M. K. (1996b). Intermembrane molecular contacts by polymyxin B mediate exchange of phospholipids. *Biochemistry*, 35(1), 299–308.
- Calderone, R. A., & Fonzi, W. A. (2001). Virulence factors of *Candida albicans*. *Trends in Microbiology*, 9(7), 327–335.
- Chan, D. I., Prenner, E. J., & Vogel, H. J. (2006). Tryptophan- and arginine-rich antimicrobial peptides: structures and mechanisms of action. *Biochimica Et Biophysica Acta*, 1758(9), 1184–1202.
- Cheng, J. T. J., Hale, J. D., Elliott, M., Hancock, R. E. W., & Straus, S. K. (2011). The importance of bacterial membrane composition in the structure and function of aurein 2.2 and selected variants. *Biochimica Et Biophysica Acta*, 1808(3), 622–633.
- Clark, D. P., Durell, S., Maloy, W. L., & Zasloff, M. (1994). Ranalexin. A novel antimicrobial peptide from bullfrog (*Rana catesbeiana*) skin, structurally related to the bacterial antibiotic, polymyxin. *The Journal of Biological Chemistry*, 269(14), 10849–10855.
- Clausell, A., Busquets, M. A., Pujol, M., Alsina, A., & Cajal, Y. (2004). Polymyxin B-lipid interactions in Langmuir-Blodgett monolayers of *Escherichia coli* lipids: a thermodynamic and atomic force microscopy study. *Biopolymers*, 75(6), 480–490.
- Clausell, A., Garcia-Subirats, M., Pujol, M., Busquets, M. A., Rabanal, F., & Cajal, Y. (2007). Gram-Negative Outer and Inner Membrane Models: Insertion of Cyclic Cationic Lipopeptides. *The Journal of Physical Chemistry B*, 111(3), 551–563.
- Clausell, A., Pujol, M., Alsina, M. A., & Cajal, Y. (2003). Influence of polymyxins on the structural dynamics of *Escherichia coli* lipid membranes. *Talanta*, 60(2-3), 225–234.
- Clausell, A., Rabanal, F., Garcia-Subirats, M., Asunción Alsina, M., & Cajal, Y. (2005). Synthesis and membrane action of polymyxin B analogues. *Luminescence : the Journal of Biological and Chemical Luminescence*, 20(3), 117–123.
- Clausell, A., Rabanal, F., Garcia-Subirats, M., Asunción Alsina, M., & Cajal, Y. (2006). Membrane Association and Contact Formation by a Synthetic Analogue of Polymyxin B and Its Fluorescent Derivatives. *The Journal of Physical Chemistry B*, 110(9), 4465–4471.
- Cohen, S. A., & Michaud, D. P. (1993). Synthesis of a Fluorescent Derivatizing Reagent, 6-Aminoquinolyl-N-Hydroxysuccinimidyl Carbamate, and Its Application for the Analysis of Hydrolysate Amino Acids via High-Performance Liquid Chromatography. *Analytical Biochemistry*, 211(2), 279–287.

- Comas, J., & Vives-Rego, J. (1997). Assessment of the effects of gramicidin, formaldehyde, and surfactants on *Escherichia coli* by flow cytometry using nucleic acid and membrane potential dyes. *Cytometry*, *29*(1), 58–64.
- Dathe, M., Nikolenko, H., Meyer, J., Beyermann, M., & Bienert, M. (2001). Optimization of the antimicrobial activity of magainin peptides by modification of charge. *FEBS Letters*, *501*(2-3), 146–150.
- Daugelavičius, R., Bakiene, E., & Bamford, D. H. (2000). Stages of Polymyxin B Interaction with the *Escherichia coli* Cell Envelope. *Antimicrobial Agents and Chemotherapy*, *44*, 2969–2978.
- de Almeida, R. F. M., Fedorov, A., & Prieto, M. (2003). Sphingomyelin/phosphatidylcholine/cholesterol phase diagram: boundaries and composition of lipid rafts. *Biophysical Journal*, *85*(4), 2406–2416.
- Díaz, M., Herrero, M., García, L. A., & Quirós, C. (2010). Application of flow cytometry to industrial microbial bioprocesses. *Biochemical Engineering Journal*, *48*(3), 385–407.
- Eftink, M. R., & Ghiron, C. A. (1976). Fluorescence quenching of indole and model micelle systems. *The Journal of Physical Chemistry*, *80*(5), 486–493.
- Eftink, M. R., & Ghiron, C. A. (1977). Exposure of tryptophanyl residues and protein dynamics. *Biochemistry*, *16*(25), 5546–5551.
- Ellens, H., Bentz, J., & Szoka, F. C. (1985). H⁺- and Ca²⁺-induced fusion and destabilization of liposomes. *Biochemistry*, *24*(13), 3099–3106.
- Epand, R. M., & Epand, R. F. (2011). Bacterial membrane lipids in the action of antimicrobial agents. *Journal of Peptide Science*, *17*(5), 298–305.
- Epand, R. M., Rotem, S., Mor, A., Berno, B., & Epand, R. F. (2008). Bacterial Membranes as Predictors of Antimicrobial Potency. *Journal of the American Chemical Society*, *130*(43), 14346–14352.
- Fauci, A. S. (2001). Infectious Diseases: Considerations for the 21st Century. *Clinical Infectious Diseases*, *32*(5), 675–685.
- Fidai, S., Farmer, S. W., & Hancock, R. E. (1997). Interaction of cationic peptides with bacterial membranes. *Methods in Molecular Biology (Clifton, N.J.)*, *78*, 187–204.
- Fjell, C. D., Hiss, J. A., Hancock, R. E. W., & Schneider, G. (2012). Designing antimicrobial peptides: form follows function. *Nature Reviews. Drug Discovery*, *11*(1), 37–51.
- Frečer, V., Ho, B., & Ding, J. L. (2004). De novo design of potent antimicrobial peptides. *Antimicrobial Agents and Chemotherapy*, *48*(9), 3349–3357.
- Friedrich, C. L., Moyles, D., Beveridge, T. J., & Hancock, R. E. (2000). Antibacterial action of structurally diverse cationic peptides on gram-positive bacteria. *Antimicrobial Agents and Chemotherapy*, *44*(8), 2086–2092.
- Fuchs, S. M., & Raines, R. T. (2006). Internalization of cationic peptides: the road less (or more?) traveled. *Cellular and Molecular Life Sciences*, *63*(16), 1819–1822.
- Gaines, G. L. (1966). The properties of liquid surfaces, *Insoluble Monolayers at Liquid-Gas Interfaces*, Wiley Interscience Publishers, New York.
- Galla, H. J., Warncke, M., & Scheit, K. H. (1985). Incorporation of the antimicrobial protein seminalplasmin into lipid bilayer membranes. *European Biophysics Journal*, *12*(4), 211–216.
- Gant, V. A., Warnes, G., Phillips, I., & Savidge, G. F. (1993). The application of flow cytometry to the study of bacterial responses to antibiotics. *Journal of Medical Microbiology*, *39*(2), 147–154.
- Gazit, E., Miller, I. R., Biggin, P. C., Sansom, M. S., & Shai, Y. (1996). Structure and orientation of the mammalian antibacterial peptide cecropin P1 within phospholipid

- membranes. *Journal of Molecular Biology*, 258(5), 860–870.
- Glaser, R. W., Sachse, C., Dürr, U. H. N., Wadhvani, P., & Ulrich, A. S. (2004). Orientation of the antimicrobial peptide PGLa in lipid membranes determined from ¹⁹F-NMR dipolar couplings of 4-CF₃-phenylglycine labels. *Journal of Magnetic Resonance*, 168(1), 153–163.
- Glaser, R. W., Sachse, C., Dürr, U. H. N., Wadhvani, P., Afonin, S., Strandberg, E., & Ulrich, A. S. (2005). Concentration-Dependent Realignment of the Antimicrobial Peptide PGLa in Lipid Membranes Observed by Solid-State. *Biophysical Journal*, 88(5), 3392–3397.
- Greenfield, N. J. (2007). Using circular dichroism spectra to estimate protein secondary structure. *Nature Protocols*, 1(6), 2876–2890.
- Gregoriadis, G. (1984). Preparation of Liposomes. CRC, Boca Raton (Florida).
- Griffin, J. H., & Judice, J. K. (2002). *Multivalent polymyxin antibiotics* (No. US6380356 B1). US Patent Office.
- Hallock, K. J., Lee, D.-K., & Ramamoorthy, A. (2003). MSI-78, an analogue of the magainin antimicrobial peptides, disrupts lipid bilayer structure via positive curvature strain. *Biophysical Journal*, 84(5), 3052–3060.
- Hancock, R. E. W., & Sahl, H.-G. (2006). Antimicrobial and host-defense peptides as new anti-infective therapeutic strategies. *Nature Biotechnology*, 24(12), 1551–1557.
- Hancock, R. E. W., Brown, K. L., & Mookherjee, N. (2006). Host defence peptides from invertebrates--emerging antimicrobial strategies. *Immunobiology*, 211(4), 315–322.
- Hancock, R., & Chapple, D. S. (1999). Peptide antibiotics. *Antimicrobial Agents and Chemotherapy*, 43, 1317–1323.
- Hartmann, M., Berditsch, M., Hawecker, J., Ardakani, M. F., Gerthsen, D., & Ulrich, A. S. (2010). Damage of the Bacterial Cell Envelope by Antimicrobial Peptides Gramicidin S and PGLa as Revealed by Transmission and Scanning Electron Microscopy. *Antimicrobial Agents and Chemotherapy*, 54(8), 3132–3142.
- Hoffmann, W., Richter, K., & Kreil, G. (1983). A novel peptide designated PYLa and its precursor as predicted from cloned mRNA of *Xenopus laevis* skin. *The EMBO Journal*, 2(5), 711–714.
- Howe, J., Andrá, J., Conde, R., Iriarte, M., Garidel, P., Koch, M. H. J., et al. (2007). Thermodynamic analysis of the lipopolysaccharide-dependent resistance of gram-negative bacteria against polymyxin B. *Biophysical Journal*, 92(8), 2796–2805.
- Huang, H. W. (2000). Action of antimicrobial peptides: two-state model. *Biochemistry*, 39, 8347–8352.
- Jelinek, R., & Kolusheva, S. (2005). Membrane interactions of host-defense peptides studied in model systems. *Current Protein & Peptide Science*, 6(1), 103–114.
- Jorgensen, J. H., & Ferraro, M. J. (2009). Antimicrobial susceptibility testing: a review of general principles and contemporary practices. *Clinical Infectious Diseases*, 49(11), 1749–1755.
- Kaiser, R. D., & London, E. (1998). Location of diphenylhexatriene (DPH) and its derivatives within membranes: comparison of different fluorescence quenching analyses of membrane depth. *Biochemistry*, 37(22), 8180–8190.
- Kanazawa, K., Sato, Y., Ohki, K., Okimura, K., Uchida, Y., Shindo, M., & Sakura, N. (2009). Contribution of each amino acid residue in polymyxin B(3) to antimicrobial and lipopolysaccharide binding activity. *Chemical & Pharmaceutical Bulletin*, 57(3), 240–244.
- Kato, T., & Shoji, T. (1980). The structure of octapeptin D (studies on antibiotics from the genus *Bacillus*. XXVIII). *The Journal of Antibiotics*, 33(2), 186–191.

- Katsuma, N., Sato, Y., Ohki, K., Okimura, K., Ohnishi, K., & Sakura, N. (2009). Development of des-fatty acyl-polymyxin B decapeptide analogs with *Pseudomonas aeruginosa*-specific antimicrobial activity. *Chemical & Pharmaceutical Bulletin*, *57*, 332–336.
- Kelly, S. M., & Price, N. C. (2000). The use of circular dichroism in the investigation of protein structure and function. *Current Protein & Peptide Science*, *1*(4), 349–384.
- Kelly, S. M., Jess, T. J., & Price, N. C. (2005). How to study proteins by circular dichroism. *Biochimica Et Biophysica Acta (BBA) - Proteins and Proteomics*, *1751*(2), 119–139.
- Kimura, Y., Matsunaga, H., & Vaara, M. (1992). Polymyxin B octapeptide and polymyxin B heptapeptide are potent outer membrane permeability-increasing agents. *The Journal of Antibiotics*, *45*(5), 742–749.
- Kinsky, S. C. (1970). Antibiotic interaction with model membranes. *Annual Review of Pharmacology*, *10*(1), 119–142.
- Konishi, M., Sugawara, K., Tomita, K., Matsumoto, K., Miyaki, T., Fujisawa, K., et al. (1983). Bu-2470, a new peptide antibiotic complex. I. Production, isolation and properties of Bu-2470 A, B1 and B2. *The Journal of Antibiotics*, *36*(6), 625–633.
- Koronkiewicz, S., & Kalinowski, S. (2004). Influence of cholesterol on electroporation of bilayer lipid membranes: chronopotentiometric studies. *Biochimica Et Biophysica Acta*, *1661*(2), 196–203.
- Landman, D., Georgescu, C., Martin, D. A., & Quale, J. (2008). Polymyxins Revisited. *Clinical Microbiology Reviews*, *21*(3), 449–465.
- Laouini, A., Jaafar-Maalej, C., Limayem-Blouza, I., Sfar, S., Charcosset, C., & Fessi, H. (2012). Preparation, Characterization and Applications of Liposomes: State of the Art. *Journal of Colloid Science and Biotechnology*, *1*(2), 147–168.
- Lasic, D. D. (1988). The mechanism of vesicle formation. *Biochemical Journal*, *256*(1), 1–11.
- Lättig-Tünnemann, G., Prinz, M., Hoffmann, D., Behlke, J., Palm-Apergi, C., Morano, I., et al. (2011). Backbone rigidity and static presentation of guanidinium groups increases cellular uptake of arginine-rich cell-penetrating peptides. *Nature Communications*, *2*, 453.
- Lee, M.-T., Sun, T.-L., Hung, W.-C., & Huang, H. W. (2013). Process of inducing pores in membranes by melittin. *Proceedings of the National Academy of Sciences of the United States of America*, *110*(35), 14243–14248.
- Lehrer, R. I., Barton, A., Daher, K. A., Harwig, S. S., Ganz, T., & Selsted, M. E. (1989). Interaction of human defensins with *Escherichia coli*. Mechanism of bactericidal activity. *The Journal of Clinical Investigation*, *84*(2), 553–561.
- Lentz, B. R. (1993). Use of fluorescent probes to monitor molecular order and motions within liposome bilayers. *Chemistry and Physics of Lipids*, *64*(1-3), 99–116.
- Lentz, B. R., Wu, J. R., Zheng, L., & Prevratil, J. (1996). The interfacial region of dipalmitoylphosphatidylcholine bilayers is perturbed by fusogenic amphipaths. *Biophysical Journal*, *71*(6), 3302–3310.
- Li, C., Budge, L. P., Driscoll, C. D., Willardson, B. M., Allman, G. W., & Savage, P. B. (1999). Incremental conversion of outer-membrane permeabilizers into potent antibiotics for Gram-negative bacteria. *Journal of the American Chemical Society*, *121*(5), 931–940.
- Maget-Dana, R. (1999). The monolayer technique: a potent tool for studying the interfacial properties of antimicrobial and membrane-lytic peptides and their interactions with lipid membranes. *Biochimica Et Biophysica Acta*, *1462*(1-2), 109–140.

- Maloy, W. L., & Kari, U. P. (1995). Structure–activity studies on magainins and other host defense peptides. *Peptide Science*, 37(2), 105–122.
- Marsh, D. (1996). Lateral pressure in membranes. *Biochimica Et Biophysica Acta (BBA) - Reviews on Biomembranes*, 1286(3), 183–223.
- Marsh, D. (2008). Energetics of hydrophobic matching in lipid-protein interactions. *Biophysical Journal*, 94(10), 3996–4013.
- Martinez, O. V., Gratzner, H. G., Malinin, T. I., & Ingram, M. (1982). The effect of some beta-lactam antibiotics on *Escherichia coli* studied by flow cytometry. *Cytometry*, 3(2), 129–133.
- Matsuzaki, K. (1999). Why and how are peptide-lipid interactions utilized for self-defense? Magainins and tachyplesins as archetypes. *Biochimica Et Biophysica Acta*, 1462(1-2), 1–10.
- Matsuzaki, K., Mitani, Y., Akada, K. Y., Murase, O., Yoneyama, S., Zasloff, M., & Miyajima, K. (1998). Mechanism of synergism between antimicrobial peptides magainin 2 and PGLa. *Biochemistry*, 37(43), 15144–15153.
- Matsuzaki, K., Murase, O., & Miyajima, K. (1995a). Kinetics of Pore Formation by an Antimicrobial Peptide, Magainin 2, in Phospholipid Bilayers. *Biochemistry*, 34(39), 12553–12559.
- Matsuzaki, K., Murase, O., Fujii, N., & Miyajima, K. (1995b). Translocation of a channel-forming antimicrobial peptide, magainin 2, across lipid bilayers by forming a pore. *Biochemistry*, 34(19), 6521–6526.
- Matsuzaki, K., Murase, O., Fujii, N., & Miyajima, K. (1996). An antimicrobial peptide, magainin 2, induced rapid flip-flop of phospholipids coupled with pore formation and peptide translocation. *Biochemistry*, 35(35), 11361–11368.
- Meyers, E., Brown, W. E., Principe, P. A., Rathnum, M. L., & Parker, W. L. (1973a). EM49, a new peptide antibiotic. I. Fermentation, isolation, and preliminary characterization. *The Journal of Antibiotics*, 26(8), 444–448.
- Meyers, E., Pansy, F. E., Basch, H. I., McRipley, R. J., Slusarchyk, D. S., Graham, S. F., & Trejo, W. H. (1973b). EM49, a new peptide antibiotic. 3. biological characterization in vitro and in vivo. *The Journal of Antibiotics*, 26(8), 457–462.
- Meyers, E., Parker, W. L., & Brown, W. E. (1976). A nomenclature proposal for the octapeptin antibiotics. *The Journal of Antibiotics*, 29(11), 1241–1242.
- Meyers, E., Parker, W. L., Brown, W. E., Linnett, P., & Strominger, J. L. (1974). EM49: a new polypeptide antibiotic active against cell membranes. *Annals of the New York Academy of Sciences*, 235(0), 493–501.
- Mika, J. T., Moiset, G., Cirac, A. D., Feliu, L., Bardají, E., Planas, M., et al. (2011). Structural basis for the enhanced activity of cyclic antimicrobial peptides: the case of BPC194. *Biochimica Et Biophysica Acta*, 1808(9), 2197–2205.
- Mingeot-Leclercq, M.-P., Tulkens, P. M., Denamur, S., Vaara, T., & Vaara, M. (2012). Novel polymyxin derivatives are less cytotoxic than polymyxin B to renal proximal tubular cells. *Peptides*, 35(2), 248–252.
- Molitor, E., Kluczny, C., Brötz, H., Bierbaum, G., Jack, R., & Sahl, H. G. (1996). Effects of the lantibiotic mersacidin on the morphology of staphylococci. *Zentralblatt Für Bakteriologie : International Journal of Medical Microbiology*, 284(2-3), 318–328.
- Moore, R. A., Bates, N. C., & Hancock, R. E. (1986). Interaction of polycationic antibiotics with *Pseudomonas aeruginosa* lipopolysaccharide and lipid A studied by using dansyl-polymyxin. *Antimicrobial Agents and Chemotherapy*, 29(3), 496–500.
- Mortensen, N. P., Fowlkes, J. D., Sullivan, C. J., Allison, D. P., Larsen, N. B., Molin, S., & Doktycz, M. J. (2009). Effects of Colistin on Surface Ultrastructure and

- Nanomechanics of *Pseudomonas aeruginosa* Cells. *Langmuir*, 25(6), 3728–3733.
- Mozsolits, H., & Aguilar, M. I. (2002). Surface plasmon resonance spectroscopy: An emerging tool for the study of peptide–membrane interactions. *Peptide Science*, 66(1), 3–18.
- Munk, J. K., Uggerhøj, L. E., Poulsen, T. J., Frimodt Møller, N., Wimmer, R., Nyberg, N. T., & Hansen, P. R. (2013). Synthetic analogs of anoplins show improved antimicrobial activities. *Journal of Peptide Science*, 19(11), 669–675.
- Needham, D., & Evans, E. (1988). Structure and mechanical properties of giant lipid (DMPC) vesicle bilayers from 20 degrees C below to 10 degrees C above the liquid crystal-crystalline phase transition at 24 degrees C. *Biochemistry*, 27(21), 8261–8269.
- Nguyen, L. T., Haney, E. F., & Vogel, H. J. (2011). The expanding scope of antimicrobial peptide structures and their modes of action. *Trends in Biotechnology*, 29(9), 464–472.
- Ogbaini-Emovon, E. (2009). Current trends in the laboratory diagnosis of tuberculosis. *Benin Journal of Postgraduate Medicine*.
- Oh, J. T., Cajal, Y., Dhurjati, P. S., Van Dyk, T. K., & Jain, M. K. (1998a). Cecropins induce the hyperosmotic stress response in *Escherichia coli*. *Biochimica Et Biophysica Acta*, 1415(1), 235–245.
- Oh, J. T., Cajal, Y., Skowronska, E. M., Belkin, S., Chen, J., Van Dyk, T. K., et al. (2000). Cationic peptide antimicrobials induce selective transcription of *micF* and *osmY* in *Escherichia coli*. *Biochimica Et Biophysica Acta*, 1463(1), 43–54.
- Oh, J. T., Van Dyk, T. K., Cajal, Y., Dhurjati, P. S., Sasser, M., & Jain, M. K. (1998b). Osmotic stress in viable *Escherichia coli* as the basis for the antibiotic response by polymyxin B. *Biochemical and Biophysical Research Communications*, 246(3), 619–623.
- Ohki, K., Sato, Y., Ohnishi, K., Uchida, Y., & Sakura, N. (2007). Chemical conversion of natural polymyxin B and colistin to their N-terminal derivatives. *Bulletin of the Chemical Society of Japan*, 80, 543–552.
- Okimura, K., Ohki, K., Sato, Y., Ohnishi, K., & Sakura, N. (2007). Semi-synthesis of polymyxin B (2-10) and colistin (2-10) analogs employing the Trichloroethoxycarbonyl (Troc) group for side chain protection of alpha, gamma-Diaminobutyric acid residues. *Chemical & Pharmaceutical Bulletin*, 55, 1724–1730.
- Olson, F., Hunt, C. A., Szoka, F. C., Vail, W. J., & Papahadjopoulos, D. (1979). Preparation of liposomes of defined size distribution by extrusion through polycarbonate membranes. *Biochimica Et Biophysica Acta*, 557(1), 9–23.
- O'Dowd, H., Kim, B., Margolis, P., Wang, W., Wu, C., Lopez, S. L., & Blais, J. (2007). Preparation of tetra-Boc-protected polymyxin B nonapeptide. *Tetrahedron Letters*, 48(11), 2003–2005.
- Papo, N., & Shai, Y. (2003). Exploring peptide membrane interaction using surface plasmon resonance: differentiation between pore formation versus membrane disruption by lytic peptides. *Biochemistry*, 42, 458–466.
- Parker, W. L., & Rathnum, M. L. (1973). EM49, a new peptide antibiotic. II. Chemical characterization. *The Journal of Antibiotics*, 26(8), 449–456.
- Parker, W. L., & Rathnum, M. L. (1975). EM49, a new peptide antibiotic IV. The structure of EM49. *The Journal of Antibiotics*, 28(5), 379–389.
- Patrzykat, A., Friedrich, C. L., Zhang, L., Mendoza, V., & Hancock, R. E. W. (2002). Sublethal concentrations of pleurocidin-derived antimicrobial peptides inhibit macromolecular synthesis in *Escherichia coli*. *Antimicrobial Agents and Chemotherapy*, 46(3), 605–614.

- Peleg, A. Y., Seifert, H., & Paterson, D. L. (2008). *Acinetobacter baumannii*: emergence of a successful pathogen. *Clinical Microbiology Reviews*, 21(3), 538–582.
- Peschel, A., & Sahl, H.-G. (2006). The co-evolution of host cationic antimicrobial peptides and microbial resistance. *Nature Reviews Microbiology*, 4(7), 529–536.
- Pogue, J. M., Marchaim, D., Kaye, D., & Kaye, K. S. (2011). Revisiting “older” antimicrobials in the era of multidrug resistance. *Pharmacotherapy*, 31(9), 912–921.
- Porro, M. (1993). Synthetic peptide for detoxification of bacterial endotoxins and treatment of septic shock. *Patent*, WO/1993/014115.
- Porro, M. (1995). Peptide for neutralizing the toxicity of Lipid A. *Patent*, WO/1995/003327.
- Porro, M., & Vaara, M. (1996). Compositions containing an antibiotic and a peptide potentiating this antibiotic. *Patent*, WO/1996/038163.
- Pouny, Y., Rapaport, D., Mor, A., Nicolas, P., & Shai, Y. (1992). Interaction of antimicrobial dermaseptin and its fluorescently labeled analogs with phospholipid membranes. *Biochemistry*, 31, 12416–12423.
- Pozo Navas, B., Lohner, K., Deutsch, G., Sevcsik, E., Riske, K. A., Dimova, R., et al. (2005). Composition dependence of vesicle morphology and mixing properties in a bacterial model membrane system. *Biochimica Et Biophysica Acta*, 1716(1), 40–48.
- Pristovsek, P., & Kidric, J. (1999). Solution structure of polymyxins B and E and effect of binding to lipopolysaccharide: an NMR and molecular modeling study. *Journal of Medicinal Chemistry*, 42(22), 4604–4613.
- Pristovsek, P., & Kidric, J. (2004). The search for molecular determinants of LPS inhibition by proteins and peptides. *Current Topics in Medicinal Chemistry*, 4(11), 1185–1201.
- Qian, C.-D., Wu, X.-C., Teng, Y., Zhao, W.-P., Li, O., Fang, S.-G., et al. (2012). Battacin (Octapeptin B5), a new cyclic lipopeptide antibiotic from *Paenibacillus tianmuensis* active against multidrug-resistant Gram-negative bacteria. *Antimicrobial Agents and Chemotherapy*, 56(3), 1458–1465.
- Qian, S., Wang, W., Yang, L., & Huang, H. W. (2008). Structure of the alamethicin pore reconstructed by x-ray diffraction analysis. *Biophysical Journal*, 94(9), 3512–3522.
- Quale, J., Shah, N., Kelly, P., Babu, E., Backer, M., Rosas-Garcia, G., et al. (2012). Activity of Polymyxin B and the Novel Polymyxin Analogue CB-182,804 Against Contemporary Gram-Negative Pathogens in New York City. *Microbial Drug Resistance*, 18(2), 132–136.
- Rawat, S. S., Kelkar, D. A., & Chattopadhyay, A. (2004). Monitoring gramicidin conformations in membranes: a fluorescence approach. *Biophysical Journal*, 87(2), 831–843.
- Rice, L. B. (2008). Federal Funding for the Study of Antimicrobial Resistance in Nosocomial Pathogens: No ESKAPE. *The Journal of Infectious Diseases*, 197(8), 1079–1081.
- Richter, K., Aschauer, H., & Kreil, G. (1985). Biosynthesis of peptides in the skin of *Xenopus laevis*: Isolation of novel peptides predicted from the sequence of cloned cDNAs. *Peptides*, 6, 17–21.
- Rosenthal, K. S., Ferguson, R. A., & Storm, D. R. (1977). Mechanism of Action of EM 49, Membrane-Active Peptide Antibiotic. *Antimicrobial Agents and Chemotherapy*, 12(6), 665–672.
- Rustici, A., Velucchi, M., Faggioni, R., Sironi, M., Ghezzi, P., Quataert, S., et al. (1993). Molecular mapping and detoxification of the lipid A binding site by synthetic

- peptides. *Science*, 259(5093), 361–365.
- Sader, H. S., Rhomberg, P. R., & Jones, R. N. (2010). Antimicrobial activity of a novel polymyxin analog (CB-182,804) tested against clinical strains of Gram-negative bacilli, including colistin-resistant organisms. *50th Interscience Conference on Antimicrobial Agents and Chemotherapy*.
- Sakura, N., Itoh, T., Uchida, Y., Ohki, K., & Okimura, K. (2004). The contribution of the N-terminal structure of polymyxin B peptides to antimicrobial and lipopolysaccharide binding activity. *Bulletin of the Chemical Society of Japan*, 77, 1915–1924.
- Sanyal, D., & Greenwood, D. (1993). An electronmicroscope study of glycopeptide antibiotic-resistant strains of *Staphylococcus epidermidis*. *Journal of Medical Microbiology*, 39(3), 204–210.
- Schindler, P. R. G., & Teuber, M. (1975). Action of Polymyxin B on Bacterial Membranes: Morphological Changes in the Cytoplasm and in the Outer Membrane of *Salmonella typhimurium* and *Escherichia coli* B. *Antimicrobial Agents and Chemotherapy*, 8(1), 95–104.
- Sessa, G., & Weissmann, G. (1968). Phospholipid spherules (liposomes) as a model for biological membranes. *Journal of Lipid Research*, 9(3), 310–318.
- Shai, Y. (1999). Mechanism of the binding, insertion and destabilization of phospholipid bilayer membranes by alpha-helical antimicrobial and cell non-selective membrane-lytic peptides. *Biochimica Et Biophysica Acta*, 1462(1-2), 55–70.
- Shimoda, M., Ohki, K., Shimamoto, Y., & Kohashi, O. (1995). Morphology of defensin-treated *Staphylococcus aureus*. *Infection and Immunity*, 63(8), 2886–2891.
- Shinitzky, M., & Barenholz, Y. (1978). Fluidity parameters of lipid regions determined by fluorescence polarization. *Biochimica Et Biophysica Acta*, 515(4), 367–394.
- Shoji, J., Sakazaki, R., Wakisaka, Y., Koizumi, K., Matsuura, S., Miwa, H., & Mayama, M. (1980). Isolation of octapeptin D (studies on antibiotics from the genus *Bacillus*. XXVII). *The Journal of Antibiotics*, 33(2), 182–185.
- Singer, S. J., & Nicolson, G. L. (1972). The fluid mosaic model of the structure of cell membranes. *Science*, 175(4023), 720–731.
- Sitaram, N., & Nagaraj, R. (1999). Interaction of antimicrobial peptides with biological and model membranes: structural and charge requirements for activity. *Biochimica Et Biophysica Acta*, 1462(1-2), 29–54.
- Solé, M., Pitart, C., Roca, I., Fàbrega, A., Salvador, P., Muñoz, L., et al. (2011). First description of an *Escherichia coli* strain producing NDM-1 carbapenemase in Spain. *Antimicrobial Agents and Chemotherapy*, 55(9), 4402–4404.
- Soravia, E., Martini, G., & Zasloff, M. (1988). Antimicrobial properties of peptides from *Xenopus* granular gland secretions. *FEBS Letters*, 228, 337–340.
- Srimal, S., Surolia, N., Balasubramanian, S., & Surolia, A. (1996). Titration calorimetric studies to elucidate the specificity of the interactions of polymyxin B with lipopolysaccharides and lipid A. *Biochemical Journal*, 315, 679–686.
- Srinivasa, B. R., & Ramachandran, L. K. (1978). Chemical modification of peptide antibiotics: Part VII--Biological activity of derivatives of polymyxin B. *Indian Journal of Biochemistry & Biophysics*, 15, 54–58.
- Steen, H. B., Boye, E., Skarstad, K., Bloom, B., Godal, T., & Mustafa, S. (1982). Applications of flow cytometry on bacteria: cell cycle kinetics, drug effects, and quantitation of antibody binding. *Cytometry*, 2(4), 249–257.
- Stewart, J. C. M. (1980). Colorimetric determination of phospholipids with ammonium ferrothiocyanate. *Analytical Biochemistry*, 104(1), 10–14.

- Strandberg, E., & Ulrich, A. S. (2004). NMR methods for studying membrane-active antimicrobial peptides. *Concepts in Magnetic Resonance Part A*, 23A(2), 89–120.
- Strandberg, E., Esteban-Martín, S., Ulrich, A. S., & Salgado, J. (2012a). Hydrophobic mismatch of mobile transmembrane helices: Merging theory and experiments. *Biochimica Et Biophysica Acta*, 1818(5), 1242–1249.
- Strandberg, E., Kanithasen, N., Tiltak, D., Bürck, J., Wadhvani, P., Zwernemann, O., & Ulrich, A. S. (2008). Solid-State NMR Analysis Comparing the Designer-Made Antibiotic MSI-103 with Its Parent Peptide PGLa in Lipid Bilayers. *Biochemistry*, 47(8), 2601–2616.
- Strandberg, E., Tiltak, D., Ehni, S., Wadhvani, P., & Ulrich, A. S. (2012b). Lipid shape is a key factor for membrane interactions of amphipathic helical peptides. *Biochimica Et Biophysica Acta*, 1818(7), 1764–1776.
- Strandberg, E., Tiltak, D., Ieronimo, M., Kanithasen, N., Wadhvani, P., & Ulrich, A. S. (2007). Influence of C-terminal amidation on the antimicrobial and hemolytic activities of cationic α -helical peptides. *Pure and Applied Chemistry*, 79(4), 717–728.
- Strandberg, E., Wadhvani, P., Tremouilhac, P., Dürr, U. H. N., & Ulrich, A. S. (2006). Solid-State NMR Analysis of the PGLa Peptide Orientation in DMPC Bilayers: Structural Fidelity of ^2H -Labels versus High Sensitivity of ^{19}F -NMR. *Biophysical Journal*, 90(5), 1676–1686.
- Strandberg, E., Zerweck, J., Wadhvani, P., & Ulrich, A. S. (2013). Synergistic Insertion of Antimicrobial Magainin-Family Peptides in Membranes Depends on the Lipid Spontaneous Curvature. *Biophysical Journal*, 104(6), L9–L11.
- Straus, S. K., & Hancock, R. E. W. (2006). Mode of action of the new antibiotic for Gram-positive pathogens daptomycin: comparison with cationic antimicrobial peptides and lipopeptides. *Biochimica Et Biophysica Acta*, 1758(9), 1215–1223.
- Sugawara, K., Yonemoto, T., Konishi, M., Matsumoto, K., Miyaki, T., & Kawaguchi, H. (1983). Bu-2470, a new peptide antibiotic complex. II. Structure determination of Bu-2470 A, B1, B2a and B2b. *The Journal of Antibiotics*, 36(6), 634–638.
- Szoka, F., & Papahadjopoulos, D. (1978). Procedure for preparation of liposomes with large internal aqueous space and high capture by reverse-phase evaporation. *Proceedings of the National Academy of Sciences of the United States of America*, 75(9), 4194–4198.
- Szoka, F., & Papahadjopoulos, D. (1980). Comparative properties and methods of preparation of lipid vesicles (liposomes). *Annual Review of Biophysics and Bioengineering*, 9(1), 467–508.
- Tam, J. P., Wu, C. R., Liu, W., & Zhang, J. W. (1991). Disulfide bond formation in peptides by dimethyl sulfoxide. Scope and applications. *Journal of the American Chemical Society*, 113, 6657–6662.
- Terabe, S., Konaka, R., & Shoji, J. (1979). Separation of polymyxins and octapeptins by high-performance liquid chromatography. *Journal of Chromatography A*, 173, 313–320.
- Teuber, M. (1974). Action of polymyxin B on bacterial membranes. *Archives of Microbiology*, 100(1), 131–144.
- Theuretzbacher, U. (2012). Accelerating resistance, inadequate antibacterial drug pipelines and international responses. *International Journal of Antimicrobial Agents*, 39(4), 295–299.
- Toke, O. (2005). Antimicrobial peptides: new candidates in the fight against bacterial infections. *Biopolymers*, 80(6), 717–735.
- Tsubery, H., Ofek, I., Cohen, S., & Fridkin, M. (2000a). Structure activity relationship

- study of polymyxin B nonapeptide. *Advances in Experimental Medicine and Biology*, 479(Chapter 18), 219–222.
- Tsubery, H., Ofek, I., Cohen, S., & Fridkin, M. (2000b). Structure-function studies of polymyxin B nonapeptide: implications to sensitization of gram-negative bacteria. *Journal of Medicinal Chemistry*, 43(16), 3085–3092.
- Tsubery, H., Ofek, I., Cohen, S., & Fridkin, M. (2001). N-terminal modifications of polymyxin B nonapeptide and their effect on antibacterial activity. *Peptides*, 22(10), 1675–1681.
- Tsubery, H., Ofek, I., Cohen, S., & Fridkin, M. (2002). Structure Activity Relationship Study of Polymyxin B Nonapeptide. *The Biology and Pathology of Innate Immunity Mechanisms*, 479(Chapter 18), 219–222.
- Tsubery, H., Yaakov, H., Cohen, S., Giterman, T., Matityahou, A., Fridkin, M., & Ofek, I. (2005). Neopeptide antibiotics that function as opsonins and membrane-permeabilizing agents for gram-negative bacteria. *Antimicrobial Agents and Chemotherapy*, 49(8), 3122–3128.
- Ulvatne, H., Haukland, H. H., Olsvik, Ø., & Vorland, L. H. (2001). Lactoferricin B causes depolarization of the cytoplasmic membrane of Escherichia coli ATCC 25922 and fusion of negatively charged liposomes. *FEBS Letters*, 492(1-2), 62–65.
- Urakawa, H., Yamada, K., Komagoe, K., Ando, S., Oku, H., Katsu, T., & Matsuo, I. (2010). Structure–activity relationships of bacterial outer-membrane permeabilizers based on polymyxin B heptapeptides. *Bioorganic & Medicinal Chemistry Letters*, 20(5), 1771–1775.
- Vaara, M. (1991). The outer membrane permeability-increasing action of linear analogues of polymyxin B nonapeptide. *Drugs Under Experimental and Clinical Research*, 17(9), 437–443.
- Vaara, M., & Vaara, T. (1983a). Polycations as outer membrane-disorganizing agents. *Antimicrobial Agents and Chemotherapy*, 24(1), 114–122.
- Vaara, M., & Vaara, T. (1983b). Sensitization of Gram-negative bacteria to antibiotics and complement by a nontoxic oligopeptide. *Nature*, 303, 526–528.
- Vaara, M., & Vaara, T. (2013). The novel polymyxin derivative NAB739 is remarkably less cytotoxic than polymyxin B and colistin to human kidney proximal tubular cells. *International Journal of Antimicrobial Agents*, 41(3), 292–293.
- Vaara, M., Fox, J., Loidl, G., Siikanen, O., Apajalahti, J., Hansen, F., et al. (2008). Novel Polymyxin Derivatives Carrying Only Three Positive Charges Are Effective Antibacterial Agents. *Antimicrobial Agents and Chemotherapy*, 52(9), 3229–3236.
- Vaara, M., Sader, H. S., Rhomberg, P. R., Jones, R. N., & Vaara, T. (2013). Antimicrobial activity of the novel polymyxin derivative NAB739 tested against Gram-negative pathogens. *Journal of Antimicrobial Chemotherapy*, 68(3), 636–639.
- van Ginkel, G., van Langen, H., & Levine, Y. K. (1989). The membrane fluidity concept revisited by polarized fluorescence spectroscopy on different model membranes containing unsaturated lipids and sterols. *Biochimie*, 71(1), 23–32.
- Vance, D. E., Vance, J. (1996). *Biochemistry of Lipids, Lipoproteins and Membranes*. Elsevier Science, Amsterdam (Netherlands).
- Velkov, T., Thompson, P. E., Nation, R. L., & Li, J. (2010). Structure–Activity Relationships of Polymyxin Antibiotics. *Journal of Medicinal Chemistry*, 53(5), 1898–1916.
- Velluz, L., Legrand, M., & Grosjean, M. (1965). *Optical circular dichroism: principles, measurements, and applications*. New York and London: Verlag Chemie Academic Press Inc.
- Verger, R., & Pattus, F. (1982). Lipid-protein interactions in monolayers. *Chemistry*

- and *Physics of Lipids*, 30(2-3), 189–227.
- Visser, P. C., Kriek, N. M. A. J., Hooft, P. A. V., Van Schepdael, A., Filippov, D. V., Marel, G. A., et al. (2003). Solid-phase synthesis of polymyxin B1 and analogues via a safety-catch approach. *The Journal of Peptide Research*, 61(6), 298–306.
- Vogler, K., & Studer, R. O. (1966). The chemistry of the polymyxin antibiotics. *Cellular and Molecular Life Sciences*, 22(6), 345–354.
- Vogler, K., Studer, R. O., Lanz, P., Lergier, W., & Bohni, E. (1961). Total synthesis of two cyclodecapeptides exerting polymyxin-like activity. *Experientia*, 17, 223–224.
- Wadhvani, P., Reichert, J., Bürck, J., & Ulrich, A. S. (2012). Antimicrobial and cell-penetrating peptides induce lipid vesicle fusion by folding and aggregation. *European Biophysics Journal*, 41(2), 177–187.
- Wadhvani, P., Strandberg, E., van den Berg, J., Mink, C., Bürck, J., Ciriello, R. A. M., & Ulrich, A. S. (2014). Dynamical structure of the short multifunctional peptide BP100 in membranes. *Biochimica Et Biophysica Acta*, 1838(3), 940–949.
- Weinstein, J., Afonso, A., Moss, E., Jr., & Miller, G. H. (1998). Selective chemical modifications of polymyxin B. *Bioorganic & Medicinal Chemistry Letters*, 8(23), 3391–3396.
- Wiegand, I., Hilpert, K., & Hancock, R. E. W. (2008). Agar and broth dilution methods to determine the minimal inhibitory concentration (MIC) of antimicrobial substances. *Nature Protocols*, 3(2), 163–175.
- Wiese, A., Gutschmann, T., & Seydel, U. (2003). Review: Towards antibacterial strategies: studies on the mechanisms of interaction between antibacterial peptides and model membranes. *Innate Immunity*, 9(2), 67–84.
- Witzke, N. M., & Heding, H. (1976). Broad-spectrum derivatives of polymyxin B and colistin. *The Journal of Antibiotics*, 29(12), 1349–1350.
- Woods, G. L. (1995). Antibacterial susceptibility tests : Dilution and disk diffusion methods. *Manual of Clinical Microbiology*, 1327–1341.
- Yang, L., Harroun, T. A., Weiss, T. M., Ding, L., & Huang, H. W. (2001). Barrel-stave model or toroidal model? A case study on melittin pores. *Biophysical Journal*, 81, 1475–1485.
- Yang, L., Weiss, T. M., Lehrer, R. I., & Huang, H. W. (2000). Crystallization of antimicrobial pores in membranes: magainin and protegrin. *Biophysical Journal*, 79, 2002–2009.
- Yeaman, M. R. (2003). Mechanisms of Antimicrobial Peptide Action and Resistance. *Pharmacological Reviews*, 55(1), 27–55.
- Zampighi, G. A., Zampighi, L. M., Fain, N., Lanzavecchia, S., Simon, S. A., & Wright, E. M. (2006). Conical electron tomography of a chemical synapse: vesicles docked to the active zone are hemi-fused. *Biophysical Journal*, 91(8), 2910–2918.
- Zaslhoff, M. (2002). Antimicrobial peptides of multicellular organisms. *Nature*, 415(6870), 389–395.
- Zhang, L. (2001). Interaction of Cationic Antimicrobial Peptides with Model Membranes. *Journal of Biological Chemistry*, 276(38), 35714–35722.
- Zhang, L., Dhillon, P., Yan, H., Farmer, S., & Hancock, R. (2000). Interactions of Bacterial Cationic Peptide Antibiotics with Outer and Cytoplasmic Membranes of *Pseudomonas aeruginosa*. *Antimicrobial Agents and Chemotherapy*, 44, 3317–3321.
- Zhao, H., & Kinnunen, P. K. J. (2002). Binding of the antimicrobial peptide temporin L to liposomes assessed by Trp fluorescence. *The Journal of Biological Chemistry*, 277(28), 25170–25177.
- Zhao, H., Sood, R., Jutila, A., Bose, S., & Fimland, G. (2006). Interaction of the antimicrobial peptide pheromone Plantaricin A with model membranes:

- implications for a novel mechanism of action. *Biochimica Et Biophysica Acta*, 1758, 1461–1474.
- Zimmerberg, J., Vogel, S. S., & Chernomordik, L. V. (1993). Mechanisms of membrane fusion. *Annual Review of Biophysics and Biomolecular Structure*, 22(1), 433–466.